DISSERTATION

Host-microbiome interaction in organ damage of cardiovascular disease
Host-Mikrobiom-Interaktion bei Organschäden durch kardiovaskuläre Erkrankungen

zur Erlangung des akademischen Grades
Doctor of Philosophy (PhD)

vorgelegt der Medizinischen Fakultät
Charité – Universitätsmedizin Berlin

von

Chia-Yu Chen

Erstbetreuer: Prof. Dr. Dominik N. Müller

Datum der Promotion: 29. November 2024

Table of contents

List of tables

List of figures

List of abbreviations

ACE inhibitor	Angiotensin-converting enzyme inhibitor
AT2	Angiotensin II receptor blockers
BH	Benjamini-hochberg
BMI	Body-mass index
BP	Blood pressure
CKD	Chronic kidney disease
CLR	Centered log-ratio
CNS	Central nervous system
COL	Colonized
CONV	Conventionally raised SPF C57BL/6J mice
CRAN	Comprehensive r archive network
CSS	Cumulative-sum scaling
CVD	Cardiovascular diseases
DASH	Dietary Approaches to Stop Hypertension
ECRC	Experimental and Clinical Research Center
FDR	False discovery rate
FPR	False positive rate
GB	Gigabyte
GF	Germ-free
GLMMs	Generalized linear mixed-effect models
GLMs	Generalized linear models
GMPR	Geometric mean of pairwise ratios
HTN	Hypertension
IBD	Inflammatory bowel disease
LMs	Linear models
MB	Megabyte
MCC	Matthews correlation coefficient
MetS	Metabolic syndrome
MiB	Mebibyte
NCEP ATP III	National cholesterol education program adult treatment panel III
Olfr78	Olfactory receptor 78

PcoA	Principal coordinates analysis
PERMANOVA	Permutational Multivariate Analysis of Variance
PPI	Proton pump inhibitor
SCFA	Short-chain fatty acid
Th1	Type 1 T helper
TMA	Trimethylamine
TMAO	Trimethylamine N-oxide
TMM	Trimmed mean of M-values
TPR	True positive rate
TSS	Total-sum scaling
VoE	Vibration of effects

Abstract

Background

The gut microbiome crucially influences human health and physiology, and it is associated with cardiovascular and kidney diseases. Understanding host-microbiome interactions is vital for novel disease therapies. Challenges remain, such as the gut microbiome's impact on hypertension-induced damage and fasting effects in metabolic syndrome (MetS) patients. Longitudinal data collection mitigates inter-individual variations, gaining popularity in microbiome research in recent years. A covariates-aware approach is essential for precise analyses; however, current tools lack effective control of multiple covariates and explicit assessment of time variable impact amidst other covariates.

Aim

To address the gap mentioned above and facilitate robust biomarker search in longitudinal microbiome analysis, an algorithm is developed and applied to microbiome datasets in order to clarify the role of the host-microbiome interaction in cardiovascular diseases (CVD), and also asses its generalizability.

Methods

LongDat, a covariate-aware longitudinal analysis algorithm, employs unique capabilities to simultaneously detect, control covariates, and assess time variable significance. It leverages generalized linear mixed-effect models (GLMMs), accommodating inter-individual variance and various data distributions. For broader distribution and reproducibility, LongDat is compiled as an R package. LongDat was applied to MetS patients' gut microbiome data undergoing fasting. In addition, the gut microbiome's role in hypertension (HTN) in colonized (COL) and germ-free (GF) mice was also explored using models and correlation tests.

Results

LongDat's performance was evaluated against existing tools using real and simulated data, illustrating its superior accuracy, runtime, and memory efficiency—particularly in scenarios with multiple covariates. When employed in the context of MetS patients undergoing fasting, LongDat unveiled alterations in the gut microbiome affecting microbial taxa, gene modules related to short-chain fatty acid (SCFA) synthesis, and indicating potential shifts in immune cells. Moreover, a comparison between COL and GF mice exposed their varied responses to HTN, with GF mice exhibiting worse renal damage. The lack of anti-inflammatory SCFA in GF mice suggests that colonization status influences HTN-relevant circulating metabolites. Additionally, correlations between the gut microbiome, functional modules, and metabolites were identified. These findings emphasize the crucial role of the gut microbiome, SCFAs, and other metabolites in HTN and overall health.

Conclusion

LongDat and the mixed effect models serve as a robust biomarker exploration tool in microbiome research, revealing fasting's potential for MetS intervention and the gut microbiome's significance in HTN development. This thesis emphasizes the essential role of covariate-aware tools in microbiome research, crucial for reproducibility and meaningful inter-study comparisons.

Zusammenfassung

Hintergrund

Das Darmmikrobiom beeinflusst die menschliche Gesundheit und wird mit Krankheiten wie Herz-Kreislauf-Erkrankungen und Nierenleiden in Verbindung gebracht. Das Verständnis von Wirt-Mikrobiom-Interaktionen ist für neue Therapien wichtig. Herausforderungen bestehen hier unter anderem bei der Erforschung des Einflusses des Mikrobioms auf durch Hypertonie verursachte Schäden oder das Fasten beim metabolischen Syndrom (MetS). Längsschnittdaten minimieren Variationen und gewinnen in Mikrobiomforschung an Bedeutung. Ein kovariatenbewusster Ansatz ist für präzise Analysen essenziell, allerdings beherrschen gegenwärtige Tools oft nicht die effektive Kontrolle multipler Kovariaten und die Bewertung des Zeitfaktors neben anderen Kovariaten.

Ziel

Um diese Lücke zu schließen und Biomarker in längsschnittdatenbasierten Mikrobiomanalysen zu finden, wurde ein Algorithmus entwickelt. Dieser wurde auf Mikrobiomdaten angewendet, um die Wirt-Mikrobiom-Interaktion bei Herz-Kreislauf-Erkrankungen zu beleuchten und seine Verallgemeinerbarkeit zu prüfen.

Methoden

Der Algorithmus LongDat erkennt, kontrolliert und bewertet Kovariaten sowie den Einfluss der Zeit. Dafür nutzt er verallgemeinerte lineare gemischte Modelle (GLMMs) für kovariatenbewusste Analysen. Um Reproduzierbarkeit zu gewährleisten und weitläufig Anwendung zu finden, wurde LongDat als R-Paket erstellt. So wurden mithilfe von LongDat Mikrobiomdaten von MetS-Patienten während des Fastens analysiert. Auch die Rolle des Mikrobioms bei Hypertonie (HTN) in besiedelten (COL) und keimfreien (GF) Mäusen wurde mit Modellen und Korrelationstests untersucht.

Ergebnisse

LongDat übertrifft aktuelle Tools sowohl in Anwendung auf reale als auch simulierte Daten hinsichtlich Genauigkeit, Laufzeit und Speichereffizienz, vor allem bei zahlreichen

Kovariaten. Bei MetS-Patienten wurden festgestellt, dass Fasten zu einer Veränderungen im Mikrobiom führt. Auch wurden Unterschiede in bakteriellen Taxa und Genmodulen, die kurzkettige Fettsäuren (SCFA) betreffen, sowie Hinweise auf Veränderungen in Immunzellen sichtbar. COL- und GF-Mäuse zeigten unterschiedliche Reaktionen auf HTN, wobei GF-Mäuse stärkere Nierenschäden aufwiesen. Das Fehlen entzündungshemmender SCFA bei GF-Mäusen legt nahe, dass der Besiedlungsstatus HTN-relevante Metabolite beeinflusst. Zudem wurden Korrelationen zwischen dem Darmmikrobiom, seinem funktionellen Potential und Metaboliten gefunden. Dies betont die Bedeutung des Mikrobioms, SCFAs und anderen Metaboliten für HTN und die menschliche Gesundheit im Allgemeinen.

Fazit

LongDat und gemischte Effektmodelle sind robuste Werkzeuge für die Mikrobiomforschung. Sie zeigen das Potential des Fastens als Internvention bei MetS und die Rolle des Mikrobioms bei HTN. Diese Dissertation unterstreicht die essentielle Rolle kovariatenbewusster Tools in der Mikrobiomforschung zur Sicherung von Reproduzierbarkeit und robuster Studienvergleiche.

1 Introduction

1.1 An overview of the gut microbiome

The human body is home to countless microorganisms. These microorganisms dwell in various environments, such as the skin, oral cavity, and gastrointestinal system (including stomach, large and small intestines). In fact, the number of microbial cells inhabiting the human body is estimated to be equal to or greater than human somatic cells[1]. The study of gut microbiome is rather recent because it was impossible to clarify the identity of these microorganisms in the past. Thanks to the rapid development of metagenomic sequencing technology in recent years, researchers are now able to characterize the composition and function of these microorganisms at a fine resolution. Nowadays, literature related to the human microbiome spawned, and in turn, facilitates the understanding of these microorganisms' impact on human health.

While microbial communities at different human body sites have distinct influences and interactions with the human body, the gut microbiome, which refers to the microorganisms living in the gastrointestinal tract collectively, has received significant interest among all the microbial communities for two reasons. First, the gut microbiome encompasses close and multifaceted relationships with human health[2]. Second, since over one thousand different microbial species have been identified in the gut microbiome so far, it stands out as the most complicated among the various microbial communities in the human body[3]. To date, it is known that the gut microbiome is highly diverse and consists of various types of microorganisms such as viruses, bacteria, archaea, and fungi[4]. This complex ecosystem is primarily composed of the taxa belonging to two dominant phyla, *Bacteroidetes* and *Firmicutes*[5]. Despite great variation between individuals whose age, health status, geography, diet, or antibiotic usage differs, the gut microbiome remains relatively stable over time if not perturbed by external factors.

The human gut microbiome can be classified into several enterotypes, namely *Bacteroides* (enterotype 1), *Prevotella* (enterotype 2), and *Ruminococcus* (enterotype 3)[6]. The enterotypes are characterized by the predominance of certain bacterial genus. Particularly, the *Bacteroides* enterotype has been divided into two subtypes, *Bacteroides* 1

and *Bacteroides* 2, mainly according to the proportion of *Faecalibacterium* and microbial cell density in the gut[7].

1.2 Host-microbiome interaction and human health

The interaction between the host and microbiome affects human health to a large extent. Host-microbiome interactions involve both direct cellular contact and the involvement of metabolites. Metabolites originate from bacteria, the host, or the environment and subsequently undergo metabolism by the bacteria[8]. One prominent example of these metabolites is the SCFA. SCFAs are a class of fatty acids consisting of less than six carbon atoms and are secreted by the gut microbiome during the fermentation of fibers in the large intestine. The main SCFAs being secreted are acetate, propionate, and butyrate[9]. In recent years, SCFAs have become a thriving research field because they are found to encompass a variety of beneficial effects on the host, including anti-obesity, anti-diabetic, anticancer, anti-inflammatory, and immune-regulating. Furthermore, it is shown that SCFAs protect the host against liver, neurological, and CVD[10].

The gut microbiome can be categorized into commensals and pathogens based on their relationship with human health. Commensals are the ones inhabiting the human gut without posing harm; on the contrary, pathogens cause disease or adverse health effects[11]. Commensals are mostly beneficial and involved in a wide range of human physiology. Some examples are outlined below.

First, commensals compete with pathogens for the resources (e.g., nutrients, living space) in the gut, making the proliferation of pathogens become more challenging, limiting the ability of pathogens to cause infections[12]. Second, commensals play an important role in training the innate and adaptive immune systems to recognize and react to potential threats, which is vital in maintaining effective immune response and the ability to defend against infections[13,14]. GF animals lacking gut microbiome exhibit compromised immune functions such as decreased immunoglobulin concentration, and have impaired innate and adaptive immune responses[15,16].

Third, commensals are involved in the regulation and development of the gastrointestinal tract. They contribute to the maturation and proper functioning of the gastrointestinal tract,

ensuring efficient digestion and absorption of nutrients[17]. Literature indicates that commensals are critical in maintaining the integrity of the intestinal barrier. The intestinal barrier is a selectively permeable structure that enables the uptake of nutrients and facilitates immune sensing, while acting as a barrier against harmful substances and bacteria simultaneously[18]. A weakened intestinal barrier allows gut bacteria, bacterial toxins, undigested food, as well as waste products to enter the bloodstream. This dysfunction triggers inflammatory responses and might result in “leaky gut syndrome”, which is a collective term including symptoms such as food sensitivities, abdominal bloating, cramps, diarrhea, constipation, and fatigue[19]. Moreover, SCFAs produced by commensal microbes are important energy sources for intestinal epithelial cells, and they strengthen the integrity of the intestinal barrier[20].

Lastly, commensals influence the function and development of the central nervous system (CNS), and disruptions in the gut microbiome may be associated with neurological problems[21]. Recent research emphasizes the significant role of the gut microbiome in shaping the gut-brain axis, which connects the central and enteric nervous systems, facilitating communication between the brain's emotional and cognitive centers and intestinal functions[22].

On the opposite side of a healthy gut microbiome, which consists of commensals, is dysbiosis, which refers to the imbalanced state of microbes in the gut. Dysbiosis occurs when the natural balance of the microbial ecosystem is disrupted, as it allows opportunistic bacteria which are originally not dominant to overgrow[23]. Dysbiosis can arise from a variety of factors specific to the host, including genetic background, health status (e.g., inflammation), and lifestyle habits. Additionally, environmental factors, such as diet (e.g., high in sugar and low in fiber), antibiotics, drugs, and hygiene, play crucial roles in leading to dysbiosis as well[24]. Lately, accumulating evidence demonstrates that dysbiosis is linked to human diseases, including autism, obesity, colorectal cancer, inflammatory bowel disease (IBD), allergy, diabetes, CVD, and kidney disease[25,26].

1.3 The role of the gut microbiome in CVD and CKD

CVD is a general term describing a range of diseases related to the heart or blood vessels. CVD stands as the major underlying cause of mortality in the world[27]. Some of the known

and well-established risk factors for CVD are unhealthy diet, insufficient physical activity, hyperglycemia, obesity, smoking, HTN, MetS, and CKD, among others[28,29]. CVD, HTN, and MetS are all associated with various forms of organ damage, such as renal damage or heart disease. Intriguingly, recent findings indicate that changes in the gut microbiome (either in composition or function), are involved in the development of CVD[30]. For example, in cross-sectional studies comparing hypertensive patients with healthy individuals, the abundance of *Prevotella* and *Klebsiella* increased. On the other hand, a reduction in the abundance of *Faecalibacterium prausnitzii* and an elevation in the levels of *Ruminococcus gnavus* was observed in patients suffering from heart failure. Besides, in atherosclerosis patients, the abundance of *Escherichia coli*, *Enterobacter aerogenes*, and *Lactobacillus salivarius* were found to rise, while *Roseburia intestinalis*, *Faecalibacterium prausnitzii*, *Prevotella copri*, and *Alistipes shahii* declined[31]. Furthermore, several microbial metabolites have appeared to influence cardiovascular disease. For instance, SCFAs mediate blood pressure (BP) through GPR-regulated pathways, and lower BP by modulating olfactory receptor 78 (Olfr78) and promoting vasodilation in mice[32]. Another example can be taken from the metabolite known as trimethylamine N-oxide (TMAO). Upon dietary intake of choline or carnitine, the gut microbiome metabolizes these compounds into trimethylamine (TMA). Subsequently, the liver converts TMA into TMAO, whose level in plasma is positively correlated with obesity, insulin resistance, risk of CVD, and mortality[33].

As previously stated, CKD is a continual kidney damage resulting in decreased glomerular filtration rate and albuminuria. CKD has been identified as a risk factor for CVD. More accurately, CVD and CKD exhibit a close interconnection, wherein dysfunction in one organ can adversely affect the other, eventually resulting in the failure of both. Similar to what has been shown in CVD, the gut microbiome plays a vital role in the progression of CKD. For example, there is a higher abundance of *Desulfovibrio*, *Escherichia/Shigella*, and *Streptococcus*, while a lower abundance of *Roseburia*, *Faecalibacterium*, *Pyramidobacter*, and *Prevotella* in CKD patients[34,35]. On the other hand, alterations in the metabolites produced by the gut microbiome have significant outcomes. Specifically, a decrease in metabolites known to promote health, such as SCFAs, while the accumulation of uremic toxins, including ammonia, indoles, and TMAO, exacerbates CKD progression. The worsening of CKD is attributed to both the excessive production of these toxins and

their reduced elimination due to impaired kidney function, ultimately contributing to the development of CKD[36].

In short, accumulating studies have indicated that the gut microbiome is pivotal in CVD and CKD progressions. Changes in the gut microbiome composition and metabolites contribute to the development of CVD and CKD. By enhancing our knowledge of the gut microbiome, novel therapies aimed at managing and treating these diseases (or their risk factors) may be developed.

1.4 The importance of longitudinal study in gut microbiome research

Based on the research design, there are two categories of microbiome data: cross-sectional and longitudinal. Cross-sectional data are obtained by evaluating more than one subjects at a single time point without follow-up, whereas longitudinal data are repeated measurements acquired sequentially from the identical subject at various time points[37,38]. Cross-sectional studies are popular since they offer notable advantages in speed and cost-effectiveness; they also excel in assessing prevalence rates and investigating connections between various factors and outcomes. Besides, ethical challenges are infrequent in cross-sectional studies because participants are not intentionally exposed or treated. Nonetheless, cross-sectional studies bear several disadvantages, including their inability to examine rare diseases and infer causal relationships. In addition, cross-sectional data are unable to account for inter-individual variations nor track intra-subject changes over time[37,39]. In contrast, longitudinal studies are specifically designed to capture the dynamics within individuals throughout the time course, as well as the variations between individuals[40,41]. Furthermore, longitudinal studies are favored over cross-sectional studies when the objective is to determine the causal impact of a specific treatment on the outcome, as the temporal sequence of treatment and outcome in longitudinal studies are clear[42]. Consequently, over recent years, there has been an increasing adoption of longitudinal data collection in the biological and medical fields, including studies related to the gut microbiome[43]. Given the high inter-subject variability observed in gut microbiome data, longitudinal studies play an important role in providing valuable insights and understanding the complex dynamics over time.

1.5 The proper analysis of longitudinal microbiome data

When it comes to analyzing longitudinal microbiome data, several factors require consideration. Microbiome data obtained through metagenomics sequencing presents unique challenges due to inherent characteristics like uneven total sequencing depth between samples, compositional structure, high sparsity, as well as overdispersion [41]. Additionally, due to the nature of longitudinal data, it is also necessary to incorporate adjustments for individual variations in the analyses.

Oftentimes, the objective of gut microbiome research is to identify the dissimilarities in the abundance of microbes among different groups (e.g., different treatments or time points). In this case, a standard procedure encompasses two stages, namely, pre-processing of the raw data and then conducting differential abundance analysis. In the first stage, the issue of uneven total sequencing depth in data acquired from metagenomic sequencing entails attention during the initial pre-processing since it can introduce bias when assessing microbial communities[44]. Thus, several data-preprocessing techniques have been devised to handle the discrepancies in sequencing depth, such as normalization, rarefaction, and transformation [45]. Commonly used methods of transformation or normalization include centered log-ratio (CLR), total-sum scaling (TSS), geometric mean of pairwise ratios (GMPR), cumulative-sum scaling (CSS), and trimmed mean of M-values (TMM)[46-48]. CLR transforms data for compositional analysis, which involves taking the log of the ratios of each value to the average of all values and centering the output values around zero. GMPR computes ratios and takes their geometric mean for normalization. TSS divides the raw absolute abundance by read depth, converting it to relative abundance, while CSS addresses TSS bias through quantile normalization. TMM tackles composition bias and calculates normalization factors. Finally, rarefaction is a process of random subsampling that ensures equal sequencing depth across all samples.

In the second stage, where differential abundance analysis is conducted, it is important to take into account the unique attributes of microbiome data. These attributes include the compositional structure, high sparsity, and overdispersion. Microbial data from metagenomic sequencing exhibit a compositional nature due to fixed total sequencing read amounts, resulting in interdependencies among feature abundances across samples[49].

Various tools have been introduced to address this compositional structure, although literature indicates that their superiority over non-compositional methods is not consistent[50]. Overdispersion refers to a situation where the data exhibits more variability than what would be anticipated based on a particular distribution[51]. On the other hand, high sparsity indicates that the data contains a high proportion of zero values[41]. Numerous approaches for microbiome data analysis have been proposed so far, and there exists a wealth of reviews comparing these approaches[45,52-54]. Yet, there is no universal pipeline (including preprocessing and differential abundance analysis) for all kinds of microbiome data, and the choice depends on the data characteristics and research objectives.

That said, the utilization of GLMMs emerges as a promising solution for the differential abundance analysis of microbiome data[55]. Longitudinal microbiome datasets violate the assumptions of simple linear models (LMs) because their values are not continuous nor normally distributed. In addition, the values of longitudinal microbiome data are autocorrelated, which means that there are correlations between measurements taken at different time points within the same individual[56]. Hence, a simple LM is unsuitable to be applied to longitudinal microbiome data, and an alternative to LMs that account for such characteristics is required. This is where GLMMs come into play. The basis of GLMMs is constructed on generalized linear models (GLMs). GLMs encompass a group of regression models that relax the strict assumptions of LM to accommodate various types of response variables, including counts, binary, proportion, continuous, categorical, and ordinal data[57,58]. For example, GLMs such as negative binomial regression and zero-inflated Poisson regression are commonly utilized to fit microbiome data since they are able to account for overdispersion and high sparsity. As mentioned earlier, due to the fact that the outcome values in longitudinal microbiome data are autocorrelated, GLMs are further extended to account for such correlation. This is achieved by integrating random effects into the framework of GLMs, resulting in the formation of GLMMs[59]. In the analysis of longitudinal microbiome data, the individual from which the sample is taken (i.e., the sample donor) is treated as a random variable, allowing for the inclusion of inter-individual variation in microbial abundance within models.

Last but not least, another crucial point when analyzing longitudinal microbiome data is the consideration of covariates. When applying model-fitting to longitudinal microbiome data, the dependent variables are the microbial features, while the independent variables

are the metadata, including the time variable and other factors (e.g., drug intake, age, weight). The goal is to examine the impact of the time variable (a proxy for treatment or intervention). Covariates refer to variables other than the time variable that may influence the outcome (microbial features), and they are commonly present in gut microbiome studies[60]. An example of a covariate may be that in a study examining the effects of a new exercise program on the gut microbiome, a potential covariate to consider would be the dietary habits of the participants. Changes in the participants' dietary patterns throughout the study could influence the observed changes in the microbiome composition, making it important to assess whether the observed effects are directly related to the exercise program or are influenced by the dietary modifications. Therefore, in order to obtain accurate results from longitudinal microbiome data analysis, it is essential to distinguish the impacts of the time variable from those of the covariates. The influence of covariates needs to be identified and accounted for to prevent drawing erroneous conclusions[61,62].

In brief, when analyzing longitudinal microbiome data, challenges related to sequencing depth, overdispersion, sparsity, and inter-individual variation need to be considered. The utilization of GLMMs is a promising solution to account for the complex characteristics of longitudinal microbiome data. Additionally, the inclusion of covariates is crucial to accurately interpret the effects of the time variable. Despite the fact that existing tools for longitudinal microbiome analysis handle some of these aspects, none of them can control for multiple covariates effectively while providing an explicit and detailed assessment of how the presence of other covariates influences the effect of the time variable[50,63-68]. Thus, the development of a new tool to bridge this gap in gut microbiome research is imperative.

1.6 Thesis outline and study aims

The primary objective of this thesis is to advance our understanding of the intricate relationship between the gut microbiome and cardiovascular and kidney diseases. The aim is to delve deeper into the influence of the gut microbiome on the development and progression of these diseases, unraveling the underlying mechanisms and identifying potential therapeutic targets. To facilitate this rigorous analysis, a novel algorithm called LongDat has been developed, enabling the integration of covariates and providing a powerful framework for investigating the intricate interplay between the gut microbiome and cardiovascular and kidney diseases. Through these endeavors, this thesis aims to contribute

to the advancement of knowledge in this critical area of research and ultimately pave the way for improved therapeutic strategies targeting these diseases.

The thesis comprises three papers that collectively contribute to the overarching goal of deepening our understanding of the gut microbiome's impact on cardiovascular and kidney diseases. The first paper introduces LongDat, the algorithm developed to enable covariate-sensitive analysis in gut microbiome research (hereafter called **Study 1**[69]). The second paper explores the effects of fasting on the gut microbiome and immunome in MetS patients, investigating the potential of fasting as a non-drug-based approach for managing MetS (hereafter called **Study 2**[70]). Lastly, the third paper goes on to study the impact of the absence of gut microbiome on inflammation and organ damage in hypertensive mice, emphasizing the importance of gut microbiome (hereafter called **Study 3**[71]). These three studies are outlined below.

Study 1[69]: This first study presents the algorithm, LongDat, which is specialized in covariate-sensitive longitudinal microbiome analysis[69]. LongDat has been specifically developed to address the gap in the current methodology of longitudinal gut microbiome research. LongDat combines GLMMs and non-parametric effect size calculations to accommodate different statistical distributions and account for inter-individual variation. Therefore, while its main application is in microbiome data analysis, LongDat is a versatile tool that can be adapted to other data types like immunome, metabolome, and transcriptome. The methodology of Longdat is presented in section 2.1, and the result of benchmarking against other existing tools, including MaAsLin2, ANCOM, lgpr, and ZIBR, is illustrated in section 3.1. MaAsLin2, similar to LongDat, focuses on microbiome analysis and utilizes GLMMs while allowing for the inclusion of covariates. However, the key distinctions lie in LongDat's explicit reporting of how the time variable's effect is influenced by other covariates, while MaAsLin2 does not provide this information. Furthermore, LongDat takes a different approach to dealing with multiple covariates compared with MaAsLin2. Besides MaAsLin2, LongDat is also evaluated alongside ANCOM, lgpr, and ZIBR, which are other R packages allowing for covariate inclusion in the analyses[64,66,68]. ANCOM employs a compositional approach, lgpr utilizes additive Gaussian process regression for modelling longitudinal data in a non-parametric way, whereas ZIBR combines zero-inflated Beta regressions and logistic models, along with random effects, to

assess the impact of time on microbial features. These tools' performances are assessed and compared using both real and simulated microbiome data for benchmarking.

Study 2[70]: As an application of the LongDat algorithm, we implemented its concept in this study. The second study inspects how fasting influences the gut microbiome of MetS patients, leading to improvement in their BP, body-mass index (BMI), and the need for antihypertensive drugs[70]. MetS is a cluster of chronic conditions induced by Western life habits, including obesity, high BP, high blood sugar levels, and abnormal cholesterol levels, that collectively increase the risk of CVD[72]. In the context of MetS, dysbiosis is associated with conditions such as insulin resistance, inflammation, and other metabolic dysregulations. Fasting refers to the practice of restraining or restricting the consumption of food and, in some cases, beverages for a defined period of time. Recently, fasting has been recognized for its capacity to enhance the abundance of beneficial microbial species, suppress the growth of pathogens, mitigate inflammation, and consequently contribute to a decrease in BP levels[73,74]. However, there is a lack of knowledge regarding the specific effects of periodic fasting on the gut microbiome and immunome in MetS patients. In this study, a protocol involving five days of fasting and then followed by three months of the modified Dietary Approaches to Stop Hypertension (DASH) diet was executed. This study represents a pioneering investigation that examines the impact of lifestyle change combined with fasting intervention in MetS patients using a comprehensive multi-omics approach, integrating analysis of the gut microbiome and immunophenotyping. Covariate-aware analyses are implemented throughout the study, such that the effect of the fasting treatment is disentangled from that of other metavariables.

Study 3[71]: The third study demonstrates the significant influence of microbial colonization on organ damage and inflammatory responses in HTN, underscoring the pivotal role of the microbiome in mediating these effects[71]. HTN emerges as a formidable risk factor, ranking among the most influential contributors to various CVDs that develop throughout an individual's lifespan[75]. The association between HTN and the gut microbiome involves inflammation, immune system, and microbial metabolites (e.g., SCFA), which have the potential to either alleviate or exacerbate cardiovascular disease and hypertensive damage[76-78]. However, the specific contribution of the gut microbiome to HTN remains unclear. Hence, this study aims to investigate the relative impact of the gut microbiome on the burden of hypertensive disease. To address this, GF mice were utilized, which allowed

the key differences in the response to hypertensive stimuli compared with COL mice to be uncovered. In this study, the partial Mantel test is utilized to partition out the effect of covariates to attain a more precise outcome.

Parts of this thesis have been assembled in publications[69-71]. The text can be similar but not identical.

2 Methods

2.1 Covariate-aware approaches of longitudinal data analysis (Study 1[69])

2.1.1 The LongDat method

2.1.1.1 LongDat package overview

To facilitate its distribution, the LongDat algorithm was compiled into an R package. The LongDat R package is built using R (>= 4.0.0), and the dependencies are lme4[79] (>= 1.1-28), glmmTMB[80] (>= 1.1.3), reshape2[81] (>= 1.4.4), emmeans[82] (>= 1.7.3), bestNormalize[83] (>= 1.8.2), tidyverse[84] (>= 1.3.1), MASS[85] (>= 7.3-56), effsize[86] (>= 0.8.1), patchwork[87] (>= 1.1.1), and car[88] (>= 3.0-12). The LongDat pipeline encompasses several functions to facilitate the generation of the input table, statistical analysis, and visualization of the output. The statistical analysis stage of the LongDat pipeline consists of three main steps, which are the evaluation of the null time model, the examination of the covariate model, and the computation of the effect size (Figure 1).

2.1.1.2 The null time model test

First, the null time model tests the association between time and each feature (overlooking covariates at this stage), utilizing GLMMs with various R packages like MASS[85], lme4[79], and glmmTMB[80]. LongDat's versatility stems from its utilization of GLMMs. Count data composed of integers (e.g., numbers of sequencing reads) is a typical data type of microbial abundance table, and is fitted by a negative binomial model[89]. Proportion data, which ranges between 0 and 1, are fitted with a beta model[90], while binary data, composed of either 0 or 1, are fitted with binary logistic regression[91]. Ordinal data (i.e., ranks) are fitted with a proportional odds model[92]. Continuous data is first normalized by the bestNormalize[83] package and then fitted with LMs. To address non-independence and between-individual variability of samples from the same donor, a random intercept model is employed in each model, where the sample donor is taken as a random variable. The significance of the time variable is inferred by the Wald chi-square test. Multiple testing is adjusted using the Benjamini-Hochberg (BH) approach or other relevant approaches[93]. The functions longdat_disc and longdat_cont employ post-hoc tests, which serve as complementary analyses to the null model test (Figure 2, 3). These tests aid in pinpointing

the specific time intervals where significant changes occur within the features. In other words, post-hoc tests help determine the specific pair of time points where differences exist. These analyses utilize the R package emmeans[82] and Spearman's correlation test, respectively.

In the case of the "count mode" where negative binomial models are used, two thresholds are set to avoid false positives when facing sparse features (i.e., features with high proportions of zeros in their values). The two thresholds are non-zero value count cut-offs and θ (theta) cut-offs. Non-zero value counts are the number of non-zero values of each feature. θ, which characterizes the level of overdispersion in the data, represents the dispersion parameter in a negative binomial model. Negative binomial regression is a generalization of Poisson regression that relaxes the assumption of equal variance and mean. Unlike Poisson regression, the variance in negative binomial regression depends on both the mean and the parameter θ, and the variance is always larger than the mean. It quantifies the degree of variability that is not accounted for by the mean-variance relationship assumed in a Poisson distribution. A higher θ indicates greater dispersion, meaning that the variance is larger than what would be expected based on the mean. Conversely, a lower θ suggests less dispersion, with the variance closer to the mean.

The negative binomial regression model operates under the assumption that the mean and variance of the response variable are related through a logarithmic link function. The negative binomial regression model is expressed as

$$log\big(E(Y)\big) = \beta^0 + \beta^1 X^1 + \beta^2 X^2 + \ldots + \beta_p X_p \qquad (1)$$

where $log(E(Y))$ represents the logarithm of the expected value of the response variable Y, $\beta_0, \ldots \beta_p$ are the regression coefficients associated with the predictor variables $X_1, \ldots X_p$. To account for overdispersion, the variance of the response variable Y is modelled as a function of the mean $E(Y)$ with an additional dispersion parameter theta (θ). The formula for the variance in a negative binomial regression is:

$$Var(Y) = E(Y) + (\theta * E(Y)^2) \qquad (2)$$

where $Var(Y)$ represents the variance of the response variable Y, and $E(Y)$ represents the expected value of Y.

Although there is no strict requirement for the minimum number of non-zero values when applying negative binomial models, it is generally recommended to have a sufficient number of non-zero values for precise parameter estimation in the negative binomial distribution. Inadequate non-zero values can result in imprecise parameter estimates and compromise the model's reliability. For example, when the number of non-zero values is low, it can violate the assumption of the negative binomial model that the variance of the data exceeds the mean. In an example dataset (gut microbiome data on species level in **Study 2**[70]), an interesting finding demonstrates a negative correlation (Spearman's rho = -0.21, p = 3×10^{-6}) between the sparsity of features (reversely represented by the number of non-zero values) and θ. This relationship is illustrated in Figure 5A, where a distinct "cloud" of microbial features with low non-zero counts (high sparsity) and high θ can be observed. In this dataset, the features that either have θ greater than 2^{20} and a number of non-zero values less than 9, or a number of non-zero values less than 5, were designated as "to be excluded", while others were designated as "to be kept". Among the significant features (BH-corrected p-values < 0.1), the raw p-values of these labeled features were significantly lower than the p-values of the features to be kept, which may result in conclusions that are shaky and lack reliability (Figure 5B). Considering this issue, the features with a low number of non-zero values from the analysis are excluded. By excluding extremely sparse features, one avoids the negative binomial models falsely resulting in extremely low p-values from really sparse features.

In the LongDat package, the longdat_disc() and longdat_cont() functions include arguments such as theta_cutoff, nonzero_count_cutoff1, and nonzero_count_cutoff2, which allow users to customize the thresholds for excluding features based on theta value and non-zero count. As different datasets might possess distinct attributes, to facilitate the selection of suitable thresholds, an auxiliary function called "theta_plot()" has been created. This function enables users to visualize the relationship between θ and non-zero counts in a similar way as Figure 5A, aiding in the decision-making process for each argument. By adjusting these values, users can tailor the analysis to their specific needs and data characteristics.

2.1.1.3 The covariate model test

Second, the covariate model test is executed only when covariates (i.e., metadata other than the time variable) are present. The covariates that demonstrate a significant association with each feature, such as the abundance of the microbiome, are chosen from the metadata through non-parametric tests like the Spearman's correlation, Wilcoxon rank-sum, or Kruskal-Wallis test. Afterward, each chosen covariate is incorporated individually as a fixed variable along with the time variable in GLMMs to investigate if the time associations could be attributed to the impact of each covariate, which aligns with the "vibration of effects" (VoE) concept[94]. VoE refers to the extent to which modifications in the combination of independent variables (such as including covariates) influence the result and significance of a model. When the VoE is large, it indicates that the relationship between independent variables and features is less reliable. An authentic correlation should maintain its statistical significance despite any changes made to the model configurations. The significance of the time variable and the covariate is determined by the Wald chi-square test. After the model tests, significant time-dependent features are categorized based on whether they fulfill the "effect not reducible to covariate," "entangled with covariate," or "effect reducible to covariate" criteria. When the time variable continues to be a significant variable in all models, it indicates that the feature is identified as an "effect not reducible to the covariate." Conversely, when the time variable becomes insignificant, but the covariate demonstrates significance in at least one of the models, the feature is classified as "effect reducible to the covariate." In case no apparent covariate exists, but in at least one model, both the covariate and time variables are not significant, the feature is denoted as "entangled with covariate." The decision tree for determining the significance of the time variable and the final signal for each feature in the LongDat output is presented in Figure 4.

2.1.1.4 Effect size calculation

Third, the effect size of the feature change between different time points is calculated. LongDat employs non-parametric methods to compute effect sizes. For continuous time variables, such as days, Spearman’s correlation is utilized, and for discrete time variables, such as before/after treatment, Cliff's delta is used[95,96]. Cliff’s delta is derived by

$$Delta = \frac{\#(x_1 > x_2) - \#(x_1 < x_2)}{n_1 n_2} \qquad (3)$$

where x_1 and x_2 represent values from group one and two, while n_1 and n_2 stand for the sample sizes of the two groups respectively. The symbol # denotes the counts. Cliff's delta ranges from -1 to 1, with -1 or 1 meaning a total difference, and 0 indicating a complete overlap between the distributions of the two groups. Spearman's correlation (rho) is calculated by

$$Rho = 1 - \frac{6\Sigma d_i^2}{N(N^2 - 1)} \qquad (4)$$

where d_i are the differences in the ranked scores between each observation in the two groups, and N is the total number of the samples. Spearman's rho varies between -1 and 1. A value of 1 implies a perfect association between ranks, while -1 signifies a complete negative association among ranks. A value of 0 denotes an absence of any association.

The estimation of effect size is determined by examining the association between the feature and the independent variable. Hence, to guarantee the correct estimation of effect size by LongDat, it is crucial that the treatment effects remain monotonic (i.e., they show no alteration in the direction of association) throughout the time intervals in the data. If the treatment effects do not maintain monotonicity, it is advisable to carry out a separate analysis on time subranges where monotonicity holds.

2.1.1.5 Randomized control test

In scenarios using the "count mode," where negative binomial models are applied, there is a concern about elevated type I error rates (false positives) associated with negative binomial regression. To provide an alert to users regarding the potential occurrence of false positives, a randomized control test is implemented. During this step, all rows within the initial dataset are randomly shuffled against the time variable. The assumption is that positive outcomes should not emerge from a randomized control test. Therefore, any signals exhibiting significance in this context are deemed false positives. If false positives are detected within this randomized control result, LongDat will issue a warning to the user upon completion, and an object named the "Randomized_control table" will be generated exclusively. This table is intended to serve as a reference for users, showcasing the effect sizes of false positive features, which can be compared with those of significant features within the original dataset. In addition, in the context of using long-

dat_disc, if false positives are present in the randomized control test, users have the option to assess a feature's significance using the Wilcoxon rank-sum test, which is a more conservative testing method. The outcome of the Wilcoxon rank-sum test is provided in the LongDat main result table alongside the default post-hoc test results, allowing users to make a more conservative evaluation of a feature's significance.

2.1.1.6 LongDat output

The above-mentioned steps yield two tables that summarize the results. The first table displays the adjusted q-values, which account for multiple testing, indicating time dependency and effect sizes for each feature. The second table shows the covariates and their respective status of relative reducibility. In case there are any false positives in the randomized control test, there will be a third table showing the effect sizes of the false positive features, so that the users can refer to the distribution of their effect sizes and check their result table. Users can visualize the result by using the function cuneiform_plot(), which creates a comprehensive cuneiform plot based on the result table (Figure 1).

2.1.2 Simulation of longitudinal data

Microbial taxonomic abundance data for a cohort was simulated longitudinally using two R packages, namely microbiomeDASim[97] and SparseDOSSA2[50]. MicrobiomeDASim allows users to define parameters such as effect size, sparsity, time points and number of samples, and uses a multivariate normal distribution to generate simulated data with a first-order autoregressive correlation for longitudinal dependency. A first-order autoregressive correlation assumes that the correlation between two observations decreases as the time interval between them increases. SparseDOSSA2, on the other hand, uses GLMMs to generate feature-covariate associations, such as the time variable and other specified covariates, and generates realistic microbial data based on real microbial communities (here, the template was stool microbiome).

2.1.2.1 Simulation of longitudinal data using microbiomeDASim

First, for the simulation of data with no covariate, 100 simulations were carried out for every combination of sample sizes (10, 20, 38, 75, 150, and 300) and effect sizes (Spearman’s rho median approximately equals 0.2 or 0.5 for features changing with time). There

were 200 features in each simulated dataset. For these datasets, 20 features were subjected to change over time or intervention, whereas the other 180 features were consistently sampled from the identical distribution across different time points. In these datasets, each individual was simulated with two time points.

Subsequently, in order to examine the impact of covariates, we generated a simulated dataset with a single covariate. A dummy variable was manually introduced to the simulated dataset to assess the effect of this covariate, which consisted of 75 samples and exhibited a median effect size of approximately 0.5. The dummy variable was designed to exhibit various levels of correlation with the time variable, including approximately 0.25, 0.5, 0.75, or 0.99, and 100 simulations were conducted for each correlation level.

Lastly, for the simulation of data with multiple covariates, the previously mentioned simulated datasets (with a sample size of 75 and an effect size median of approximately 0.5) were manually added with either 1, 2, 4, 8, or 16 dummy variables that were correlated with the time variable. In the process of testing the performance of different statistical tools, dummy variables were added to a simulated dataset that correlated with the time variable at different Spearman's rho values of about 0.25, 0.5, 0.75, or 0.99, and 100 simulations were conducted for each correlation level. In comparing the performance of Maaslin2 and LongDat, 100 simulations were run for every combination of tool, sample size, and effect size. The dataset, in this case, consists of 200 features, where 20 of which changed with time and the remaining 180 did not. To compare LongDat, ZIBR, lgpr, and ANCOM, 50 simulations were carried out for every combination of effect size, sample size, and tool. In this case, the dataset consists of 100 features, 10 of which changed with time and 90 that did not. The reason for reducing the number of features and simulations was because of the high computational resources (low speed and high memory) required by ANCOM, lgpr, and ZIBR.

2.1.2.2 Simulation of longitudinal data using SparseDOSSA2

First, for the simulation of data with no covariate, 100 simulations were executed for every combination of sample sizes (10, 20, 38, 75, 150, and 300) and effect sizes (the median of Spearman's rho approximately equals 0.2 or 0.5 for features changing with time). Each simulated dataset comprised 332 features, out of which 33 were spiked, indicating

changes with time or under intervention, whereas the other features were sampled from the identical distribution over time. In these datasets, each individual was simulated with two time points.

Next, for the simulation of data with covariates, the simulated dataset with 332 features and different sample sizes had 1, 4, or 16 dummy variables added to it manually, which correlated with the time variable. The dummy variables were randomly chosen to achieve a Spearman's rho of approximately 0.25, 0.5, 0.75, or 0.99 with the time variable. A hundred simulations were conducted for every correlation level,.

Finally, for the simulation of negative control data, 100 sets of data with two time points, 150 individuals, and 332 microbial features were generated through simulations with effect size equals to zero for all microbial features (i.e., there is no spiked feature in the simulated data). This is done to examine the influence of systematic effects on sampling depth, which could arise in clinical datasets with low biomass. To this end, 6 versions of the data were created with varying sequencing depths (i.e., the total microbial abundance of each feature). This approach ensured that any signal detected in the simulated data reflected only systematic bias. During the simulations, the overall abundances of each individual at both the initial and subsequent time points were subjected to rarefaction. In versions 1 and 2, the total abundances were rarefied to 50000 and 1000, respectively. In version 3, the initial time point underwent rarefaction to 50000, while the second time point was rarefied to 5000. Version 4 involved rarefying the first time point to 5000 and the second time point to 50000. In version 5, the first time point was rarefied to 50000 and the second time point to 1000. Finally, in version 6, the first time point underwent rarefaction to 1000, while the second time point was rarefied to 50000. When employing LongDat's count mode which uses negative binomial models, versions 3 to 6 were additionally subjected to rarefaction. The rarefaction was performed to either 5000 or 1000, depending on the sequencing depth that is the lowest, in order to achieve equal sequencing depths between the two time points.

2.1.2.3 Normalization, transformation and rarefaction of SparseDOSSA2-simulated data

Various R packages were utilized to pre-process (either normalization or transformation) the raw simulated microbial features obtained from SparseDOSSA2, including TSS[98], CSS[99], TMM[100], GMPR[46], CLR[101], rarefaction[102]. TSS involves dividing absolute abundance by read depth (the total sum of abundance in each individual), resulting in relative abundance values ranging from 0 to 1. CSS, which is a quantile normalization technique designed to counter the biases introduced by TSS, rescales the relative abundances of taxa within samples based on the cumulative sum of their ranks. TMM is a normalization approach that estimates correction factors for library sizes by calculating weighted mean log ratios between samples after filtering highly expressed and large log ratio genes. GMPR computes the ratios for each pair of values, and then followed by calculating their geometric mean to normalize the data. The CLR transformation, which is commonly employed in compositional data analysis, involves taking the log ratios of every component's abundance to the geometric mean of all components, resulting in values that are centered around zero. Finally, rarefaction is a technique that employs random subsampling to ensure uniform sequencing depth across all samples. The available combinations of tools (LongDat, lgpr, MaAsLin2, and ZIBR) and normalization/transformation methods were restricted by the tool's specific input format requirement.

2.1.2.4 Semi-synthetic evaluation of metagenomic data

In order to conduct a semi-synthetic assessment using real microbiome data, the first two time points of the stool microbiome data obtained in **Study 2**[70] were chosen. The data was collected on a clinical group of individuals with MetS who were undergoing either the fasting arm or the DASH arm of the study. The fasting arm involved a seven-day fast which consisted of two days with a maximum calorie intake of 1200 kcal/day followed by five days with an intake of 300-350 kcal/day. After this, the MetS patients followed the DASH diet for three months. Gut microbial abundances at the genus level were used for analysis, and the time variable was shuffled randomly against other variables to remove any association between the time variable and microbes, and also between the time variable and covariates. This was done to ensure that no real intervention or passage of time signal remained. Data normalization or rarefaction was carried out as described in the 2.1.2.3 section.

2.1.3 Running LongDat and other tools on longitudinal data

2.1.3.1 Running LongDat

The simulated longitudinal data were analyzed using the "longdat_cont()" function in the LongDat package. In this analysis, the time intervals between samplings were regarded as continuous variables, while the data type was considered as count or relative abundance data. The running time and memory usage were recorded using the peakRAM[103] R package. Feature associations were deemed significant if their BH-corrected null-model q-values are below 0.1 and post-hoc test q-values are below 0.05. The analysis was conducted on LongDat under CentOS Linux 7 and R version 4.1.1 with an 8 gigabytes (GB) memory allocation.

2.1.3.2 Running Maaslin2

To analyze simulated longitudinal data, the function "Maaslin2()" from the MaAsLin2[104] package was utilized. The time variable was treated as a continuous variable, and the mode was specified as either "NEGBIN" (negative binomial model) or "LM" (linear model). Features having a BH-corrected q-value less than 0.1 were regarded as significant. MaAsLin2 was executed on CentOS Linux 7 and R version 4.1.1 with 8 GB of memory allocated.

2.1.3.3 Running ANCOM

The simulated longitudinal data was analyzed using ANCOM in the ancom.R script (available at https://github.com/FrederickHuangLin/ANCOM-Code-Archive). The time variable was regarded as a factor, and the random formula was set to sample ID, whereas all the covariates present are included in the adjust formula. Features with W statistics exceeding a cut-off calculated by multiplying the count of taxa by 0.7 were deemed significant. ANCOM was executed on CentOS Linux 7 with R version 4.1.1, and 350 GB of memory was allocated.

2.1.3.4 Running ZIBR

Simulated longitudinal data was analyzed using the "zibr()" function from the ZIBR[66] package. The time variable was considered a continuous variable and all covariates were included in the analysis. Features were deemed significant if their joint q-values corrected with BH were less than 0.1. The ZIBR analysis was conducted with CentOS Linux 7 and R version 4.1.1 with 8 GB of memory allocated.

2.1.3.5 Running lpr

The analysis of simulated longitudinal data involved the use of the "lgp()" function in the lgpr[64] package. The time variable was regarded as a continuous variable, while all covariates present were incorporated for analysis. Sample ID was used as the random variable. One hundred drawing samples were obtained from a Stan model, with four Markov chains. Features were deemed significant if the ratio of the total explained variance met or exceeded a 95% threshold after selecting the time variable. The lgpr analysis was executed under CentOS Linux 7 with R version 4.1.1, and 8 GB of memory was allocated.

2.1.4 Evaluation of real microbiome and immunome data

The study under reanalysis in this work examined the effects of fasting on Metabolic Syndrome (MetS) patients, as reported by **Study 2**[70]. There are two arms in this study, with a fasting and a DASH arm. MetS patients participating in the fasting arm of the study followed a specific seven-day fasting protocol. This regimen involved two days of consuming a maximum calorie of 1200 kcal per day, followed by five days of consuming a restricted range of 300-350 kcal per day. After the fasting period, there was a three-month re-feeding stage, during which MetS patients adhered to the DASH diet. The species-level microbial abundance and immunome data from the fasting arm were re-analyzed using LongDat to showcase its effectiveness and performance.

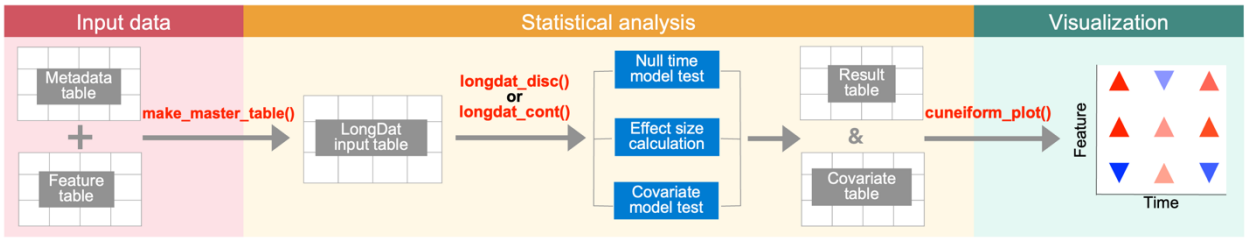

Figure 1. An overview of the LongDat package. Main functions are shown in bold red text. The function "make_master_table()" is used for creating an input table by combining user-provided metadata and feature tables. The functions "longdat_disc()" and "longdat_cont()" enable covariate-aware analyses by performing various tests, including null time model tests, effect size calculations, and covariate model tests, on the input tables to assess the significance of the time variable (representing treatment). The function "longdat_disc()" is designed for datasets with discrete time values (e.g., before and after treatment), while "longdat_cont()" is suitable for datasets with continuous time representation (e.g., day). Lastly, the function "cuneiform_plot()" creates a summary figure of the resulting table. This figure has been published as figure 1 in Chen *et al*., 2023[69] (under CC BY 4.0 license).

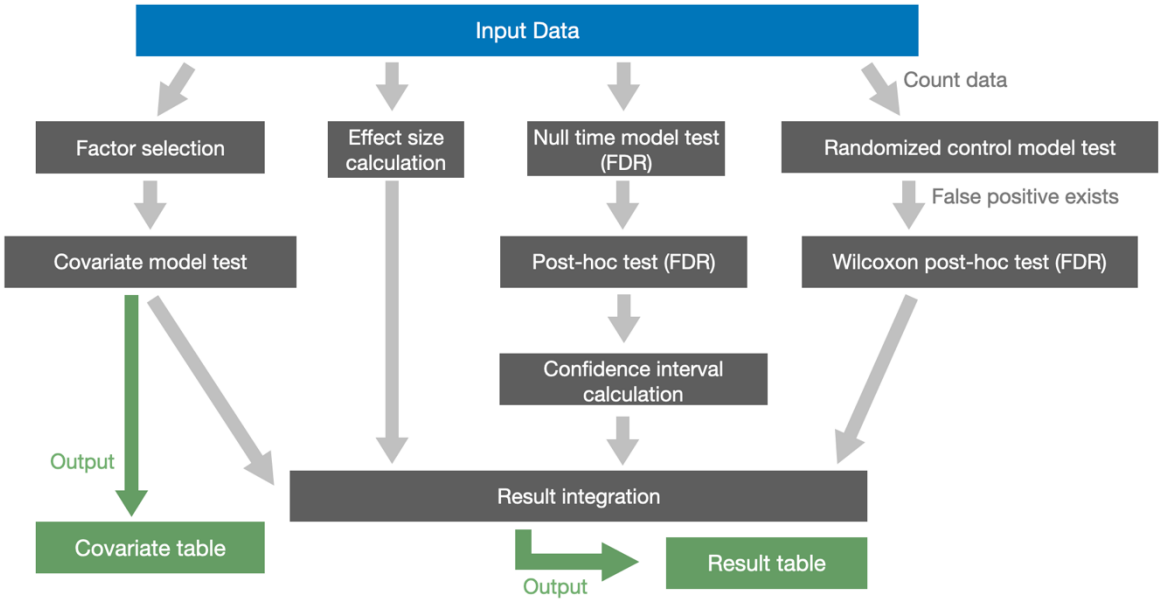

Figure 2. Scheme of the function longdat_disc(). Source: own representation.

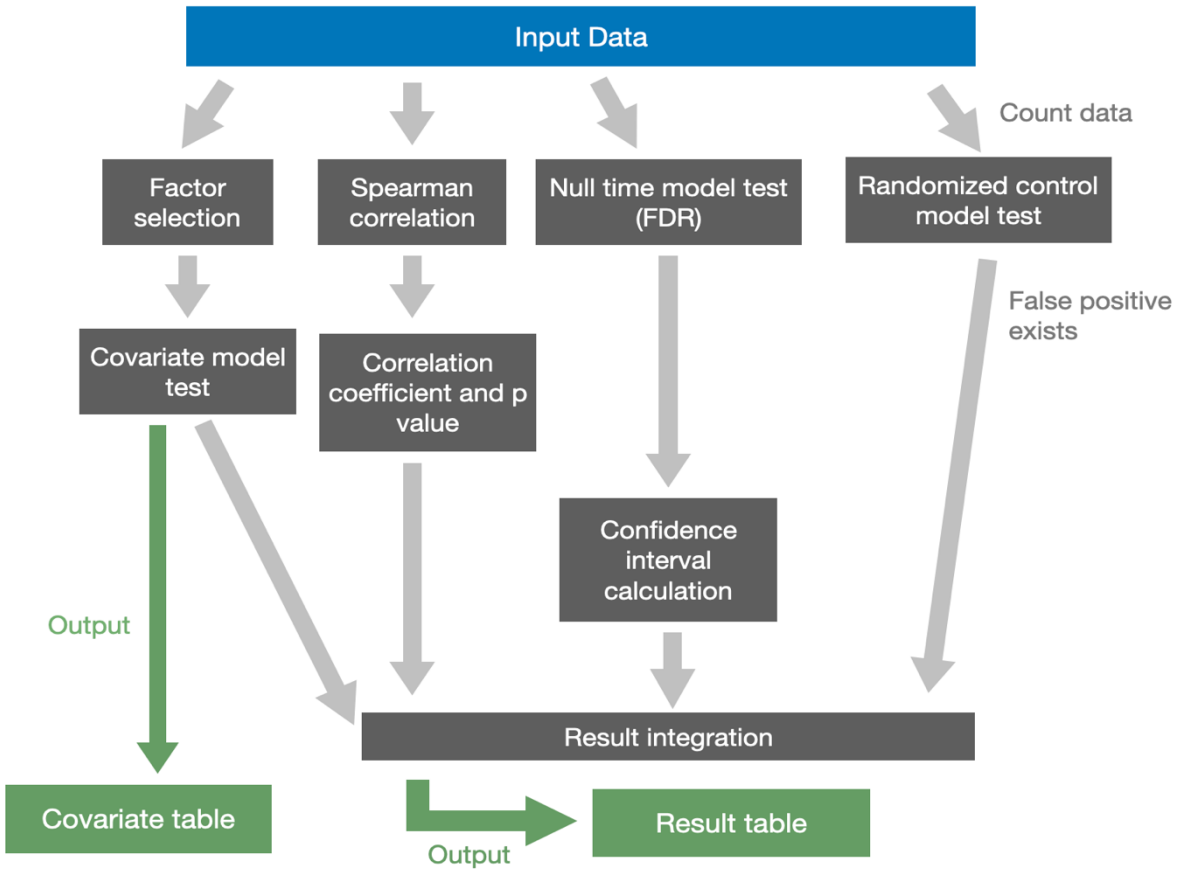

Figure 3. Scheme of the function longdat_disc(). Source: own representation.

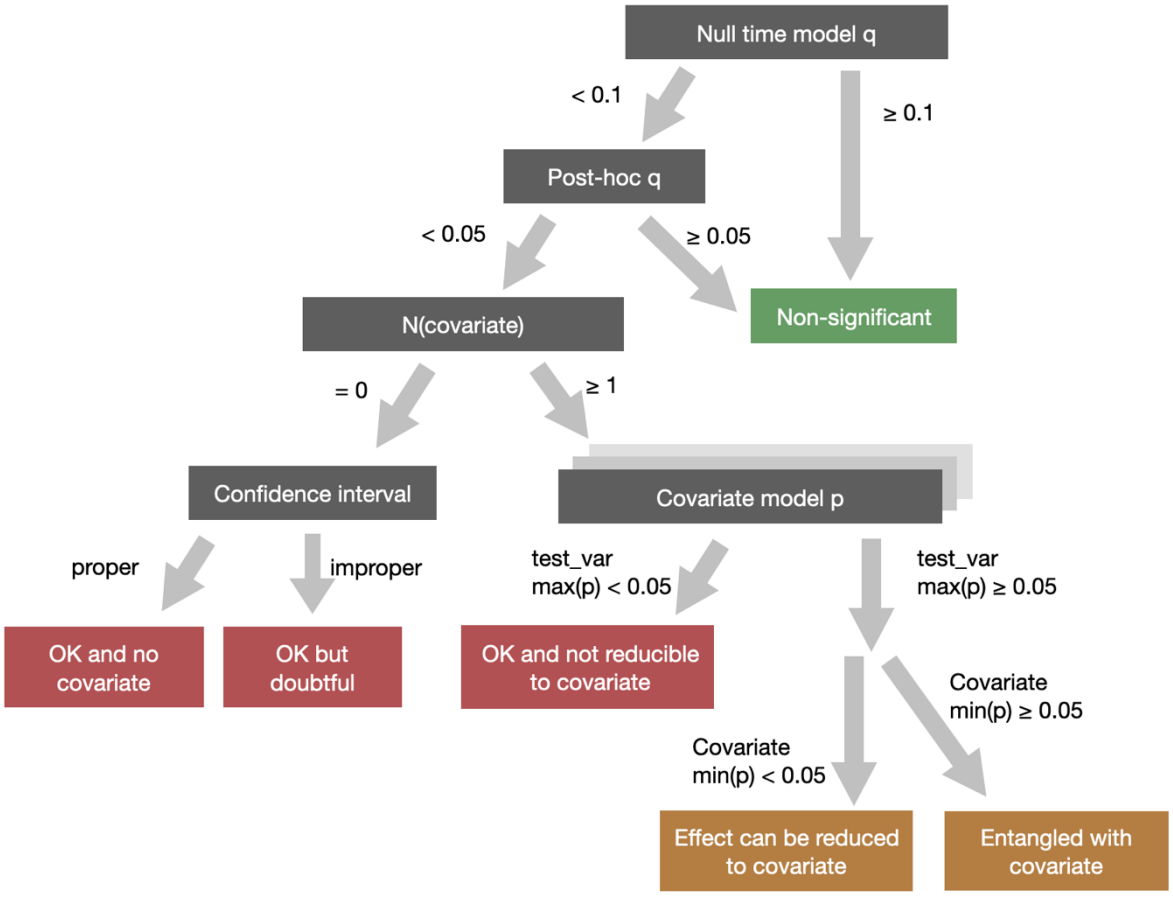

Figure 4. Decision tree for determining the significance of the time variable and the final signal (colored boxes) for each feature in the LongDat output. The threshold of the p-values can be adjusted by the users. Source: own representation.

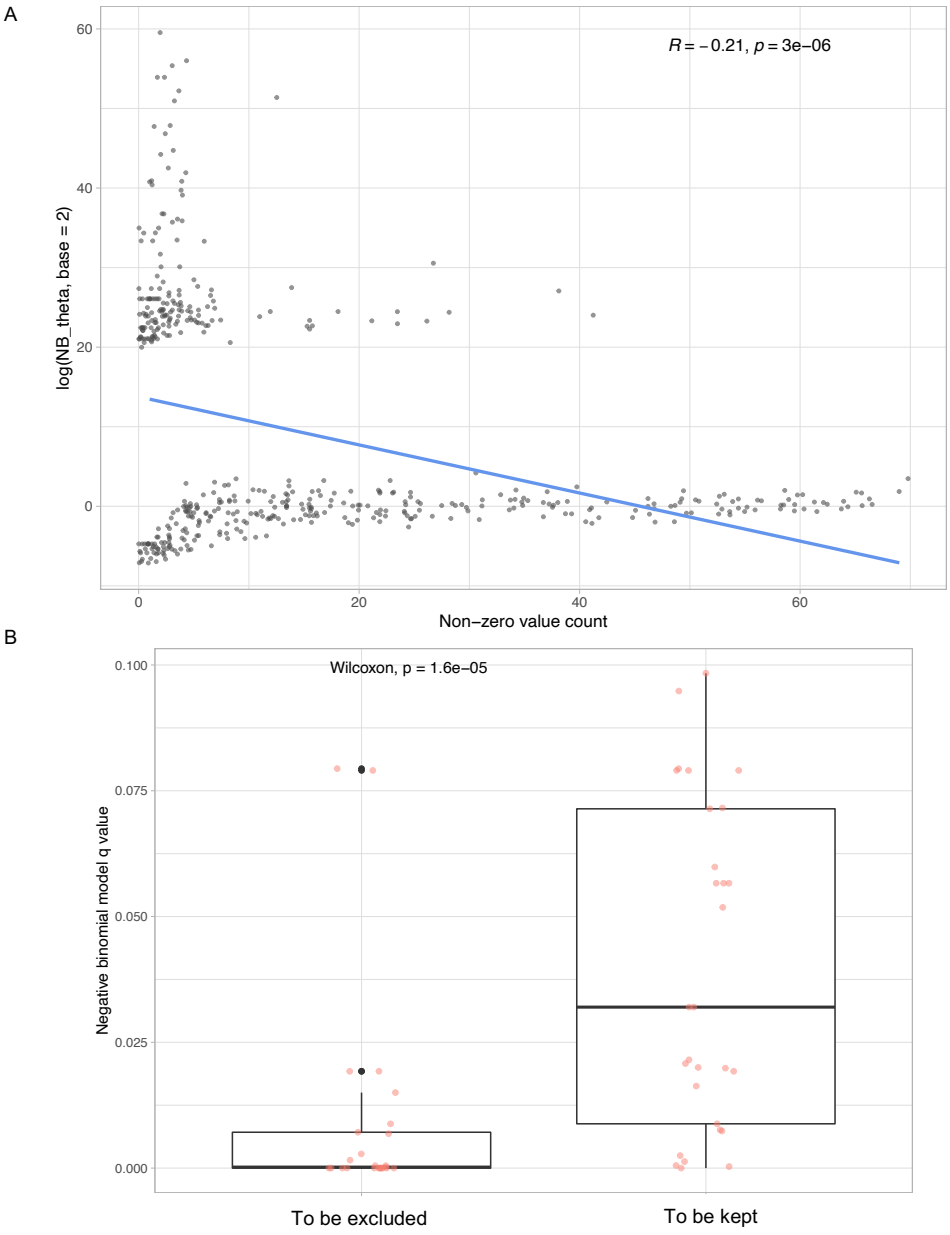

Figure 5. The sparsity is an important factor when fitting negative binomial models. (A) The scatter plot shows the result of negative binomial models applied to the microbiome data (species level) theta values (taken log base 2) versus the number of non-zero counts in Study 2. The blue line is added by using ggplot2::geom_smooth(method = "lm"). The p-value comes from Spearman's rho test. (B) The box plot shows the raw p-values of the significant features (BH-corrected p-value < 0.1). The features that either have a theta value greater than 2^{20} and less than 9 non-zero values, or a number of non-zero values less than 5, were labeled as "to be excluded", while others were labeled as "to be kept". The scattered points show the original data. Source: own representation.

2.2 Fasting effects in patients with MetS (Study 2[70])

2.2.1 Experimental procedures

This project is conducted as a randomized controlled trial, and aimed to investigate the effects of periodic fasting and a modified DASH diet on patients with MetS. This study received ethical approval from the ethics committees of Charité-Universitätsmedizin Berlin and was registered at ClinicalTrials.gov. Patients who met the inclusion criteria and did not meet any exclusion criteria were asked for and provided informed consent. Patients with MetS (including male and female), as defined by the National Cholesterol Education Program Adult Treatment Panel III (NCEP ATP III) criteria, were included in the study. In addition to the NCEP ATP III criteria, patients had to have a diagnosis of systolic HTN.

Both the fasting and DASH arms received dietary interventions in the form of a group-based behavioral intervention. The intervention for the fasting arm combined periodic fasting (7 days) and a modified DASH diet. The periodic fasting included 2 days of calorie-restricted vegan meals followed by 5 days of taking vegetable juices and broth. When the fasting was completed, the modified DASH diet intervention focused on a plant-based diet with reduced sugar, fat and sodium. The baseline is referred to as time point 1 (V1), and time point 2 (V2) is after seven days of fasting (for the fasting arm) or DASH (for the DASH arm), while time point 3 (V3) is after three months of DASH diet for both arms. Randomization was performed using block randomization with varying block lengths and stratification factors. Outcome measures (e.g., 24-hour ambulatory systolic BP) were evaluated at baseline, one week, and twelve weeks after randomization. Physician-assessed outcomes such as BP, body weight, body fat percentage, and laboratory measurements were documented. Peripheral blood mononuclear cell analysis was performed to study immune cell profiles.

Fecal samples were collected and stored for DNA-based sequencing. DNA was extracted and purified. Next, the 16S rRNA gene was amplified and then sequenced on the MiSeq platform. Metagenomic DNA libraries were constructed, sequenced on the NovaSeq platform, and processed using NGLess[105]. Sequences were filtered and mapped to the human genome. Non-human sequences were mapped to the SILVA[106] database and IGC

gene catalog. LotuS v1.62[107] pipeline was used for sequence processing, and the taxonomic classification was based on the SILVA database. Marker gene-based OTUs were generated. Raw counts were rarefied with RTK v0.93.1[102] prior to downstream analysis. Functional analyses included binning IGC genes to KEGG KOs[108], KEGG modules, and Gut Microbial Modules[109].

The experimental procedures above were conducted by my collaborator, András Maifeld (ECRC, Müller/Dechend lab) and other co-authors. Full information about the experimental procedures and individual contributions can be found in Maifeld et al., 2021[70].

2.2.2 Data statistical analyses

2.2.2.1 General analysis and machine learning

The comparison of body weight and BP changes between responders and non-responders was conducted using a Wilcoxon rank-sum test. Alpha and beta diversity analysis of the microbiome data was performed using various metrics, including Shannon diversity, richness, evenness, Chao1 index, Simpson's and Inverse Simpson's metrics. Unpaired Wilcoxon rank-sum tests were used to examine significance. Beta diversity was evaluated using community distances between samples, and multivariate analysis was executed using Principal Coordinates Analysis (PcoA) and Permutational Multivariate Analysis of Variance (PERMANOVA) tests.

To ensure the reliability of univariate analysis involving clinical, immunome, or microbiome features, covariate effects of medication changes were taken into account through a two-step process. In step one, a nested model comparison was conducted for each feature, incorporating predictors (e.g., age, patient ID), and normalized medication dosage at each time point. An additional predictor of time points V1-V3 was included in the model. Likelihood ratio tests were employed to compare these models, and p-values were adjusted using the BH method applied within every data space. In step two, features with FDR values below 0.1 were selected for post-hoc tests. Wilcoxon rank-sum tests were performed for comparisons between values at each pair of time points, with FDR adjustments for multiple testing. Results were considered significant if the BH-adjusted p-value was below 0.05. Non-parametric effect sizes (i.e., Cliff’s delta) were calculated.

To explore interactions among taxa, immune cells, and phenotypes, a two-step test was utilized. Initially, Spearman's correlation test was conducted to examine the associations between the variables. Then, a post-hoc test where mixed-effects models were fitted on rank-transformed variables and patient ID was treated as a random effect, was employed to account for sample dependency. Correlations were visualized using R packages circlize[110].

Machine-learning techniques were used to predict treatment response at the individual level. A leave-one-patient-out cross-validation method was employed to evaluate the performance of the predictive model. The input variables were standardized, and a logistic regression algorithm was used for binary classification. A forward-stepwise selection method was applied to identify the ten most relevant input variables for outcome prediction. The resulting predictive model was validated by assessing its ability to accurately predict blood-pressure response in independent participants. The overall performance of the model was estimated by averaging the results across all predicted clinical responses.

2.2.2.2 Comparative re-analysis of previous data

Data from Mesnage et al.[111], the sole existing cohort examining fasting effects and encompassing both BP data and stool sequencing, was employed for validation purposes. This dataset was subjected to analysis in a manner identical to the approach used for the main study dataset.

The statistical analyses above were conducted by my collaborator, András Maifeld (ECRC, Müller/Dechend lab) and other co-authors.

2.2.2.3 Enterotyping

The fecal microbiome samples from the fasting arm were classified into enterotypes using the DirichletMultinomial[112] R package v1.32.0 based on the abundance table at the genus level. The dmn() function in the package fits a Dirichlet-Multinomial model to count data, and a parameter k represents the number of Dirichlet components (clusters) to be modeled. The optimal k value is determined by Laplace goodness of fit. Then heatmaps showing the dominant taxa in each cluster are plotted with the function heatmapdmn() to facilitate the assignment of enterotypes.

2.3 Impact of gut microbiome on hypertensive organ damage in mice (Study 3[71])

2.3.1 Experimental procedures

In this study, axenic wild-type C57BL/6J mice were maintained in an isolator with a 12:12 hour day-night cycle and constant access to water and food. Male mice were randomized into GF or passive bacterial colonization groups at 4 weeks of age. At 12 weeks of age, mice received either Angiotensin II + 1% NaCl or sham treatment and were euthanized after 2 weeks for sample collection, including blood, feces, spot urine, and organs (Figure 6). Echocardiography and Ang II pressor response assessments were conducted under isoflurane inhalation anesthesia. The study involved 40 mice (GF n=5, COL n=5, GF+HTN n= 16, COL + HTN n = 14), with five (GF+HTN n=3, COL+ HTN n = 2) taken out of the experiment due to ethical termination criteria. Additionally, cells and tissues derived from conventionally raised SPF C57BL/6J mice (CONV) were utilized in in vitro experiments as a control group.

Immunophenotyping was performed using single-cell suspensions of splenocytes from euthanized mice. The full details of this method are described in Avery et al., 2022[71]. Briefly, erythrocytes were lysed, and flow cytometry analysis was conducted using surface antibodies for staining and intracellular antigens for staining. A total of 10^6 cells per panel were analyzed, excluding dead cells. The data were recorded using a BD FACS Canto II and analyzed with FlowJo software. In vitro Type 1 T helper (Th17) polarization experiments involved isolating cells from the mesenteric lymph nodes of GF or CONV mice. CD4+ T cells were sorted using magnetic activation and then exposed to anti-CD3 and anti-CD28 stimulation under Th17 polarizing situations. The influence of Ang II on Th17 cell polarization was assessed by culturing the cells with Ang II or vehicle for 96 hours. For SCFA pre-incubation, cells were incubated with a mix of sodium butyrate and sodium propionate, or sodium chloride as a control, before the addition of Th17 polarizing cytokines and Ang II. The cells were then measured for Th17-specific markers.

Urine analysis was conducted on a subset of experimental mice. Spot urine was collected upon sacrifice, and various parameters were measured using the AU480 clinical chemistry analyzer. Turbidimetric and enzymatic methods were used to measure urinary albumin and creatinine, respectively. Histology staining was performed on heart and renal tissue collected from the mice. Cryosections of the tissue were fixed, blocked, and stained

with primary and secondary antibodies. Immunofluorescence staining and image analysis software were used to quantify cardiac interstitial and perivascular fibrosis, as well as infiltrating immune cells. Kidney cryosections were stained for infiltrating immune cells and Nephrin, and tissue fixed with formalin was stained with Masson's trichrome to analyze perivascular fibrosis. Every histological staining was digitally scanned by using a slide scanner.

Quantitative real-time RT-PCR was conducted on RNA isolated from the kidney and heart apex. cDNA synthesis was followed by target gene expression quantification using TaqMan or SYBR Green assays on QuantStudio 3. The expression was normalized to the 18S housekeeping gene as a reference.

Metabolomics analysis involved using the MxP Quant 500 kit for the analysis of metabolites from serum samples. Sample preparation included transferring serum to a 96-well plate, adding specific solutions for metabolite extraction, and utilizing LC-MS and FIA-MS methods for analysis. Data were processed and normalized. Valid metabolites above the limit of detection were used for subsequent statistical analysis. Fecal SCFA measurements were performed using GC-MS and analyzed with Thermo Scientific Xcalibur Software.

DNA isolation and extraction were conducted, and the extracted DNA passed quality control was subjected to metagenomics sequencing using the Illumina NovaSeq 6000 PE150 platform. The sequencing data were processed using NGless[105], and taxonomic classification was performed by aligning the reads to mOTUs. Functional annotation was done using the global microbial gene catalogue[113] gmgc v1.0 and MouseGutCatalog v0.9. The results were visualized using KronaTools. Additionally, fecal qPCR was done using an Applied Biosystems QuantStudio 3 system to quantify specific bacterial genes. Copy numbers per gram of feces were calculated, and standard curves were used for quantification. The generated microbiome data is publicly accessible in the NCBI database under BioProject PRJNA812410.

The experimental procedures above were led by my collaborators, Dr. Ellen Avery (ECRC Müller/Dechend lab) and Dr. Hendrik Bartolomaeus (ECRC Wilck lab). Full information about experimental procedures and individual contributions can be found in Avery et al.,

2022[71]. The shotgun sequencing preprocessing was done by another co-author, Dr. Ulrike Löber (ECRC, Forslund lab).

2.3.2 Statistical analysis

The statistical analyses done by my collaborators and I were performed using R version 4.0.2 or GraphPad Prism 6. Two-way ANOVA was used for analyzing univariate data, considering HTN and microbiome status as the factors of interest. If either factor or both were significant, Sidak's multiple comparison test was used for post-hoc analysis to determine the specific source of variation. Relative changes were assessed by expressing the values of HTN mice as percentage of the average of the corresponding sham group, followed by an unpaired two-tailed Student's t-test for comparing COL and GF. A significance level of $p < 0.05$ was used. PCoA and PERMANOVA were executed in R using the vegan[114] package, with Euclidean distances for kidney, heart, metabolome, and immunome data, and Bray-Curtis dissimilarity for microbiome data. The analysis of effect size was conducted using Cliff's delta with the orddom[115] package in R and visualized using ggplot2[116]. The in-depth description of my analyses and graphical approaches are detailed below.

2.3.2.1 Heat map of metabolites and microbiome

Initially, metabolites and microbiome species were filtered based on their significant changes between the sham and Ang2 groups using the Wilcoxon rank-sum test. Subsequently, Spearman's correlation was computed between the chosen metabolites and genera, and the p-values were adjusted using the BH correction. The same procedure was applied to determine Spearman's correlation between metabolites and functional modules. These correlation matrices were then combined to generate the final heatmap using the gplots[117] package in R.

2.3.2.2 Mantel test

The Mantel test is a type of regression analysis that investigates the association between distance matrices, which represent the pairwise similarities among samples. An advantageous aspect of the Mantel test is its flexibility in handling variables of various types, including categorical or rank variables, by utilizing distance matrices. This adaptability makes the Mantel test a versatile approach for exploring relationships between diverse

types of data. The Mantel tests are performed by using the R packages vegan[114] and ncf[118].

2.3.2.3 Pluznick study data preprocessing

The raw 16S sequences from the fecal microbiome sequencing of the Pluznick study were obtained from the NCBI Sequence Read Archive under the BioProject PRJNA514044. To analyze the 16S amplicons, LotuS[107] v1.62 software was employed, utilizing the SILVA[106], Greengenes[119], and HITdb[120] databases. This analysis generated abundance tables for the microbiome at all taxonomic levels. The abundance tables were then subjected to rarefaction using the RTK[102] method. Specifically, the abundance table at the genus level was selected for comparison with our study. For further analysis, PCoA was performed using the vegan[114] package in R, with Bray-Curtis distances used as the dissimilarity measure.

2.3.2.4 Comparative analysis with Pluznick study

To compare the fecal microbiome data obtained in our study with the data that was published by Cheema and Pluznick[121] (here called the "Pluznick" data), we needed to reannotate our shotgun next-generation sequencing data. This reannotation process aimed to transform our data into a format that could be directly compared to the published 16S sequencing data. Dr. Ulrike Löber (ECRC, Forslund lab) carried out this reannotation task. Additionally, the metabolites from the Pluznick study underwent a curation process to identify overlapping metabolites that shared identical biochemical names, CAS IDs, HMDB IDs, and/or PubChem IDs. Dr. Ellen Avery (ECRC, Müller/Dechend lab) performed this curation process.

The dissimilarity in microbial composition between our data and the Pluznick data was visualized using PCoA by using the vegan[114] R package, and the Euclidean distance metric was utilized. To compare the alterations in metabolites between the sham and HTN groups at an individual level, several steps were followed. First, a Wilcoxon rank-sum test was conducted within the GF or COL groups for each study, with any resulting missing values (NAs) removed. Then, the direction of alteration for every metabolite in the corresponding group from the Pluznick data or our data was compared. The significance of the difference between the GF and COL groups was assessed using a chi-squared test. To compare the effect size of every metabolite individually between the

sham and HTN groups in GF or COL/CONV groups of the Pluznick data or our study, Cliff's delta was computed using the orddom[115] R package. The discrepancy between the effect sizes in the GF or COL groups was determined by calculating the absolute difference in effect sizes between the two studies. For visualizing the results, the ggplot2[116] package was utilized, and the ggpubr[122] package was applied to include the Wilcoxon rank-sum test results. The geom_density_2d() in the ggplot2 package, which was used to add a layer of 2D kernel density contours to the plot. The 2D kernel density plot uses a nonparametric method called kernel density estimation for probability density functions to create a representation with a smoothed density of the scatterplot. This plot displays the average trend observed in the scatterplot.

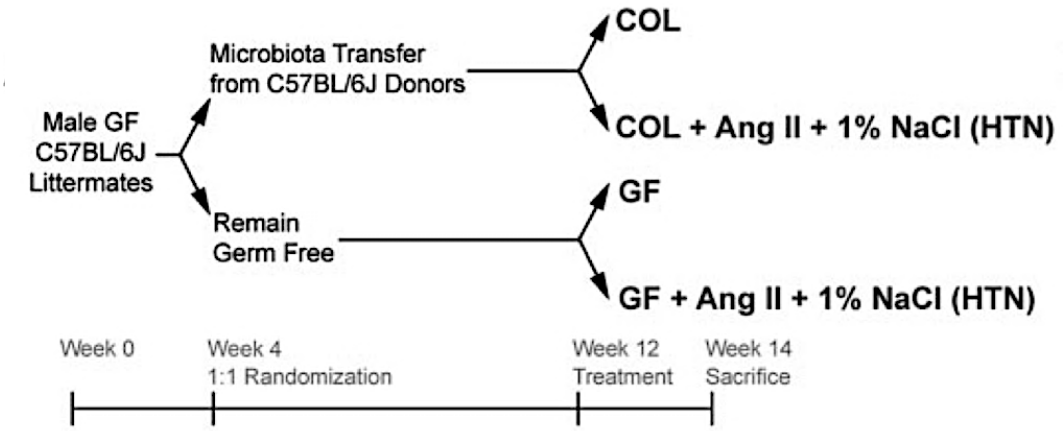

Figure 6. Description of the study protocol. The sample sizes are GF Sham n = 5; GF + HTN n = 12; COL Sham n = 5; COL + HTN n = 12. This figure is published as figure 1 in Avery et al., 2022[71] (under CC BY-NC 4.0 license). Reprinted by permission of Oxford University Press on behalf of the European Society of Cardiology.

3. Results

3.1 Results of benchmarking analysis of LongDat compared with other tools (Study 1[69])

Part of the content of this chapter has been published as a research article[69], the text can be similar but not identical.

LongDat, an algorithm tailored for covariate-aware analysis on high-dimensional longitudinal data, was created and subsequently packaged into an R package for ease of distribution and enhanced reproducibility. The analysis of microbiome absolute or relative abundance data is the main focus of LongDat, although its usage can be extended to other data types, like proportion (e.g., immunome), binary (e.g., survival), and ordinal data (e.g., pain level). In order to demonstrate that LongDat surpasses other existing tools, benchmarking tests were conducted on LongDat and other microbiome-analysis-centered tools that could consider covariates in their analyses, including MaAsLin2[50] (the closest published counterpart of LongDat), lgpr[64], ZIBR[66], and ANCOM[68] to evaluate their speed and performance. To ensure the consistency of the benchmarking results across multiple benchmarking platforms, the tools were evaluated using two independent simulation R packages, namely microbiomeDASim[97] and SparseDOSSA2[123].

The results of microbiomeDASim simulations showed that, in terms of accuracy, true positive rate (TPR), false discovery rate (FDR), and Matthews correlation coefficient (MCC), LongDat performed similarly to MaAsLin2 on data without covariates. However, LongDat outperformed MaAsLin2 when the data had multiple covariates (Figure 7A). As the number of covariates in the simulated data increased, the performance gap between LongDat and MaAsLin2 became more evident. Notably, LongDat maintained a controlled FDR of zero regardless of the tested effects and sample sizes, whereas MaAsLin2's FDR escalated and TPR diminished, particularly with more than four covariates present. The reason for this phenomenon is that LongDat treats covariates by iterating over every covariate in parallel models, while MaAsLin2 incorporates all covariates into a single model. This difference gives rise to the profound discrepancy when analyzing longitudinal microbiome data with multiple covariates as observed here, making LongDat more appropriate in such cases. In addition, the runtime of LongDat was longer than that of MaAsLin2, and this

was because LongDat had a covariate model test part, which conferred robustness to LongDat when dealing with multiple covariates (see section 2.1.1.3). MaAsLin2, on the other hand, lacked this feature (Figure 7B). As for ANCOM, lgpr, and ZIBR, their computational efficiency was found to be unsatisfactory. ANCOM was observed to require excessive memory, while lgpr and ZIBR were slow in execution (Figure 8B). In terms of performance, the TPR of ANCOM and ZIBR dropped, while the FDR of lgpr and ZIBR surged as the number of covariates increased (Figure 8A).

The results of SparseDOSSA2 reconfirmed the findings of the microbiomeDASim benchmarking. The performance of LongDat and MaAsLin2 was assessed using linear or negative binomial models on data pre-processed differently, including TSS-normalized, CSS-normalized, TMM-normalized, CLR-normalized, GMPR-normalized, or rarefied. Regardless of the pre-processing method and the model used, LongDat performed similarly to MaAsLin2 on simulated data without covariates, but outperformed MaAsLin2 when more than four covariates were present (Figure 9A - H). On the other hand, ZIBR and lgpr (ANCOM was excluded in this benchmarking because its memory requirement was too large to run on MDC clusters) again suffered from high FDR and long runtime, particularly when multiple covariates were present in the data (Figure 10A - H). When comparing preprocessing methods and models, MaAsLin2's negative binomial model has higher TPR and FDR (and thus similar accuracy and MCC) than its LM, except when fitting LMs on CLR-transformed data, which performed the worst. Similar outcomes are yielded by LongDat using either linear or negative binomial models with various normalization or rarefaction techniques, except when CLR is paired with the LM, which performed poorly. Even though the negative binomial model and rarefied count data combination resulted in a higher FDR compared with the LM TSS-normalized data, we hold the belief that rarefaction is indispensable for certain circumstances. For instance, when longitudinal negative control data with different sequencing depths at two time points were simulated, a near-zero FPR was obtained when the rarefied count data was fitted with a negative binomial model (Figure 11). However, applying the LM to non-rarefied TSS-normalized data led to a high FPR when there was substantial variation in sequencing depth between the two time points. As a result, it can be deduced that LMs are appropriate for analyzing TSS-normalized data only if no consistent deviation in sequencing depth across different groups or time periods. Or else, the analysis might produce numerous false positives.

Notably, a one-size-fits-all solution does not exist, and choosing the most suitable approach primarily relies on the data's characteristics.

To evaluate the performance of LongDat using data other than simulated data (microbiomeDASim and SparseDOSSA2), a semi-synthetic assessment was conducted. This was accomplished by randomly shuffling the time variable against other variables in the microbiome data at the genus level from **Study 2**[70]. The comparison was made between the significant associations in the data before and after shuffling. The outcomes from LongDat's analysis demonstrated minimal to almost negligible instances of false positive findings within the shuffled data, irrespective of the presence of covariates in the analysis process (Figure 12). On the other hand, MaAsLin2, ZIBR, and lgpr were all affected by the addition of covariates in the analyses. MaAsLin2 identified fewer significant associations in the unrandomized data and more false positives in the randomized data compared with LongDat. ZIBR and lgpr resulted in significantly higher rates of false positives than LongDat. As previously observed, it was confirmed by the analysis that LongDat is able to effectively minimize false positive results in both semi-synthetic and simulated evaluations, indicating its robustness.

Given that MaAsLin2 is the sole alternative tool capable of handling the entire benchmark without being hindered by memory and runtime limitations, the following analyses primarily concentrate on comparing MaAsLin2 and LongDat. To assess their effectiveness in identifying covariate effects, a dummy variable that correlates with the time variable was introduced. Whether the dummy variable, when employed as the input time variable instead, was erroneously identified as showing an independent association with the simulated feature, was then examined (Figure 13A, 13B). LongDat requires only one run for this evaluation. MaAsLin2 lacks a corresponding component in its covariate model testing compared to the LongDat pipeline's second part; consequently, two separate MaAsLin2 runs were conducted to ensure comparable outcomes with LongDat. One run included covariates in the model, while the other run was performed without covariates. The findings indicate that both LongDat and MaAsLin2 achieved similar performance in correctly detecting covariate effects. The medians of the success rates for both tools remained at approximately 0.95, as determined by the FDR threshold or family-wise error rate, even in cases where the time and dummy variables exhibited a strong correlation. The similarity in performance might be due to the fact that LongDat

and MaAsLin2 are both based on GLMMs. These results demonstrate the accuracy and reliable identification of covariates by both LongDat and MaAsLin2.

To further show the performance of LongDat on real data, and compare it with that of MaAsLin2, a comparative analysis of LongDat and MaAsLin2 using real gut microbial data from **Study 2**[70] investigating the effects of fasting on MetS patients was conducted[70]. The study objective was to examine the impact of fasting while accounting for changes in medication. Initially, without considering any covariates (i.e., drug variables) in the MaAsLin2 analysis, both LongDat and MaAsLin2 found 27 species that exhibited significant changes in their abundances during the intervention, with 19 species showing consistent results between the two methods (Figure 14A, 14B). However, when covariates were included in the analysis, MaAsLin2 reported only two species as significantly different in abundance. This limitation arose because the models in MaAsLin2 encountered errors (indicated by "NA" values in p-values and standard errors) when more than one fixed variables were incorporated into one single model. In contrast, LongDat overcomes this issue by including only one covariate at a time and iterating over all covariates. As a result, LongDat demonstrates greater robustness than MaAsLin2 when analyzing datasets with multiple covariates, albeit with a longer runtime.

Finally, to showcase the versatility of LongDat beyond microbiome data, LongDat was applied to the immunome data obtained from **Study 2**[70] (Figures 15, 16). The immunome data encompass both proportion (percentage) and non-proportion (non-percentage) data, which were analyzed using the proportion and measurement modes of LongDat, respectively. These findings demonstrate that LongDat is capable of handling diverse data types, extending its applicability beyond microbiome counts.

Altogether, the results in this study demonstrate that LongDat is a reliable tool for analyzing longitudinal microbiome data, particularly in situations involving multiple covariates (Table 1).

Table 1. Summary of the comparison of all tools. This table has been published in Chen *et al*., 2023[69] as table S1 (under CC BY 4.0 license).

	TPR	FDR	TPR and FDR affected by the number of covariates	Memory requirement	Speed	Able to include covariates in analysis	Provides covariate effect of each feature	Multiple test correction	Needs* arbitrary cutoff
LongDat	Low when sample size is small	Generally low	Not affected	Small	Medium	Yes	Yes	Yes	No
MaAsLin2 (Mallick et al. 2021)	Low when there are multiple covariates	High when there are multiple covariates	Highly affected	Small	Fast	Yes	No	Yes	No
ANCOM (Mandal et al. 2015)	Low when sample size is small	Generally low	Affected	Large	Medium	Yes	No	Yes	Yes**
ZIBR (Chen et al. 2016)	Low when there are multiple covariates	Generally high	Highly affected	Small	Slow	Yes	No	Yes	No
lgpr (Timonen et al. 2021)	Low when sample size is small	High when sample size is small	Highly affected	Medium	Slow	Yes	No	No	Yes***

TPR: true positive rate; FDR: false discovery rate

*Indicates if the user needs to select an arbitrary threshold to decide the significance of the tested variable on a feature.

**Relies on W statistics, which is the number of each feature is tested to be significantly different against other features.

***Relies on the ratio of total explained variance in a model.

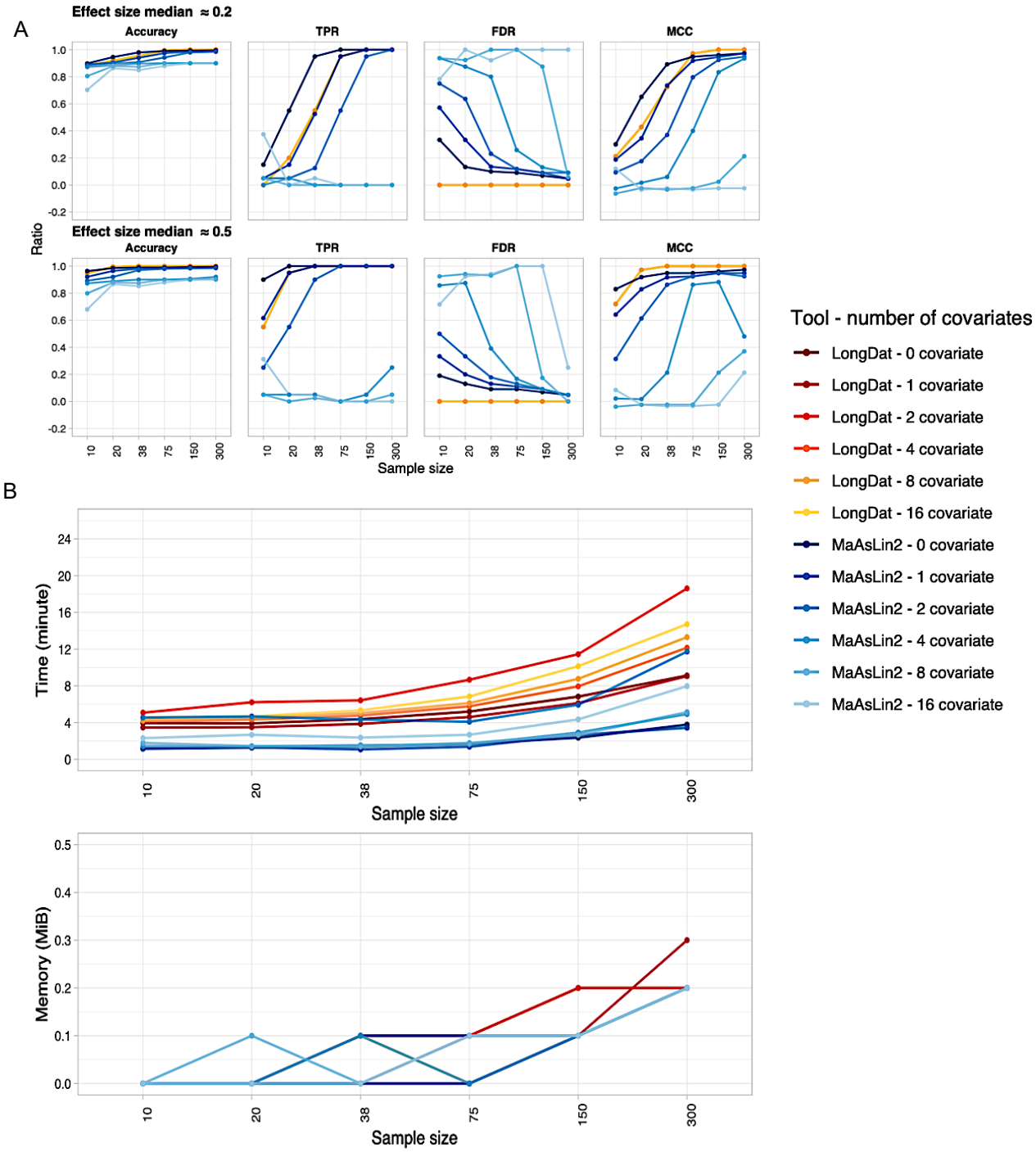

Figure 7. Comparison of the performance of LongDat and MaAsLin2. Both tools are employing the negative binomial model on the microbiomeDASim-simulated longitudinal data with different numbers of covariates. The line plots demonstrate the median values of (A) accuracy, true positive rate (TPR), false discovery rate (FDR), Matthews correlation coefficient (MCC), and (B) runtime and memory usage. This figure has been published in Chen *et al.*, 2023[69] as figures S3 and S4 (under CC BY 4.0 license).

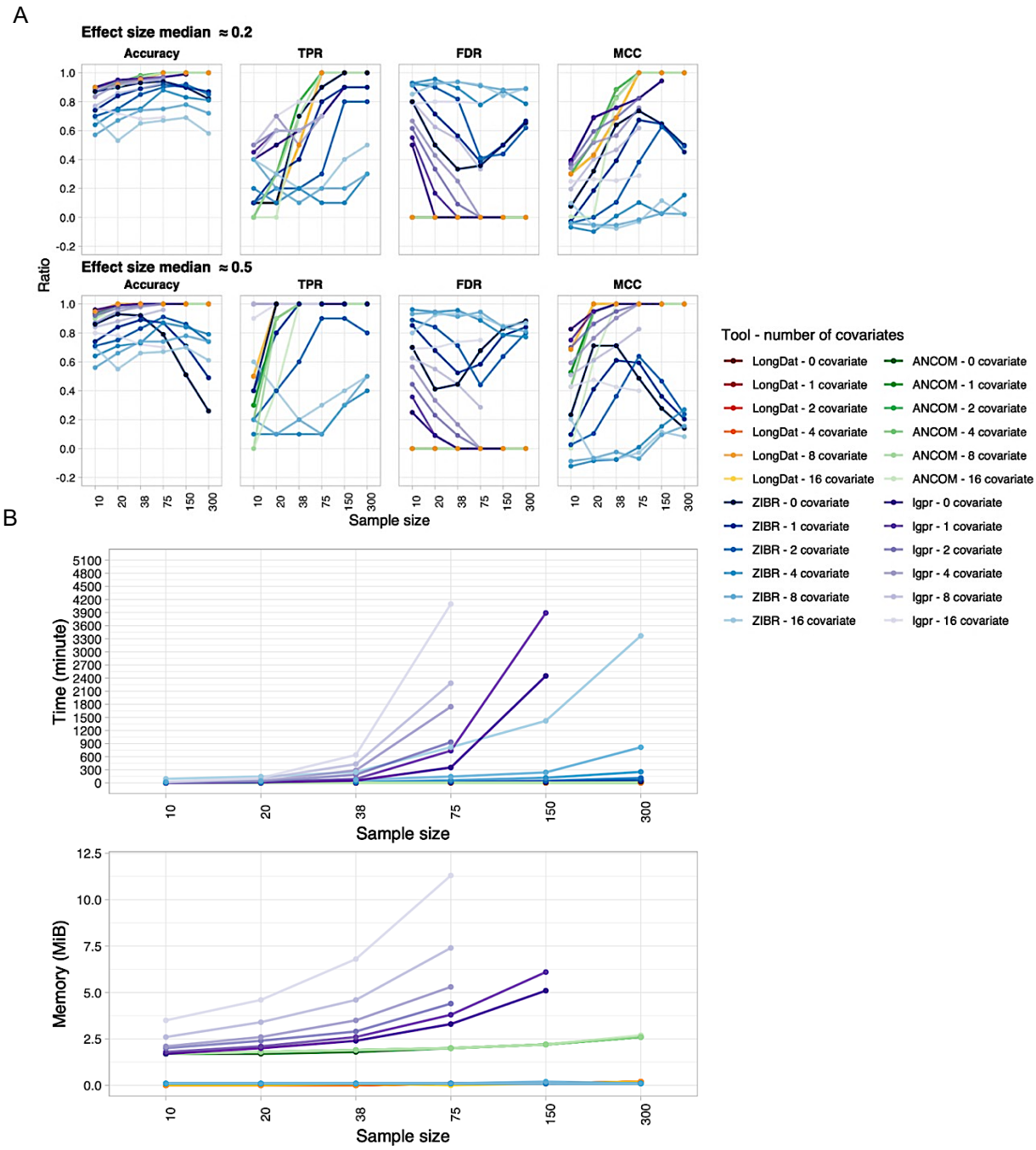

Figure 8. Comparison of LongDat, lgpr, ZIBR, and ANCOM. This is comparing the performance of the tools when analyzing longitudinal data simulated by microbiomeDASim with zero to multiple covariates. The line plots show the medians of (A) accuracy, true positive rate (TPR), false discovery rate (FDR), and Matthews correlation coefficient (MCC), and (B) runtime and memory usage. This figure has been published in Chen *et al*., 2023[69], as figures S10 and S11 (under CC BY 4.0 license).

A

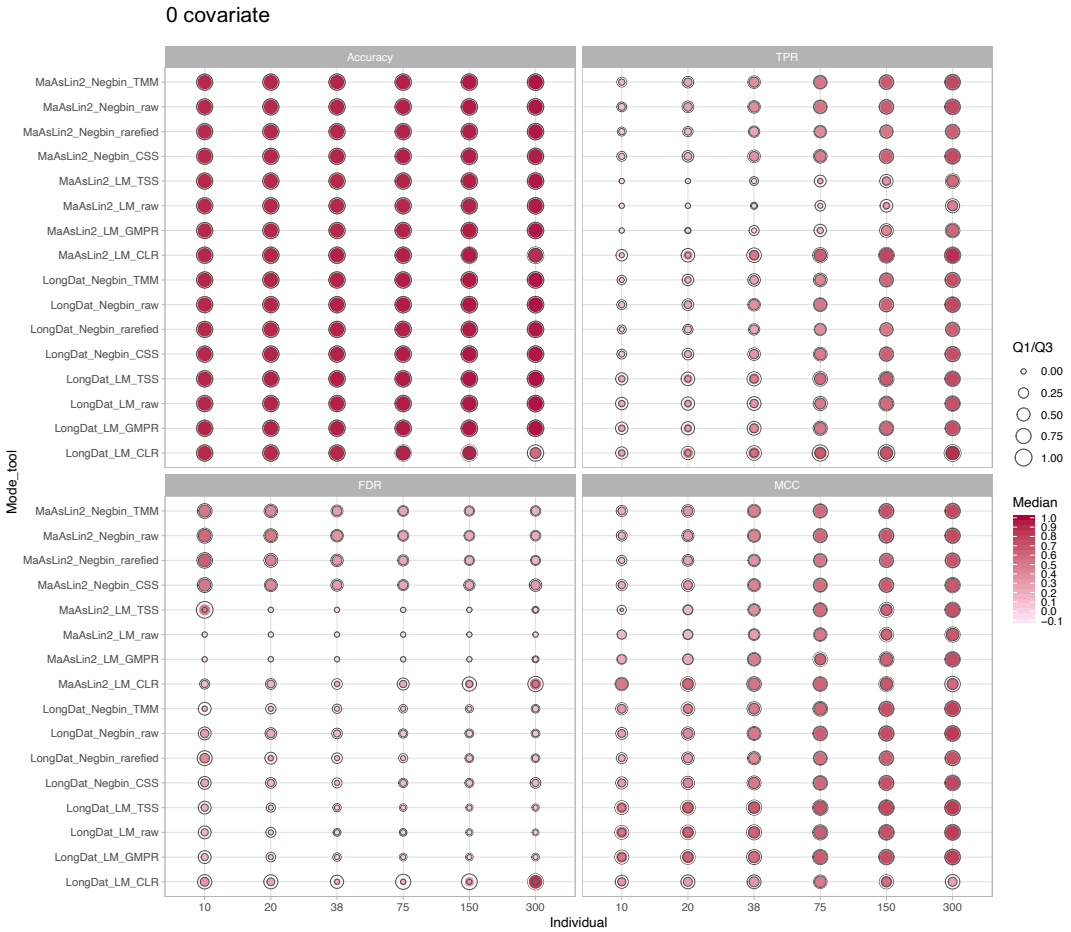
0 covariate
Accuracy
TPR
FDR
MCC
MaAsLin2_Negbin_TMM
MaAsLin2_Negbin_raw
MaAsLin2_Negbin_rarefied
MaAsLin2_Negbin_CSS
MaAsLin2_LM_TSS
MaAsLin2_LM_raw
MaAsLin2_LM_GMPR
MaAsLin2_LM_CLR
LongDat_Negbin_TMM
LongDat_Negbin_raw
LongDat_Negbin_rarefied
LongDat_Negbin_CSS
LongDat_LM_TSS
LongDat_LM_raw
LongDat_LM_GMPR
LongDat_LM_CLR
Mode_tool
10
20
38
75
150
300
Individual
Q1/Q3
0.00
0.25
0.50
0.75
1.00
Median
1.0
0.9
0.8
0.7
0.6
0.5
0.4
0.3
0.2
0.1
0.0
−0.1

B


1 covariate
Accuracy
TPR
FDR
MCC
MaAsLin2_Negbin_TMM
MaAsLin2_Negbin_raw
MaAsLin2_Negbin_rarefied
MaAsLin2_Negbin_CSS
MaAsLin2_LM_TSS
MaAsLin2_LM_raw
MaAsLin2_LM_GMPR
MaAsLin2_LM_CLR
LongDat_Negbin_TMM
LongDat_Negbin_raw
LongDat_Negbin_rarefied
LongDat_Negbin_CSS
LongDat_LM_TSS
LongDat_LM_raw
LongDat_LM_GMPR
LongDat_LM_CLR
Mode_tool
10
20
38
75
150
300
Individual
Q1/Q3
0.00
0.25
0.50
0.75
1.00
Median
1.0
0.9
0.8
0.7
0.6
0.5
0.4
0.3
0.2
0.1
0.0
−0.1

C


4 covariates
Accuracy
TPR
FDR
MCC
MaAsLin2_Negbin_TMM
MaAsLin2_Negbin_raw
MaAsLin2_Negbin_rarefied
MaAsLin2_Negbin_CSS
MaAsLin2_LM_TSS
MaAsLin2_LM_raw
MaAsLin2_LM_GMPR
MaAsLin2_LM_CLR
LongDat_Negbin_TMM
LongDat_Negbin_raw
LongDat_Negbin_rarefied
LongDat_Negbin_CSS
LongDat_LM_TSS
LongDat_LM_raw
LongDat_LM_GMPR
LongDat_LM_CLR
Mode_tool
10
20
38
75
150
300
Individual
Q1/Q3
0.00
0.25
0.50
0.75
1.00
Median
1.0
0.9
0.8
0.7
0.6
0.5
0.4
0.3
0.2
0.1
0.0
−0.1

D

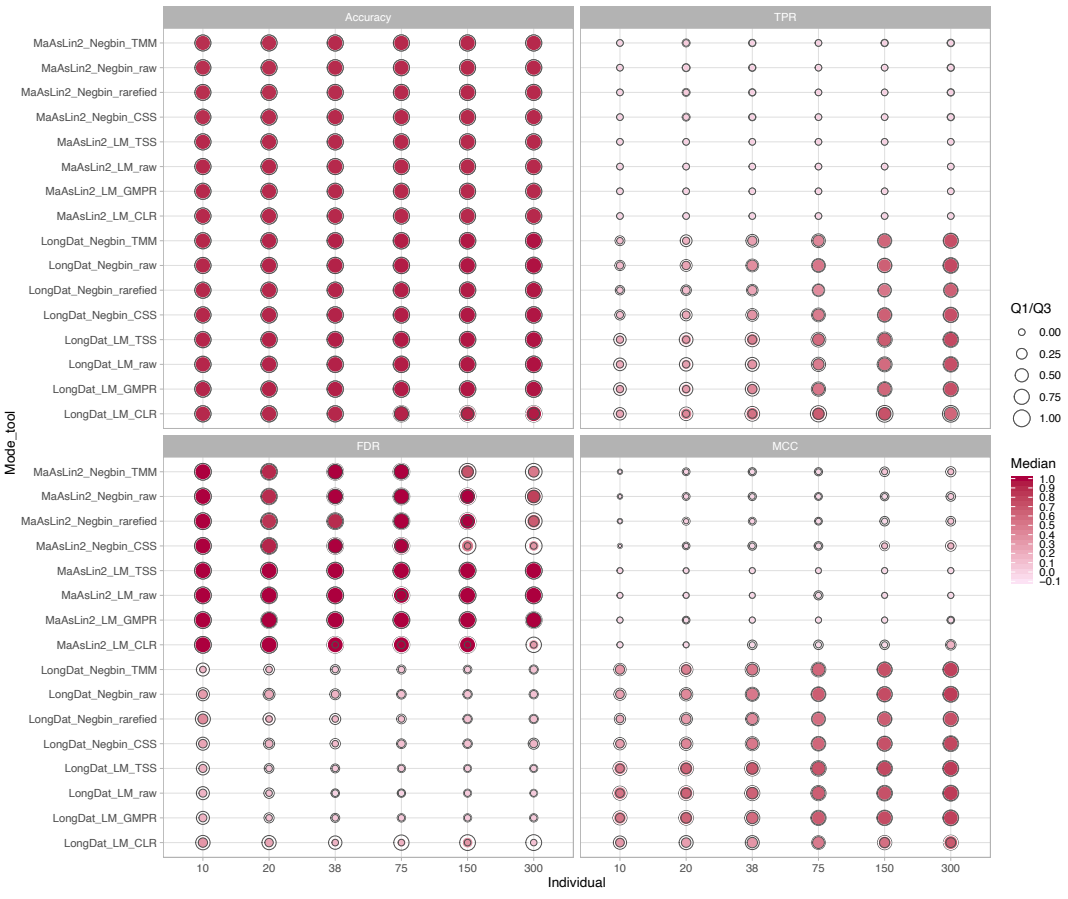
16 covariates
Accuracy
TPR
FDR
MCC
MaAsLin2_Negbin_TMM
MaAsLin2_Negbin_raw
MaAsLin2_Negbin_rarefied
MaAsLin2_Negbin_CSS
MaAsLin2_LM_TSS
MaAsLin2_LM_raw
MaAsLin2_LM_GMPR
MaAsLin2_LM_CLR
LongDat_Negbin_TMM
LongDat_Negbin_raw
LongDat_Negbin_rarefied
LongDat_Negbin_CSS
LongDat_LM_TSS
LongDat_LM_raw
LongDat_LM_GMPR
LongDat_LM_CLR
Mode_tool
10
20
38
75
150
300
Individual
Q1/Q3
0.00
0.25
0.50
0.75
1.00
Median
1.0
0.9
0.8
0.7
0.6
0.5
0.4
0.3
0.2
0.1
0.0
−0.1

E

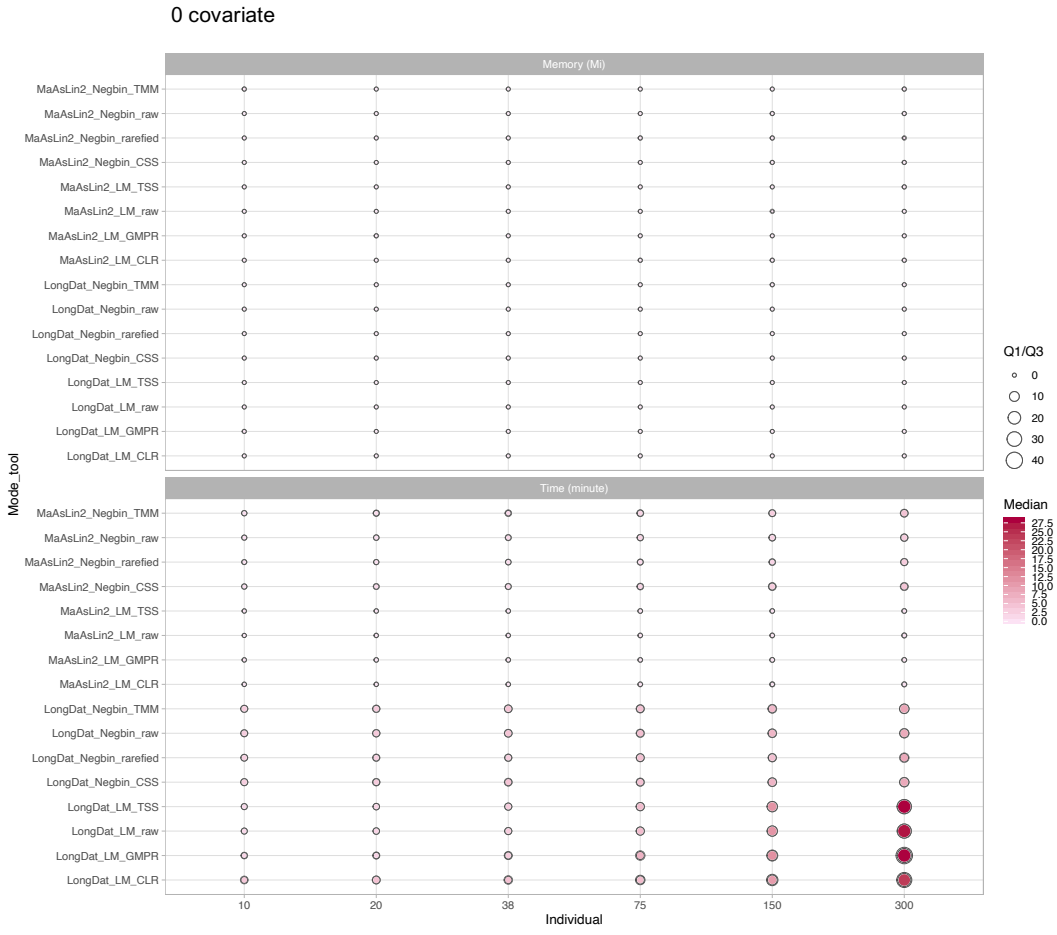
0 covariate
Memory (Mi)
Time (minute)
MaAsLin2_Negbin_TMM
MaAsLin2_Negbin_raw
MaAsLin2_Negbin_rarefied
MaAsLin2_Negbin_CSS
MaAsLin2_LM_TSS
MaAsLin2_LM_raw
MaAsLin2_LM_GMPR
MaAsLin2_LM_CLR
LongDat_Negbin_TMM
LongDat_Negbin_raw
LongDat_Negbin_rarefied
LongDat_Negbin_CSS
LongDat_LM_TSS
LongDat_LM_raw
LongDat_LM_GMPR
LongDat_LM_CLR
Mode_tool
10
20
38
75
150
300
Individual
Q1/Q3
0
10
20
30
40
Median
27.5
25.0
22.5
20.0
17.5
15.0
12.5
10.0
7.5
5.0
2.5
0.0

F

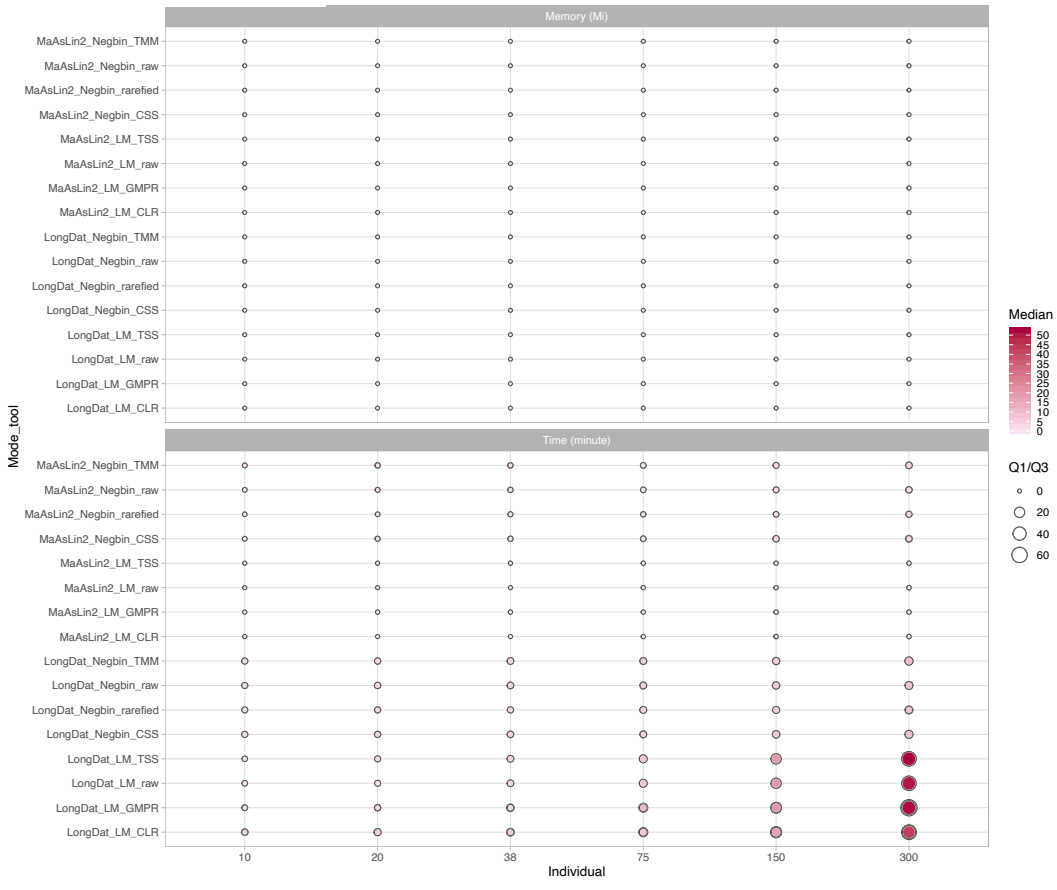
1 covariate
Memory (Mi)
Time (minute)
MaAsLin2_Negbin_TMM
MaAsLin2_Negbin_raw
MaAsLin2_Negbin_rarefied
MaAsLin2_Negbin_CSS
MaAsLin2_LM_TSS
MaAsLin2_LM_raw
MaAsLin2_LM_GMPR
MaAsLin2_LM_CLR
LongDat_Negbin_TMM
LongDat_Negbin_raw
LongDat_Negbin_rarefied
LongDat_Negbin_CSS
LongDat_LM_TSS
LongDat_LM_raw
LongDat_LM_GMPR
LongDat_LM_CLR
Mode_tool
10
20
38
75
150
300
Individual
Median
50
45
40
35
30
25
20
15
10
5
0
Q1/Q3
0
20
40
60

G

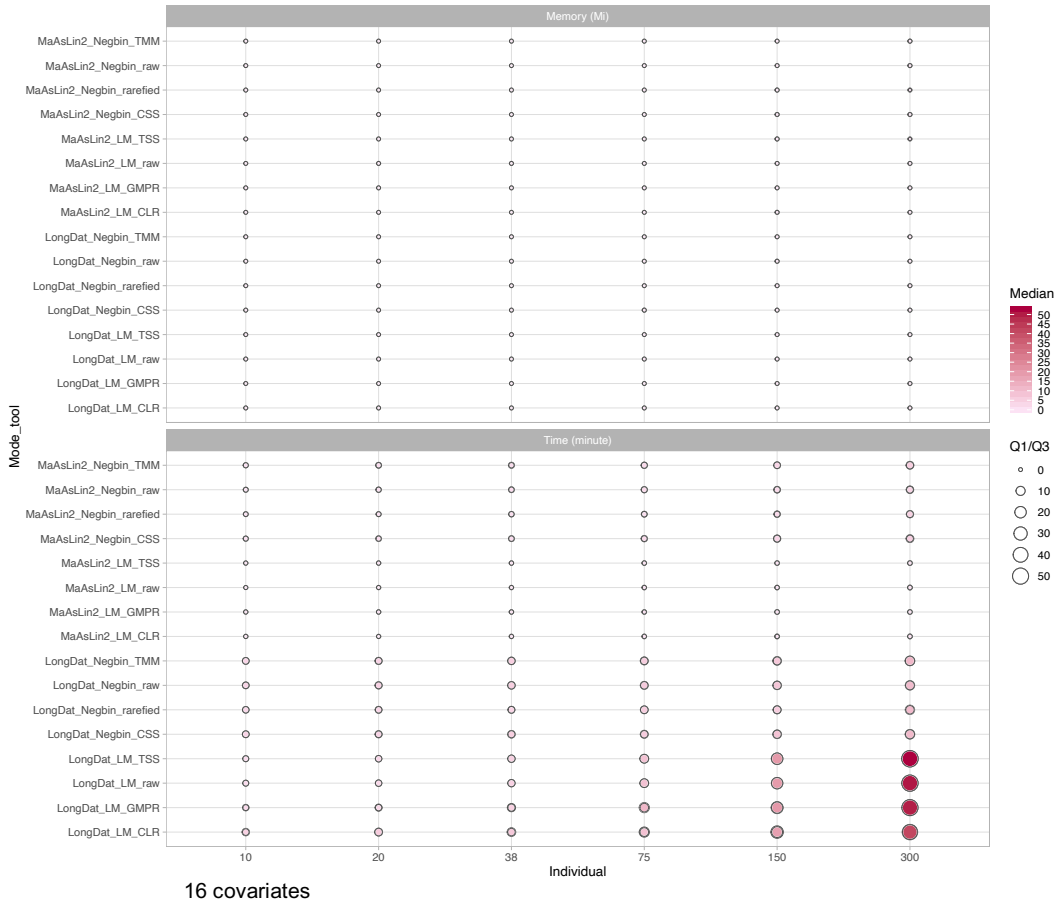
4 covariates
Memory (Mi)
Time (minute)
Mode_tool
MaAsLin2_Negbin_TMM
MaAsLin2_Negbin_raw
MaAsLin2_Negbin_rarefied
MaAsLin2_Negbin_CSS
MaAsLin2_LM_TSS
MaAsLin2_LM_raw
MaAsLin2_LM_GMPR
MaAsLin2_LM_CLR
LongDat_Negbin_TMM
LongDat_Negbin_raw
LongDat_Negbin_rarefied
LongDat_Negbin_CSS
LongDat_LM_TSS
LongDat_LM_raw
LongDat_LM_GMPR
LongDat_LM_CLR
10
20
38
75
150
300
Individual
Median
50
45
40
35
30
25
20
15
10
5
0
Q1/Q3
0
10
20
30
40
50

H

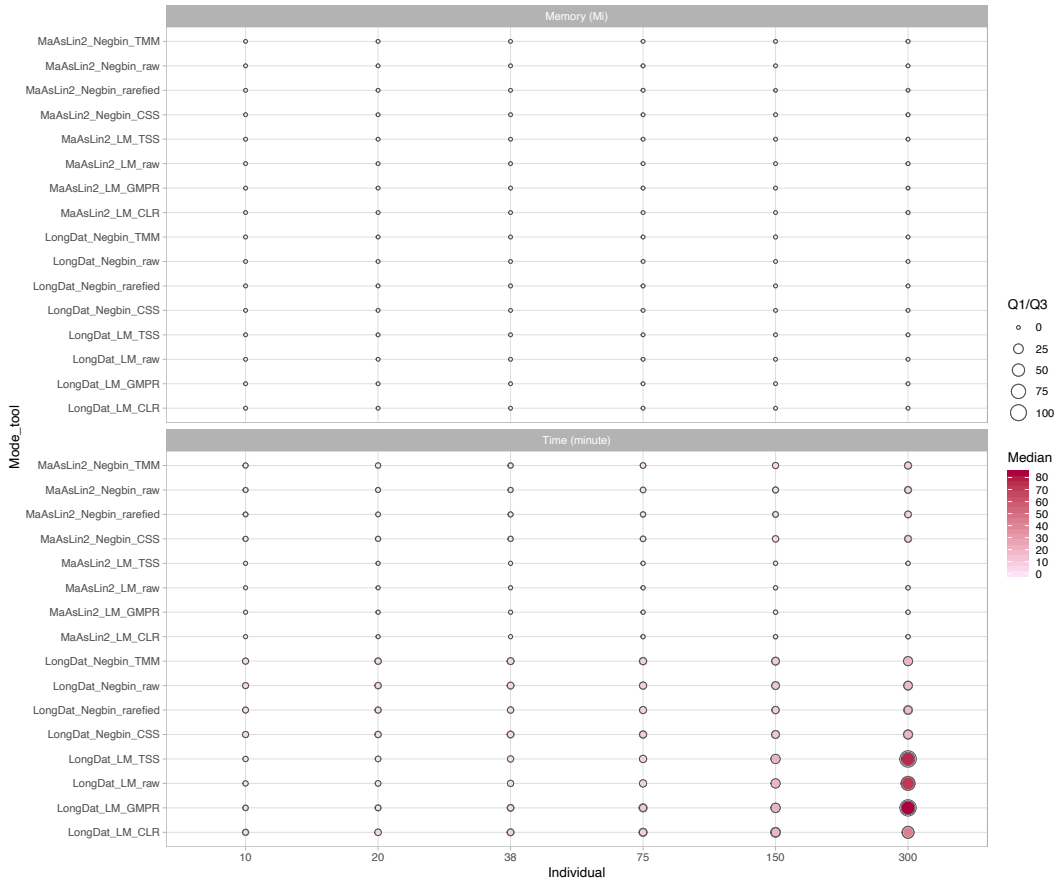
16 covariates
Memory (Mi)
Time (minute)
Mode_tool
MaAsLin2_Negbin_TMM
MaAsLin2_Negbin_raw
MaAsLin2_Negbin_rarefied
MaAsLin2_Negbin_CSS
MaAsLin2_LM_TSS
MaAsLin2_LM_raw
MaAsLin2_LM_GMPR
MaAsLin2_LM_CLR
LongDat_Negbin_TMM
LongDat_Negbin_raw
LongDat_Negbin_rarefied
LongDat_Negbin_CSS
LongDat_LM_TSS
LongDat_LM_raw
LongDat_LM_GMPR
LongDat_LM_CLR
10
20
38
75
150
300
Individual
Q1/Q3
0
25
50
75
100
Median
80
70
60
50
40
30
20
10
0

Figure 9. Comparison of different modes of LongDat and MaAsLin2. This is comparing their performance and computational resource requirement when applied to longitudinal data simulated by SparseDOSSA2 with (A, E) 0 covariate; (B, F) 1 covariate; (C, G) 4 covariates; (D, H) 16 covariates. (A, B, C, D) The circles show the first quartiles, medians, and third quartiles of (A) accuracy, true positive rate (TPR), false discovery rate (FDR), and Matthews correlation coefficient (MCC), and (E, F, G, H) runtime and total used memory. The filled circles (red) are the medians, while the inner and outer hollow circles are the first and third quartiles, respectively. 1 mebibyte (MiB) ≈ 1.05 megabyte (MB). Negbin: negative binomial model; LM: linear model; TMM: trimmed mean of M-values; raw: raw counts; rarefied: rarefied counts; CSS: cumulative-sum scaling; TSS: total-sum scaling; GMPR: geometric mean of pairwise ratios; CLR: centered log-ratio. This figure has been published in Chen *et al*., 2023[69] as figures S5-S8 (under CC BY 4.0 license).

A


0 covariate
Accuracy
TPR
FDR
MCC
ZIBR_TSS
LongDat_Negbin_TMM
LongDat_Negbin_raw
LongDat_Negbin_rarefied
LongDat_Negbin_CSS
LongDat_LM_TSS
LongDat_LM_raw
LongDat_LM_GMPR
LongDat_LM_CLR
lgpr_TSS
lgpr_TMM
lgpr_raw
lgpr_rarefied
lgpr_GMPR
lgpr_CSS
lgpr_CLR
Mode_tool
10
20
38
75
150
300
Individual
Median
0.9
0.8
0.7
0.6
0.5
0.4
0.3
0.2
0.1
0.0
Q1/Q3
0.00
0.25
0.50
0.75
1.00

B

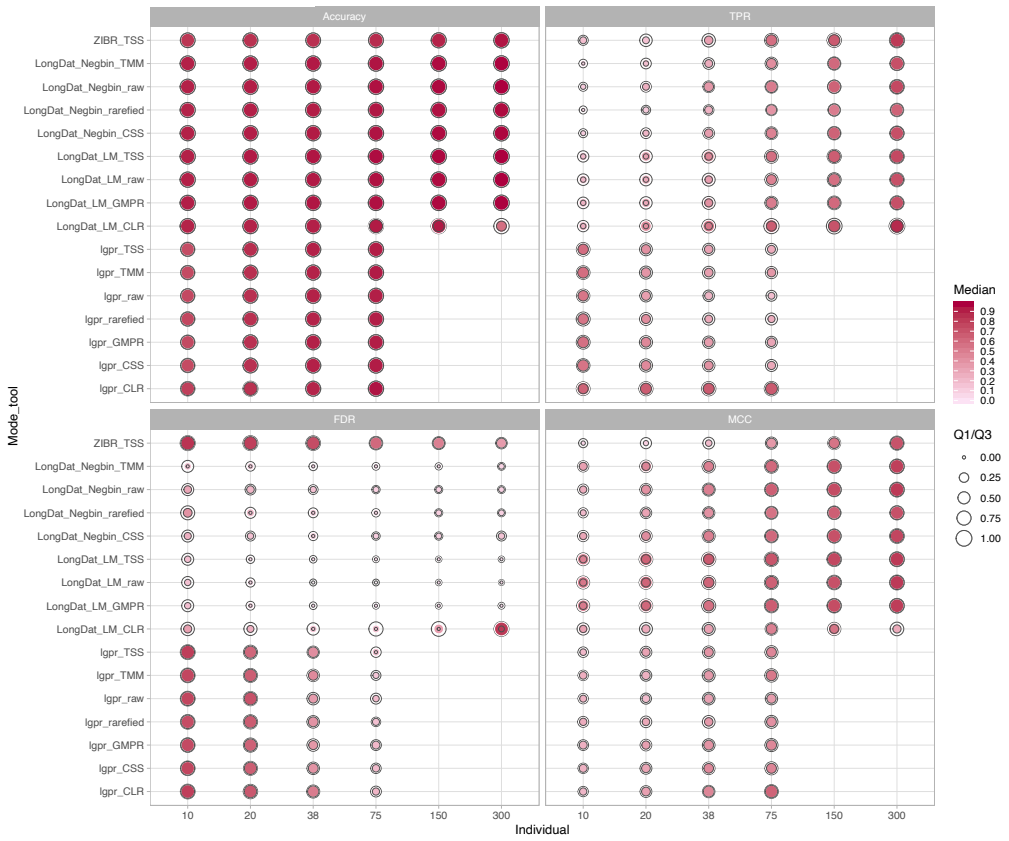
1 covariate
Accuracy
TPR
FDR
MCC
ZIBR_TSS
LongDat_Negbin_TMM
LongDat_Negbin_raw
LongDat_Negbin_rarefied
LongDat_Negbin_CSS
LongDat_LM_TSS
LongDat_LM_raw
LongDat_LM_GMPR
LongDat_LM_CLR
lgpr_TSS
lgpr_TMM
lgpr_raw
lgpr_rarefied
lgpr_GMPR
lgpr_CSS
lgpr_CLR
Mode_tool
10
20
38
75
150
300
Individual
Median
0.9
0.8
0.7
0.6
0.5
0.4
0.3
0.2
0.1
0.0
Q1/Q3
0.00
0.25
0.50
0.75
1.00

C

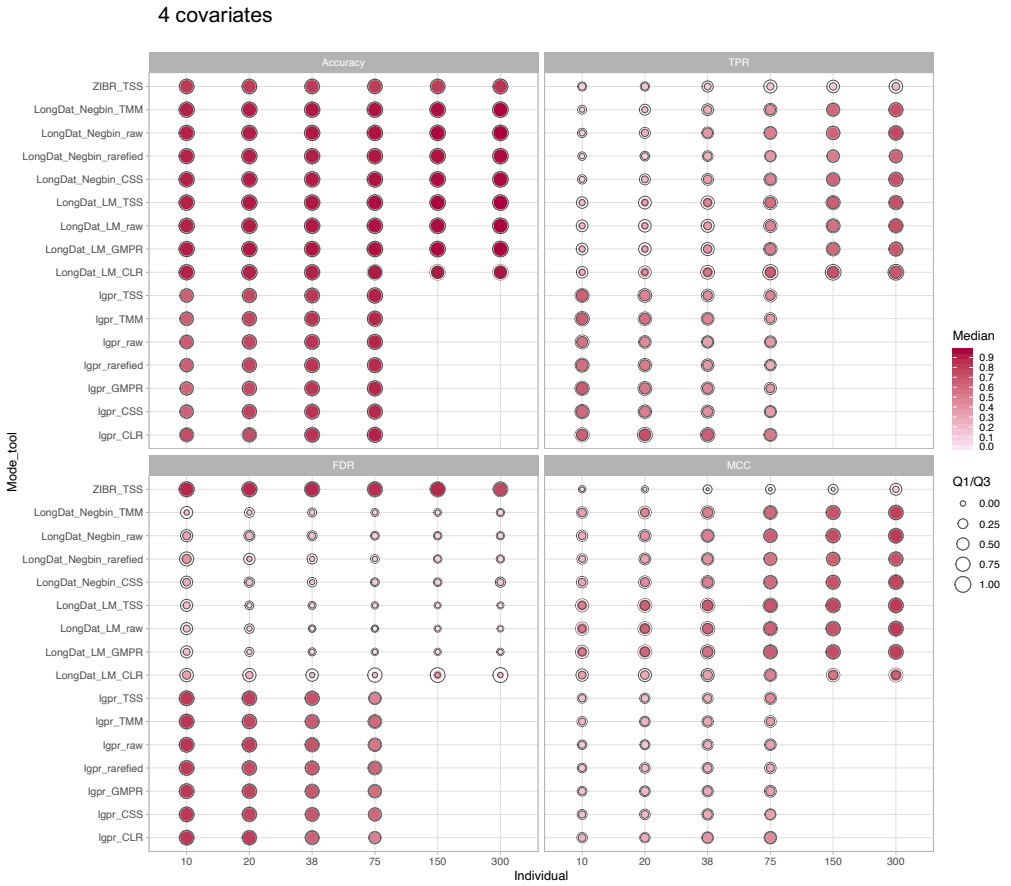
4 covariates
Accuracy
TPR
FDR
MCC
ZIBR_TSS
LongDat_Negbin_TMM
LongDat_Negbin_raw
LongDat_Negbin_rarefied
LongDat_Negbin_CSS
LongDat_LM_TSS
LongDat_LM_raw
LongDat_LM_GMPR
LongDat_LM_CLR
lgpr_TSS
lgpr_TMM
lgpr_raw
lgpr_rarefied
lgpr_GMPR
lgpr_CSS
lgpr_CLR
Mode_tool
10
20
38
75
150
300
Individual
Median
0.9
0.8
0.7
0.6
0.5
0.4
0.3
0.2
0.1
0.0
Q1/Q3
0.00
0.25
0.50
0.75
1.00

D

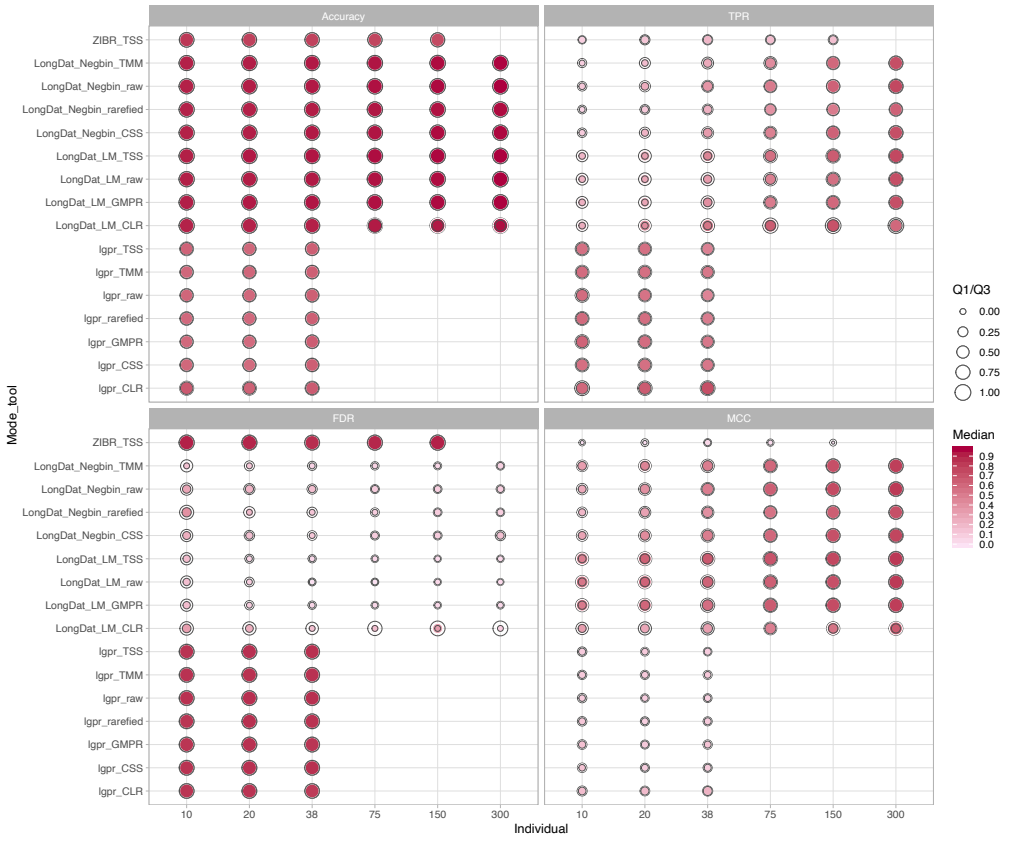
16 covariates
Accuracy
TPR
FDR
MCC
ZIBR_TSS
LongDat_Negbin_TMM
LongDat_Negbin_raw
LongDat_Negbin_rarefied
LongDat_Negbin_CSS
LongDat_LM_TSS
LongDat_LM_raw
LongDat_LM_GMPR
LongDat_LM_CLR
lgpr_TSS
lgpr_TMM
lgpr_raw
lgpr_rarefied
lgpr_GMPR
lgpr_CSS
lgpr_CLR
Mode_tool
10
20
38
75
150
300
Individual
Q1/Q3
0.00
0.25
0.50
0.75
1.00
Median
0.9
0.8
0.7
0.6
0.5
0.4
0.3
0.2
0.1
0.0

E


0 covariate
Memory (Mi)
Time (minute)
ZIBR_TSS
LongDat_Negbin_TMM
LongDat_Negbin_raw
LongDat_Negbin_rarefied
LongDat_Negbin_CSS
LongDat_LM_TSS
LongDat_LM_raw
LongDat_LM_GMPR
LongDat_LM_CLR
lgpr_TSS
lgpr_TMM
lgpr_raw
lgpr_rarefied
lgpr_GMPR
lgpr_CSS
lgpr_CLR
Mode_tool
10
20
38
75
150
300
Individual
Q1/Q3
0
1000
2000
3000
4000
5000
Median
5000
4500
4000
3500
3000
2500
2000
1500
1000
500
0

F


1 covariate
Memory (Mi)
Time (minute)
ZIBR_TSS
LongDat_Negbin_TMM
LongDat_Negbin_raw
LongDat_Negbin_rarefied
LongDat_Negbin_CSS
LongDat_LM_TSS
LongDat_LM_raw
LongDat_LM_GMPR
LongDat_LM_CLR
lgpr_TSS
lgpr_TMM
lgpr_raw
lgpr_rarefied
lgpr_GMPR
lgpr_CSS
lgpr_CLR
Mode_tool
10
20
38
75
150
300
Individual
Q1/Q3
0
1000
2000
3000
Median
3000
2500
2000
1500
1000
500
0

G

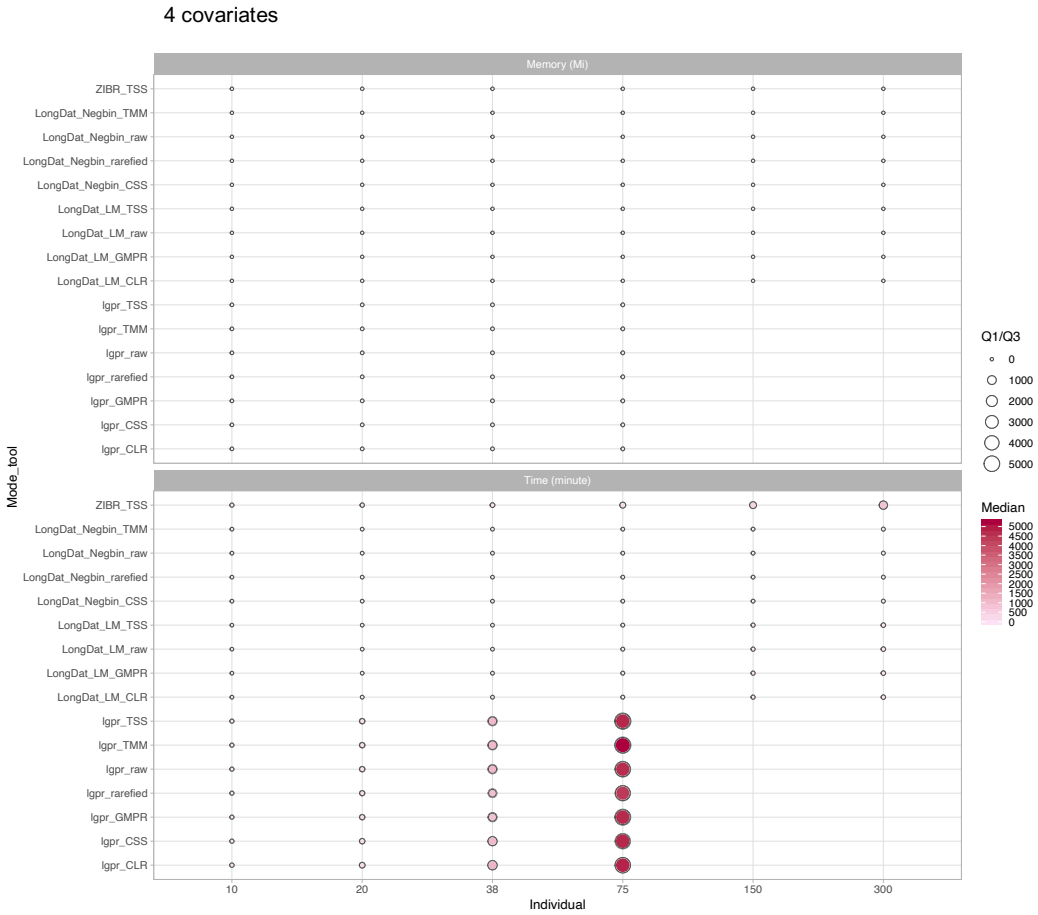
4 covariates
Memory (Mi)
Time (minute)
ZIBR_TSS
LongDat_Negbin_TMM
LongDat_Negbin_raw
LongDat_Negbin_rarefied
LongDat_Negbin_CSS
LongDat_LM_TSS
LongDat_LM_raw
LongDat_LM_GMPR
LongDat_LM_CLR
lgpr_TSS
lgpr_TMM
lgpr_raw
lgpr_rarefied
lgpr_GMPR
lgpr_CSS
lgpr_CLR
Mode_tool
10
20
38
75
150
300
Individual
Q1/Q3
0
1000
2000
3000
4000
5000
Median
5000
4500
4000
3500
3000
2500
2000
1500
1000
500
0

H


16 covariates
Memory (Mi)
Time (minute)
ZIBR_TSS
LongDat_Negbin_TMM
LongDat_Negbin_raw
LongDat_Negbin_rarefied
LongDat_Negbin_CSS
LongDat_LM_TSS
LongDat_LM_raw
LongDat_LM_GMPR
LongDat_LM_CLR
lgpr_TSS
lgpr_TMM
lgpr_raw
lgpr_rarefied
lgpr_GMPR
lgpr_CSS
lgpr_CLR
Mode_tool
10
20
38
75
150
300
Individual
Q1/Q3
0
1000
2000
3000
4000
5000
Median
4500
4000
3500
3000
2500
2000
1500
1000
500
0

Figure 10. Comparison of different modes of LongDat, lgpr and ZIBR. This is comparing their performance and computational resource requirement when applied to longitudinal data simulated by SparseDOSSA2 with (A, E) 0 covariate; (B, F) 1 covariate; (C, G) 4 covariates; (D, H) 16 covariates. (A, B, C, D) The circles show the first quartiles, medians, and third quartiles of (A) accuracy, true positive rate (TPR), false discovery rate (FDR), and Matthews correlation coefficient (MCC), and (E, F, G, H) runtime and total used memory. The filled circles (red) are the medians, while the inner and outer hollow circles are the first and third quartiles, respectively. 1 mebibyte (MiB) ≈ 1.05 megabyte (MB). Negbin: negative binomial model; LM: linear model; TMM: trimmed mean of M-values; raw: raw counts; rarefied: rarefied counts; CSS: cumulative-sum scaling; TSS: total-sum scaling; GMPR: geometric mean of pairwise ratios; CLR: centered log-ratio. This figure has been published in Chen *et al*., 2023[69], as figures S12-S15 (under CC BY 4.0 license).

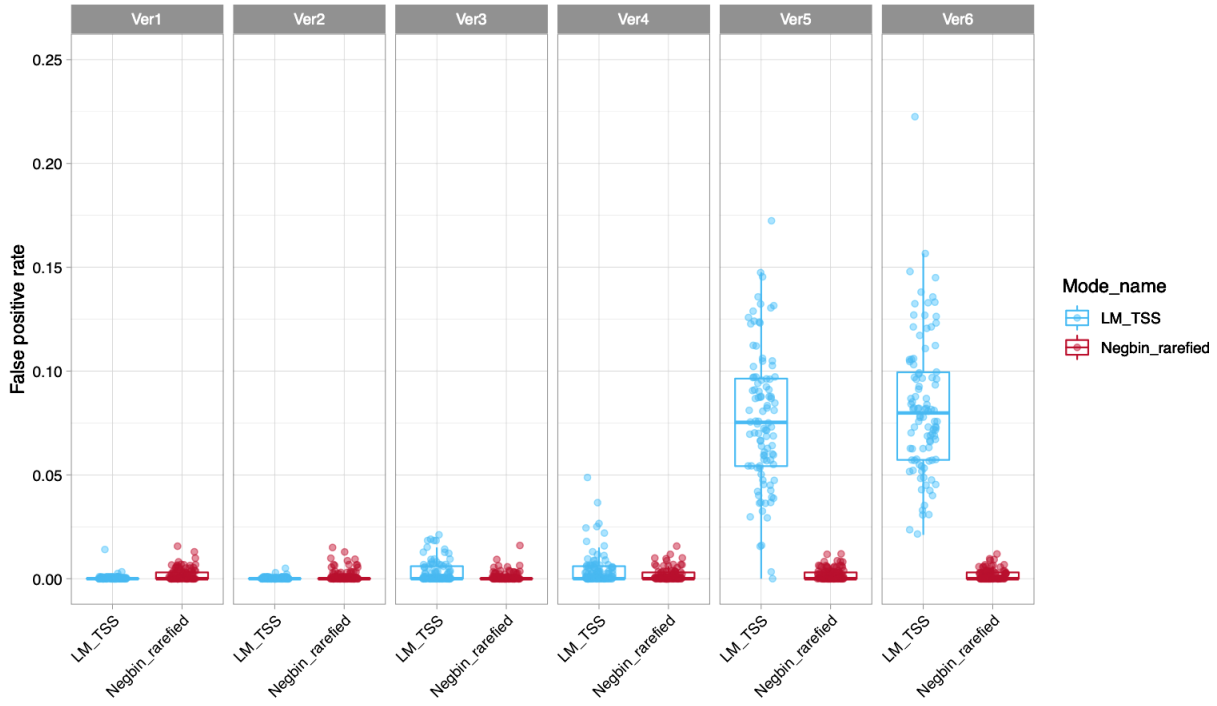

Figure 11. Evaluation of the false positive rates (FPR) of various modes of LongDat. This data, simulated by SparseDOSSA2, is a negative control longitudinal data consisting of 150 individuals, 332 microbes, and had no time-varying features (i.e., the effect size was zero for all features) at two time points. We compared the performance of two different models, an LM paired with TSS normalization and a negative binomial model paired with rarefied count, through 100 simulations for each mode and tool pairing. Versions 1 through 6 were created using the same raw simulated data. In versions 1 and 2, the total abundances for each individual at both time points were rarefied to 50000 and 1000, respectively. In version 3, the total abundances at the first time point were rarefied to 50000, while the ones at the second time point were rarefied to 5000, whereas in version 4, the total abundances at the first time point were rarefied to 5000, while those at the second time point were rarefied to 50000. In version 5, the overall abundances were adjusted using rarefaction to 50,000 at the initial time point and 1,000 at the second time point. On the other hand, in version 6, the total abundances were rarefied to 1,000 at the first time point and 50,000 at the second time point. Furthermore, for the negative binomial model, versions 3 to 6 were subjected to additional rarefaction at both time points, with the specific rarefaction threshold being determined by the lowest sequencing depth. This threshold was set at either 5000 or 1000. Microbes having BH-corrected model test q-values lower than 0.1 and BH-corrected post-hoc test q-values lower than 0.05 are deemed to be significant. Negbin: negative binomial model; LM: linear model; rarefied: rarefied counts; TSS: total-sum scaling. This figure has been published in Chen *et al.*, 2023[69], as figure S9 (under CC BY 4.0 license).

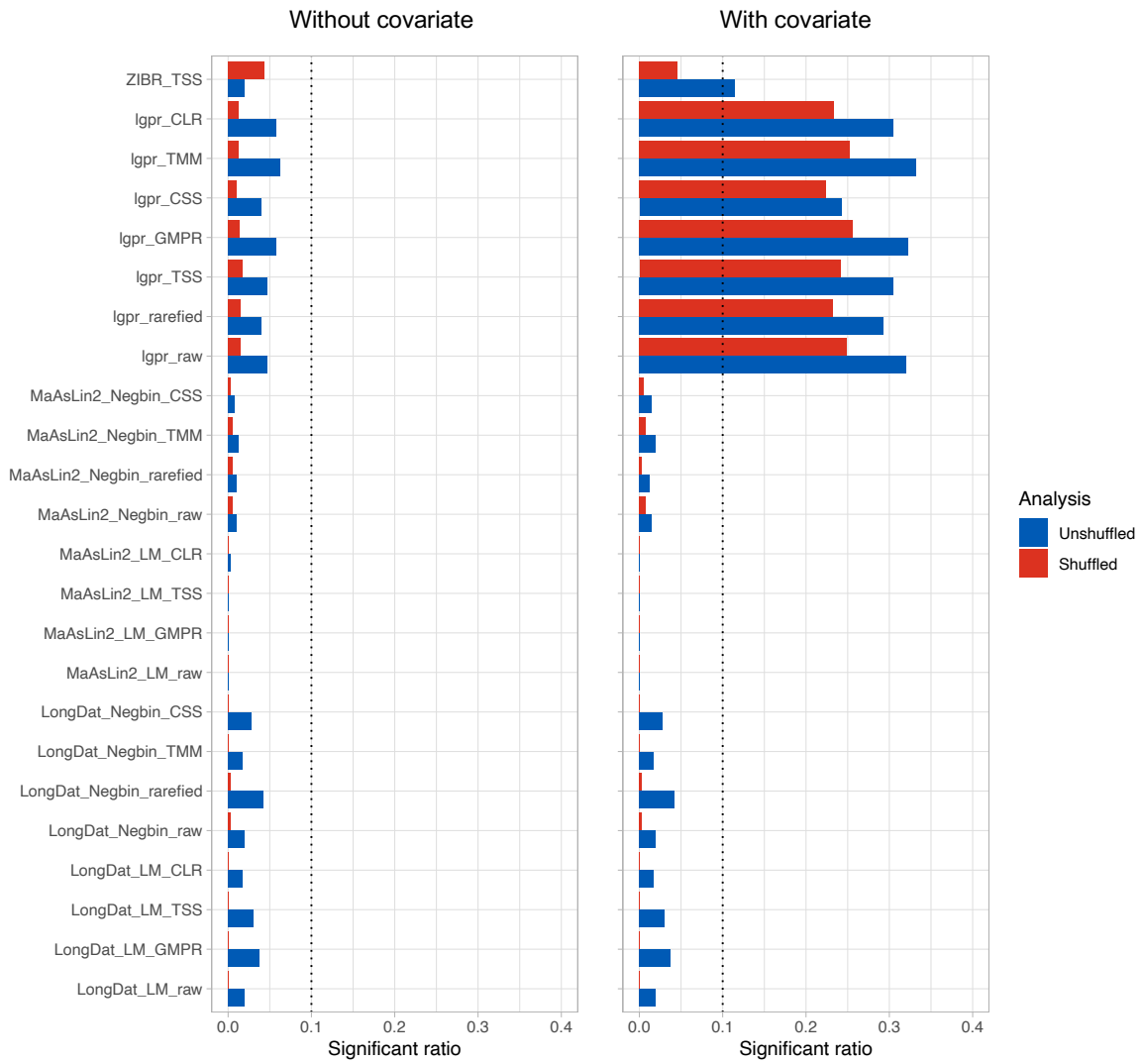

Figure 12. Bar charts illustrating the proportion of significant associations discovered in genus-level fasting microbiome data before and after shuffling. This is testing the significance of the time variable in the original (unshuffled) and time-shuffled datasets, without (left panel) and with (right panel) covariates included in the analyses. A significance threshold (BH-corrected) of 0.1 was established, and for every shuffled test, 100 simulations were conducted. Negbin: negative binomial model; LM: linear model; TMM: trimmed mean of M-values; raw: raw counts; rarefied: rarefied counts; CSS: cumulative-sum scaling; TSS: total-sum scaling; GMPR: geometric mean of pairwise ratios; CLR: centered log-ratio. This figure has been published in Chen *et al.*, 2023[69], as figure S16 (under CC BY 4.0 license).

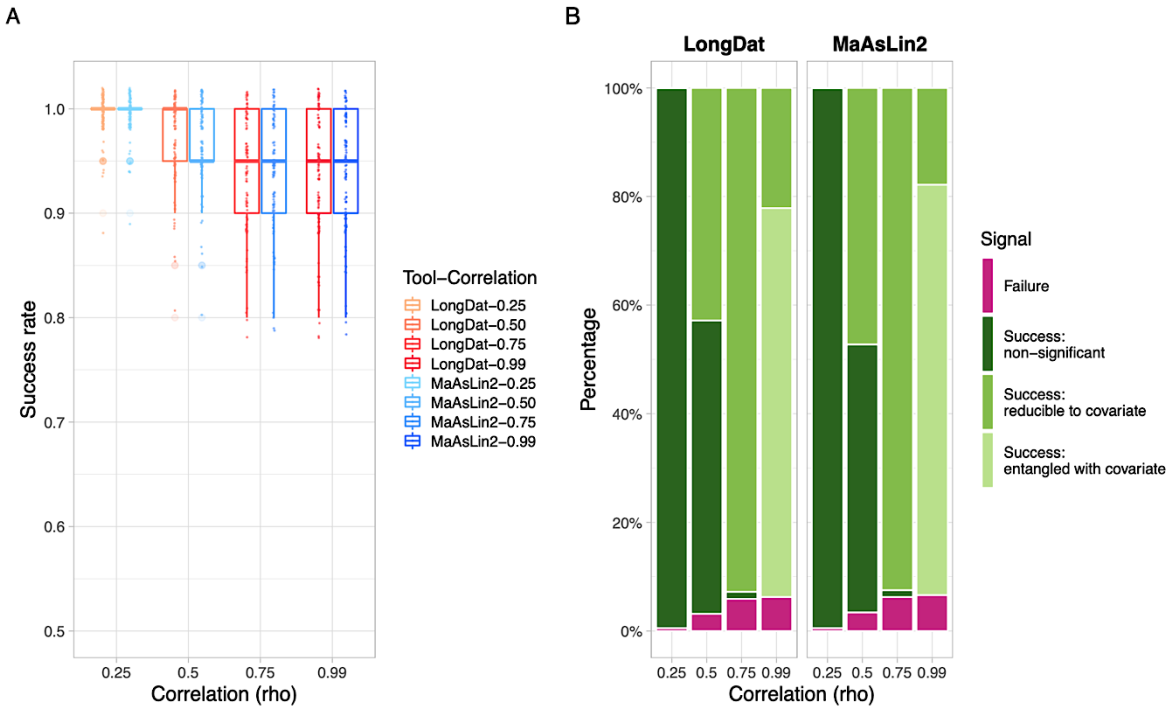

Figure 13. Assessment of covariate-sensitive analysis performance of LongDat and MaAsLin2 when applied to longitudinal data simulated by microbiomeDASim. To evaluate the performance of LongDat and MaAsLin2 in identifying covariates, simulated longitudinal data from microbiome-DASim was utilized. For this comparison, a dummy variable was introduced into the simulated dataset, and its significance was examined. The success criteria involve the tools designating the dummy variable as “non-significant”, “reducible to covariate” or “entangled with covariate” (where the time variable functions as the covariate in this case). Conversely, failure happens if a tool inaccurately identifies the dummy variable as significant while indicating the time variable as non-significant. (A) The success rates of LongDat and MaAsLin2 in detecting and interpreting covariate effects at various levels of correlation between the time and the dummy variable are depicted in the box plot. (B) The bar chart displays the distribution of success and failure rates across different correlation levels. Each correlation degree was tested through 100 simulations. This figure has been published in Chen et al., 2023[69], as figure 4 (under CC BY 4.0 license).

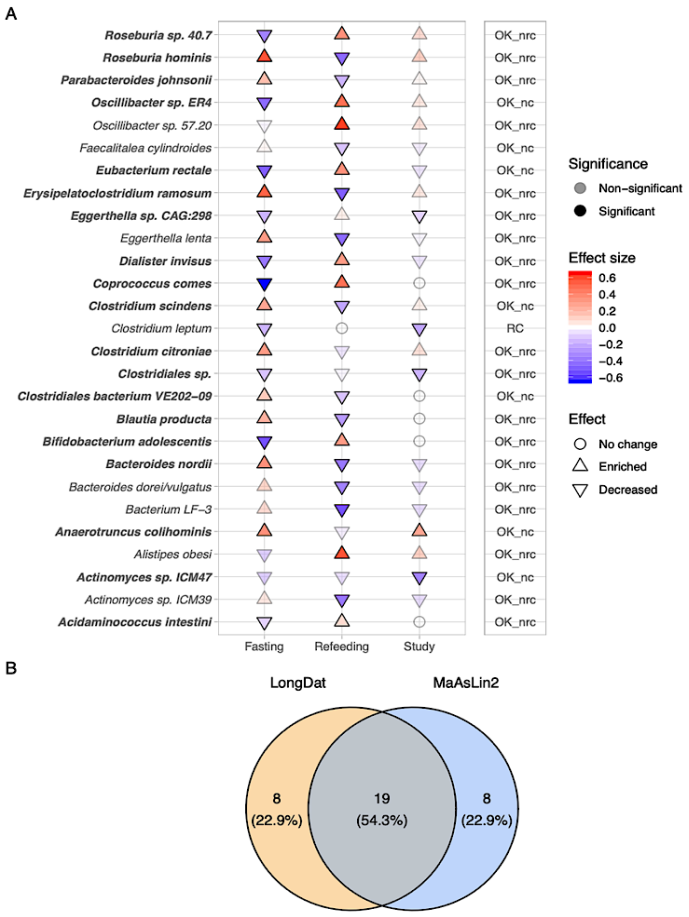

Figure 14. Comparison between LongDat and MaAsLin2 results of analyzing species-level microbiome data from Study 2. (A) The left panel of the cuneiform plot showcases the gut microbes (at the species level) which exhibit significant differences in abundance within at least one time interval in the study[70]. The time intervals are represented as "fasting" (day 0 to 7), "refeeding" (day 7 to 90), and "study" (day 0 to 90), reflecting their respective durations. Species highlighted in bold indicate those that showed significance in both the LongDat and MaAsLin2 results. The panel on the right provides the covariate status for every microbe. OK_nc: OK and no covariate. Time/intervention has a significant effect, and no covariate is found. OK_nrc: OK and not reducible to any covariate. The effect of time/intervention is statistically significant and remains unaffected by the inclusion of all other covariates in the model. RC: Effect reducible to covariate. Time/intervention demonstrates significance when analyzed independently, but its impact is better elucidated by the inclusion of a covariate in the model, while the reverse does not hold true. Microbes are deemed significant if their BH-corrected model test q-values are below 0.1 and their BH-corrected post-hoc test q-values are below 0.05. (B) The Venn diagram depicts the microbial species identified as significant by LongDat and MaAsLin2, with numbers representing the counts and percentages within each category. It is important to note that covariates were not considered in the MaAsLin2 analysis conducted in this study. This figure has been published in Chen *et al*., 2023[69], as figure 5 (under CC BY 4.0 license).

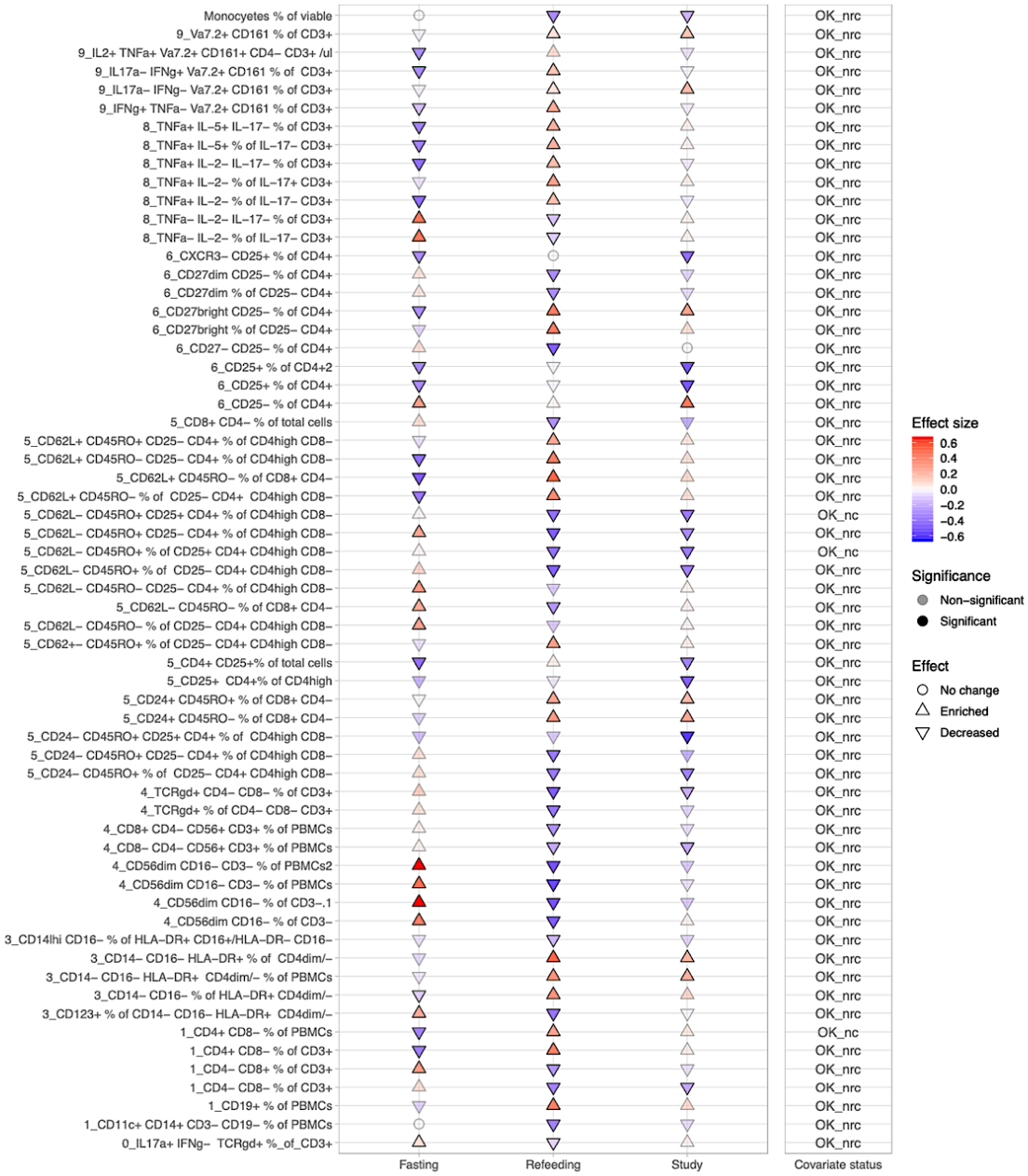

Figure 15. The result of the LongDat algorithm analyzing the immunome data (proportion data) in Study 2. The left panel of the cuneiform plot illustrates the immune cells that exhibit significant variations in their abundance within at least one time interval. The time intervals are categorized as "fasting" (day 0 to 7), "refeeding" (day 7 to 90), and "study" (day 0 to 90) to indicate the specific durations. The covariate status of each feature is presented on the right panel. OK_nrc: OK and not reducible to any covariate. The effect of time/intervention is statistically significant and remains unaffected by the inclusion of all other covariates in the model. Features with model test q-values below 0.1 and post-hoc test q-values below 0.05 are considered significant. This figure has been published in Chen *et al.*, 2023[69], as figure S18 (under CC BY 4.0 license).

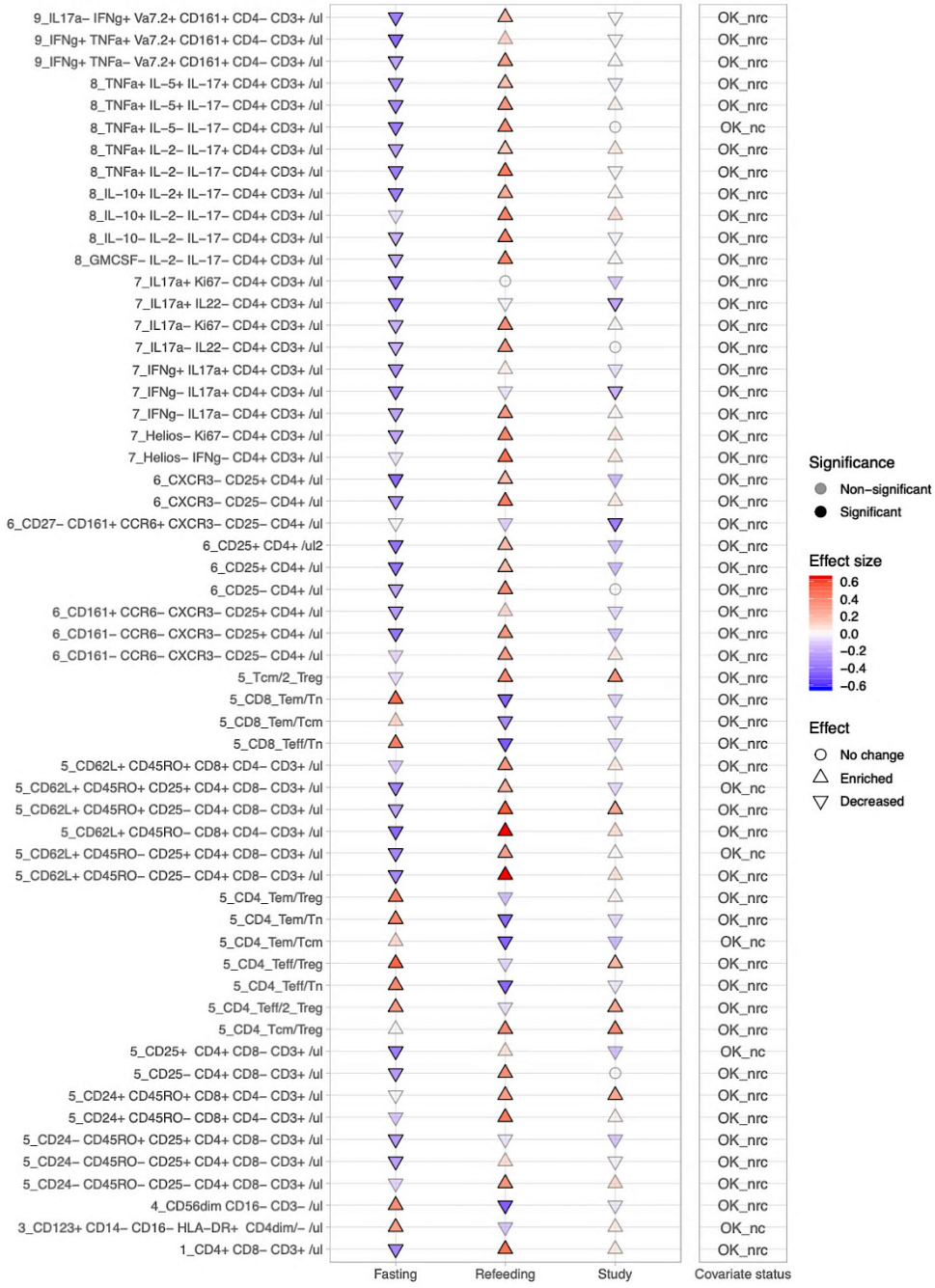

Figure 16. The result of the LongDat algorithm analyzing the immunome data (non-proportion data) in the Study 2. The left panel of the cuneiform plot illustrates the immune cells that exhibit significant variations in their abundance within at least one time interval. The time intervals are categorized as "Fasting" (day 0 to 7), "Refeeding" (day 7 to 90), and "Study" (day 0 to 90) to indicate the specific durations. The covariate status of each feature is presented on the right panel. OK_nrc: OK and not reducible to any covariate. The effect of time/intervention is statistically significant and remains unaffected by the inclusion of all other covariates in the model. Features with model test q-values below 0.1 and post-hoc test q-values below 0.05 are considered significant. This figure has been published in Chen *et al.*, 2023[69], as figure S19 (under CC BY 4.0 license).

3.2 Effects of fasting on the gut microbiome in MetS patients (Study 2[70])

Part of the content of this chapter has been published as a research article[70], the text can be similar but not identical.

In **Study 2[70]**, we investigated the impact of fasting on the gut microbiome and immune system in MetS patients. My collaborator, Dr. András Maifeld (ECRC, Müller/Dechend lab), and his colleagues collected and analyzed the data from a cohort of MetS patients either undergoing five days of fasting followed by three months of a modified DASH diet (fasting arm), or solely three months of DASH diet (DASH arm). Potential covariates such as medication, age, and sex were controlled for in our statistical analyses. Briefly, the results showed significant differences in microbial composition and host immune cell composition during fasting, which partially reversed after a three-month refeeding period. Fasting resulted in changes in immune cell composition, including a reduction in pro-inflammatory T cells and an increase in monocytes and specific T cell subsets. Moreover, fasting led to shifts in the abundance of commensal bacteria (e.g., *Eubacterium rectale* and *Coprococcus comes*) and alterations in microbial metabolic capacity related to SCFAs. The combination of fasting and a modified DASH diet led to a continuous decrease in systolic BP and body weight, surpassing the effects of the DASH diet alone. Analysis of the gut microbiome and immune system of BP responders (i.e., the patients whose systolic BP decreased significantly upon fasting and thus needed less antihypertensive drugs) revealed unique characteristics associated with successful fasting treatment, such as changes in specific microbial taxa (e.g., decreased Clostridiales, *Faecalibacterium,* and *Eubacterium* at baseline in BP-responders), and immune features. Network analysis showed correlations between certain immune cell populations, microbial taxa, and BP. These findings suggest that fasting can influence the gut microbiome and immunome, leading to improvements in BP and body weight in individuals with MetS.

Within this research project, I made a direct contribution by conducting the analysis of enterotypes. Utilizing the DirichletMultinomial R package, I applied this statistical method to the microbiome data obtained from the fasting arm of the study. The purpose was to classify the gut microbiomes of the participants into distinct enterotypes, representing specific clusters or groupings based on their microbial composition. There are four distinct

enterotypes identified, namely *Ruminococcus*, *Prevotella*, *Bacteroides* 1, and *Bacteroides* 2 in our study (Figures 17, 18). Based on the findings presented in Figures 19 A-C, an intriguing pattern emerged from the analysis: a higher percentage of BP responders experienced changes in their enterotypes during the intervention period compared with non-responders (47% vs. 29%). However, it is worth noting that the chi-squared test conducted on the contingency table did not yield significant results ($p = 0.65$). Nevertheless, this finding suggests a potential connection between changes in enterotype and the physiological response to the fasting intervention.

In addition to the analysis of enterotypes, I have significantly contributed to this project by developing the LongDat algorithm. This algorithm draws its roots from the scripts initially conceived by Prof. Dr. Sofia Forslund (ECRC), which is to disentangle the influences of covariates (e.g., medication) from the effects of fasting. My contribution transcends the mere refinement of existing informal in-house scripts; rather, it represents a comprehensive overhaul involving substantial improvements, effectively evolving Longdat into a markedly enhanced algorithm. I dedicated substantial effort to rewriting the codes, focusing on conciseness, readability, and transparency to enhance the reproducibility of the research findings. Aside from this, I incorporated various user-friendly features to streamline the analysis process. Firstly, I added a covariate selection step to optimize time efficiency by including only relevant variables in the analysis, such that the burden of analyzing unnecessary variables is alleviated. Secondly, I differentiated the functions for continuous and discrete time variables, customizing them to their respective characteristics. For example, the effect size calculation differs between the two, using correlation for continuous variables and Cliff's delta for discrete variables. Thirdly, acknowledging the diverse nature of data encountered in high-dimensional analyses, I expanded the package's usability to accommodate different data types, such as count, binary, ordinal, and measurement data, by incorporating GLMMs into the package. Moreover, I introduced two novel functions to enhance the overall user experience. The first function simplifies the data preparation process, making it easier for researchers to input their data into LongDat seamlessly. The second function allows for the visualization of result tables, aiding researchers in interpreting and presenting their findings effectively. With these features, LongDat is a comprehensive pipeline that enables users to perform covariate-aware analysis on high-dimensional data with ease, from raw data to visualization. Finally, I revised the script for submission to The Comprehensive R Archive Network (CRAN),

ensuring the package's availability to the scientific community and promoting robust biomarker search by accounting for covariates. The details of the LongDat package, including its methodology (Section 2.1) and results (Section 3.1), can be found in the respective sections. The reanalysis of the gut microbiome and immunome data in this project is demonstrated in Figures 14-16. The figures clearly depict the effect size and statistical significance of changes observed during the intervention, while considering the covariate status. These visual representations effectively capture the dynamics and impact of each feature throughout the study, enabling users to easily identify patterns and focus on their targeted features. The latest LongDat algorithm was employed to reanalyze the gut microbiome data from the fasting group in this study. Table 2 presents the species that exhibit significant enrichment or depletion during the fasting and refeeding stages. The table highlights the influences of the covariates on the effect of the time variable, which is the proxy of fasting or refeeding treatment. A visualization of this result table is shown in Figure 14A.

In short conclusion, this study examined the effects of fasting on the gut microbiome and immune system in MetS patients. The results showed significant changes in microbial composition, immune cell composition, and metabolic capacity during fasting. These findings suggest that fasting can influence the gut microbiome and immunome, leading to improvements in BP and body weight in individuals with MetS. My contribution to the project involves analyzing enterotypes and developing the LongDat algorithm, which enhances reproducibility and facilitates covariate-aware analysis of high-dimensional data in the future.

Table 2. Result table of the reanalysis of the gut microbiome data in the fasting group using the LongDat algorithm. This table is adapted from tables S2 and S3 that are published in Chen *et al*., 2023[69] (under CC BY 4.0 license).

Feature	Signal	Fasting effect	Refeeding effect	Study effect	Covariates
Acidaminococcus intestini	OK_nrc	Decreased	Enriched	NS	ACE inhibitor, antidiabetics, statin, AT2 blocker
Actinomyces sp. ICM39	OK_nrc	NS	Decreased	NS	Beta blocker, thyroid
*Actinomyces sp.*ICM47	OK_nc	NS	NS	Decreased	-
Alistipes obesi	OK_nrc	NS	Enriched	NS	Metformin, statin, xanthan oxidase inhibitor
Anaerotruncus colihominis	OK_nc	Enriched	NS	Enriched	-
Bacteroides nordii	OK_nrc	Enriched	Decreased	NS	AT2 blocker, metformin, PPI, statin, vitamin D, xanthan oxidase inhibitor
Bacteroides sp. *dorei*/*vulgatus*	OK_nrc	NS	Decreased	NS	Thyroid
Bifidobacterium adolescentis	OK_nrc	Decreased	Enriched	NS	Thyroid
Blautia producta	OK_nrc	Enriched	Decreased	NS	Beta blocker, PPI, thyroid
Clostridiales bacterium VE202.09	OK_nc	Enriched	Decreased	NS	-
Clostridium scindens	OK_nc	Enriched	Decreased	NS	-
Coprococcus comes	OK_nrc	Decreased	Enriched	NS	Beta blocker, PPI
Dialister invisus	OK_nrc	Decreased	Enriched	NS	ACE inhibitor, AT2 blocker, statin, thyroid
Eggerthella lenta/ *Clostridioides difficile*	OK_nrc	Enriched	Decreased	NS	Beta blocker, calcium antagonist, thyroid
Eggerthella sp. CAG 298	OK_nrc	Decreased	NS	Decreased	Diuretic, thyroid
Erysipelotrichaceae sp./ *Coprobacillus*/ *Erysipelatoclostridium ramosum*	OK_nrc	Enriched	Decreased	NS	ACE inhibitor, AT2 blocker, calcium antagonist, PPI, thyroid vitamin D
Eubacterium rectale	OK_nc	Decreased	Enriched	NS	-
Faecalitalea cylindroides	OK_nc	NS	Decreased	NS	-
Oscillibacter sp. 57_20	OK_nrc	NS	Enriched	NS	PPI, xanthan oxidase inhibitor
Oscillibacter sp.ER4	OK_nc	Decreased	Enriched	NS	-
Parabacteroides johnsonii	OK_nrc	Enriched	Decreased	NS	Thyroid

Roseburia hominis	OK_nrc	Enriched	Decreased	NS	PPI
Roseburia sp. 40_7	OK_nrc	Decreased	Enriched	NS	AT2 blocker
Clostridium citroniae	OK_nrc	Enriched	NS	NS	Beta blocker, PPI, thyroid, xanthan oxidase inhibitor
Clostridium leptum	RC	Decreased	NS	Decreased	Diuretic*, metformin, xanthan oxidase inhibitor
Bacterium LF 3	OK_nrc	NS	Decreased	NS	Xanthan oxidase inhibitor,
Unknown Clostridiales Family XIII Incertae Sedis	OK_nrc	Decreased	NS	Decreased	Antidiabetics, beta blocker

AT2 blocker = Angiotensin II receptor blocker

ACE inhibitor = Angiotensin-converting enzyme inhibitors

PPI = Proton pump inhibitors

*Covariates in red indicate that the effect of the time variable (proxy of the treatment) is reducible to the effect of the covariate.

OK_nc: OK and no covariate. Time/intervention has a significant effect, and no covariate is found. OK_nrc: OK and not reducible to any covariate. The effect of time/intervention is statistically significant and remains unaffected by the inclusion of all other covariates in the model. RC: Effect reducible to covariate. Time/intervention demonstrates significance when analyzed independently, but its impact is better elucidated by the inclusion of a covariate in the model, while the reverse does not hold true. Microbes are deemed significant if their BH-corrected model test q-values are below 0.1 and their BH-corrected post-hoc test q-values are below 0.05.

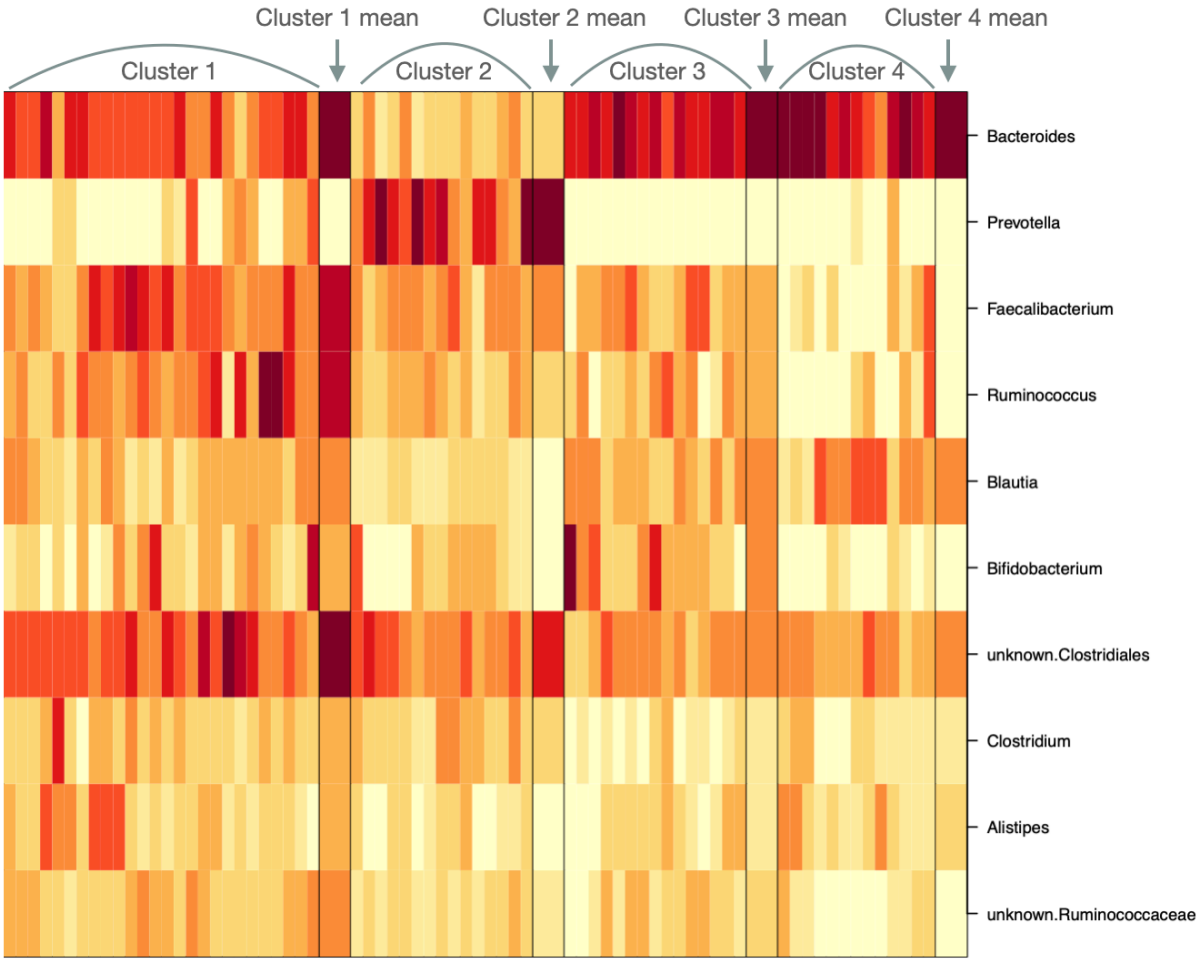

Figure 17. The fecal microbiome shotgun sequencing data from the fasting arm was subjected to enterotype classification using the DirichletMultinomial R package. Each narrow column represents a single sample, while the broader columns represent the group means. The color scale represents squared-root counts, with darker colors indicating higher counts. Based on this analysis, four distinct clusters were identified and designated as specific enterotypes based on the dominant microbial taxa. The *Ruminococcus* enterotype was assigned to cluster one, while cluster two was classified as the *Prevotella* enterotype. Clusters three and four have a high proportion of *Bacteroides*, but cluster four is depleted of *Faecalibacterium*. Therefore, cluster three was designated as the *Bacteroides* 1 enterotype, and cluster four was assigned as the *Bacteroides* 2 enterotype. Source: own representation.

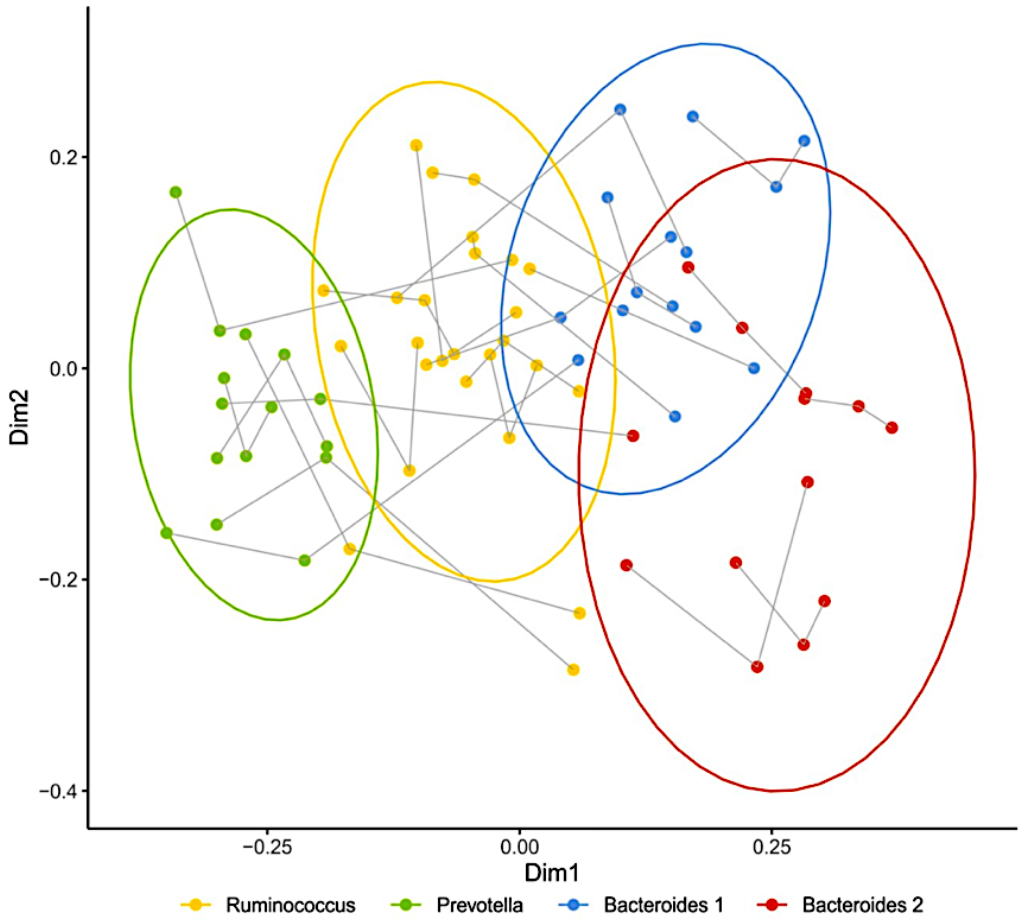

Figure 18. The PCoA (Bray-Curtis distance) representing the variation in the gut microbiome community at the genus level. Paired samples from the same individual are connected by grey lines. The ellipses indicate the 95% confidence interval. This figure has been published in Maifeld et al., 2021[70], as figure S7 (reproduced with permission from Springer Nature, under CC BY 4.0 license).

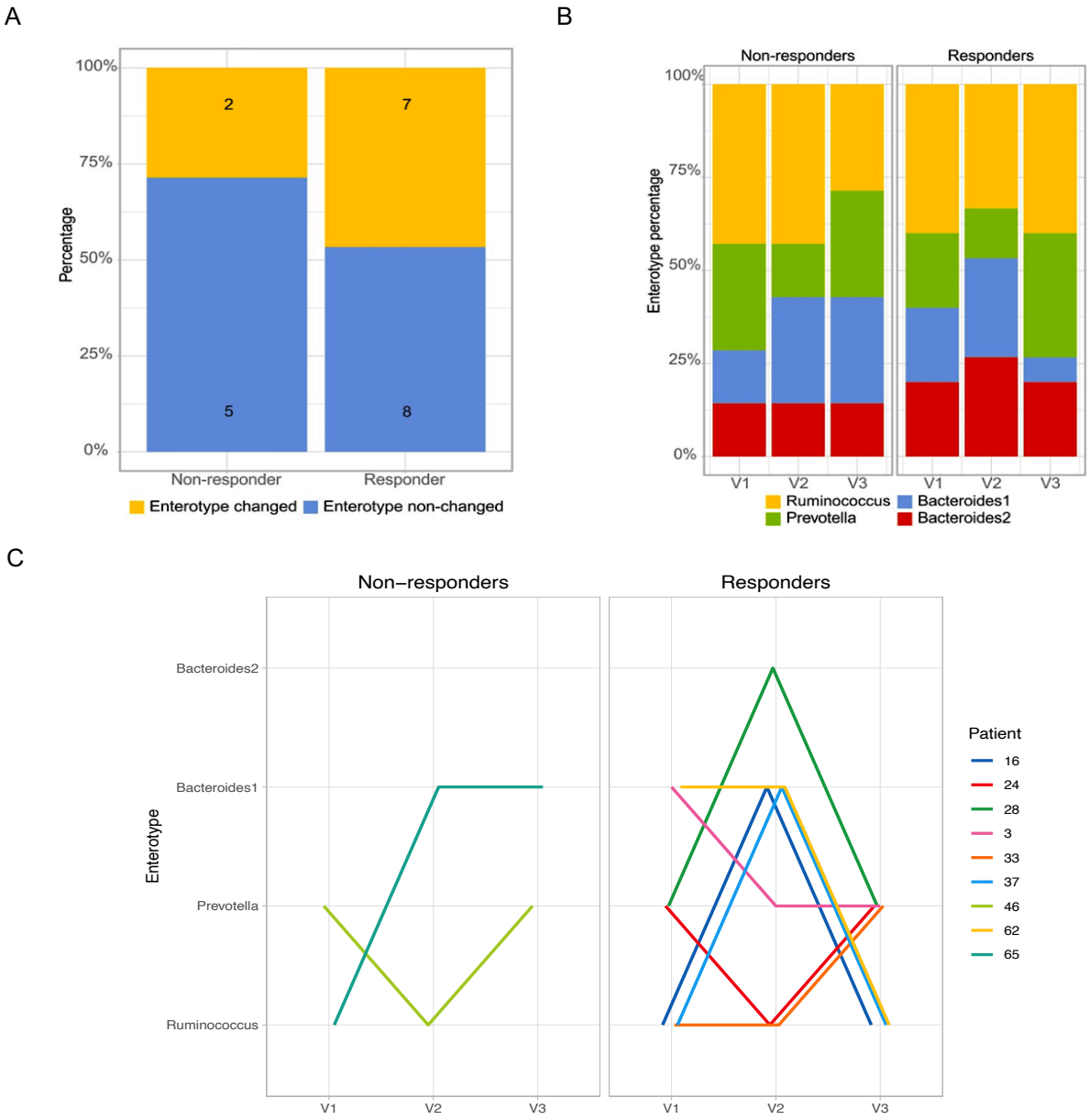

Figure 19. Comparison of the enterotyping results between responders and non-responders. (A) The bar plot shows the percentage of individuals whose enterotypes changed or remained unchanged throughout the study. The raw counts of samples falling within each outcome group are denoted by the numbers. (B) The bar plot displays the proportion of enterotypes observed at each time point. V1 = before fasting; V2 = after seven days of fasting; V3 = after three months of DASH diet (refeeding stage). (C) The line plot illustrates the enterotypes of the patients whose enterotype was altered throughout the study in BP responders and non-responders. Each patient is represented by a colored line. Figures A and B have been published in Maifeld et al., 2021[70], as figure S7 (reproduced with permission from Springer Nature, under CC BY 4.0 license). Source of figure C: own representation.

3.3 Gut microbial colonization affects hypertensive organ damage in mice (Study 3[71])

Part of the content of this chapter has been published as a research article[71], the text can be similar but not identical.

In **Study 3[71]**, we quantified the impact of gut microbiome on inflammation and organ damage associated with HTN in mice. In brief, my collaborator, Dr. Ellen Avery (ECRC, Müller/Dechend lab), and other co-authors conducted experiments using GF and COL mice to investigate the influence of microbial colonization on HTN-induced organ damage. Our results showed that upon HTN induction, GF mice exhibited a significantly larger extent of albuminuria and a stronger increase in T-helper cells and leukocytes in the kidney compared with COL mice. Additionally, GF mice displayed accentuated kidney fibrosis, suggesting a heightened susceptibility of the kidney to microbial influence. However, cardiac damage showed similar levels in both groups. Within COL mice, HTN triggered an alteration to the gut microbiome composition when compared with the sham group, such as a decreased abundance of *Dubosiella newyorkensis* and *Bifidobacterium pseudologum*, and an increased abundance of *Enterococcus*. To explore the role of microbiome-derived metabolites, we conducted serum metabolome analysis. The analysis revealed significant differences in metabolite profiles between GF and COL mice upon HTN induction. Interestingly, various classes of metabolites showed similar changes in both groups, indicating a microbiome-independent effect. Furthermore, there was little overlap in the individual metabolites whose abundance changed in response to HTN within GF or COL mice. The serum metabolome was significantly influenced by the microbiome, as evidenced by the correlations observed between metabolites and microbial species. Notably, GF mice lacked important anti-hypertensive metabolites, including SCFAs such as propionate and butyrate, which are hypothesized to contribute to their observed phenotype. Moreover, the disturbed inflammatory status of GF mice under HTN induction, along with an increase in specific immune cells, suggests that the conditioning of naive T-cells in GF and COL mice can influence the polarization of pro-inflammatory T-cells and the severity of organ damage in HTN. Our findings highlight the notable influence of the microbiome and its metabolites, such as SCFAs, on immune cells associated with HTN and the observed damage in the heart and kidneys.

In this research project, my contribution focuses on three key aspects. Firstly, a thorough examination was conducted to explore the correlations between the serum metabolites and the fecal microbiome, aiming to uncover potential associations between these components. The analysis, illustrated in Figure 20, unveiled a wide range of significant correlations observed between the fecal microbiome and the serum metabolites, as well as the functional profile (represented by KEGG modules) and the serum metabolites. Microbial species, including *Lactobacillus johnsonii*, *Enterococcus.faecium/hirae*, *Bifidobacterium pseudolongum*, and *Dubosiella newyorkensis* displayed significant associations with various metabolites such as sphingomyelins, phosphatidylcholines, triacylglycerides, and amino acids. These findings provide valuable insights into the intricate interplay between the composition of the fecal microbiome and the abundance of specific metabolites in the serum. Furthermore, as anticipated, the analysis also revealed numerous significant correlations between the functional profile and the metabolites, further enhancing our understanding of the complex relationships between the functional activities of the microbiome and the comprehensive metabolite landscape.

Secondly, I investigated the similarity between the fecal and cecal microbiome collected in this study and also identified the important factors for microbiome and metabolome compositions by utilizing the Mantel test (Table 3). The Mantel test, a statistical method widely used in ecological studies, allowed the estimation of correlation between two distance matrices, particularly suitable for analyzing multivariate data such as microbial abundance. The results of the Mantel test provided a p-value and the Mantel r coefficient, ranging from -1 to 1, where values near -1 or 1 suggest strong negative or positive correlations, respectively, while 0 suggests no relationship. In addition, I employed the partial Mantel test, an extension of the Mantel test, to assess the relationship between matrices while accounting for the influence of a potential covariate (Table 4). This approach enabled the assessment of the unique contributions of each variable and their independent associations by statistically controlling the effect of a third matrix. Hence, the partial Mantel test is another example of partitioning out the effect of covariates to achieve a more accurate result. Throughout this study, I conducted multiple rounds of Mantel and partial Mantel tests to explore the associations among various distance matrices, including the fecal microbiome, cecal microbiome, metabolome, treatment, and colonization status, as presented in Tables 3 and 4. The Mantel test results revealed a strong and positive correlation (Mantel r = 0.99) between the distance matrices of the fecal and cecal microbiome,

confirming their highly similar structures. Additionally, the metabolome distance matrix exhibited significant positive correlations with both the fecal and cecal microbiome distance matrices, indicating a close relationship between the metabolome and microbiome, consistent with the findings presented in the heatmap (Figure 20). Furthermore, the partial Mantel test outcomes demonstrated that the impact of treatment (Ang/Sham) on the microbiome was more pronounced than its origin (fecal/cecal), which aligns with the previous finding of high similarity between the fecal and cecal microbiome. Lastly, the results indicated that both treatment (Ang/Sham) and colonization status (GF/COL) significantly influenced the metabolome. In summary, the Mantel and partial Mantel tests provided insights into the similarity between the fecal and cecal microbiome, the association between the metabolome and microbiome, and the importance of treatment and colonization status in shaping these metabolome compositions.

Finally, for the purpose of comparing the results with existing literature, a comparative analysis was conducted to assess the congruity between the findings of this study and the Pluznick[121] study, which was a research exploring the impact of HTN on the microbiome and metabolome in GF and CONV mice. The raw data of the Pluznick study were processed by Dr. Ellen Avery (ECRC, Müller/Dechend lab) and Dr. Ulrike Löber (ECRC, Forslund lab) to ensure comparability with this study. Unexpectedly, a notable disparity was observed at the genus level when comparing the microbiome profiles of the COL mice in our study and the Pluznick dataset, where the microbiome clustered based on study rather than treatment (Figure 21A). This discrepancy led us to hypothesize that the metabolome response would exhibit a similar pattern. Intriguingly, when comparing the metabolome data from the Pluznick study with our own (referred to as Avery), a significantly greater overlap was found in the response of the metabolites to HTN among the GF groups, compared with the COL/CONV groups (Figures 21B, 21C). That is, there is a notable reduction in dissimilarity in the impact of HTN on serum metabolites of GF mice across these two datasets. This implies that the congruity of the serum metabolome in the GF groups in the two datasets is greater than that of the COL groups. These findings provide supporting evidence for the notion that the composition of the COL microbiome exerts a large influence on the alterations observed in the serum metabolome in response to HTN.

In conclusion, **Study 3**[71] demonstrates the significant impact of gut microbiome on hypertensive disease. GF mice showed worse organ damage, especially in the kidneys, compared with COL mice. The composition of immune cells and inflammatory state, as well as the metabolome, differed between the two groups. These findings highlight the importance of gut microbiome in the development and progression of HTN. In this research project, my contribution focused on exploring the correlations between serum metabolites, fecal and cecal microbiome, and their potential implications in various biological processes. In addition, I provided valuable insights into the similarity between the fecal and cecal microbiome, the association between the metabolome and microbiome, and the influence of treatment and colonization status on these metabolome compositions. Finally, I contributed to the validation of our findings by comparing our study with an independent dataset, emphasizing the significant influence of the gut microbiome on serum metabolome changes as a response to HTN.

Table 3. Mantel test results. Source: own representation.

Variable 1	Variable 2	Mantel p-value and r
Fecal microbiome (species) distance matrix (Bray-Curtis)	Cecal microbiome (species) distance matrix (Bray-Curtis)	0.001*, 0.99
Metabolome distance matrix (Euclidean)	Fecal microbiome (species) distance matrix (Bray-Curtis)	0.005*, 0.28
Metabolome distance matrix (Euclidean)	Cecal microbiome (species) distance matrix (Bray-Curtis)	0.022*, 0.42

* Denotes significance ($p < 0.05$)

Table 4. Partial Mantel test results. Source: own representation.

Variable 1	Variable 2	Variable 3	p12.3, r12.3	p13.2, r13.2
Microbiome (species) distance matrix (Bray-Curtis)	Treatment congruence (Same Ang/Sham or not)	Microbiome origin congruence (Same fecal/cecal or not)	0.005*, 0.28	0.41, -0.027
Metabolome distance matrix (Euclidean)	Treatment congruence (Same Ang/Sham or not)	Colonization congruence (Same GF/COL or not)	0.024*, 0.18	0.002*, 0.23

* Denotes signifiance ($p < 0.05$)

p12.3 is the Mantel p-value of the correlation between variables 1 and 2 when controlling for variable 3, and vice versa.

r12.3 is the Mantel r of the correlation between variables 1 and 2 when controlling for variable 3, and vice versa.

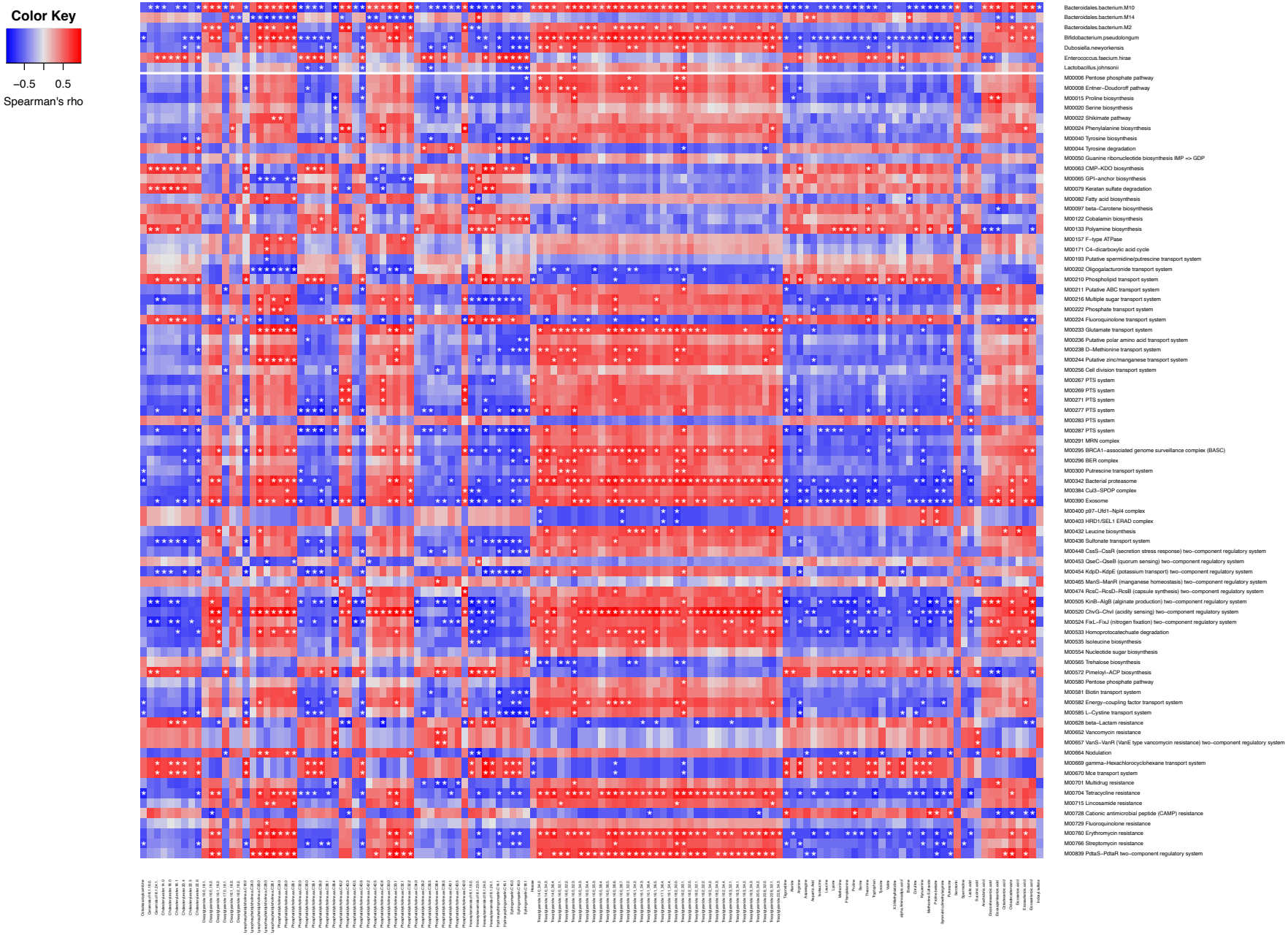
Color Key
−0.5
0.5
Spearman's rho
Bacteroidales.bacterium.M10
Bacteroidales.bacterium.M14
Bacteroidales.bacterium.M2
Bifidobacterium.pseudolongum
Dubosiella.newyorkensis
Enterococcus.faecium.hirae
Lactobacillus.johnsonii
M00006 Pentose phosphate pathway
M00008 Entner−Doudoroff pathway
M00015 Proline biosynthesis
M00020 Serine biosynthesis
M00022 Shikimate pathway
M00024 Phenylalanine biosynthesis
M00040 Tyrosine biosynthesis
M00044 Tyrosine degradation
M00050 Guanine ribonucleotide biosynthesis IMP => GDP
M00063 CMP−KDO biosynthesis
M00065 GPI−anchor biosynthesis
M00079 Keratan sulfate degradation
M00082 Fatty acid biosynthesis
M00097 beta−Carotene biosynthesis
M00122 Cobalamin biosynthesis
M00133 Polyamine biosynthesis
M00157 F−type ATPase
M00171 C4−dicarboxylic acid cycle
M00193 Putative spermidine/putrescine transport system
M00202 Oligogalacturonide transport system
M00210 Phospholipid transport system
M00211 Putative ABC transport system
M00216 Multiple sugar transport system
M00222 Phosphate transport system
M00224 Fluoroquinolone transport system
M00233 Glutamate transport system
M00236 Putative polar amino acid transport system
M00238 D−Methionine transport system
M00244 Putative zinc/manganese transport system
M00256 Cell division transport system
M00267 PTS system
M00269 PTS system
M00271 PTS system
M00277 PTS system
M00283 PTS system
M00287 PTS system
M00291 MRN complex
M00295 BRCA1−associated genome surveillance complex (BASC)
M00296 BER complex
M00300 Putrescine transport system
M00342 Bacterial proteasome
M00384 Cul3−SPOP complex
M00390 Exosome
M00400 p97−Ufd1−Npl4 complex
M00403 HRD1/SEL1 ERAD complex
M00432 Leucine biosynthesis
M00436 Sulfonate transport system
M00448 CssS−CssR (secretion stress response) two−component regulatory system
M00453 QseC−QseB (quorum sensing) two−component regulatory system
M00454 KdpD−KdpE (potassium transport) two−component regulatory system
M00465 ManS−ManR (manganese homeostasis) two−component regulatory system
M00474 RcsC−RcsD−RcsB (capsule synthesis) two−component regulatory system
M00505 KinB−AlgB (alginate production) two−component regulatory system
M00520 ChvG−ChvI (acidity sensing) two−component regulatory system
M00524 FixL−FixJ (nitrogen fixation) two−component regulatory system
M00533 Homoprotocatechuate degradation
M00535 Isoleucine biosynthesis
M00554 Nucleotide sugar biosynthesis
M00565 Trehalose biosynthesis
M00572 Pimeloyl−ACP biosynthesis
M00580 Pentose phosphate pathway
M00581 Biotin transport system
M00582 Energy−coupling factor transport system
M00585 L−Cystine transport system
M00628 beta−Lactam resistance
M00652 Vancomycin resistance
M00657 VanS−VanR (VanE type vancomycin resistance) two−component regulatory system
M00664 Nodulation
M00669 gamma−Hexachlorocyclohexane transport system
M00670 Mce transport system
M00701 Multidrug resistance
M00704 Tetracycline resistance
M00715 Lincosamide resistance
M00728 Cationic antimicrobial peptide (CAMP) resistance
M00729 Fluoroquinolone resistance
M00760 Erythromycin resistance
M00766 Streptomycin resistance
M00839 PdtaS−PdtaR two−component regulatory system

Figure 20. The heatmap depicting the correlations between serum metabolites, bacterial species, and functional microbial modules within the COL group. Serum metabolites are on the x-axis, while bacterial species and functional microbial modules are on the y-axis. Variables that showed significant alterations between the HTN and sham groups in the Wilcoxon rank-sum test are selected. Spearman's correlations were calculated, and the results were adjusted for multiple testing with BH-correction. White asterisk indicates the Spearman's $q < 0.05$. This figure was created by Chia-Yu Chen, and its adapted version has been published in Avery et al., 2022[71], as figure S7 (under CC BY-NC 4.0 license). Reprinted by permission of Oxford University Press on behalf of the European Society of Cardiology. Dr. Ellen Avery and Dr. Ulrike Löber generated and annotated the metabolomics and microbiome data, and I did the analysis and created this figure.

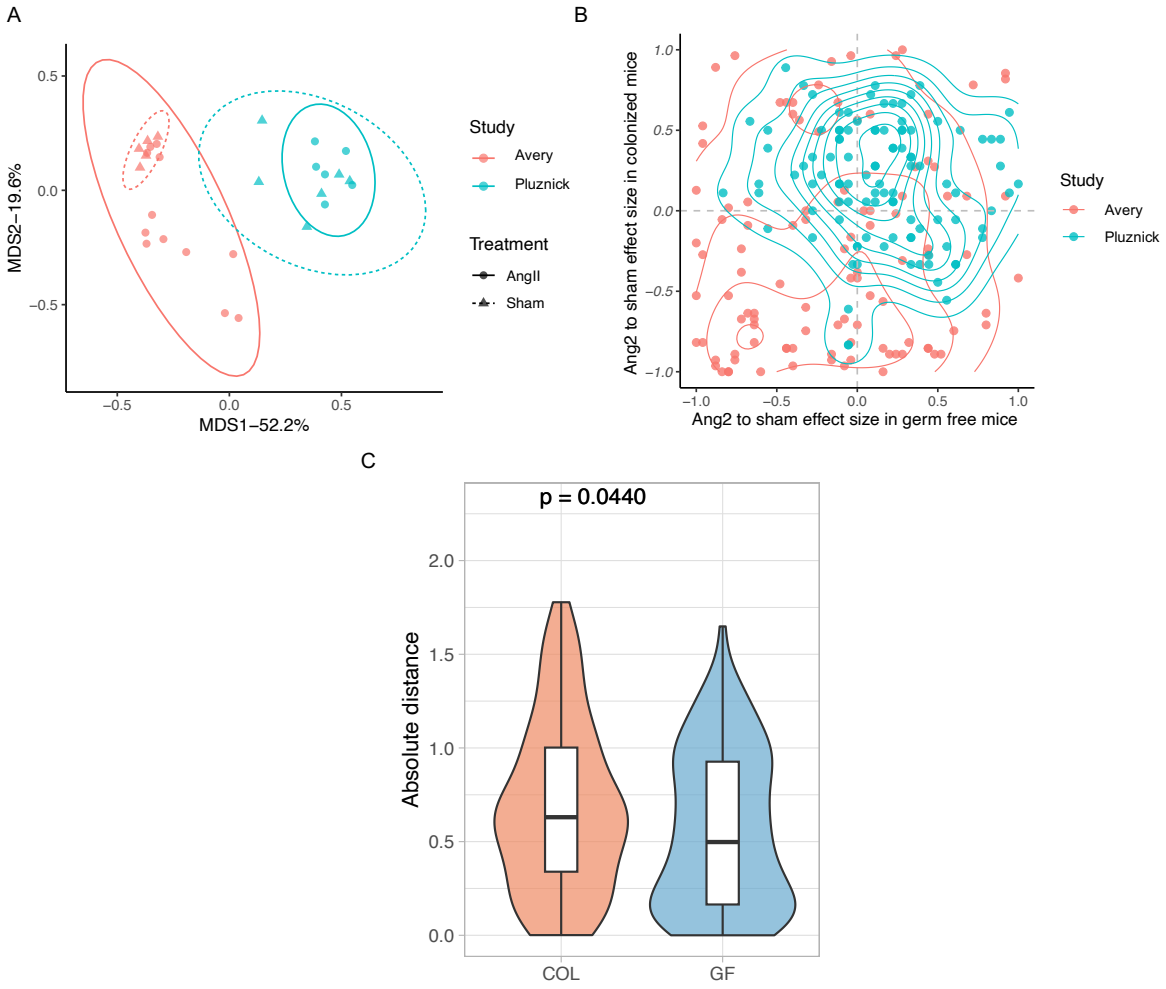

Figure 21. Comparison of the serum metabolites between the Pluznick and Avery studies. (A) Principal coordinate analysis (PCoA) shows the dissimilarities between the microbiome (genus level) of the COL mice which underwent different treatment from each study, which was done using Euclidean distance scaling of microbiome data published by Cheema and Pluznick[121] (referred to as Pluznick) and our data (referred to as Avery). (B) The metabolites measured in the serum of mice in both Pluznick and Avery studies are included. The Y-axis displays the effect size of HTN compared with sham in COL mice, while the X-axis depicts the effect size of HTN compared with sham in GF mice. The contours indicating densities are added by using the function geom_density_2d() in the ggplot2 package. (C) The quantification of the distance in Figure 21B within each metabolite between the GF and COL groups from the Pluznick and Avery studies is shown. The y-axis shows the absolute value of the difference in the effect size between the two studies. The statistical significance, indicated by $p < 0.05$, was determined using the Wilcoxon rank-sum test. This figure was created by Chia-Yu Chen and its adapted version has been published in Avery et al., 2022[71], as figure S10 (under CC BY-NC 4.0 license). Reprinted by permission of Oxford University Press on behalf of the European Society of Cardiology. Dr. Ellen Avery annotated the metabolomics data from Pluznick and Avery studies, and I created these plots.

4. Discussion

4.1 Short summary of the results

The main goal of this thesis is to advance our understanding of the intricate relationship between the gut microbiome and cardiovascular and kidney diseases in a covariate-aware manner. To facilitate this investigation, a specialized algorithm named LongDat[69] has been developed, specifically designed for the covariate-sensitive analysis of high-dimensional longitudinal data. By incorporating LongDat into the analysis pipeline, we were able to disentangle the effects of covariates, such as medication and baseline characteristics, from the specific effects of fasting and the DASH diet. LongDat is subjected to benchmarking against existing tools, with the results of this assessment, based on either simulated or real data, substantiating LongDat's efficiency and competency in comparison to its counterparts. Covariate-sensitive methods were implemented throughout **Studies 2[70] and 3[71]**. In **Study 2[70]**, significant changes in microbial composition, immune cell composition, and metabolic capacity during fasting were found. The findings suggest that fasting influences the gut microbiome and immunome, leading to improvements in BP and body weight in individuals with MetS. In **Study 3[71]**, it is found that the GF mice displayed more severe kidney damage and distinct metabolic profiles compared with COL mice, highlighting the influence of the presence of gut microbiome and microbiome-derived metabolites on immune cells and organ damage in HTN. Overall, these findings provide valuable insights into the role of the host-microbiome interaction in the development and progression of CVD and kidney diseases, as well as the potential therapeutic implications of targeting the gut microbiome.

4.2 Interpreting and integrating results with the current state of research

To the best of my knowledge, LongDat presented in **Study 1[69]** is the first algorithm developed specifically to address the challenge of multiple covariates commonly encountered in longitudinal data analysis, particularly in the field of biomedical studies. Initially developed for microbiome analysis, LongDat can be adapted for other types of high-dimensional data with robust methods like GLMMs and non-parametric tests. LongDat automates the analysis process, eliminating the need for users to program linear modeling functions. LongDat provides standardized output, enabling easy integration, comparison, and visualization of findings. When compared with existing longitudinal data

analyzing tools that also allow the inclusion of covariates during analysis[64,66,68,104], the LongDat algorithm proves to be highly effective and efficient in several key aspects. Firstly, it demonstrates acceptable speed, allowing for timely analysis of large-scale longitudinal datasets. This efficiency is particularly beneficial when dealing with extensive data sets characterized by numerous time points and subjects, which are common in biomedical studies. Moreover, LongDat exhibits low memory usage, minimizing the computational resources required for data analysis. This advantage is especially crucial when working with high-dimensional longitudinal data, where memory constraints can significantly impact the feasibility of analyses. Most importantly, LongDat excels in its ability to handle multiple covariates, a vital feature in studying complex relationships such as those involving the gut microbiome, immune system, and cardiovascular health. LongDat stands out among other existing tools, particularly in scenarios with multiple covariates, owing to its distinctive approach to handling them. Unlike other methods, LongDat adopts a unique strategy of iterating over each covariate through parallel models, leading to a more robust and effective analysis. By accommodating numerous covariates, the LongDat algorithm enables comprehensive analyses, leading to more accurate results.

The implementation of the LongDat algorithm, the mixed effect models, Mantel and partial Mantel tests in this thesis yields critical insights into the complicated interplay between the gut microbiome, immune system, and cardiovascular and kidney health, specifically by disentangling the effect of covariates and treatment in the analyses. In **Study 2[70]**, fasting induced changes in the population levels of key commensal bacteria, which were subsequently restored upon refeeding[70]. LongDat goes above and beyond merely identifying the abundance of altered features (e.g., gut microbial species) during fasting and refeeding. It goes a step further by pinpointing the covariates that have a significant impact on each feature, and determining whether the effect of time is being confounded by these covariates. An illustrative case can be observed in Table 2, where the gut microbiome data of MetS patients in the fasting arm were reanalyzed at the species level. Notably, the SCFA producer, *Clostridium leptum*, was found to decrease during fasting[124]. However, the result of LongDat found that the observed effect of time, which serves as a proxy for treatment, could be attributed to diuretics. Hence, it would be inaccurate to consider fasting as the primary reason for the decline in *Clostridium leptum*. Instead, the main contributing factor appears to be the use of diuretics. Diuretics are medications used to

increase urine production and are employed to treat conditions like HTN, heart failure, kidney disorders, liver cirrhosis, and hypercalcemia[125]. The impact of diuretics on the gut microbiome has been demonstrated to exhibit significant synergistic effects in patients with type 2 diabetes, particularly when administered in conjunction with other medications like aspirin, angiotensin-converting enzyme inhibitors (ACE inhibitors), and beta-blockers. These diuretics show pronounced effects on the abundance of the gut microbiome. For example, it is known that diuretics influence the levels of *Roseburia*[126]. Furthermore, it has been observed that diuretics also induce shifts in microbial composition and richness in cirrhosis patients[127].

Aside from diuretics, as shown in Table 2, other covariates were also detected, although the effect of time cannot be reduced to these covariates. These covariates, some of them being drugs commonly used to treat HTN, include ACE inhibitors, antidiabetics, statins, angiotensin II receptor blockers (AT2 blockers), beta blockers, thyroid hormone, metformin, xanthine oxidase inhibitors, proton pump inhibitors (PPIs), vitamin D, and calcium antagonists. Among them, there is evidence in the literature supporting the capacity of ACE inhibitors, statins, AT2 blockers, beta blockers, thyroid hormone, metformin, PPIs, vitamin D, calcium antagonists, and antidiabetics to modify or impact the composition of the gut microbiome in humans or mice[128-134]. While the precise mechanisms of how these drugs influence the gut microbiome remain unclear, it is likely that they directly affect the gut microenvironment, and in turn, promote or inhibit the growth of specific bacteria. For example, metformin has been found to foster the growth of beneficial bacteria, contributing to its therapeutic effects in enhancing insulin resistance and glucose regulation.

In recent years, gut microbiome research has been a thriving research field; nevertheless, it confronts obstacles stemming from inconsistent discoveries. These discrepancies might arise from a lack of control and inadequate reporting of covariate impacts in publications[62,126,135]. The demonstrated influence of various drugs highlights the importance of covariate-aware analysis. Understanding the effects of these covariates on the gut microbiome is essential for obtaining accurate and meaningful results. The longitudinal data analysis in **Study 2[70]**, performed exclusively with the LongDat algorithm, empowers the identification and consideration of covariates like drug usage, which hold significant influences over the gut microbiome. Particularly, when dealing with multiple covariates in the

data, LongDat stands as the sole and essential tool that seamlessly and reliably handles the analysis, preventing failures (e.g., inflated FDR, unreasonable runtime, excessive memory usage, or NAs in the results) associated with such complexity. In short, LongDat proves vital in identifying covariate effects that would otherwise be overlooked in naïve analyses, ultimately improving the consistency and reliability of gut microbiome research. The utilization of LongDat in this study also contributes to the broader scientific community by making the algorithm available on platforms such as CRAN and GitHub. This availability enables researchers in the biomedical fields to apply LongDat to their own datasets and thus promotes the good practice of covariate-aware research.

Study 2[70] represents the first comprehensive investigation using high-resolution multi-omics to characterize fasting in MetS patients. It includes detailed clinical assessments, immunophenotyping, and sequencing of the gut microbiome. The main biomedical-wise discovery in **Study 2[70]** is that the combination of fasting and a modified DASH diet for three months triggers unique and coordinated changes in both the gut microbiome and immune system. These changes result in a lasting decrease in BP, a benefit not observed in patients solely on the DASH diet. Specifically, fasting induced significant changes in the gut microbiome, including shifts in butyrate-producing bacteria (e.g., *Eubacterium rectale* and *Coprococcus comes)*, which are also reported in previous literature[135]. These changes were observed during the fasting phase and partially reverted after refeeding. Despite many fasting-induced shifts being temporary, a lasting improvement in BP was observed in the patients. It is revealed that individuals who responded positively to the fasting+DASH intervention for BP improvement had depleted SCFA-producing taxa and gene modules at the baseline. During fasting or refeeding, these taxa and gene modules increased, counteracting the initial depletion. The improved availability of SCFAs in the body is considered a vital mechanism for the observed improvement, as SCFA has been shown to lower BP[136].

Gut microbial dysbiosis is associated with HTN in humans and rodents[137,138]. However, the overall contribution of the microbiome to HTN remains understudied. In **Study 3[71]**, by comparing the HTN-induced inflammation and organ damage between GF and COL mice, it is found that GF mice displayed significantly higher mean arterial pressure, more severe albuminuria, and increased T-helper cells and leukocytes in the kidneys. These results

indicate a heightened susceptibility of the kidneys to microbial influence, whereas the cardiac damage levels were similarly severe between the two groups. The proposition is that the reduced overall damage observed in COL mice is probably attributed to the existence of SCFAs, which have been shown to regulate BP[139]. On the other hand, when comparing COL+sham mice with COL+HTN mice, there is a decrease in the abundance of *Dubosiella newyorkensis* and *Bifidobacterium pseudolongum*, accompanied by an increase in the abundance of *Enterococcus*. Interestingly, *Dubosiella newyorkensis* is a recently discovered species and a potential probiotics known for its anti-aging properties in aged mice by reducing oxidative stress, and the ability to inhibit the renin-angiotensin system[140-142]. *Bifidobacterium pseudolongum* is a prevalent commensal species in the animal gut, known for its ability to improve metabolic health and alleviate intestinal inflammation[143,144]. The correlation analysis revealed a positive association between *Dubosiella newyorkensis* and serotonin, while *Bifidobacterium pseudolongum* showed a negative correlation with kynurenine. Both serotonin and kynurenine are metabolites derived from tryptophan and are linked to conditions like HTN, heart disease, and obesity[145-147]. These results shed light on the complex interaction between the gut microbiome and serum metabolites in the context of CVD.

The implementation of the LongDat algorithm was not employed in **Study 3[71]** as a result of the cross-sectional nature of the data used in the study. Nonetheless, the research incorporated the principles of covariate-aware analysis. This was exemplified through the application of the partial Mantel test, a statistical tool used to disentangle the effects of colonization status and treatment on the serum metabolome, as well as the treatment and origin (fecal vs cecal) on gut microbiome composition. The results indicate that both colonization status and the HTN-inducing treatment significantly impact the metabolome. This observation is consistent with previous literature showing notable alterations in plasma metabolome during HTN induction[121]. Additionally, it has been demonstrated that the microbiome is crucial in explaining variations in the metabolome among germ-free, gnotobiotic, and specific-pathogen-free mice[148]. On the other hand, although previous study states that the microbial composition in the cecum of humans exhibits both quantitative and qualitative distinctions compared with the microbial composition in the feces[149], the microbiome of COL mice in **Study 3[71]** is much more affected by the treatment than the origin of the microbiome, implying a substantial systematic change in the microbiome upon HTN induction.

The findings of **Study 3**[71] are contradictory to the Karbach study[150] where GF mice were protected from HTN when compared with COL mice. Two potential reasons for the discrepancy were proposed, including differences in experimental protocols and the distinct microbiome backgrounds of the COL mice used. From the comparative analysis of the microbiome and metabolome of the Pluznick study[121] and the data from **Study 3**[71], it is found that there are significant differences in the microbiomes of the CONV/COL mice between the two studies. Importantly, the serum metabolome of GF mice showed less distance between the two studies compared with the CONV/COL mice. This suggests that the microbiome has an observable influence on serum metabolome changes as a response to HTN and may explain the conflicting results between the Karbach studies and **Study 3**[71]. Hence, transparent documentation and accessibility of microbiome data in future studies are crucial to ensure reproducibility and comparability between studies.

4.3 Limitations

Despite the careful execution of all three studies, it is important to acknowledge the presence of certain limitations that should be addressed. One limitation of the LongDat algorithm presented in **Study 1**[69] is that it reports standardized nonparametric effect sizes of discrete and continuous variables (Cliff's delta and Spearman's rho, respectively), computed independently of other covariates. As a result, when the time effect (the proxy of the treatment effect) is reported as significant, and its effect is not reducible to covariates, it is considered reliable. However, while the direction of the effect is correct, the estimation of its strength is not ideal as it does not consider the influence of covariates that may independently affect the measured feature. Currently, there is a lack of knowledge regarding partial effect size metrics, which are standardized and directional, that could help address this limitation. Nonetheless, active efforts are underway to search for such metrics to potentially incorporate them in later versions of the LongDat algorithm. Furthermore, LongDat currently does not support the inclusion of interactive terms, such as those between the time variable and covariates. This feature is planned to be added in future updates of the LongDat algorithm to expand its usage.

In **Study 2**[70], the study has several limitations. Firstly, the participants were exclusively from a Caucasian-European background, which may introduce selection bias. Further research is needed to determine if the findings are applicable to a more diverse patient

population. Additionally, the study design did not allow for investigating fasting's long-term effects without the following DASH diet on immunome, microbiome or BP. Next, identified alterations in microbiome taxonomic and functional features, microbial metabolites, and immunome suggest potential explanations for the intervention's efficacy. However, causal conclusions necessitate further experimental work. For example, one can validate the BP-associated bacteria by introducing them into animal models such as mice and then observe the difference in phenotypes. Moreover, the relatively low number of patients in the study may lead to insufficient power, and thus limit the comprehensive understanding of fasting-associated host and microbiome features, necessitating larger studies for validation. Notwithstanding these limitations, the core findings in **Study 2**[70] persist in parallel with findings from other studies, with the strongest microbiome alteration replicated across various studies[135]. Therefore, **Study 2**[70] demonstrates the potential of fasting followed by a DASH diet as a non-drug-based approach for treating MetS patients.

Finally, in **Study 3**[71], there are also a few limitations to be acknowledged. For starters, the low number of samples in each group may result in limited statistical power to detect changes in the microbiome or immunome analysis. To address this, future studies could consider increasing the sample size to enhance the robustness of the findings. Secondly, as previously mentioned, the implanted microbiome plays a significant role in shaping the metabolome and phenotype related to HTN. However, in this study, only one type of microbiome (i.e., the microbiome comes from a single environmental source) for passive bacterial colonization was utilized. To validate and generalize the results in **Study 3**[71], it would be necessary to investigate the effects of different compositions of implanting microbiomes in follow-up studies, or consider using wildling mice (mice possessing the genetic background of laboratory mice but harboring the microbiome of wild mice) as an alternative[151].

4.4 Implications for practice and future application

The LongDat[69] algorithm serves as an ideal tool for the analysis of longitudinal data, with a particular focus on investigating intervention effects while accounting for covariates throughout the study. Initially designed as a specialized microbiome analysis tool, LongDat has undergone enhancements to accommodate a diverse range of high-dimensional

data types, making its usage more flexible and versatile. LongDat offers a seamless and efficient alternative to cumbersome programming models and non-parametric tests from scratch, automating the data analysis process. By utilizing LongDat, users gain access to standardized output, complete with effect sizes, and visually engaging representations that elucidate the impacts of covariates for every feature. This enables users to integrate, compare, and visually explore their results with ease. In order to promote covariate-aware analysis within the scientific community and enhance reproducibility, I have compiled the LongDat algorithm into an R package, leveraging the widely adopted R environment. This integration ensures that LongDat can be easily downloaded and installed from CRAN, the standard repository for R packages, making it accessible to a broad range of researchers and facilitating its adoption in scientific research.

In addition to its broader utilization in the science community, the LongDat algorithm is set to play a crucial role in the analysis of the CRC1365 project, "Renoprotection." The aim of the Renoprotection project is to clarify the interaction between the gut microbiome and immune cells of the host, and further investigate how this interaction affects the pathogenesis of HTN-induced CKD. This project involves the generation of longitudinal data on metagenome, metabolome, immunome, and phenotype. It is divided into multiple stages, including data collection from HTN-induced CKD development in double-transgenic rats, exploring the effects of microbiome-targeting drugs on CKD, and evaluating different gut microbiome effects on CKD progression through fecal microbiome transplants. By incorporating LongDat in the analyses, the goal is to ensure covariate-aware analysis and proper evaluation of longitudinal data. The result is anticipated to pave the way for innovative and improved therapeutic strategies for CKD.

The research findings from **Studies 2[70] and 3[71]** highlight the substantial impact of the gut microbiome and its metabolites on the conditions of MetS and HTN, both of which are major risk factors for CVD. Promisingly, the positive results observed with fasting followed by a DASH diet during the refeeding phase suggest a potential intervention to effectively manage high BP in MetS patients. Additionally, the discovery that COL mice, as opposed to their GF counterparts, are protected from damage through anti-inflammatory SCFAs, introduces a novel approach to address HTN and inflammation. The potential of elevating SCFA levels through direct supplementation or via influencing the gut microbiome to pro-

mote SCFA-generating microbial species, such as through dietary fiber or nutritional therapies, emerges as a promising strategy. In summary, both fasting and SCFA supplementation offer promising prospects for managing conditions related to MetS and HTN. These strategies provide an opportunity to propel non-pharmacological approaches that enhance patient outcomes, creating novel avenues for mitigating CVD considering the significant role of MetS and HTN as contributing risk factors.

5. Conclusions

In this thesis, LongDat was developed as a covariate-aware algorithm tailored for analyzing high-dimensional longitudinal data. The challenge of multiple covariates commonly encountered in longitudinal microbiome data analysis was addressed by LongDat, offering a unique and efficient approach to detect and control for these covariates. LongDat enhances the consistency and reliability of gut microbiome research, enabling users to perform covariate-aware analyses with increased efficiency and accuracy. By applying LongDat to gut microbiome data from MetS patients, significant changes in microbial composition, and immune cell composition during fasting were uncovered. These findings suggest that the gut microbiome and immunome are influenced by fasting, leading to improvements in BP and body weight in individuals with MetS. LongDat algorithm's ability to identify and account for covariates, played a crucial role in disentangling the effects of fasting and the DASH diet, providing a clearer understanding of the intervention's impact. Additionally, insights into the role of the gut microbiome in HTN development as revealed by the study comparing HTN impacts between COL and GF mice. GF mice displayed more severe kidney damage and distinct metabolic profiles compared with COL mice, highlighting the influence of the presence of gut microbiome and microbiome-derived metabolites on immune cells and organ damage in HTN. The presence of anti-inflammatory SCFAs in COL mice seemed to protect them from damage, implying a novel approach to address HTN and inflammation.

Overall, via covariate-aware methods, the thesis advances the understanding of the intricate relationship between the gut microbiome and diseases, shedding light on potential therapeutic implications. The findings from this thesis offer valuable insights into the role of host-microbiome interaction in MetS, HTN and organ damage, paving the way for non-pharmacological interventions in the realm of CVD and kidney diseases. Last but not least, this thesis has convincingly demonstrated that better comparability and reproducibility of scientific studies can only be achieved by providing a thoroughly transparent report of the microbiome composition, drug usage, diet, lifestyle, and any other covariates that might influence the outcome. Consequently, embracing transparency and covariate-aware analyses will foster greater trust and confidence in the scientific community and facilitate meaningful progress in the field of biomedical research.

Reference list

1 Gilbert, J. A., Blaser, M. J., Caporaso, J. G., Jansson, J. K., Lynch, S. V. & Knight, R. Current understanding of the human microbiome. *Nature Medicine* **24**, 392-400 (2018). https://doi.org:10.1038/nm.4517

2 Cani, P. D. Human gut microbiome: hopes, threats and promises. *Gut* **67**, 1716-1725 (2018). https://doi.org:10.1136/gutjnl-2018-316723

3 Sankar, S. A., Lagier, J.-C., Pontarotti, P., Raoult, D. & Fournier, P.-E. The human gut microbiome, a taxonomic conundrum. *Systematic and Applied Microbiology* **38**, 276-286 (2015). https://doi.org:https://doi.org/10.1016/j.syapm.2015.03.004

4 Hugon, P., Lagier, J.-C., Colson, P., Bittar, F. & Raoult, D. Repertoire of human gut microbes. *Microbial Pathogenesis* **106**, 103-112 (2017). https://doi.org:https://doi.org/10.1016/j.micpath.2016.06.020

5 Magne, F., Gotteland, M., Gauthier, L., Zazueta, A., Pesoa, S., Navarrete, P. & Balamurugan, R. The Firmicutes/Bacteroidetes Ratio: A Relevant Marker of Gut Dysbiosis in Obese Patients? *Nutrients* **12**, 1474 (2020).

6 Arumugam, M., Raes, J., Pelletier, E., Le Paslier, D., Yamada, T., Mende, D. R., Fernandes, G. R., Tap, J., Bruls, T., Batto, J. M., Bertalan, M., Borruel, N., Casellas, F., Fernandez, L., Gautier, L., Hansen, T., Hattori, M., Hayashi, T., Kleerebezem, M., Kurokawa, K., Leclerc, M., Levenez, F., Manichanh, C., Nielsen, H. B., Nielsen, T., Pons, N., Poulain, J., Qin, J., Sicheritz-Ponten, T., Tims, S., Torrents, D., Ugarte, E., Zoetendal, E. G., Wang, J., Guarner, F., Pedersen, O., de Vos, W. M., Brunak, S., Doré, J., Antolín, M., Artiguenave, F., Blottiere, H. M., Almeida, M., Brechot, C., Cara, C., Chervaux, C., Cultrone, A., Delorme, C., Denariaz, G., Dervyn, R., Foerstner, K. U., Friss, C., van de Guchte, M., Guedon, E., Haimet, F., Huber, W., van Hylckama-Vlieg, J., Jamet, A., Juste, C., Kaci, G., Knol, J., Lakhdari, O., Layec, S., Le Roux, K., Maguin, E., Mérieux, A., Melo Minardi, R., M'Rini, C., Muller, J., Oozeer, R., Parkhill, J., Renault, P., Rescigno, M., Sanchez, N., Sunagawa, S., Torrejon, A., Turner, K., Vandemeulebrouck, G., Varela, E., Winogradsky, Y., Zeller, G., Weissenbach, J., Ehrlich, S. D. & Bork, P. Enterotypes of the human gut microbiome. *Nature* **473**, 174-180 (2011). https://doi.org:10.1038/nature09944

7 Vieira-Silva, S., Falony, G., Belda, E., Nielsen, T., Aron-Wisnewsky, J., Chakaroun, R., Forslund, S. K., Assmann, K., Valles-Colomer, M., Nguyen, T. T. D., Proost, S., Prifti, E., Tremaroli, V., Pons, N., Le Chatelier, E., Andreelli, F., Bastard, J.-P., Coelho, L. P., Galleron, N., Hansen, T. H., Hulot, J.-S., Lewinter, C., Pedersen, H. K., Quinquis, B., Rouault, C., Roume, H., Salem, J.-E., Søndertoft, N. B., Touch, S., Alves, R., Amouyal, C., Galijatovic, E. A. A., Barthelemy, O., Batisse, J.-P., Berland, M., Bittar, R., Blottière, H., Bosquet, F., Boubrit, R., Bourron, O., Camus, M., Cassuto, D., Ciangura, C., Collet, J.-P., Dao, M.-C., Debedat, J., Djebbar, M., Doré, A., Engelbrechtsen, L., Fellahi, S., Fromentin, S., Giral, P., Graine, M., Hartemann, A., Hartmann, B., Helft, G., Hercberg, S., Hornbak, M., Isnard, R., Jaqueminet, S., Jørgensen, N. R., Julienne, H., Justesen, J., Kammer, J., Kerneis, M., Khemis, J., Krarup, N., Kuhn, M., Lampuré, A., Lejard, V., Levenez, F., Lucas-Martini, L., Massey, R., Maziers, N., Medina-Stamminger, J., Moitinho-Silva, L., Montalescot, G., Moutel, S., Le Pavin, L. P., Poitou-Bernert, C., Pousset, F., Pouzoulet, L., Schmidt, S., Silvain, J., Svendstrup, M., Swartz, T., Vanduyvenboden, T., Vatier, C., Verger, E., Walther, S., Dumas, M.-E., Ehrlich, S. D., Galan, P., Gøtze, J. P., Hansen, T., Holst, J. J., Køber, L., Letunic, I., Nielsen,

J., Oppert, J.-M., Stumvoll, M., Vestergaard, H., Zucker, J.-D., Bork, P., Pedersen, O., Bäckhed, F., Clément, K., Raes, J. & MetaCardis, C. Statin therapy is associated with lower prevalence of gut microbiota dysbiosis. *Nature* **581**, 310-315 (2020). https://doi.org:10.1038/s41586-020-2269-x

8 Hertli, S. & Zimmermann, P. Molecular interactions between the intestinal microbiota and the host. *Molecular Microbiology* **117**, 1297-1307 (2022). https://doi.org:https://doi.org/10.1111/mmi.14905

9 Silva, Y. P., Bernardi, A. & Frozza, R. L. The Role of Short-Chain Fatty Acids From Gut Microbiota in Gut-Brain Communication. *Frontiers in Endocrinology* **11** (2020). https://doi.org:10.3389/fendo.2020.00025

10 Xiong, R.-G., Zhou, D.-D., Wu, S.-X., Huang, S.-Y., Saimaiti, A., Yang, Z.-J., Shang, A., Zhao, C.-N., Gan, R.-Y. & Li, H.-B. Health Benefits and Side Effects of Short-Chain Fatty Acids. *Foods* **11**, 2863 (2022).

11 Khan, R., Petersen, F. C. & Shekhar, S. Commensal Bacteria: An Emerging Player in Defense Against Respiratory Pathogens. *Frontiers in Immunology* **10** (2019). https://doi.org:10.3389/fimmu.2019.01203

12 McLaren, M. R. & Callahan, B. J. Pathogen resistance may be the principal evolutionary advantage provided by the microbiome. *Philosophical Transactions of the Royal Society B: Biological Sciences* **375**, 20190592 (2020). https://doi.org:doi:10.1098/rstb.2019.0592

13 Negi, S., Das, D. K., Pahari, S., Nadeem, S. & Agrewala, J. N. Potential Role of Gut Microbiota in Induction and Regulation of Innate Immune Memory. *Frontiers in Immunology* **10** (2019). https://doi.org:10.3389/fimmu.2019.02441

14 Zheng, D., Liwinski, T. & Elinav, E. Interaction between microbiota and immunity in health and disease. *Cell Research* **30**, 492-506 (2020). https://doi.org:10.1038/s41422-020-0332-7

15 Čaja, F., Stakheev, D., Chernyavskiy, O., Křížan, J., Dvořák, J., Rossmann, P., Štěpánková, R., Makovický, P., Makovický, P., Kozáková, H. & Vannucci, L. Immune activation by microbiome shapes the colon mucosa: Comparison between healthy rat mucosa under conventional and germ-free conditions. *Journal of Immunotoxicology* **18**, 37-49 (2021). https://doi.org:10.1080/1547691X.2021.1887412

16 Gomez de Agüero, M., Ganal-Vonarburg, S. C., Fuhrer, T., Rupp, S., Uchimura, Y., Li, H., Steinert, A., Heikenwalder, M., Hapfelmeier, S., Sauer, U., McCoy, K. D. & Macpherson, A. J. The maternal microbiota drives early postnatal innate immune development. *Science* **351**, 1296-1302 (2016). https://doi.org:doi:10.1126/science.aad2571

17 Di Mauro, A., Neu, J., Riezzo, G., Raimondi, F., Martinelli, D., Francavilla, R. & Indrio, F. Gastrointestinal function development and microbiota. *Italian Journal of Pediatrics* **39**, 15 (2013). https://doi.org:10.1186/1824-7288-39-15

18 Alam, A. & Neish, A. Role of gut microbiota in intestinal wound healing and barrier function. *Tissue Barriers* **6**, 1539595 (2018). https://doi.org:10.1080/21688370.2018.1539595

19 Twardowska, A., Makaro, A., Binienda, A., Fichna, J. & Salaga, M. Preventing Bacterial Translocation in Patients with Leaky Gut Syndrome: Nutrition and Pharmacological Treatment Options. *International Journal of Molecular Sciences* **23**, 3204 (2022).

20 Martin-Gallausiaux, C., Marinelli, L., Blottière, H. M., Larraufie, P. & Lapaque, N. SCFA: mechanisms and functional importance in the gut. *Proceedings of the Nutrition Society* **80**, 37-49 (2021). https://doi.org:10.1017/S0029665120006916

21 Sharon, G., Sampson, T. R., Geschwind, D. H. & Mazmanian, S. K. The Central Nervous System and the Gut Microbiome. *Cell* **167**, 915-932 (2016). https://doi.org:https://doi.org/10.1016/j.cell.2016.10.027

22 Ma, Q., Xing, C., Long, W., Wang, H. Y., Liu, Q. & Wang, R.-F. Impact of microbiota on central nervous system and neurological diseases: the gut-brain axis. *Journal of Neuroinflammation* **16**, 53 (2019). https://doi.org:10.1186/s12974-019-1434-3

23 Martín, R., Miquel, S., Ulmer, J., Kechaou, N., Langella, P. & Bermúdez-Humarán, L. G. Role of commensal and probiotic bacteria in human health: a focus on inflammatory bowel disease. *Microbial Cell Factories* **12**, 71 (2013). https://doi.org:10.1186/1475-2859-12-71

24 Hrncir, T. Gut Microbiota Dysbiosis: Triggers, Consequences, Diagnostic and Therapeutic Options. *Microorganisms* **10** (2022). https://doi.org:10.3390/microorganisms10030578

25 DeGruttola, A. K., Low, D., Mizoguchi, A. & Mizoguchi, E. Current Understanding of Dysbiosis in Disease in Human and Animal Models. *Inflamm Bowel Dis* **22**, 1137-1150 (2016). https://doi.org:10.1097/mib.0000000000000750

26 Wilkins, L. J., Monga, M. & Miller, A. W. Defining Dysbiosis for a Cluster of Chronic Diseases. *Scientific Reports* **9**, 12918 (2019). https://doi.org:10.1038/s41598-019-49452-y

27 Savoji, H., Mohammadi, M. H., Rafatian, N., Toroghi, M. K., Wang, E. Y., Zhao, Y., Korolj, A., Ahadian, S. & Radisic, M. Cardiovascular disease models: A game changing paradigm in drug discovery and screening. *Biomaterials* **198**, 3-26 (2019). https://doi.org:https://doi.org/10.1016/j.biomaterials.2018.09.036

28 Bays, H. E., Taub, P. R., Epstein, E., Michos, E. D., Ferraro, R. A., Bailey, A. L., Kelli, H. M., Ferdinand, K. C., Echols, M. R., Weintraub, H., Bostrom, J., Johnson, H. M., Hoppe, K. K., Shapiro, M. D., German, C. A., Virani, S. S., Hussain, A., Ballantyne, C. M., Agha, A. M. & Toth, P. P. Ten things to know about ten cardiovascular disease risk factors. *American Journal of Preventive Cardiology* **5**, 100149 (2021). https://doi.org:https://doi.org/10.1016/j.ajpc.2021.100149

29 Podkowińska, A. & Formanowicz, D. Chronic Kidney Disease as Oxidative Stress- and Inflammatory-Mediated Cardiovascular Disease. *Antioxidants* **9**, 752 (2020).

30 Ahmad, A. F., Dwivedi, G., O'Gara, F., Caparros-Martin, J. & Ward, N. C. The gut microbiome and cardiovascular disease: current knowledge and clinical potential. *American Journal of Physiology-Heart and Circulatory Physiology* **317**, H923-H938 (2019). https://doi.org:10.1152/ajpheart.00376.2019

31 Zhao, Y. & Wang, Z. Gut microbiome and cardiovascular disease. *Curr Opin Cardiol* **35**, 207-218 (2020). https://doi.org:10.1097/hco.0000000000000720

32 Pluznick, J. L., Protzko, R. J., Gevorgyan, H., Peterlin, Z., Sipos, A., Han, J., Brunet, I., Wan, L.-X., Rey, F., Wang, T., Firestein, S. J., Yanagisawa, M., Gordon, J. I., Eichmann, A., Peti-Peterdi, J. & Caplan, M. J. Olfactory receptor responding to gut microbiota-derived signals plays a role in renin secretion and blood pressure regulation. *Proceedings of the National Academy of Sciences* **110**, 4410-4415 (2013). https://doi.org:doi:10.1073/pnas.1215927110

33 Duttaroy, A. K. Role of Gut Microbiota and Their Metabolites on Atherosclerosis, Hypertension and Human Blood Platelet Function: A Review. *Nutrients* **13**, 144 (2021).

34 Zhao, J., Ning, X., Liu, B., Dong, R., Bai, M. & Sun, S. Specific alterations in gut microbiota in patients with chronic kidney disease: an updated systematic review. *Renal Failure* **43**, 102-112 (2021). https://doi.org:10.1080/0886022X.2020.1864404

35 Yang, C.-Y., Chen, T.-W., Lu, W.-L., Liang, S.-S., Huang, H.-D., Tseng, C.-P. & Tarng, D.-C. Synbiotics Alleviate the Gut Indole Load and Dysbiosis in Chronic Kidney Disease. *Cells* **10**, 114 (2021).

36 Magliocca, G., Mone, P., Di Iorio, B. R., Heidland, A. & Marzocco, S. Short-Chain Fatty Acids in Chronic Kidney Disease: Focus on Inflammation and Oxidative Stress Regulation. *International Journal of Molecular Sciences* **23**, 5354 (2022).

37 Wang, X. & Cheng, Z. Cross-Sectional Studies: Strengths, Weaknesses, and Recommendations. *Chest* **158**, S65-S71 (2020). https://doi.org:https://doi.org/10.1016/j.chest.2020.03.012

38 Smith, G. in *Essential Statistics, Regression, and Econometrics (Second Edition)* (ed Gary Smith) 1-25 (Academic Press, 2015).

39 Levin, K. A. Study design III: Cross-sectional studies. *Evidence-Based Dentistry* **7**, 24-25 (2006). https://doi.org:10.1038/sj.ebd.6400375

40 White, R. T. & Arzi, H. J. Longitudinal Studies: Designs, Validity, Practicality, and Value. *Research in Science Education* **35**, 137-149 (2005). https://doi.org:10.1007/s11165-004-3437-y

41 Kodikara, S., Ellul, S. & Lê Cao, K.-A. Statistical challenges in longitudinal microbiome data analysis. *Briefings in Bioinformatics* **23** (2022). https://doi.org:10.1093/bib/bbac273

42 Toh, S. & Hernán, M. A. Causal Inference from Longitudinal Studies with Baseline Randomization. *The International Journal of Biostatistics* **4** (2008). https://doi.org:doi:10.2202/1557-4679.1117

43 Liu, C., Cripe, T. P. & Kim, M.-O. Statistical Issues in Longitudinal Data Analysis for Treatment Efficacy Studies in the Biomedical Sciences. *Molecular Therapy* **18**, 1724-1730 (2010). https://doi.org:https://doi.org/10.1038/mt.2010.127

44 Pan, A. Y. Statistical analysis of microbiome data: The challenge of sparsity. *Current Opinion in Endocrine and Metabolic Research* **19**, 35-40 (2021). https://doi.org:https://doi.org/10.1016/j.coemr.2021.05.005

45 Weiss, S., Xu, Z. Z., Peddada, S., Amir, A., Bittinger, K., Gonzalez, A., Lozupone, C., Zaneveld, J. R., Vázquez-Baeza, Y., Birmingham, A., Hyde, E. R. & Knight, R. Normalization and microbial differential abundance strategies depend upon data characteristics. *Microbiome* **5**, 27 (2017). https://doi.org:10.1186/s40168-017-0237-y

46 Chen, L., Reeve, J., Zhang, L., Huang, S., Wang, X. & Chen, J. GMPR: A robust normalization method for zero-inflated count data with application to microbiome sequencing data. *PeerJ* **6**, e4600 (2018). https://doi.org:10.7717/peerj.4600

47 McKnight, D. T., Huerlimann, R., Bower, D. S., Schwarzkopf, L., Alford, R. A. & Zenger, K. R. Methods for normalizing microbiome data: An ecological perspective. *Methods in Ecology and Evolution* **10**, 389-400 (2019). https://doi.org:https://doi.org/10.1111/2041-210X.13115

48 Mulè, M. P., Martins, A. J. & Tsang, J. S. Normalizing and denoising protein expression data from droplet-based single cell profiling. *Nature Communications* **13**, 2099 (2022). https://doi.org:10.1038/s41467-022-29356-8

49 Tsilimigras, M. C. B. & Fodor, A. A. Compositional data analysis of the microbiome: fundamentals, tools, and challenges. *Annals of Epidemiology* **26**, 330-335 (2016). https://doi.org:https://doi.org/10.1016/j.annepidem.2016.03.002

50 Ma, S., Ren, B., Mallick, H., Moon, Y. S., Schwager, E., Maharjan, S., Tickle, T. L., Lu, Y., Carmody, R. N., Franzosa, E. A., Janson, L. & Huttenhower, C. A statistical model for describing and simulating microbial community profiles. *PLoS Comput Biol* **17**, e1008913 (2021). https://doi.org:10.1371/journal.pcbi.1008913

51 Dean, C. B. & Lundy, E. R. in *Wiley StatsRef: Statistics Reference Online* 1-9.
52 Calgaro, M., Romualdi, C., Waldron, L., Risso, D. & Vitulo, N. Assessment of statistical methods from single cell, bulk RNA-seq, and metagenomics applied to microbiome data. *Genome Biology* **21**, 191 (2020). https://doi.org:10.1186/s13059-020-02104-1
53 Swift, D., Cresswell, K., Johnson, R., Stilianoudakis, S. & Wei, X. A review of normalization and differential abundance methods for microbiome counts data. *WIREs Computational Statistics* **n/a**, e1586 (2022). https://doi.org:https://doi.org/10.1002/wics.1586
54 Nearing, J. T., Douglas, G. M., Hayes, M. G., MacDonald, J., Desai, D. K., Allward, N., Jones, C. M. A., Wright, R. J., Dhanani, A. S., Comeau, A. M. & Langille, M. G. I. Microbiome differential abundance methods produce different results across 38 datasets. *Nature Communications* **13**, 342 (2022). https://doi.org:10.1038/s41467-022-28034-z
55 Xia, Y. & Sun, J. in *Bioinformatic and Statistical Analysis of Microbiome Data: From Raw Sequences to Advanced Modeling with QIIME 2 and R* (eds Yinglin Xia & Jun Sun) 615-674 (Springer International Publishing, 2023).
56 Gibbons, S. M., Kearney, S. M., Smillie, C. S. & Alm, E. J. Two dynamic regimes in the human gut microbiome. *PLOS Computational Biology* **13**, e1005364 (2017). https://doi.org:10.1371/journal.pcbi.1005364
57 Lindsey, J. K. & Jones, B. Choosing among generalized linear models applied to medical data. *Stat Med* **17**, 59-68 (1998). https://doi.org:Doi 10.1002/(Sici)1097-0258(19980115)17:1<59::Aid-Sim733>3.0.Co;2-7
58 McCue, T., Carruthers, E. H., Dawe, J., Liu, S., Robar, A. N. & Johnson, K. R.
59 Bolker, B. M., Brooks, M. E., Clark, C. J., Geange, S. W., Poulsen, J. R., Stevens, M. H. H. & White, J.-S. S. Generalized linear mixed models: a practical guide for ecology and evolution. *Trends in Ecology & Evolution* **24**, 127-135 (2009). https://doi.org:https://doi.org/10.1016/j.tree.2008.10.008
60 Field-Fote, E. Mediators and Moderators, Confounders and Covariates: Exploring the Variables That Illuminate or Obscure the “Active Ingredients” in Neurorehabilitation. *Journal of Neurologic Physical Therapy* **43**, 83-84 (2019). https://doi.org:10.1097/npt.0000000000000275
61 Pedersen, H. K., Forslund, S. K., Gudmundsdottir, V., Petersen, A. Ø., Hildebrand, F., Hyötyläinen, T., Nielsen, T., Hansen, T., Bork, P., Ehrlich, S. D., Brunak, S., Oresic, M., Pedersen, O. & Nielsen, H. B. A computational framework to integrate high-throughput ‘-omics’ datasets for the identification of potential mechanistic links. *Nature Protocols* **13**, 2781-2800 (2018). https://doi.org:10.1038/s41596-018-0064-z
62 Morris, T. P., Walker, A. S., Williamson, E. J. & White, I. R. Planning a method for covariate adjustment in individually randomised trials: a practical guide. *Trials* **23**, 328 (2022). https://doi.org:10.1186/s13063-022-06097-z
63 longitudinal: Analysis of Multiple Time Course Data (CRAN, 2021).
64 Timonen, J., Mannerström, H., Vehtari, A. & Lähdesmäki, H. lgpr: an interpretable non-parametric method for inferring covariate effects from longitudinal data. *Bioinformatics* **37**, 1860-1867 (2021). https://doi.org:10.1093/bioinformatics/btab021
65 Gonçalves, M. H. & Cabral, M. S. cold: An R Package for the Analysis of Count Longitudinal Data. *J Stat Softw* **99**, 1 - 34 (2021). https://doi.org:10.18637/jss.v099.i03

66 Chen, E. Z. & Li, H. A two-part mixed-effects model for analyzing longitudinal microbiome compositional data. *Bioinformatics* **32**, 2611-2617 (2016). https://doi.org:10.1093/bioinformatics/btw308

67 Asar, Ö. & İlk, Ö. mmm: An R package for analyzing multivariate longitudinal data with multivariate marginal models. *Computer Methods and Programs in Biomedicine* **112**, 649-654 (2013). https://doi.org:https://doi.org/10.1016/j.cmpb.2013.07.022

68 Mandal, S., Van Treuren, W., White, R. A., Eggesbø, M., Knight, R. & Peddada, S. D. Analysis of composition of microbiomes: a novel method for studying microbial composition. *Microbial Ecology in Health and Disease* **26**, 27663 (2015). https://doi.org:10.3402/mehd.v26.27663

69 Chen, C.-Y., Löber, U. & Forslund, S. K. LongDat: an R package for covariate-sensitive longitudinal analysis of high-dimensional data. *Bioinformatics Advances* **3** (2023). https://doi.org:10.1093/bioadv/vbad063

70 Maifeld, A., Bartolomaeus, H., Lober, U., Avery, E. G., Steckhan, N., Marko, L., Wilck, N., Hamad, I., Susnjar, U., Mahler, A., Hohmann, C., Chen, C. Y., Cramer, H., Dobos, G., Lesker, T. R., Strowig, T., Dechend, R., Bzdok, D., Kleinewietfeld, M., Michalsen, A., Muller, D. N. & Forslund, S. K. Fasting alters the gut microbiome reducing blood pressure and body weight in metabolic syndrome patients. *Nat Commun* **12**, 1970 (2021). https://doi.org:10.1038/s41467-021-22097-0

71 Avery, E. G., Bartolomaeus, H., Rauch, A., Chen, C. Y., N'Diaye, G., Löber, U., Bartolomaeus, T. U. P., Fritsche-Guenther, R., Rodrigues, A. F., Yarritu, A., Zhong, C., Fei, L., Tsvetkov, D., Todiras, M., Park, J. K., Markó, L., Maifeld, A., Patzak, A., Bader, M., Kempa, S., Kirwan, J. A., Forslund, S. K., Müller, D. N. & Wilck, N. Quantifying the impact of gut microbiota on inflammation and hypertensive organ damage. *Cardiovascular Research* (2022). https://doi.org:10.1093/cvr/cvac121

72 Silveira Rossi, J. L., Barbalho, S. M., Reverete de Araujo, R., Bechara, M. D., Sloan, K. P. & Sloan, L. A. Metabolic syndrome and cardiovascular diseases: Going beyond traditional risk factors. *Diabetes/Metabolism Research and Reviews* **38**, e3502 (2022). https://doi.org:https://doi.org/10.1002/dmrr.3502

73 Shi, H., Zhang, B., Abo-Hamzy, T., Nelson, J. W., Ambati, C. S. R., Petrosino, J. F., Bryan, R. M. & Durgan, D. J. Restructuring the Gut Microbiota by Intermittent Fasting Lowers Blood Pressure. *Circulation Research* **128**, 1240-1254 (2021). https://doi.org:doi:10.1161/CIRCRESAHA.120.318155

74 Mohr, A. E., Gumpricht, E., Sears, D. D. & Sweazea, K. L. Recent advances and health implications of dietary fasting regimens on the gut microbiome. *American Journal of Physiology-Gastrointestinal and Liver Physiology* **320**, G847-G863 (2021). https://doi.org:10.1152/ajpgi.00475.2020

75 Kjeldsen, S. E. Hypertension and cardiovascular risk: General aspects. *Pharmacological Research* **129**, 95-99 (2018). https://doi.org:https://doi.org/10.1016/j.phrs.2017.11.003

76 Sittipo, P., Lobionda, S., Lee, Y. K. & Maynard, C. L. Intestinal microbiota and the immune system in metabolic diseases. *Journal of Microbiology* **56**, 154-162 (2018). https://doi.org:10.1007/s12275-018-7548-y

77 Yang, F., Chen, H., Gao, Y., An, N., Li, X., Pan, X., Yang, X., Tian, L., Sun, J., Xiong, X. & Xing, Y. Gut microbiota-derived short-chain fatty acids and hypertension: Mechanism and treatment. *Biomedicine & Pharmacotherapy* **130**, 110503 (2020). https://doi.org:https://doi.org/10.1016/j.biopha.2020.110503

78 Avery, E. G., Bartolomaeus, H., Maifeld, A., Marko, L., Wiig, H., Wilck, N., Rosshart, S. P., Forslund, S. K. & Müller, D. N. The Gut Microbiome in Hypertension.

Circulation Research **128**, 934-950 (2021). https://doi.org:doi:10.1161/CIRCRESAHA.121.318065

79 Bates, D., Machler, M., Bolker, B. M. & Walker, S. C. Fitting Linear Mixed-Effects Models Using lme4. *J Stat Softw* **67**, 1-48 (2015). https://doi.org:DOI 10.18637/jss.v067.i01

80 Brooks, M. E., Kristensen, K., Benthem, K. J. v., Magnusson, A., Berg, C. W., Nielsen, A., Skaug, H. J., Maechler, M. & Bolker, B. M. Modeling Zero-Inflated Count Data With glmmTMB. *bioRxiv preprint* **bioRxiv:132753** (2017). https://doi.org:https://doi.org/10.1101/132753

81 Wickham, H. Reshaping Data with the reshape Package. *J Stat Softw* **21**, 1 - 20 (2007). https://doi.org:10.18637/jss.v021.i12

82 emmeans: Estimated Marginal Means, aka Least-Squares Means. R package version 1.6.3. (CRAN, 2021).

83 Peterson, R. A. Finding Optimal Normalizing Transformations via bestNormalize. *The R Journal* **13**, 310-329 (2021).

84 Wickham, H., Averick, M., Bryan, J. & Chang, W. Welcome to the Tidyverse. *Journal of Open Source Software* **4**, 1686 (2019).

85 Venables, W. N. & Ripley, B. D. *Modern Applied Statistics with S*. Fourth edn, (Springer, 2002).

86 effsize: Efficient Effect Size Computation v. R package version 0.8.1 (CRAN, 2020).

87 Palleja, A., Mikkelsen, K. H., Forslund, S. K., Kashani, A., Allin, K. H., Nielsen, T., Hansen, T. H., Liang, S., Feng, Q., Zhang, C., Pyl, P. T., Coelho, L. P., Yang, H., Wang, J., Typas, A., Nielsen, M. F., Nielsen, H. B., Bork, P., Wang, J., Vilsboll, T., Hansen, T., Knop, F. K., Arumugam, M. & Pedersen, O. Recovery of gut microbiota of healthy adults following antibiotic exposure. *Nat Microbiol* **3**, 1255-1265 (2018). https://doi.org:10.1038/s41564-018-0257-9

88 Fox, J. & Weisberg, S. *An {R} Companion to Applied Regression*. Third edn, (Sage, 2019).

89 Ver Hoef, J. M. & Boveng, P. L. Quasi-Poisson vs. negative binomial regression: how should we model overdispersed count data? *Ecology* **88**, 2766-2772 (2007). https://doi.org:10.1890/07-0043.1

90 Ferrari, S. & Cribari-Neto, F. Beta Regression for Modelling Rates and Proportions. *Journal of Applied Statistics* **31**, 799-815 (2004). https://doi.org:10.1080/0266476042000214501

91 Nick, T. G. & Campbell, K. M. in *Topics in Biostatistics* (ed Walter T. Ambrosius) 273-301 (Humana Press, 2007).

92 Liu, X. Ordinal Regression Analysis: Fitting the Proportional Odds Model Using Stata, SAS and SPSS. *Journal of Modern Applied Statistical Methods* **8**, 632-645 (2009). https://doi.org:10.22237/jmasm/1257035340

93 Benjamini, Y. & Hochberg, Y. Controlling the False Discovery Rate: A Practical and Powerful Approach to Multiple Testing. *Journal of the Royal Statistical Society: Series B (Methodological)* **57**, 289-300 (1995). https://doi.org:https://doi.org/10.1111/j.2517-6161.1995.tb02031.x

94 Tierney, B. T., Tan, Y., Kostic, A. D. & Patel, C. J. Gene-level metagenomic architectures across diseases yield high-resolution microbiome diagnostic indicators. *Nat Commun* **12**, 2907 (2021). https://doi.org:10.1038/s41467-021-23029-8

95 Macbeth, G., Razumiejczyk, E. & Ledesma, R. D. Vol. 10 545-555 (Universitas Psychologica, 2011).

96 Ruscio, J. Constructing Confidence Intervals for Spearman's Rank Correlation with Ordinal Data: A Simulation Study Comparing Analytic and Bootstrap Methods. *Journal of Modern Applied Statistical Methods* **7** 416-434 (2008).
97 Williams, J., Bravo, H. C., Tom, J. & Paulson, J. N. microbiomeDASim: Simulating longitudinal differential abundance for microbiome data. *F1000Res* **8**, 1769 (2019). https://doi.org:10.12688/f1000research.20660.2
98 Badri, M., Kurtz, Z. D., Bonneau, R. & Müller, C. L. Shrinkage improves estimation of microbial associations under different normalization methods. *NAR Genomics and Bioinformatics* **2** (2020). https://doi.org:10.1093/nargab/lqaa100
99 Metwally, A. A., Yang, J., Ascoli, C., Dai, Y., Finn, P. W. & Perkins, D. L. MetaLonDA: a flexible R package for identifying time intervals of differentially abundant features in metagenomic longitudinal studies. *Microbiome* **6**, 32 (2018). https://doi.org:10.1186/s40168-018-0402-y
100 Robinson, M. D., McCarthy, D. J. & Smyth, G. K. edgeR: a Bioconductor package for differential expression analysis of digital gene expression data. *Bioinformatics* **26**, 139-140 (2010). https://doi.org:10.1093/bioinformatics/btp616
101 van den Boogaart, K. G. & Tolosana-Delgado, R. "compositions": A unified R package to analyze compositional data. *Computers & Geosciences* **34**, 320-338 (2008). https://doi.org:https://doi.org/10.1016/j.cageo.2006.11.017
102 Saary, P., Forslund, K., Bork, P. & Hildebrand, F. RTK: efficient rarefaction analysis of large datasets. *Bioinformatics* **33**, 2594-2595 (2017). https://doi.org:10.1093/bioinformatics/btx206
103 peakRAM: Monitor the Total and Peak RAM Used by an Expression or Function (CRAN, 2017).
104 Mallick, H., Rahnavard, A., McIver, L. J., Ma, S., Zhang, Y., Nguyen, L. H., Tickle, T. L., Weingart, G., Ren, B., Schwager, E. H., Chatterjee, S., Thompson, K. N., Wilkinson, J. E., Subramanian, A., Lu, Y., Waldron, L., Paulson, J. N., Franzosa, E. A., Bravo, H. C. & Huttenhower, C. Multivariable association discovery in population-scale meta-omics studies. *PLOS Computational Biology* **17**, e1009442 (2021). https://doi.org:10.1371/journal.pcbi.1009442
105 Coelho, L. P., Alves, R., Monteiro, P., Huerta-Cepas, J., Freitas, A. T. & Bork, P. NG-meta-profiler: fast processing of metagenomes using NGLess, a domain-specific language. *Microbiome* **7**, 84 (2019). https://doi.org:10.1186/s40168-019-0684-8
106 Quast, C., Pruesse, E., Yilmaz, P., Gerken, J., Schweer, T., Yarza, P., Peplies, J. & Glöckner, F. O. The SILVA ribosomal RNA gene database project: improved data processing and web-based tools. *Nucleic Acids Res* **41**, D590-596 (2013). https://doi.org:10.1093/nar/gks1219
107 Hildebrand, F., Tadeo, R., Voigt, A. Y., Bork, P. & Raes, J. LotuS: an efficient and user-friendly OTU processing pipeline. *Microbiome* **2**, 30 (2014). https://doi.org:10.1186/2049-2618-2-30
108 Kanehisa, M., Furumichi, M., Sato, Y., Kawashima, M. & Ishiguro-Watanabe, M. KEGG for taxonomy-based analysis of pathways and genomes. *Nucleic Acids Research* **51**, D587-D592 (2022). https://doi.org:10.1093/nar/gkac963
109 Vieira-Silva, S., Falony, G., Darzi, Y., Lima-Mendez, G., Garcia Yunta, R., Okuda, S., Vandeputte, D., Valles-Colomer, M., Hildebrand, F., Chaffron, S. & Raes, J. Species–function relationships shape ecological properties of the human gut microbiome. *Nature Microbiology* **1**, 16088 (2016). https://doi.org:10.1038/nmicrobiol.2016.88

110 Gu, Z., Gu, L., Eils, R., Schlesner, M. & Brors, B. circlize Implements and enhances circular visualization in R. *Bioinformatics* **30**, 2811-2812 (2014). https://doi.org:10.1093/bioinformatics/btu393
111 Mesnage, R., Grundler, F., Schwiertz, A., Le Maho, Y. & Wilhelmi de Toledo, F. Changes in human gut microbiota composition are linked to the energy metabolic switch during 10 d of Buchinger fasting. *J Nutr Sci* **8**, e36 (2019). https://doi.org:10.1017/jns.2019.33
112 Holmes, I., Harris, K. & Quince, C. Dirichlet Multinomial Mixtures: Generative Models for Microbial Metagenomics. *PLOS ONE* **7**, e30126 (2012). https://doi.org:10.1371/journal.pone.0030126
113 Coelho, L. P., Alves, R., del Río, Á. R., Myers, P. N., Cantalapiedra, C. P., Giner-Lamia, J., Schmidt, T. S., Mende, D. R., Orakov, A., Letunic, I., Hildebrand, F., Van Rossum, T., Forslund, S. K., Khedkar, S., Maistrenko, O. M., Pan, S., Jia, L., Ferretti, P., Sunagawa, S., Zhao, X.-M., Nielsen, H. B., Huerta-Cepas, J. & Bork, P. Towards the biogeography of prokaryotic genes. *Nature* **601**, 252-256 (2022). https://doi.org:10.1038/s41586-021-04233-4
114 Dixon, P. VEGAN, a package of R functions for community ecology. *J Veg Sci* **14**, 927-930 (2003). https://doi.org:DOI 10.1111/j.1654-1103.2003.tb02228.x
115 Ordinal Dominance Statistics (orddom): An R Project for Statistical Com- puting package to compute ordinal, nonparametric alternatives to mean comparison v. R package Version 3.1 (CRAN, 2013).
116 Wickham, H. *ggplot2: Elegant Graphics for Data Analysis.*, (Springer-Verlag, 2016).
117 gplots: Various R Programming Tools for Plotting Data (2012).
118 ncf: Spatial Covariance Functions v. 1.3-2 (CRAN, 2022).
119 McDonald, D., Price, M. N., Goodrich, J., Nawrocki, E. P., DeSantis, T. Z., Probst, A., Andersen, G. L., Knight, R. & Hugenholtz, P. An improved Greengenes taxonomy with explicit ranks for ecological and evolutionary analyses of bacteria and archaea. *The ISME Journal* **6**, 610-618 (2012). https://doi.org:10.1038/ismej.2011.139
120 Ritari, J., Salojärvi, J., Lahti, L. & de Vos, W. M. Improved taxonomic assignment of human intestinal 16S rRNA sequences by a dedicated reference database. *BMC Genomics* **16**, 1056 (2015). https://doi.org:10.1186/s12864-015-2265-y
121 Cheema, M. U. & Pluznick, J. L. Gut Microbiota Plays a Central Role to Modulate the Plasma and Fecal Metabolomes in Response to Angiotensin II. *Hypertension* **74**, 184-193 (2019). https://doi.org:10.1161/hypertensionaha.119.13155
122 ggpubr: 'ggplot2' Based Publication Ready Plots v. 0.6.0 (CRAN, 2023).
123 Bartolomaeus, T. U. P., Birkner, T., Bartolomaeus, H., Lober, U., Avery, E. G., Mahler, A., Weber, D., Kochlik, B., Balogh, A., Wilck, N., Boschmann, M., Muller, D. N., Marko, L. & Forslund, S. K. Quantifying technical confounders in microbiome studies. *Cardiovasc Res* **117**, 863-875 (2021). https://doi.org:10.1093/cvr/cvaa128
124 Kabeerdoss, J., Sankaran, V., Pugazhendhi, S. & Ramakrishna, B. S. Clostridium leptum group bacteria abundance and diversity in the fecal microbiota of patients with inflammatory bowel disease: a case–control study in India. *BMC Gastroenterology* **13**, 20 (2013). https://doi.org:10.1186/1471-230X-13-20
125 Qavi, A. H., Kamal, R. & Schrier, R. W. Clinical Use of Diuretics in Heart Failure, Cirrhosis, and Nephrotic Syndrome. *International Journal of Nephrology* **2015**, 975934 (2015). https://doi.org:10.1155/2015/975934
126 Forslund, S. K., Chakaroun, R., Zimmermann-Kogadeeva, M., Markó, L., Aron-Wisnewsky, J., Nielsen, T., Moitinho-Silva, L., Schmidt, T. S. B., Falony, G., Vieira-

Silva, S., Adriouch, S., Alves, R. J., Assmann, K., Bastard, J.-P., Birkner, T., Caesar, R., Chilloux, J., Coelho, L. P., Fezeu, L., Galleron, N., Helft, G., Isnard, R., Ji, B., Kuhn, M., Le Chatelier, E., Myridakis, A., Olsson, L., Pons, N., Prifti, E., Quinquis, B., Roume, H., Salem, J.-E., Sokolovska, N., Tremaroli, V., Valles-Colomer, M., Lewinter, C., Søndertoft, N. B., Pedersen, H. K., Hansen, T. H., Amouyal, C., Andersson Galijatovic, E. A., Andreelli, F., Barthelemy, O., Batisse, J.-P., Belda, E., Berland, M., Bittar, R., Blottière, H., Bosquet, F., Boubrit, R., Bourron, O., Camus, M., Cassuto, D., Ciangura, C., Collet, J.-P., Dao, M.-C., Djebbar, M., Doré, A., Engelbrechtsen, L., Fellahi, S., Fromentin, S., Galan, P., Gauguier, D., Giral, P., Hartemann, A., Hartmann, B., Holst, J. J., Hornbak, M., Hoyles, L., Hulot, J.-S., Jaqueminet, S., Jørgensen, N. R., Julienne, H., Justesen, J., Kammer, J., Krarup, N., Kerneis, M., Khemis, J., Kozlowski, R., Lejard, V., Levenez, F., Lucas-Martini, L., Massey, R., Martinez-Gili, L., Maziers, N., Medina-Stamminger, J., Montalescot, G., Moute, S., Neves, A. L., Olanipekun, M., Le Pavin, L. P., Poitou, C., Pousset, F., Pouzoulet, L., Rodriguez-Martinez, A., Rouault, C., Silvain, J., Svendstrup, M., Swartz, T., Vanduyvenboden, T., Vatier, C., Walther, S., Gøtze, J. P., Køber, L., Vestergaard, H., Hansen, T., Zucker, J.-D., Hercberg, S., Oppert, J.-M., Letunic, I., Nielsen, J., Bäckhed, F., Ehrlich, S. D., Dumas, M.-E., Raes, J., Pedersen, O., Clément, K., Stumvoll, M., Bork, P. & The MetaCardis, C. Combinatorial, additive and dose-dependent drug–microbiome associations. *Nature* **600**, 500-505 (2021). https://doi.org:10.1038/s41586-021-04177-9

127 Cortez, K. J., Roilides, E., Quiroz-Telles, F., Meletiadis, J., Antachopoulos, C., Knudsen, T., Buchanan, W., Milanovich, J., Sutton, D. A., Fothergill, A., Rinaldi, M. G., Shea, Y. R., Zaoutis, T., Kottilil, S. & Walsh, T. J. Alterations in the Gut Microbiome in the Progression of Cirrhosis to Hepatocellular Carcinoma. *Clinical Microbiology Reviews* **21**, 157-197 (2008). https://doi.org:doi:10.1128/cmr.00039-07

128 Hu, X., Li, H., Zhao, X., Zhou, R., Liu, H., Sun, Y., Fan, Y., Shi, Y., Qiao, S., Liu, S., Liu, H. & Zhang, S. Multi-omics study reveals that statin therapy is associated with restoration of gut microbiota homeostasis and improvement in outcomes in patients with acute coronary syndrome. *Theranostics* **11**, 5778-5793 (2021). https://doi.org:10.7150/thno.55946

129 Robles-Vera, I., Toral, M., de la Visitación, N., Sánchez, M., Gómez-Guzmán, M., Muñoz, R., Algieri, F., Vezza, T., Jiménez, R., Gálvez, J., Romero, M., Redondo, J. M. & Duarte, J. Changes to the gut microbiota induced by losartan contributes to its antihypertensive effects. *British Journal of Pharmacology* **177**, 2006-2023 (2020). https://doi.org:https://doi.org/10.1111/bph.14965

130 Tangestani, H., Boroujeni, H. K., Djafarian, K., Emamat, H. & Shab-Bidar, S. Vitamin D and The Gut Microbiota: a Narrative Literature Review. *Clin Nutr Res* **10**, 181-191 (2021). https://doi.org:10.7762/cnr.2021.10.3.181

131 Weersma, R. K., Zhernakova, A. & Fu, J. Interaction between drugs and the gut microbiome. *Gut* **69**, 1510-1519 (2020). https://doi.org:10.1136/gutjnl-2019-320204

132 Li, Y., Zhao, D., Qian, M., Liu, J., Pan, C., Zhang, X., Duan, X., Zhang, Y., Jia, W. & Wang, L. Amlodipine, an anti-hypertensive drug, alleviates non-alcoholic fatty liver disease by modulating gut microbiota. *British Journal of Pharmacology* **179**, 2054-2077 (2022). https://doi.org:https://doi.org/10.1111/bph.15768

133 Ojo, O., Wang, X., Ojo, O. O., Brooke, J., Jiang, Y., Dong, Q. & Thompson, T. The Effect of Prebiotics and Oral Anti-Diabetic Agents on Gut Microbiome in Patients

with Type 2 Diabetes: A Systematic Review and Network Meta-Analysis of Randomised Controlled Trials. *Nutrients* **14**, 5139 (2022).

134 Bargiel, P., Szczuko, M., Stachowska, L., Prowans, P., Czapla, N., Markowska, M., Petriczko, J., Kledzik, J., Jędrzejczyk-Kledzik, A., Palma, J., Zabielska, P. & Maciejewska-Markiewicz, D. Microbiome Metabolites and Thyroid Dysfunction. *Journal of Clinical Medicine* **10**, 3609 (2021).

135 Forslund, S. K. Fasting intervention and its clinical effects on the human host and microbiome. *Journal of Internal Medicine* **293**, 166-183 (2023). https://doi.org:https://doi.org/10.1111/joim.13574

136 Pluznick, J. L. Microbial Short-Chain Fatty Acids and Blood Pressure Regulation. *Current Hypertension Reports* **19**, 25 (2017). https://doi.org:10.1007/s11906-017-0722-5

137 Yang, T., Santisteban, M. M., Rodriguez, V., Li, E., Ahmari, N., Carvajal, J. M., Zadeh, M., Gong, M., Qi, Y., Zubcevic, J., Sahay, B., Pepine, C. J., Raizada, M. K. & Mohamadzadeh, M. Gut Dysbiosis Is Linked to Hypertension. *Hypertension* **65**, 1331-1340 (2015). https://doi.org:doi:10.1161/HYPERTENSIONAHA.115.05315

138 Li, J., Zhao, F., Wang, Y., Chen, J., Tao, J., Tian, G., Wu, S., Liu, W., Cui, Q., Geng, B., Zhang, W., Weldon, R., Auguste, K., Yang, L., Liu, X., Chen, L., Yang, X., Zhu, B. & Cai, J. Gut microbiota dysbiosis contributes to the development of hypertension. *Microbiome* **5**, 14 (2017). https://doi.org:10.1186/s40168-016-0222-x

139 Wu, Y., Xu, H., Tu, X. & Gao, Z. The Role of Short-Chain Fatty Acids of Gut Microbiota Origin in Hypertension. *Front Microbiol* **12**, 730809 (2021). https://doi.org:10.3389/fmicb.2021.730809

140 Cox, L. M., Sohn, J., Tyrrell, K. L., Citron, D. M., Lawson, P. A., Patel, N. B., Iizumi, T., Perez-Perez, G. I., Goldstein, E. J. C. & Blaser, M. J. Description of two novel members of the family Erysipelotrichaceae: Ileibacterium valens gen. nov., sp. nov. and Dubosiella newyorkensis, gen. nov., sp. nov., from the murine intestine, and emendation to the description of Faecalibaculum rodentium. *Int J Syst Evol Microbiol* **67**, 1247-1254 (2017). https://doi.org:10.1099/ijsem.0.001793

141 Liu, T.-h., Wang, J., Zhang, C.-y., Zhao, L., Sheng, Y.-y., Tao, G.-s. & Xue, Y.-z. Gut microbial characteristical comparison reveals potential anti-aging function of Dubosiella newyorkensis in mice. *Frontiers in Endocrinology* **14** (2023). https://doi.org:10.3389/fendo.2023.1133167

142 Liu, T.-h., Chen, M.-h., Tu, W.-q., Liang, Q.-e., Tao, W.-c., Jin, Z., Xiao, Y. & Chen, L.-g. Network and 16S rRNA Sequencing-Combined Approach Provides Insightal Evidence of Vitamin K2 for Salt-Sensitive Hypertension. *Frontiers in Nutrition* **8** (2021). https://doi.org:10.3389/fnut.2021.639467

143 Bo, T.-b., Wen, J., Zhao, Y.-c., Tian, S.-j., Zhang, X.-y. & Wang, D.-h. Bifidobacterium pseudolongum reduces triglycerides by modulating gut microbiota in mice fed high-fat food. *The Journal of Steroid Biochemistry and Molecular Biology* **198**, 105602 (2020). https://doi.org:https://doi.org/10.1016/j.jsbmb.2020.105602

144 Guo, W., Mao, B., Cui, S., Tang, X., Zhang, Q., Zhao, J. & Zhang, H. Protective Effects of a Novel Probiotic Bifidobacterium pseudolongum on the Intestinal Barrier of Colitis Mice via Modulating the Pparγ/STAT3 Pathway and Intestinal Microbiota. *Foods* **11**, 1551 (2022).

145 Song, P., Ramprasath, T., Wang, H. & Zou, M.-H. Abnormal kynurenine pathway of tryptophan catabolism in cardiovascular diseases. *Cellular and Molecular Life Sciences* **74**, 2899-2916 (2017). https://doi.org:10.1007/s00018-017-2504-2

146 Nagy, B. M., Nagaraj, C., Meinitzer, A., Sharma, N., Papp, R., Foris, V., Ghanim, B., Kwapiszewska, G., Kovacs, G., Klepetko, W., Pieber, T. R., Mangge, H., Olschewski, H. & Olschewski, A. Importance of kynurenine in pulmonary hypertension. *American Journal of Physiology-Lung Cellular and Molecular Physiology* **313**, L741-L751 (2017). https://doi.org:10.1152/ajplung.00517.2016

147 MacLean, M. R. & Dempsie, Y. Serotonin and pulmonary hypertension—from bench to bedside? *Current Opinion in Pharmacology* **9**, 281-286 (2009). https://doi.org:https://doi.org/10.1016/j.coph.2009.02.005

148 Brown, K., Thomson, C. A., Wacker, S., Drikic, M., Groves, R., Fan, V., Lewis, I. A. & McCoy, K. D. Microbiota alters the metabolome in an age- and sex-dependent manner in mice. *Nature Communications* **14**, 1348 (2023). https://doi.org:10.1038/s41467-023-37055-1

149 Marteau, P., Pochart, P., Doré, J., Béra-Maillet, C., Bernalier, A. & Corthier, G. Comparative Study of Bacterial Groups within the Human Cecal and Fecal Microbiota. *Applied and Environmental Microbiology* **67**, 4939-4942 (2001). https://doi.org:doi:10.1128/AEM.67.10.4939-4942.2001

150 Karbach, S. H., Schönfelder, T., Brandão, I., Wilms, E., Hörmann, N., Jäckel, S., Schüler, R., Finger, S., Knorr, M., Lagrange, J., Brandt, M., Waisman, A., Kossmann, S., Schäfer, K., Münzel, T., Reinhardt, C. & Wenzel, P. Gut Microbiota Promote Angiotensin II–Induced Arterial Hypertension and Vascular Dysfunction. *Journal of the American Heart Association* **5**, e003698 (2016). https://doi.org:doi:10.1161/JAHA.116.003698

151 Rosshart, S. P., Herz, J., Vassallo, B. G., Hunter, A., Wall, M. K., Badger, J. H., McCulloch, J. A., Anastasakis, D. G., Sarshad, A. A., Leonardi, I., Collins, N., Blatter, J. A., Han, S.-J., Tamoutounour, S., Potapova, S., Foster St. Claire, M. B., Yuan, W., Sen, S. K., Dreier, M. S., Hild, B., Hafner, M., Wang, D., Iliev, I. D., Belkaid, Y., Trinchieri, G. & Rehermann, B. Laboratory mice born to wild mice have natural microbiota and model human immune responses. *Science* **365**, eaaw4361 (2019). https://doi.org:doi:10.1126/science.aaw4361

Statutory Declaration

“I, Chia-Yu Chen, by personally signing this document in lieu of an oath, hereby affirm that I prepared the submitted dissertation on the topic “Host-microbiome interaction in organ damage of cardiovascular disease” (German title: Host-Mikrobiom-Interaktion bei Organschäden durch kardiovaskuläre Erkrankungen), independently and without the support of third parties, and that I used no other sources and aids than those stated. All parts which are based on the publications or presentations of other authors, either in letter or in spirit, are specified as such in accordance with the citing guidelines. The sections on methodology (in particular regarding practical work, laboratory regulations, statistical processing) and results (in particular regarding figures, charts and tables) are exclusively my responsibility.

Furthermore, I declare that I have correctly marked all of the data, the analyses, and the conclusions generated from data obtained in collaboration with other persons, and that I have correctly marked my own contribution and the contributions of other persons (cf. declaration of contribution). I have correctly marked all texts or parts of texts that were generated in collaboration with other persons.

My contributions to any publications to this dissertation correspond to those stated in the below joint declaration made together with the supervisor. All publications created within the scope of the dissertation comply with the guidelines of the ICMJE (International Committee of Medical Journal Editors; http://www.icmje.org) on authorship. In addition, I declare that I shall comply with the regulations of Charité – Universitätsmedizin Berlin on ensuring good scientific practice.

I declare that I have not yet submitted this dissertation in identical or similar form to another Faculty.

The significance of this statutory declaration and the consequences of a false statutory declaration under criminal law (Sections 156, 161 of the German Criminal Code) are known to me.”

Date Signature

Declaration of your own contribution to the publications

Chia-Yu Chen contributed the following to the below-listed publications:

Study 1:

Chen, C.-Y., Löber, U. & Forslund, S. K. LongDat: an R package for covariate-sensitive longitudinal analysis of high-dimensional data. Bioinformatics Advances 3 (2023). https://doi.org/10.1093/bioadv/vbad063

Contribution:

Chia-Yu Chen is the sole first author of this paper. She developed the LongDat R algorithm and then compiled it into an R package, conducting performance assessments via benchmarking against alternative tools, and applying it across diverse datasets. All figures and tables presented herein are a direct result of her efforts. Her supervisor, Sofia Forslund, played a pivotal role in conceptualizing the methodology, offering guidance in analysis and visualization, while collaborator Ulrike Löber contributed to methodological conception. The paper is majorly written by Chia-Yu Chen, and refined through collaborative revision by Ulrike Löber and Sofia Forslund.

Study 2:

Maifeld, A., Bartolomaeus, H., Lober, U., Avery, E. G., Steckhan, N., Marko, L., Wilck, N., Hamad, I., Susnjar, U., Mahler, A., Hohmann, C., **Chen, C.-Y.**, Cramer, H., Dobos, G., Lesker, T. R., Strowig, T., Dechend, R., Bzdok, D., Kleinewietfeld, M., Michalsen, A., Muller, D. N. & Forslund, S. K. Fasting alters the gut microbiome reducing blood pressure and body weight in metabolic syndrome patients. Nat Commun 12, 1970 (2021). https://doi.org/10.1038/s41467-021-22097-0

Contribution:

Chia-Yu Chen contributed to this paper by analyzing gut microbiome data and generating Figure S7 of the paper, as well as writing the related method. She provided input during the paper writing process and took part in revising the final manuscript. She also made substantial contributions by creating the LongDat algorithm, which evolved from the initial scripts written by Sofia Forslund for this paper. Through Chia-Yu Chen's efforts, the code underwent a comprehensive transformation to expand its usage as well as improve clarity and reproducibility. Furthermore, she introduced user-friendly elements and functions, culminating in the compilation of the scripts into an R package, thereby ensuring the replicability of the results.

Study 3:

Avery, E. G., Bartolomaeus, H., Rauch, A., **Chen, C.-Y.**, N'Diaye, G., Löber, U., Bartolomaeus, T. U. P., Fritsche-Guenther, R., Rodrigues, A. F., Yarritu, A., Zhong, C., Fei, L., Tsvetkov, D., Todiras, M., Park, J. K., Markó, L., Maifeld, A., Patzak, A., Bader, M., Kempa, S., Kirwan, J. A., Forslund, S. K., Müller, D. N. & Wilck, N. Quantifying the impact of gut microbiota on inflammation and hypertensive organ damage. Cardiovascular Research (2022). https://doi.org/10.1093/cvr/cvac121

Contribution:

Chia-Yu Chen has been engaged in comprehensive analyses of both gut microbiome and serum metabolome data. Her active engagement included in-depth discussions with Ellen Avery regarding the statistical methodologies employed in this study, as well as conducting comparative analyses with other pertinent studies. Chia-Yu created Figures S7 and S10, alongside composing the associated method section. She provided input during the paper writing process and took part in composing and revising the final manuscript.

_____

Signature of doctoral candidate

Printing copies of the publications

Study 1:

Bioinformatics Advances, 2023, vbad063
https://doi.org/10.1093/bioadv/vbad063
Advance Access Publication Date: 18 May 2023
Original Article

Software

LongDat: an R package for covariate-sensitive longitudinal analysis of high-dimensional data

Chia-Yu Chen [1,2,3,4], **Ulrike Löber** [1,2,3,4] **and Sofia K. Forslund**[1,2,3,4,5,*]

[1]Max-Delbrück-Center for Molecular Medicine in the Helmholtz Association (MDC), Berlin 13125, Germany, [2]Experimental and Clinical Research Center, A Cooperation between the Max-Delbrück-Center for Molecular Medicine in the Helmholtz Association and the Charité – Universitätsmedizin Berlin, Berlin 13125, Germany, [3]Charité - Universitätsmedizin Berlin, Corporate Member of Freie Universität Berlin and Humboldt-Universität zu Berlin, Berlin 10117, Germany, [4]DZHK (German Centre for Cardiovascular Research), partner site Berlin, Berlin 10785, Germany and [5]Structural and Computational Biology Unit, European Molecular Biology Laboratory, Heidelberg 69117, Germany

*To whom correspondence should be addressed.
Associate Editor: Marieke Kuijjer

Received on August 24, 2022; revised on April 15, 2023; editorial decision on April 30, 2023; accepted on May 17, 2023

Abstract

Summary: We introduce LongDat, an R package that analyzes longitudinal multivariable (cohort) data while simultaneously accounting for a potentially large number of covariates. The primary use case is to differentiate direct from indirect effects of an intervention (or treatment) and to identify covariates (potential mechanistic intermediates) in longitudinal data. LongDat focuses on analyzing longitudinal microbiome data, but its usage can be expanded to other data types, such as binary, categorical and continuous data. We tested and compared LongDat with other tools (i.e. MaAsLin2, ANCOM, lgpr and ZIBR) on both simulated and real data. We showed that LongDat outperformed these tools in accuracy, runtime and memory cost, especially when there were multiple covariates. The results indicate that the LongDat R package is a computationally efficient and low-memory-cost tool for longitudinal data with multiple covariates and facilitates robust biomarker searches in high-dimensional datasets.
Availability and implementation: The R package LongDat is available on CRAN (https://cran.r-project.org/web/packages/LongDat/) and GitHub (https://github.com/CCY-dev/LongDat).
Contact: chia-yu.chen@mdc-berlin.de or sofia.forslund@mdc-berlin.de
Supplementary information: Supplementary data are available at *Bioinformatics Advances* online.

1 Introduction

Recent years have seen the spawning of high-dimensional data (i.e. data with a large number of features) as biotechnology develops rapidly (Assent, 2012; Witten *et al.*, 2010). For instance, metabolomics, immunomics and metagenomics are becoming prevalent. Among them, count data derived from microbial metagenomics sequencing especially require specific methods to tackle since they have several inherent properties, including uneven sequencing depth across samples, compositional structure, overdispersion and high sparsity (Kodikara *et al.*, 2022; Zhang *et al.*, 2017). When the research aim is to find out the differences in the abundance of microbial features between groups (e.g. time points, treatments), a typical workflow consists of pre-processing and differential abundance analysis steps. Uneven sequencing depth in metagenomic shotgun sequencing needs to be addressed at the pre-processing step because it is known to cause bias in evaluating microbial communities (Sanchez-Cid *et al.*, 2022). Therefore, data-preprocessing approaches such as normalization, transformation and rarefaction have been developed to deal with varying sequencing depth (Lin *et al.*, 2020). When it comes to differential abundance analysis, we need to consider the typical characteristics of microbiome data, including () compositional structure, (ii) overdispersion and (iii) high sparsity. Microbial data from shotgun sequencing are inherently compositional since the total amount of reads each sequencing run can generate is fixed. Thus the abundances of features are not independent of each other (Gloor *et al.*, 2017). Tools have been proposed to account for the compositional structure (Mandal *et al.*, 2015). However, some literature shows that the compositional methods do not always outperform the non-compositional methods (Mallick *et al.*, 2021). Overdispersion denotes a larger variability observed in data than expected from a specific distribution, while high sparsity implies that the data are inflated with zeros. When fitting models to the microbiome data, overdispersion and high sparsity should be addressed. For example, models like negative binomial regression and zero-inflated Poisson regression have been introduced to solve overdispersion and high-sparsity problems (Mallick *et al.*, 2021; Zhang *et al.*, 2017). Collectively, many different microbiome data

© The Author(s) 2023. Published by Oxford University Press.

This is an Open Access article distributed under the terms of the Creative Commons Attribution License (https://creativecommons.org/licenses/by/4.0/), which permits unrestricted reuse, distribution, and reproduction in any medium, provided the original work is properly cited.

Downloaded from https://academic.oup.com/bioinformaticsadvances/article/3/1/vbad063/7172481 by Duke University user on 21 August 2023

analysis methods have been proposed so far, and there are plentiful reviews on their comparisons (Calgaro *et al.*, 2020; Swift *et al.*, 2023; Weiss *et al.*, 2017). However, there is no universal method for analyzing all types of microbiome data. Hence, it depends on the characteristics of the data and the user's research aim to opt for an appropriate method in different scenarios.

Microbiome data can be divided into cross-sectional and longitudinal based on its study design. Cross-sectional data are collected by examining multiple subjects at one time point (Levin, 2006). In contrast, longitudinal data from observational or intervention cohorts are repeated measurements from the same individuals at different time points (Liu *et al.*, 2010). Compared with cross-sectional studies, longitudinal studies account for individual variation and enable researchers to trace changes over time (Hua *et al.*, 2009). Thus, longitudinal data collection has become more common in biological and medical fields nowadays (Liu *et al.*, 2010). When fitting models to longitudinal microbiome data, microbiome features are the dependent variables, while the metadata (i.e. information about the individuals) are the independent variables. The metadata may include the time variable and other variables, such as dietary supplements, changes in meals and weight. The aim of longitudinal microbiome data analysis is to investigate the effect of the time variable since it is the proxy for treatment or intervention in longitudinal data. Accordingly, all variables in the metadata except for the time variables are referred to as covariates, which are defined as the factors other than the variable we are interested in (here the time variable) that might associate with the outcome (here microbiome features) (Field-Fote, 2019). Examples of covariates include, for example, how patients benefiting from a dietary intervention (coded as a time variable) may have their medication dosages reduced during the course of a trial, raising the question of whether observed -omics signature changes are direct effects of the intervention or indirect effects following from the alteration of medication regime (Maifeld *et al.*, 2021). Consequently, to ensure proper analyses of longitudinal microbiome data, it is important to disentangle the time variable's effects from the covariates' effects. In other words, covariates should be uncovered and controlled for to avoid false conclusions (Pedersen *et al.*, 2018). In addition, two other critical points need to be considered when analyzing longitudinal microbiome data. First, selecting appropriate statistical tests from empirical data distributions is important for obtaining proper interpretations (Nahm, 2016). Second, inter-individual variation (e.g. differences in microbial abundance levels between individuals) should be addressed. Several tools dealing with longitudinal microbiome data already exist, and some allow taking in covariates for analysis (Asar *et al.*, 2013; Chen *et al.*, 2016; Gonçalves *et al.*, 2021; Mallick *et al.*, 2021; Mandal *et al.*, 2015; Opgen-Rhein *et al.*, 2021; Timonen *et al.*, 2021). Nevertheless, none of these tools reports explicitly on how the effect of time variable is affected by the presence of other covariates while detecting and simultaneously controlling for them. Therefore, we developed LongDat, an R package capable of performing the tasks as described above.

LongDat is developed and tested centered on microbiome data. However, we extended its utility to work on different data types (e.g. immunome, metabolome, transcriptome). The key to LongDat's flexibility to adapt to input data with different statistical distributions lies in the utilization of generalized linear models (GLMs) and non-parametric effect size calculations in the pipeline. GLMs can fit skewed data (e.g. data with overdispersion and high sparsity), allow non-constant variances (heteroscedasticity) and model various data types, such as continuous, categorical and ordinal data (Lindsey *et al.*, 1998). To account for inter-individual variation in longitudinal data, we treat sample donor origin (i.e. individual) as a random effect, expanding the GLMs framework to the generalized linear mixed models (GLMMs) (Bolker *et al.*, 2009). LongDat utilizes GLMMs to test the significance of the time variable without and with the presence of covariates in the models, respectively. Subsequently, the effect size of the time variable on each microbiome feature is calculated. In a longitudinal setting, an effect size is defined as the degree of feature difference before and after treatment. Reporting effect sizes in the result is in line with the current best practice, which urges researchers to report effect sizes along with *P*-values in biomedical research (Sullivan *et al.*, 2012). *P*-values from the abovementioned model tests indicate the statistical significance of the time variable (proxy of treatments), whereas standardized and directional effect sizes allow users to interpret the magnitude of effects both manually and within automated frameworks. In the LongDat pipeline, directional non-parametric effect sizes (e.g. Spearman's rho and Cliff's delta) are applied to handle both normally and non-normally distributed data (Marfo *et al.*, 2019). LongDat focuses on analyzing monotonic (i.e. the direction of change is fixed) treatment effects within time intervals while reporting covariates for each feature.

In this report, we describe the method of the LongDat R package and validate its performance by comparing it with its closest published counterpart to date, MaAsLin2 (Mallick *et al.*, 2021). We tested the performance of LongDat and MaAsLin2 on simulated, semi-synthetic and real microbiome data. MaAsLin2 is an R package similar to LongDat in several aspects. They both focus on microbiome analysis, adopt GLMMs and allow covariates to be included in the models. The main difference between MaAsLin2 and LongDat is that MaAsLin2 does not explicitly report how the effect of the time variable is affected by the presence of other covariates. In addition, the ways of treating covariates in the two tools differ. MaAsLin2 takes in all covariates along with the time variable into a model at once, while LongDat loops over each covariate in parallel models (see Methods). This distinction leads to significant differences in the results of analyzing longitudinal microbiome data with many covariates, making LongDat more suitable when there are multiple covariates (see Results). Aside from MaAsLin2, we also compared LongDat with other R packages which allow covariates to be included in the analysis, namely ANCOM (Mandal *et al.*, 2015), lgpr (Timonen *et al.*, 2021) and ZIBR (Chen *et al.*, 2016). ANCOM is a microbiome-oriented tool that utilizes the compositional method. Lgpr uses additive Gaussian process regression (a Bayesian method) to achieve non-parametric modeling of longitudinal data. ZIBR incorporates logistic models and zero-inflated Beta regressions with random effects to test the effect of time on microbiome features. Since normalization and rarefaction of the microbial count data might induce considerable changes to the analysis result, we compared the performances of these tools when different normalization or rarefaction techniques were applied, including total-sum scaling (TSS), cumulative-sum scaling (CSS), trimmed mean of M-values (TMM), geometric mean of pairwise ratios (GMPR), centered log-ratio (CLR), rarefaction (Chen *et al.*, 2018; McKnight *et al.*, 2019; Mulè *et al.*, 2022). TSS divides absolute abundance by the total sum of read depth and converts it into relative abundance ranging between 0 and 1. CSS is a quantile normalization method that addresses the bias arising from TSS. The purpose of TMM is to tackle the problem of composition bias and calculate normalization factors that aid in comparing different libraries. GMPR computes the ratio between each pair of values and then takes the geometric mean of those ratios to normalize data. CLR transformation, commonly used for compositional data analysis, takes the logarithm of the ratios of each component to the geometric mean of all components, and then centers the resulting values around zero. Lastly, rarefaction randomly subsamples the data to obtain an equivalent sequencing depth across all samples. Altogether, we assessed how these tools performed with various normalization or rarefaction techniques.

The real microbiome data used in this study for comparison are from our previous study, which reported on a clinical cohort investigating fasting effects on patients with metabolic syndrome (MetS) (Maifeld *et al.*, 2021). By reanalyzing this dataset in which MetS patients benefit from a dietary intervention while medication dosages were altered subsequently during the trial course as an indirect effect following improved health, we demonstrated the need to resolve the time variable (proxy of dietary intervention) and covariate effects in real data. The research question is whether the beneficial outcome is a direct effect of the intervention or an indirect effect following the alteration of the medication regimen. Below we show that LongDat could disentangle the intervention's beneficial direct

Downloaded from https://academic.oup.com/bioinformaticsadvances/article/3/1/vbad063/7172481 by Duke University user on 21 August 2023

effect from the indirect effect of the changes in drug dosage. Finally, to demonstrate LongDat's flexibility to deal with other datatypes besides microbiome data, we also applied LongDat to the immunome data in the study described above.

2 Methods

2.1 The LongDat method

The LongDat pipeline comprises three major steps, namely the null time model test, covariate model test and effect size calculation (Fig. 1).

1. *Null time model test.* We test whether time associates significantly with each feature (dependent variable), regardless of covariates. LongDat incorporates several R packages specializing in GLMMs, such as MASS, lme4 and glmmTMB (Bates *et al.*, 2015; Brooks *et al.*, 2017; Venables *et al.*, 2002), providing high flexibility for input data types. A negative binomial model is used to fit count data composed of integers (Ver Hoef *et al.*, 2007), such as numbers of sequencing reads. A beta model is applied to proportion data (i.e. that range between 0 and 1) (Ferrari *et al.*, 2004). For binary data (consisting of either 0 or 1), binary logistic regression is performed (Nick *et al.*, 2007). For ordinal data (where the features correspond to ranks), a proportional odds model is adopted (Liu, 2009). Finally, continuous data are first normalized and then fitted by linear models. Each model is a random intercept model with the sample donor origin treated as a random factor to account for between-individual variability and non-independence of samples from the same donor. *P*-values are adjusted for multiple testing using the Benjamini-Hochberg method or other approaches (Benjamini *et al.*, 1995).
2. *Covariate model test.* If covariates are present in a dataset, this step identifies them and disentangles their effects from those of variables of interest (here, the time variable). In the metadata, covariates that exhibit significant association with each feature (e.g. microbiome abundance) via non-parametric tests (i.e. the Wilcoxon rank-sum, Kruskal-Wallis or Spearman's correlation test) are selected. And then, each selected covariate is included one by one as a fixed effect, together with the time variable, in GLMMs to examine whether or not the time associations can be reduced to the influence of each covariate, reflecting the 'vibration of effects' (VoE) concept (Tierney *et al.*, 2021). VoE is the degree to which different combinations of independent variables (e.g. adding covariates) change the outcome and assessed significance of a model. The larger the VoE, the less robust the association is between features and independent variables. That is, a true association should remain significant across all model configurations. Significant time-dependent features are subsequently classified as fulfilling conditions of 'effect not reducible to covariate', 'entangled with covariate' or 'effect reducible to covariate' according to these model tests. If the time variable remains a significant predictor in all models, the feature will be flagged as 'effect not reducible to covariate'. If the time variable loses significance but the covariate does show significance in any of the models, the feature is marked as 'effect reducible to covariate'. If there is no clear covariate but at least one model in which the covariate and time both failed to show significance, the feature will be labeled 'entangled with covariate'.
3. *Effect size calculation.* Non-parametric effect size calculations are implemented. These are Spearman correlation for continuous time variables (e.g. day) and Cliff's delta for discrete time variables (e.g. before/after treatment) (Macbeth *et al.*, 2010). Effect size calculation is based on a naïve association between the independent variable and the feature, without being partitioned by covariates. Therefore, to ensure LongDat calculates the correct effect size, treatment effects should be monotonic (i.e. no change in the direction of association) within the time interval of the input data. If this is not the case, analyses should be done separately on time subranges of the data for which monotony holds.

All results of the steps mentioned above are summarized into two tables. One table lists the significance estimate (*q*-values adjusted for multiple testing) of time dependence and effect sizes across all features. The other table lists relevant covariates with relative reducibility status for each of them.

2.2 LongDat package overview

LongDat is built with R (≥4.0.0), and its dependencies include lme4 (≥1.1-28) (Bates *et al.*, 2015), glmmTMB (≥1.1.3) (Brooks *et al.*, 2017), reshape2 (≥1.4.4) (Wickham, 2007), emmeans (≥1.7.3) (Lenth, 2021), bestNormalize (≥1.8.2) (Peterson, 2021), MASS (≥7.3-56) (Venables *et al.*, 2002), tidyverse (≥1.3.1) (Wickham *et al.*, 2019), effsize (≥0.8.1) (Torchiano, 2020), patchwork (≥1.1.1) (Pedersen, 2020) and car (≥3.0-12) (Fox *et al.*, 2019). There are four main functions that are the most relevant to users of the LongDat package (Fig. 1). For more detailed tutorials for LongDat, please visit GitHub (https://github.com/CCY-dev/LongDat), or install LongDat and then access its vignettes with the command 'browseVignettes("LongDat")'.

2.3 Simulation of longitudinal data with microbiomeDASim

Longitudinal data corresponding to microbiome taxonomic abundance measurements from a cohort were simulated using microbiomeDASim (Williams *et al.*, 2019). MicrobiomeDASim is an R package aimed at simulating longitudinal differential microbiome

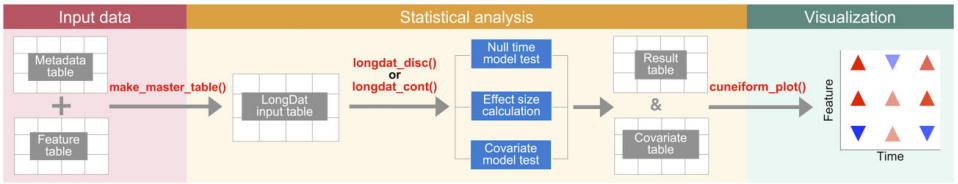

Fig. 1. LongDat pipeline overview. Flowchart of LongDat showing the major functions (bold text in red) and steps. The function 'make_master_table()' creates a master table that can be taken as input by joining metadata and feature tables provided by the user. The two functions 'longdat_disc()' and 'longdat_cont()' both perform covariate-sensitive analyses. The main components of them are the null time model test, the effect size calculation and the covariate model test, applied to input master tables to perform covariate-aware tests for the significance of the time variable (the proxy of treatment). The function 'longdat_disc()' is suitable for data where time is discrete (e.g. a before/after treatment dataset), whereas 'longdat_cont()' is for data with time represented as a continuous variable (e.g. day). Finally, the function 'cuneiform_plot()' generates a summarizing plot of the result table. For more detailed tutorials of LongDat application, please visit GitHub (https://github.com/CCY-dev/LongDat), or refer to its vignettes

Downloaded from https://academic.oup.com/bioinformaticsadvances/article/3/1/vbad063/7172481 by Duke University user on 21 August 2023

data. It allows the users to define sparsity, effect size, number of samples and time points. Here, simulated data were generated from a multivariate normal distribution, and the parameter encoding the longitudinal dependency within individuals was a first-order autoregressive correlation structure.

1. *Simulated data with no covariate.* For each sample size (10, 20, 38, 75, 150 and 300) and effect size (Spearman's rho median ≈ 0.2 or 0.5 for time-varying features) combination, 100 simulations were performed. Each simulated dataset contained 200 features. Among them, 20 features changed over time/under intervention, while the remaining 180 were sampled from the same distribution across time points. Two time points were simulated for each individual.
2. *Simulated data with a single covariate for covariate effect analysis.* A dummy variable correlating with the time variable was manually added to the aforementioned simulated dataset (sample size = 75, effect size median ≈ 0.5). The dummy variable was sampled to correlate with the time variable at a Spearman's rho of approximately 0.25, 0.5, 0.75 or 0.99. For each correlation level, 100 simulations were performed. For the negative-control data, we shuffled the time variable against all other variables randomly within each individual to wipe out the association between the time variable and the features, and the association between the time variable and the covariates.
3. *Simulated data with multiple covariates.* 1, 2, 4, 8 or 16 dummy variables correlating with the time variable were manually added to the abovementioned simulated dataset (sample size = 75, effect size median ≈ 0.5). The dummy variables were randomly sampled to correlate with the time variable at a Spearman's rho of approximately 0.25, 0.5, 0.75 or 0.99. For each correlation level, 100 simulations were performed. For the comparison between LongDat and Maaslin2, each dataset contained 200 features (20 changed over time and 180 did not), and for each combination of sample size, effect size and tool, 100 simulations were performed. For the comparison between LongDat, ANCOM, lpgr and ZIBR, each dataset contained 100 features (10 changed over time and 90 did not), and 50 simulations were performed for each combination of sample size, effect size and tool. The reduction of feature number and simulation number was due to the heavy computational resource ANCOM (large memory), lgpr (long runtime) and ZIBR (long runtime) required.

2.4 Simulation of longitudinal data with SparseDOSSA2

Besides microbiomeDASim, another set of longitudinal microbial data was simulated using SparseDOSSA2 (Ma *et al.*, 2021). SparseDOSSA2 is an R package specialized for simulating realistic new microbiome data templated on real microbial communities. In these longitudinal data simulations, SparseDOSSA2 adopts generalized linear models to create feature-covariate associations (here, the time variable and other covariates) specified by users, and the template was based on stool microbiome. We followed the tutorial of SparseDOSSA2 (https://github.com/biobakery/biobakery/wiki/SparseDOSSA2) as a complementary approach to the above to simulate longitudinal microbial data for benchmarking.

1. *Simulated data with no covariate.* For each sample size (10, 20, 38, 75, 150 and 300) and effect size (Spearman's rho median ≈ 0.2 or 0.5 for time-varying features) combination, 100 simulations were performed. Each simulated dataset contained 332 features. Among them, 33 features were spiked (changed over time/under intervention), while the remaining ones were sampled from the same distribution across time points. Two time points were simulated for each individual.
2. *Simulated data with multiple covariates.* 1, 4 or 16 dummy variables correlating with the time variable were manually added to the abovementioned simulated dataset with 332 features and varying sample sizes. The dummy variables were randomly sampled to correlate with the time variable at a Spearman's rho of approximately 0.25, 0.5, 0.75 or 0.99. For each correlation level, 100 simulations were performed.
3. *Simulated negative control data.* Simulations were done to generate 100 sets of data with two time points, 150 individuals, 332 microbes and zero effect size for all microbial features (i.e. no spiked feature). Six versions of the data with different sequencing depths (the sum of microbial abundance of each feature) were further generated, to test the impact of systematic effects on sampling depth as may occur, for example, in clinical low biomass datasets. Accordingly, for these simulated data, any signal detected will reflect such systematic bias only. In versions one and two of the simulation, both of the total abundances at the first and second time points of each individual were rarefied to 50 000 and 1000, respectively. In version three, the total abundances at the first time point were rarefied to 50 000 and the second time point to 5000, while in version four, the total abundances at the first time point were rarefied to 5000 and the second time point to 50 000. In version five, the total abundances at the first time point were rarefied to 50 000 and the second time point to 1000, while in version six, the total abundances at the first time point were rarefied to 1000 and the second time point to 50 000. When applying LongDat count mode (running negative binomial models), versions three to six were further rarefied to either 5000 or 1000 (as per the lowest sequencing depth) at both time points, such that the sequencing depths are the same between the two time points, reflecting how a user concerned over unequal sampling depths would preprocess the data for this method.

2.5 Normalization of the data simulated by SparseDOSSA2

Several R packages were used to normalize or transform the raw simulated microbial features from SparseDOSSA2, TSS, rarefaction (Saary *et al.*, 2017), CLR (van den Boogaart *et al.*, 2008), GMPR (Chen *et al.*, 2018), TMM (Robinson *et al.*, 2010) and CSS (Metwally *et al.*, 2018). The combinations of the tools (LongDat, MaAsLin2, lgpr, ZIBR) and the normalization methods are limited by each tool's requirement of the input format.

2.6 Running LongDat on simulated longitudinal data

The function 'longdat_cont()' in the LongDat package was used for analyzing simulated longitudinal data, where the time between samplings was treated as a continuous variable and the data type as count data. The R package peakRAM was adopted to record running time and memory usage (Quinn, 2017). Feature associations with Benjamini-Hochberg (BH)-corrected null-model q-value < 0.1 and BH-corrected post-hoc test q-values < 0.05 were considered significant. LongDat was run under CentOS Linux 7 and R version 4.1.1 with 8 GB of memory allocated.

2.7 Running MaAsLin2 on simulated longitudinal data

The function 'Maaslin2()' in the MaAsLin2 package was used for analyzing simulated longitudinal data, where the time between samplings was treated as a continuous variable, and the mode was set as 'NEGBIN' for negative binomial model mode and 'LM' for linear model mode (Mallick *et al.* 2021). Since MaAsLin2 lacks a covariate model test component that corresponds to the second part of the LongDat pipeline, we ran MaAsLin2 with two separate runs (with and without simulated covariate included as a fixed effect,

Downloaded from https://academic.oup.com/bioinformaticsadvances/article/3/1/vbad063/7172481 by Duke University user on 21 August 2023

respectively) for each simulated data with covariates, such that the MaAsLin2 result is comparable with that of LongDat. Features with BH-corrected q-value < 0.1 were considered significant. MaAsLin2 was run under CentOS Linux 7 and R version 4.1.1 with 8 GB of memory allocated.

2.8 Running ANCOM on simulated longitudinal data

The function ANCOM in the ancom. R Rscript (https://github.com/FrederickHuangLin/ANCOM-Code-Archive) was used for analyzing simulated longitudinal data. The time between samplings was treated as a factor, while the random formula was set as sample ID, and the adjust formula included all the present covariates. Features were considered significant if their W statistics passed the cutoff of the number of taxa multiplied by 0.7. ANCOM was run under CentOS Linux 7 and R version 4.1.1 with 350 GB of memory allocated.

2.9 Running ZIBR on simulated longitudinal data

The function 'zibr()' in the ZIBR package (Chen *et al.*, 2016) was used for analyzing simulated longitudinal data, where the time between samplings was treated as a continuous variable. All covariates in the data were included for analyses, while subjects and time points were specified. Features with joint P values corrected by BH < 0.1 were considered significant. ZIBR was run under CentOS Linux 7 and R version 4.1.1 with 8 GB of memory allocated.

2.10 Running lgpr on simulated longitudinal data

The function 'lgp()' in the lgpr package (Timonen *et al.*, 2021) was used for analyzing simulated longitudinal data, where the time between samplings was treated as a continuous variable. Sample ID was set as the random effect, and all covariates in the data were included for analyses. The number of drawing samples from a Stan model was 100, and the number of Markov chains was 4. If the time variable was selected using a 95% threshold for the proportion of total explained variance, then the feature was considered significant. Lgpr was run under CentOS Linux 7 and R version 4.1.1 with 8 GB of memory allocated.

2.11 Semi-synthetic evaluation of metagenomic data: Fasting study

To perform a semi-synthetic evaluation based on real microbiome data, we selected the first and second time points from the stool microbiome data, using bacterial genus abundances. Next, we randomly shuffled the time variable against all other variables for each individual to eliminate any associations between the time variable and the microbes, as well as between the time variable and the covariates, such that no real signal of the intervention or of the passage of time should remain. Data were normalized or rarefied as the methods in the 'normalization of the data simulated by SparseDOSSA2' section.

2.12 Evaluation of real metagenomic and immunome data: Fasting study

The fasting study reanalyzed here reported on a clinical cohort investigating fasting effects on patients with MetS (Maifeld *et al.*, 2021). This study has two arms, one being the fasting arm and the other being the DASH (Dietary Approaches to Stop Hypertension, DASH) arm. MetS patients in the fasting arm first underwent seven-day fasting, which consists of two days in which the patients took in a maximum of 1200 kcal/day and five days in which the patients took in 300–350 kcal/day. And then, there was a three-month refeeding stage where MetS patients were asked to follow the DASH diet. Microbial abundance at the species level and the immunome data of the fasting arm were reanalyzed to demonstrate the value and performance of LongDat.

3 Results

3.1 LongDat outperforms MaAsLin2 when there are multiple covariates in the simulated data

First, we compared the performance of LongDat with its closest counterpart up to date, MaAsLin2, by running them on microbiomeDASim-simulated longitudinal datasets templated on microbiome data from cohort studies without covariates. The default setting of MaAsLin2 was doing total-sum scaling (TSS) that converted the data into relative abundance and then fitting linear model (LM). However, this default setting performs worse than using the negative binomial model in terms of accuracy, true positive rate (TPR), false discovery rate (FDR) and Matthews correlation coefficient (MCC) (Supplementary Fig. S1). Therefore, we focused on the MaAsLin2 negative binomial model mode results instead of its default setting. Both LongDat and MaAsLin2 use negative binomial models to fit the data. LongDat and MaAsLin2 have comparable accuracy ranging between 0.9 and 1 (Fig. 2). While MaAsLin2 achieves a higher TPR when sample sizes are small, this comes at the cost of a higher FDR. In contrast, the FDR median of LongDat was controlled at zero across all tested effects and sample sizes, while TPR increases with sample size (Supplementary Fig. S2). LongDat and MaAsLin2 have comparable memory footprints, whereas LongDat has a longer runtime (Fig. 3A and B) due to the additional covariate model test, which MaAsLin2 does not possess. Although MaAsLin2 and LongDat perform similarly on simulated data without covariates, their difference in performance rises as the number of covariates increases in the simulated data (Supplementary Figs S3A, B, S4A and B). The performance of LongDat remains stable across all numbers of covariates. In contrast, FDR escalates and TPR diminishes in MaAsLin2 as the number of covariates increases, especially when more than four covariates are present.

Apart from evaluating LongDat and MaAsLin2 using microbiomeDASim-simulated data, we utilized SparseDOSSA2, another microbiome data simulation tool, to validate that the benchmarking outcome of LongDat is consistent between different simulation tools. Here, we assessed the performance of LongDat and MaAsLin2 using various modes, such as linear or negative binomial models, on simulated data that was either raw, normalized or rarefied. The benchmarking of performance and requirement of computational resources on SparseDOSSA2-simulated data with 0 (Supplementary Fig. S5A and B), 1 (Supplementary Fig. S6A and B), 4 (Fig. S7 and S7B) and 16 covariates (Supplementary Fig. S8A and B) are presented. Within a broader perspective, these results reproduce our findings in the benchmarking using microbiomeDASim-simulated data, where MaAsLin2 and LongDat perform similarly on simulated data in the absence of covariates. However, as the number of covariates increases, the performance gap between the two methods becomes more evident. The performance of LongDat remains stable across all numbers of covariates while FDR surges and TPR diminishes in MaAsLin2, particularly when more than four covariates are present. Upon closer examination of each normalization method, MaAsLin2's negative binomial model mode generally produces higher TPR but also higher FDR than its linear model mode (except when run on CLR-transformed data, which has a high FDR), thus similar accuracy and MCC. On the other hand, LongDat produces comparable outcomes when either linear or negative binomial models are run on data processed through different normalization or rarefaction methods (except for CLR paired with linear model, which performs the worst). Specifically, we believe rarefaction is necessary for some situations, although the pair of negative binomial model and rarefied count data has higher FDR than the pair of linear model TSS-normalized data. For example, we simulated longitudinal negative control data with two time points in which the sequencing depths varied systematically between the two points. In this scenario, the negative binomial model applied to rarefied count data maintains a near-zero false positive rate (FPR), while the linear model applied to non-rarefied TSS-normalized data results in a high FPR when the depth variation between the two time points was large (Supplementary Fig. S9). Therefore, we conclude that the use of linear models to analyze TSS-normalized data is reasonable

Downloaded from https://academic.oup.com/bioinformaticsadvances/article/3/1/vbad063/7172481 by Duke University user on 21 August 2023

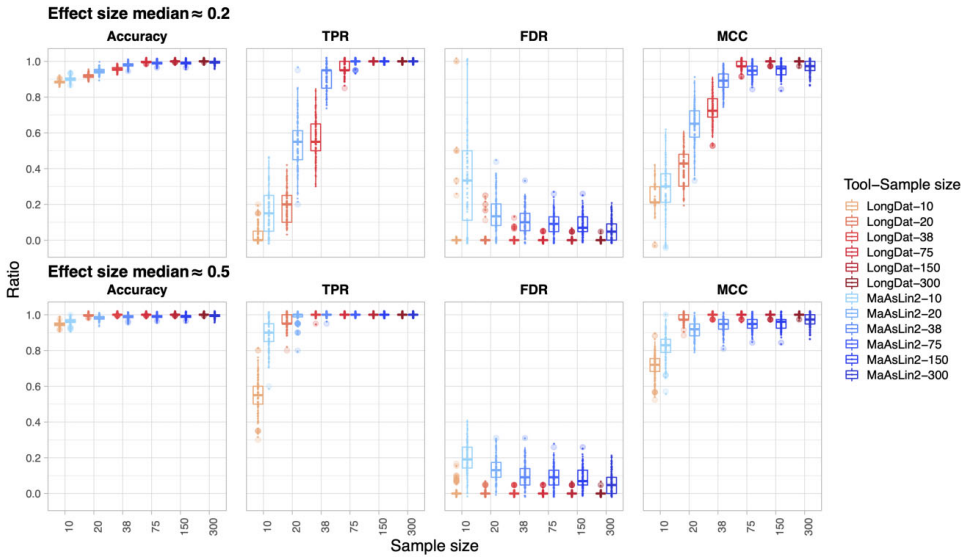

Fig. 2. Comparison of LongDat and MaAsLin2 (using the negative binomial model mode) on performance and power applied to microbiomeDASim-simulated longitudinal data. The box plots show the accuracy, true positive rate (TPR), false discovery rate (FDR) and Matthews correlation coefficient (MCC). The upper panel features a low effect size (median ≈ 0.2) while the lower panel features a medium effect size (median ≈ 0.5). For each combination of sample size, effect size and tool, 100 simulations were performed

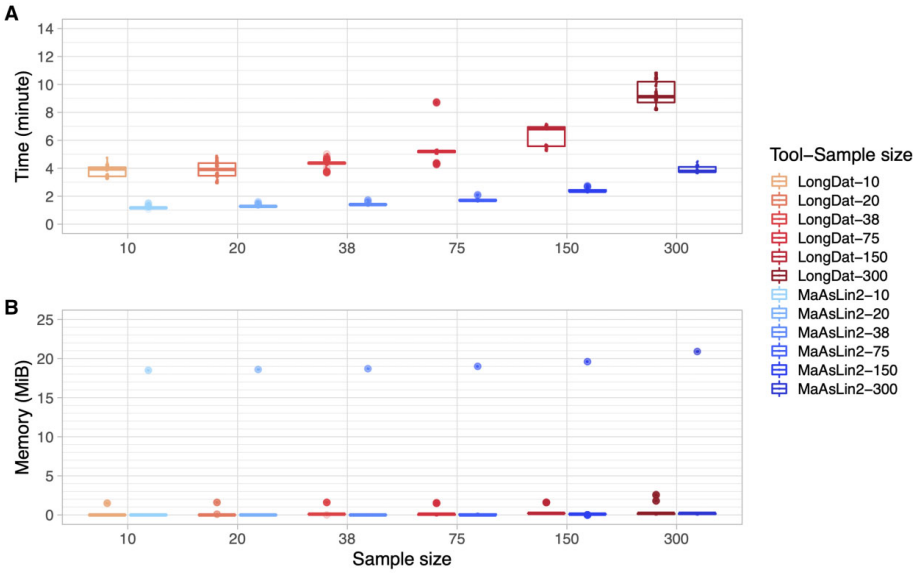

Fig. 3. Comparison of LongDat and MaAsLin2 (using the negative binomial model mode) on computational resource profiling applied to microbiomeDASim-simulated longitudinal data. Runtime (**A**) and total used memory (**B**) required by LongDat and MaAsLin2 when run on simulated data with 200 features and various sample sizes. For each sample size, 200 simulations were performed. 1 mebibyte (MiB) ≈ 1.05 megabyte (MB)

Downloaded from https://academic.oup.com/bioinformaticsadvances/article/3/1/vbad063/7172481 by Duke University user on 21 August 2023

only when there is no systematic bias in sequencing depth between groups or time points; otherwise, the analysis may result in many false positives. There is no method suitable for all scenarios; instead, the selection of an appropriate approach highly depends on the data's nature.

3.2 LongDat outperforms ANCOM in computational efficiency and outperforms lgpr and ZIBR in overall performance when tested on simulated data

In addition to MaAsLin2, we also compared LongDat with several other tools capable of analyzing longitudinal microbiome data, including ANCOM, lgpr and ZIBR, by examining their performances when multiple covariates are present (Supplementary Figs S10A, B, S11A and B). Here the simulated data were generated by microbiomeDASim. The results show that the FDR of ANCOM remains around zero as LongDat does and has comparable accuracy, TPR and MCC when there are less than four covariates, whereas TPR dwindles as the number of covariates increases. The major drawback of ANCOM is that it needs large memory (requires 350 GB to be allocated or else errors would occur and halt) to run through each simulated dataset (here each containing 100 features), making it challenging to run ANCOM on a large scale. ZIBR does not perform well because its FDR is high, and its accuracy, TPR and MCC are low across all numbers of covariates. Moreover, ZIBR needs much time to run through each dataset with large sample sizes (e.g. around 55 h to finish a run with 300 samples and 16 covariates). Lastly, while lgpr has better TPR than LongDat when the sample size is small ($\leq$38), it simultaneously has a high level of FDR. The primary shortcoming of lgpr is that its run time (e.g. around 65 h with 150 samples and 1 covariate) is substantially longer than all other tools, and it could not finish any run within the time limit (96 h) of the high-performance computing cluster we used. This impedes lgpr from being widely applied to microbiome data in a common research environment. From these results, we concluded that LongDat is the ideal tool for data with multiple covariates since it has decent performance and low computational resource requirements (Supplementary Table S1).

As we did with the comparison between LongDat and MaAsLin2, we employed SparseDOSSA2 to assess the performance of LongDat, lgpr and ZIBR, in addition to the microbiomeDASim-simulated data comparison. ANCOM's high memory requirement (>350 GB) for SparseDOSSA2-simulated data analysis caused it to fail to run on the high-performance computing cluster we utilized, leading to its exclusion from the analysis here. The assessment of computational resource requirements and performance benchmarking using SparseDOSSA2-simulated data with varying numbers of covariates (0, 1, 4 and 16) is depicted in Supplementary Figures S12A, B, S13A, B, S14A, B, S15A and B, respectively. These findings confirm our earlier observations based on microbiomeDASim-simulated data. ZIBR, which operates on TSS-normalized data, has a high FDR and takes a long time to execute. lgpr performs better than LongDat in terms of TPR for small sample sizes, regardless of normalization or rarefaction, but it also has a high FDR. The primary disadvantage of lgpr is that it takes significantly longer to run than any of the other tools, making it not able to complete any run within the time limit (96 h) of the high-performance computing cluster we used when the sample size is relatively large. The performances of both ZIBR and lgpr decline as the number of covariates increases. In contrast, LongDat maintains decent performance and computational resource requirements regardless of the number of covariates.

3.3 The performance of LongDat was evaluated using semi-synthetic data, demonstrating a low false positive rate

To estimate the performance of LongDat based on data aside from simulated data (microbiomeDASim and SparseDOSSA2), we conducted a semi-synthetic evaluation as well. In this evaluation, we shuffled the time variable against all other variables in the fasting microbiome data (at the genus level). Next, we compared the ratio of significant associations between unshuffled and shuffled data. The result of LongDat indicates few to no false positives in the shuffled data in all modes, regardless of whether covariates were included or excluded in the analysis (Supplementary Fig. S16). Conversely, MaAsLin2, lgpr and ZIBR were all influenced by the presence of covariates in their analyses. MaAsLin2 identifies fewer significant associations in the unshuffled data and more false positives in the shuffled data than LongDat. ZIBR and lgpr result in much higher false positive rates than LongDat. Consistent with prior analyses, we confirmed that LongDat is robust against false positive findings in both simulated and semi-synthetic evaluations.

3.4 LongDat provides a more smooth and more efficient workflow than MaAsLin2 despite similar performance

Since MaAsLin2 is the only alternate tool where memory and runtime scaling do not preclude its application to our full benchmark, the analyses below focus on the comparison between MaAsLin2 and LongDat. To compare the performance of LongDat and MaAsLin2 on detecting covariate effects, we added a dummy variable correlating with the time variable and tested whether this dummy variable, when instead used as the time input variable, was wrongly reported as exhibiting a relationship to the simulated feature independent of time (Fig. 4A and B). LongDat requires only a single run for this test. In contrast, MaAsLin2 lacks a covariate model test component corresponding to the LongDat pipeline's second part, so we ran MaAsLin2 in two separate runs (with and without covariate included in the model, respectively) to generate comparable results with LongDat. We found that LongDat and MaAsLin2 achieved similar performance, with the median success rate for both tools in correctly concluding covariate effects remaining at $\sim$0.95 (as per FDR threshold/family-wise error rate) even when the dummy and time variables were strongly correlated. As a negative control, we tested how LongDat performs when both the features and covariates are not associated with time by shuffling the time variable randomly within each individual (Supplementary Fig. S17). Here we tested if the shuffled time variable was reported as significant. We found no false positive occurred across all correlation degrees (the correlation between the time variable and covariate was, in fact, destroyed because time was shuffled). These results demonstrate that both LongDat and MaAsLin2 perform well in accuracy and correctly flagging covariates.

In the simulated data, with rho being as high as 0.99 between the dummy and time variables, we demonstrated that LongDat could distinguish data generated from different underlying ground truths even when there is substantial confounding. It is worth noting that LongDat does not label the dummy variable as 'non-significant' (i.e. having no relationship with the feature at all) but rather as 'reducible to covariate' or 'entangled with covariate' when the correlation degree is high. These two labels do not signify that the dummy variable is irrelevant to the features but instead intend to communicate that its association with the features might be from an indirect association. In real data, however, it will be more challenging to discern between the dummy and the time variables if they are highly correlated. In that case, more investigation or experiments are required to confirm which variable has direct versus indirect influence, necessitating more careful inspection and domain knowledge before robust conclusions can be drawn.

3.5 LongDat performs more robustly than MaAsLin2 in real data with multiple covariates

Subsequently, to compare the performance of LongDat and MaAsLin2 on real data, we reanalyzed gut microbial data from a clinical cohort investigating fasting effects on patients with MetS (Maifeld *et al.*, 2021). One aim of the study was to investigate how fasting affects blood pressure while controlling for changes in medication. When no covariates (i.e. medication variables) were included in the MaAsLin2 analysis, LongDat and MaAsLin2 each identified 27 microbial species that were significantly altered in abundance throughout the intervention, with 19 of them being consistent

Downloaded from https://academic.oup.com/bioinformaticsadvances/article/3/1/vbad063/7172481 by Duke University user on 21 August 2023

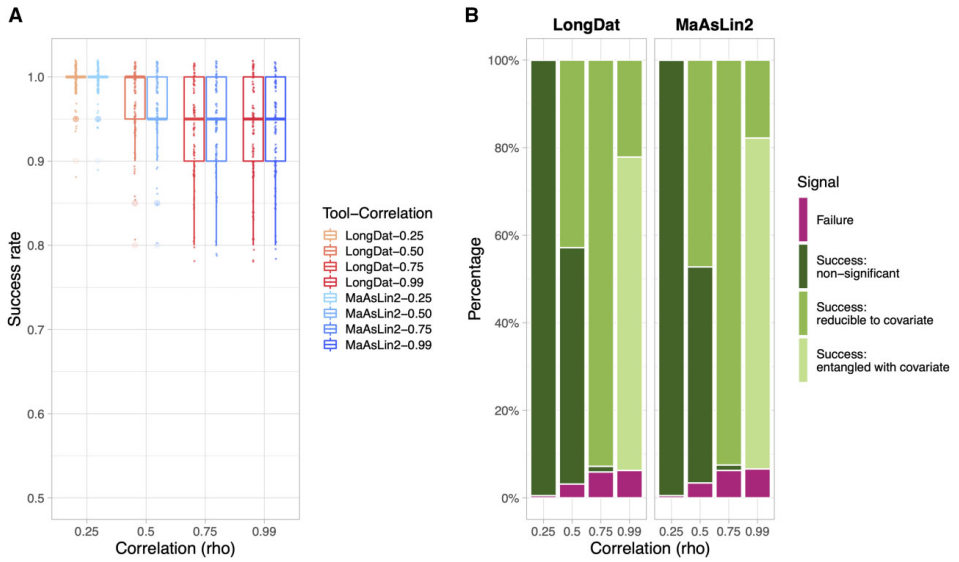

Fig. 4. Comparison of LongDat and MaAsLin2 on covariate-sensitive analysis applied to microbiomeDASim-simulated longitudinal data. To compare the ability of LongDat and MaAsLin2 on detecting covariates, a dummy variable was added to the simulated data and was tested for its effect. 'Success' is defined as a tool indicating the dummy variable as either 'non-significant', 'reducible to covariate' or 'entangled with covariate' (time is the covariate here), whereas 'failure' occurs when a tool wrongly concludes that the dummy variable is significant and the time variable is not. (**A**) The box plot shows the success rate of using LongDat and MaAsLin2 to filter out and conclude covariate effects at different degrees of correlation between the dummy variable and time. (**B**) The bar chart illustrates the proportion of success and failure across correlation degrees. For each degree of correlation, 100 simulations were done

between the two (Fig. 5A and B; Supplementary Tables S2, S3 and S4). However, when covariates were included, only two species were reported significantly different in abundance by MaAsLin2 (Supplementary Table S5). This is because models fitting most of the significantly affected species returned errors (showed NA in *P*-values and standard errors) when multiple fixed effects were included. LongDat avoids this problem by having only one covariate in a model at one time and loops over all of them. Thus, LongDat performs more robustly than MaAsLin2 for this type of data when multiple covariates are present in the dataset, but at the cost of higher runtime.

3.6 LongDat can be applied to other data types, such as immunome data

Finally, to demonstrate that LongDat can run on other data types besides microbiome data, we applied LongDat to the immunome data from the same fasting study mentioned above (Supplementary Figs S18 and S19; Supplementary Tables S6–S9). The immunome data consist of proportion (percentage) and non-proportion (non-percentage) data, so they were analyzed by LongDat proportion mode and measurement mode, respectively. These results show that LongDat can tackle other types of data in addition to microbiome counts.

4 Discussion

We introduce LongDat, an R package that analyzes longitudinal data for intervention (or treatment) effects while accounting for covariates throughout the intervention. LongDat was developed and tested as a microbiome analysis tool, and we made it able to work on other high-dimensional data types by using flexible and robust approaches, chiefly GLMMs and non-parametric tests. The resulting output allows convenient downstream analysis and interpretation. Instead of proposing a new theory or mathematical tool to deal with the problems of high-dimensional data, multiple covariates and different data types (distribution), we packaged the GLMMs and non-parametric tests together to automate the process of analyzing high-dimensional data. LongDat relieves the users of the burden of having to program the R linear modeling functions from scratch. With the standardized output, including effect sizes reported in Cliff's delta, and the visualization of the significances and influences of covariates for each feature, it is easier for biologists to integrate, compare and visualize their findings. Though here we do not present a theoretical advance, we believe LongDat is a practical and convenient modeling tool immediately applicable to the scale of problems faced, e.g. in cohort- or intervention-centered systems medical research, and therefore promotes high-dimensional data analysis in the biomedical research field. One limitation of LongDat is that it reports standardized non-parametric effect sizes of discrete (Cliff's delta) or continuous (Spearman's rho) variables, both of which are calculated independently of other covariates. Thus, when covariates are present in the data, the reported effect size is not a perfect estimate as it does not incorporate covariates for calculation. We currently are not aware of any partial standardized directional effect size metrics that would let us circumvent this obstacle, but we are actively searching for them to include in later versions of LongDat.

By conducting simulations using two independent tools, namely microbiomeDASim and SparseDOSSA2, we confirm that the statements below are consistent across benchmarking platforms. The advantages of LongDat over the most similar existing tool, MaAsLin2, include lower FDR, the ability to explicitly report covariate effects and their effect sizes, and thus a more convenient functionality in reporting and describing covariates for each feature. The latter, which reports the influence of covariates on the tested variable, is the exclusive feature of LongDat that no other tool possesses to the best of our knowledge. The other important feature of LongDat is that it can handle multiple covariates at once and maintain stable performance. This feature is achieved by having only one

Downloaded from https://academic.oup.com/bioinformaticsadvances/article/3/1/vbad063/7172481 by Duke University user on 21 August 2023

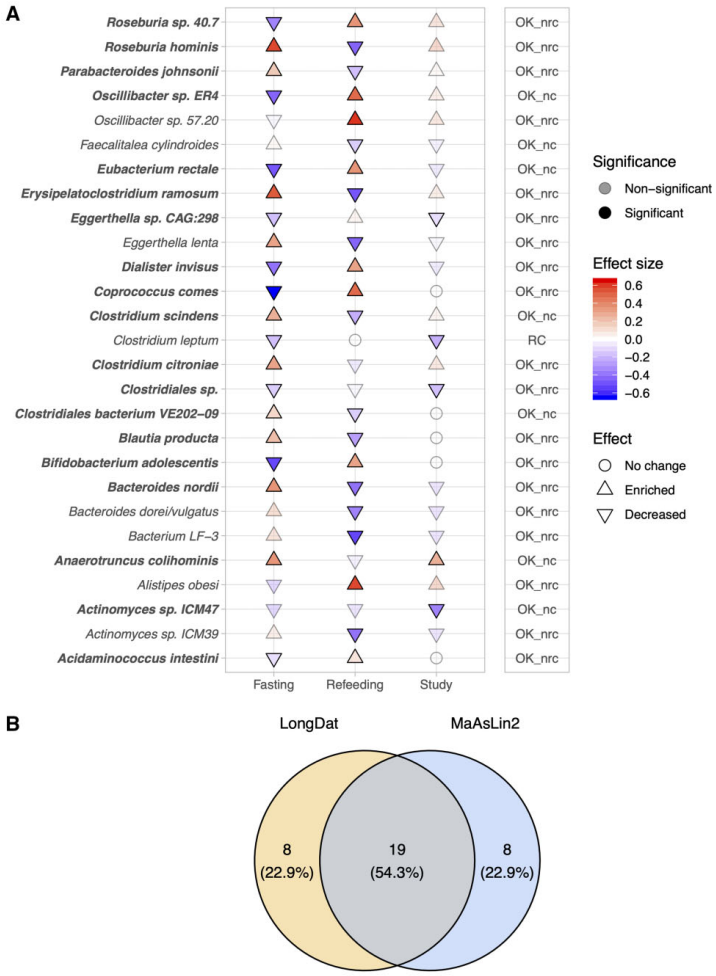

Fig. 5. Comparison of LongDat and MaAsLin2 on analyzing real microbiome data. (**A**) The cuneiform plot on the left panel shows the gut microbes (species level) that display significant differences in their abundance in at least one of the time intervals in the assessed study (Maifeld *et al.*, 2021). In that study, metabolic disease patients underwent 7-day fasting and then a 3-month re-feeding period. In the plot, 'fasting' indicates the time elapsed from Day 0 to 7, while 'refeeding' indicates Day 7 to 90, and 'study' indicates the overall duration from Day 0 to 90. Bold species are the ones that appeared significant in both LongDat and MaAsLin2 results. The right panel reports the covariate status of each microbe as follows. *OK_nc*: OK and no covariate. Time/intervention has significant effect and there is no covariate. *OK_nrc*: OK and not reducible to any covariate. Time/intervention has significant effect, and its effect is independent of all tracked covariates. *RC*: Effect reducible to covariate. Time/intervention when tested on its own achieves significance; however, its effect is better explained by that of a covariate (whereas the inverse is not true). Microbes with BH-corrected model test q-values < 0.1 and BH-corrected post-hoc test q-values < 0.05 are regarded as significant. (**B**) The Venn diagram shows the significant species found by LongDat and MaAsLin2. Numbers indicate counts and percentages of each category. Note that for MaAsLin2, covariates were not included in the analyses here. When covariates were included in MaAsLin2 analysis, only 2 of the species showed significance here remained significant, while all others returned error due to NA in *P*-values and standard errors (Supplementary Table S5)

covariate in a model at one time and looping over them instead of including all covariates at once, which forms a lengthy formula. This approach grants LongDat robustness when facing multiple covariates, but at the cost of higher runtime. By contrast, the performance of MaAsLin2 is highly dependent on the number of covariates in the data. While MaAsLin2 and LongDat have comparable accuracy when there are no covariates, we observe a trade-off between TPR and FDR in them. Hence, MaAsLin2 and LongDat are suitable in different scenarios depending on the priorities of the application. For instance, when a lower FDR is more emphasized in an analysis, or when there are many covariates in a study, LongDat will be a better choice. In contrast, if a higher TPR and power are prioritized, and no covariate is in the data, then MaAsLin2 is a good option.

In addition to MaAsLin2, we also compared LongDat with three other tools: ANCOM, lgpr and ZIBR. While the performance of ANCOM is fairly good when the number of covariates is low, ANCOM suffers from the need for huge memory to run. On the

Downloaded from https://academic.oup.com/bioinformaticsadvances/article/3/1/vbad063/7172481 by Duke University user on 21 August 2023

other hand, the performances of both lgpr and ZIBR are highly dependent on the number of covariates, and both tools suffer from long runtime. Furthermore, ANCOM and lgpr rely on arbitrary cutoffs (W statistics and the proportion of total explained variance, respectively), which might pose inconvenience and confusion to the users. Despite the unfavorable ZIBR results shown here, we believe in the potential of the zero-inflated models (represented by ZIBR here) since they characterize the distribution of highly sparse microbiome data well. We will keep track of its development (or other related zero-inflated models) and plan to integrate it into the future version of LongDat.

To investigate the impact of normalization and rarefaction on analysis results, we conducted benchmarking tests on each tool using different preprocessing methods. Interestingly, we find that LongDat and MaAsLin2 have similar overall performance (based on accuracy and MCC) when analyzing data without any covariates, irrespective of the modes (negative binomial or linear model) and preprocessing methods (except for the CLR transformation). However, the discrepancy in the performance of LongDat and MaAsLin2 widens as the number of covariates increases. While all modes of MaAsLin2 struggle to maintain high true positive rates and low false discovery rates with four or more covariates, LongDat remains stable and performs well across all scenarios. Meanwhile, ZIBR and lgpr did not excel in this round of benchmarking test because of high FDR and extremely long runtime that impedes the users from applying them effectively. Furthermore, by simulating datasets with high variation in sequencing depth between time points (or groups), we underscored that the choice of normalization or rarefaction technique should be tailored to the specific characteristics of the data. In the example above, rarefaction is required to remove the systematic bias between time points, which leads to false positive findings. Ultimately, we believe that there is no one-size-fits-all approach to data preprocessing and analysis, and researchers should carefully select appropriate protocols according to the unique features of their data.

In conclusion, our comprehensive benchmarking, including independent simulation tools, semi-synthetic and real data evaluations, demonstrates that the LongDat package we present here is a computationally efficient and low-memory-cost analysis tool for longitudinal data with multiple covariates, and facilitates robust biomarker searches in high-dimensional datasets.

Acknowledgement

We sincerely thank Morgan Essex for her insightful comments and revisions that significantly improved the manuscript in all aspects.

Author contributions

Chia-Yu Chen (Conceptualization [equal], Formal analysis [lead], Investigation [lead], Methodology [equal], Project administration [lead], Software [lead], Validation [lead], Visualization [lead], Writing—original draft [lead], Writing—review & editing [equal]), Ulrike Löber (Conceptualization [supporting], Methodology [supporting], Software [supporting], Supervision [supporting], Writing—review & editing [equal]) and Sofia Forslund (Conceptualization [equal], Formal analysis [supporting], Funding acquisition [lead], Investigation [supporting], Methodology [equal], Project administration [supporting], Resources [lead], Software [supporting], Supervision [lead], Validation [supporting], Visualization [supporting], Writing—original draft [supporting], Writing—review & editing [equal]).

Funding

This work was supported by the German Research Foundation (Deutsche Forschungsgemeinschaft, DFG) Collaborative Research Center (CRC) 1365 'Renoprotection'; the DFG as part of a Clinical Research Unit (CRU) 339 'Food Allergy and Tolerance' [428049112]; and the German Federal Ministry of Education and Research [EMBARK; 01KI1909B] under the frame of JPI-AMR [EMBARK; JPIAMR2019-109] to U.L.

Conflict of interest: All authors declare that they have no conflicts of interest.

Data availability

The scripts for simulating longitudinal data, running LongDat, ANCOM, lgpr, ZIBR and MaAsLin2, and also the raw data for the fasting study are available at https://github.com/CCY-dev/LongDat_paper_supplement.git. The stool sequencing data of the fasting study are deposited on NCBI under the accession PRJNA698459.

References

Asar,Ö. *et al.* (2013) mmm: an R package for analyzing multivariate longitudinal data with multivariate marginal models. *Comput. Methods Programs Biomed.*, **112**, 649–654.

Assent,I. (2012) Clustering high dimensional data. *WIREs Data Min. Knowledge Discov.*, **2**, 340–350.

Bates,D. *et al.* (2015) Fitting linear mixed-effects models using lme4. *J. Stat. Soft.*, **67**, 1–48.

Benjamini,Y. *et al.* (1995) Controlling the false discovery rate: a practical and powerful approach to multiple testing. *J. R. Stat. Soc. Ser. B (Methodological)*, **57**, 289–300.

Bolker,B.M. *et al.* (2009) Generalized linear mixed models: a practical guide for ecology and evolution. *Trends Ecol. Evol.*, **24**, 127–135.

Brooks,M.E. *et al.* (2017) Modeling zero-inflated count data with glmmTMB. *bioRxiv preprint*: 132753.

Calgaro,M. *et al.* (2020) Assessment of statistical methods from single cell, bulk RNA-seq, and metagenomics applied to microbiome data. *Genome Biol.*, **21**, 191.

Chen,E.Z. *et al.* (2016) A two-part mixed-effects model for analyzing longitudinal microbiome compositional data. *Bioinformatics*, **32**, 2611–2617.

Chen,L. *et al.* (2018) GMPR: a robust normalization method for zero-inflated count data with application to microbiome sequencing data. *PeerJ*, **6**, e4600.

Ferrari,S. *et al.* (2004) Beta regression for modelling rates and proportions. *J. Appl. Stat.*, **31**, 799–815.

Field-Fote,E. (2019) Mediators and moderators, confounders and covariates: exploring the variables that illuminate or obscure the "active ingredients" in neurorehabilitation. *J. Neurol. Phys. Therapy*, **43**, 83–84.

Fox,J. *et al.* (2019) *An {R} Companion to Applied Regression*. Sage, California, USA.

Gloor,G.B. *et al.* (2017) Microbiome datasets are compositional: and this is not optional. *Front. Microbiol.*, **8**, 1–6.

Gonçalves,M.H. *et al.* (2021) Cold: an R package for the analysis of count longitudinal data. *J. Stat. Soft.*, **99**, 1–34.

Hua,Z. *et al.* (2009) Study design: cross-sectional, longitudinal, case, and group. In: Wei, L., and Moyer, M.G. (eds) *The Blackwell Guide to Research Methods in Bilingualism and Multilingualism*, pp. 88–107. Wiley Interscience/John Wiley and Sons, Hoboken, USA.

Kodikara,S. *et al.* (2022) Statistical challenges in longitudinal microbiome data analysis. *Brief. Bioinf.*, **23**, bbac273.

Lenth,R.V. (2021) *emmeans: Estimated Marginal Means, aka Least-Squares Means*. R Package Version 1.6.3., CRAN, Vienna, Austria.

Levin,K.A. (2006) Study design III: cross-sectional studies. *Evid. Based Dent.*, **7**, 24–25.

Lin,H. *et al.* (2020) Analysis of microbial compositions: a review of normalization and differential abundance analysis. *NPJ Biofilms Microbiomes*, **6**, 60.

Lindsey,J.K. *et al.* (1998) Choosing among generalized linear models applied to medical data. *Statist. Med.*, **17**, 59–68.

Liu,C. *et al.* (2010) Statistical issues in longitudinal data analysis for treatment efficacy studies in the biomedical sciences. *Mol. Ther.*, **18**, 1724–1730.

Liu,X. (2009) Ordinal regression analysis: fitting the proportional odds model using stata, SAS and SPSS. *J. Mod. App. Stat. Meth.*, **8**, 632–642.

Ma,S. *et al.* (2021) A statistical model for describing and simulating microbial community profiles. *PLoS Comput. Biol.*, **17**, e1008913.

Macbeth,G. *et al.* (2010) Cliff's Delta calculator: a non-parametric effect size program for two groups of observations. *Univ. Psychol.*, **10**, 545–555.

Maifeld,A. *et al.* (2021) Fasting alters the gut microbiome reducing blood pressure and body weight in metabolic syndrome patients. *Nat. Commun.*, **12**, 1970.

Mallick,H. *et al.* (2021) Multivariable association discovery in population-scale meta-omics studies. *PLoS Comput. Biol.*, **17**, e1009442.

Mandal,S. *et al.* (2015) Analysis of composition of microbiomes: a novel method for studying microbial composition. *Microb. Ecol. Health Dis.*, **26**, 27663.

Marfo,P. *et al.* (2019) The accuracy of effect-size estimates under normals and contaminated normals in meta-analysis. *Heliyon*, **5**, e01838.

Downloaded from https://academic.oup.com/bioinformaticsadvances/article/3/1/vbad063/7172481 by Duke University user on 21 August 2023

McKnight,D.T. *et al.* (2019) Methods for normalizing microbiome data: an ecological perspective. *Methods Ecol. Evol.*, **10**, 389–400.
Metwally,A.A. *et al.* (2018) MetaLonDA: a flexible R package for identifying time intervals of differentially abundant features in metagenomic longitudinal studies. *Microbiome*, **6**, 32.
Mulè,M.P. *et al.* (2022) Normalizing and denoising protein expression data from droplet-based single cell profiling. *Nat. Commun.*, **13**, 2099.
Nahm,F.S. (2016) Nonparametric statistical tests for the continuous data: the basic concept and the practical use. *Korean J. Anesthesiol.*, **69**, 8–14.
Nick,T.G. *et al.* (2007) Logistic regression. In: Ambrosius, W.T. (ed.) *Topics in Biostatistics*. Humana Press, Totowa, NJ, pp. 273–301.
Opgen-Rhein,R. *et al.* (2021) *Longitudinal: Analysis of Multiple Time Course Data*. CRAN, Vienna, Austria.
Pedersen,H.K. *et al.* (2018) A computational framework to integrate high-throughput '-omics' datasets for the identification of potential mechanistic links. *Nat. Protoc.*, **13**, 2781–2800.
Pedersen,T.L. (2020) *Patchwork: The Composer of Plots*. CRAN, Vienna, Austria.
Peterson,R.A. (2021) Finding optimal normalizing transformations via bestNormalize. *R. J.*, **13**, 310–329.
Quinn,T. (2017) *peakRAM: Monitor the Total and Peak RAM Used by an Expression or Function*. CRAN, Vienna, Austria.
Robinson,M.D. *et al.* (2010) edgeR: a bioconductor package for differential expression analysis of digital gene expression data. *Bioinformatics*, **26**, 139–140.
Saary,P. *et al.* (2017) RTK: efficient rarefaction analysis of large datasets. *Bioinformatics*, **33**, 2594–2595.
Sanchez-Cid,C. *et al.* (2022) Sequencing depth has a stronger effect than DNA extraction on soil bacterial richness discovery. *Biomolecules*, **12**, 364.
Sullivan,G.M. *et al.* (2012) Using effect size—or why the P value is not enough. *J. Grad. Med. Educ.*, **4**, 279–282.
Swift,D. *et al.* (2023) A review of normalization and differential abundance methods for microbiome counts data. *WIREs Comput. Stat.*, **15**, e1586.
Tierney,B.T. *et al.* (2021) Gene-level metagenomic architectures across diseases yield high-resolution microbiome diagnostic indicators. *Nat. Commun.*, **12**, 2907.
Timonen,J. *et al.* (2021) lgpr: an interpretable non-parametric method for inferring covariate effects from longitudinal data. *Bioinformatics*, **37**, 1860–1867.
Torchiano,M. (2020) *effsize: Efficient Effect Size Computation*. CRAN, Vienna, Austria.
van den Boogaart,K.G. *et al.* (2008) "compositions": a unified R package to analyze compositional data. *Comput. Geosci.*, **34**, 320–338.
Venables,W.N. *et al.* (2002) *Modern Applied Statistics with S*. Springer, New York.
Ver Hoef,J.M. *et al.* (2007) Quasi-Poisson vs. negative binomial regression: how should we model overdispersed count data? *Ecology*, **88**, 2766–2772.
Weiss,S. *et al.* (2017) Normalization and microbial differential abundance strategies depend upon data characteristics. *Microbiome*, **5**, 27.
Wickham,H. (2007) Reshaping data with the reshape package. *J. Stat. Soft.*, **21**, 1–20.
Wickham,H. *et al.* (2019) Welcome to the Tidyverse. *JOSS*, **4**, 1686.
Williams,J. *et al.* (2019) microbiomeDASim: simulating longitudinal differential abundance for microbiome data. *F1000Res.*, **8**, 1769.
Witten,D.M. *et al.* (2010) Survival analysis with high-dimensional covariates. *Stat. Methods Med. Res.*, **19**, 29–51.
Zhang,X. *et al.* (2017) Negative binomial mixed models for analyzing microbiome count data. *BMC Bioinformatics*, **18**, 4.

Downloaded from https://academic.oup.com/bioinformaticsadvances/article/3/1/vbad063/7172481 by Duke University user on 21 August 2023

Study 2:

nature COMMUNICATIONS

ARTICLE

https://doi.org/10.1038/s41467-021-22097-0 OPEN

Fasting alters the gut microbiome reducing blood pressure and body weight in metabolic syndrome patients

András Maifeld[1,2,3,4], Hendrik Bartolomaeus[1,2,3,4], Ulrike Löber[1,3,4], Ellen G. Avery[1,3,4,5], Nico Steckhan[2,6], Lajos Markó[1,2,3], Nicola Wilck[1,3,7,8], Ibrahim Hamad[9,10], Urša Šušnjar[1], Anja Mähler[1,2,3], Christoph Hohmann[6], Chia-Yu Chen[1,2,3,4], Holger Cramer[11], Gustav Dobos[11], Till Robin Lesker[12], Till Strowig[12,13], Ralf Dechend[1,2,3,14], Danilo Bzdok[15,16,17], Markus Kleinewietfeld[9,10], Andreas Michalsen[2,6,18]✉, Dominik N. Müller[1,2,3,4,18]✉ & Sofia K. Forslund[1,2,3,4,18]✉

Periods of fasting and refeeding may reduce cardiometabolic risk elevated by Western diet. Here we show in the substudy of NCT02099968, investigating the clinical parameters, the immunome and gut microbiome exploratory endpoints, that in hypertensive metabolic syndrome patients, a 5-day fast followed by a modified Dietary Approach to Stop Hypertension diet reduces systolic blood pressure, need for antihypertensive medications, body-mass index at three months post intervention compared to a modified Dietary Approach to Stop Hypertension diet alone. Fasting alters the gut microbiome, impacting bacterial taxa and gene modules associated with short-chain fatty acid production. Cross-system analyses reveal a positive correlation of circulating mucosa-associated invariant T cells, non-classical monocytes and $CD4^+$ effector T cells with systolic blood pressure. Furthermore, regulatory T cells positively correlate with body-mass index and weight. Machine learning analysis of baseline immunome or microbiome data predicts sustained systolic blood pressure response within the fasting group, identifying $CD8^+$ effector T cells, Th17 cells and regulatory T cells or Desulfovibrionaceae, Hydrogenoanaerobacterium, *Akkermansia*, and Ruminococcaceae as important contributors to the model. Here we report that the high-resolution multi-omics data highlight fasting as a promising non-pharmacological intervention for the treatment of high blood pressure in metabolic syndrome patients.

A full list of author affiliations appears at the end of the paper.

Fasting can prolong survival and reduce disease burden in rodent models, and possibly in humans[1]. In contrast, today's Western diet promotes cardiometabolic disease (CMD)[2]. How diet affects the gut microbiota, immune system and subsequently host (patho)physiology is not fully understood, and information is lacking on how periodic fasting affects the gut microbiome in patients with metabolic syndrome (MetS). To reduce CMD risk, exercise and a healthy diet are often prescribed. Shifting from a "Western diet" to a healthier "Mediterranean-like" DASH diet[3] to achieve optimal nutrition and negative energy balance is recommended, although compliance is a major hurdle. Our study is the first of its kind to investigate the effects of a lifestyle modification in combination with fasting therapy in patients with MetS using a multi-omics approach by combining gut microbiome analysis and deep immunophenotyping. The "Western diet" is known to induce metabolic inflammation, accelerating CMD[4]. The gut microbiota is a delicate ecosystem that plays a pivotal role in health and disease. Dysbiosis has been observed as a characteristic of several inflammatory, cardiovascular, and metabolic disorders (e.g. obesity)[5], including hypertension[6,7]. The "healthy" gut microbiome is relatively stable, although various factors such as antibiotics, intestinal infections, and profound dietary or lifestyle changes, such as moving on or off a "Western diet", can induce transient or persistent changes to this ecosystem. Traditionally, fasting plays an important role in different cultural and religious practices. Dramatic caloric restriction not only affects host health and physiology, but also has an impact on the microbiome[8–10]. Here, we studied the role of fasting in cardiovascular risk patients with MetS (Table 1). Five days of fasting followed by 3 months of a modified DASH diet induced distinct microbiome and immunome changes not seen under DASH alone, as well as a sustained SBP benefit even 3 months post-intervention. Applying machine-learning algorithms, we were able to make effective predictions regarding which patients would respond positively to treatment via BP reduction from either baseline immunome or 16S microbiome data. The microbial signature for BP responsiveness generalizes to a recently published cohort investigating the impact of fasting in 15 healthy male volunteers, as do many of the microbiome changes upon fasting. These data highlight fasting followed by a shift to a health-promoting diet as a promising non-pharmacological intervention for patients with hypertensive MetS, with possible implications for a wider spectrum of health states.

Table 1 Patient characteristics at baseline.

	FASTING + DASH	DASH
Females/Males	23/12	21/15
Age (year)	58 ± 8	62 ± 8
Height (cm)	171 ± 8	171 ± 9
Office SBP (mm Hg)	136 ± 15	138 ± 16
Office DBP (mm Hg)	88 ± 11	88 ± 9
24 h ABPM SBP (mm Hg)	132 ± 9	131 ± 9
24 h ABPM DBP (mm Hg)	81 ± 8	81.4 ± 7
24 h ABPM MAP (mm Hg)	104 ± 8	104 ± 7
24 h ABPM peripheral resistance (mm Hg*s/ml)	1.4 ± 0.1	1.3 ± 0.1
SBP day (mm Hg)	134 ± 10	133 ± 10
DBP day (mm Hg)	83 ± 9	84 ± 7
SBP nocturnal (mm Hg)	120 ± 12	121 ± 10
DBP nocturnal (mm Hg)	71.5 ± 8	71.6 ± 7
Weight (kg)	99 ± 17	96 ± 17
BMI (kg/m^2)	34 ± 4.9	33 ± 4.7
Hip circumference (cm)	115 ± 20	113 ± 17
Waist circumference (cm)	116 ± 11	114 ± 12
Waist to hip ratio	1.1 ± 0.7	1.0 ± 0.2
Body fat percentage (%)	42 ± 8	39 ± 10
HOMA index	2.8 ± 2.1	3.4 ± 2.4
Insulin (mU/l)	10.4 ± 6.4	12.1 ± 7.4
Plasma glucose (mg/dl)	105 ± 20	110 ± 20
Hb-A1C (%)	5.8 ± 0.4	5.9 ± 0.7
Hb-A1C IFCC (mmol/mol)	39.6 ± 4.8	41.2 ± 7.4
Triglyceride (mg/dl)	166 ± 106	169 ± 109
Cholesterol (mg/dl)	220 ± 48	222 ± 54
HDL (mg/dl)	50 ± 11	51 ± 10
LDL(mg/dl)	137 ± 36	140 ± 45
LDL/HDL ratio	2.8 ± 0.7	2.8 ± 0.9
CRP (mg/l)	0.4 ± 0.4	0.3 ± 0.3
IL-6 (pg/ml)	3.1 ± 2.0	2.8 ± 2.2
Creatinine (mg/dl)	0.9 ± 0.2	0.9 ± 0.2
eGFR Cockroft-Gault (ml/min)	120 ± 39	107 ± 32

Mean values and +/− one standard deviation are shown

Results

Fasting affects the gut microbiome and immunome. As we have previously reported a major influence of common MetS drugs on the microbiota[11], we accounted for any changes in medication regime or dosage in our statistical tests, alongside controlling for important demographic features such as age and sex. There were substantial and significant (PERMANOVA $P = 0.001$) differences in microbial composition within individuals during fasting, reflecting a characteristic intervention-induced shift, which later partially reverted following a 3-month refeeding period on a DASH diet (Fig. 1d, Supplementary Data 1 and Fig. 1a). This was echoed by analogous significant (PERMANOVA $P = 0.001$) changes in host immune cell composition during the intervention, revealing a fasting-specific signature, which likewise largely reversed during refeeding (Fig. 1e, Supplementary Data 1). We did not observe significant changes to the microbiome species richness/alpha diversity (between-group Mann–Whitney U (MWU) $P > 0.05$, within-individual likelihood ratio test FDR > 0.1 for all comparisons; Supplementary Data 2; Shannon: Fig. 1b, Supplementary Fig. 2) after either fasting or refeeding in the present dataset, though a trend of reduced, then restored diversity was seen in the longitudinal tests. Similarly, there were no significant changes between time points in the intersample gut taxonomic variability/beta diversity (Bray–Curtis distance, Fig. 1c. DASH without fasting neither affected the microbial composition nor the host immune cell composition ($P = 0.374$ and $P = 0.378$, respectively, Supplementary Fig. 1B, C).

Fasting resulted in a reduction of $CD3^+$, $CD4^+$ T cells, and $CD19^+$ B cells, while the frequency of $CD8^+$ T cells was unaltered. In contrast, fasting increased the abundance of monocytes ($CD14^+CD11c^+CD19^-CD3^-$) and $TCR\gamma/\delta^+$ T cells. However, these changes were reversed upon refeeding (Fig. 1h, Supplementary Data 1). Of note, frequency of $CD123^+CD14^-CD16^-HLA\text{-}DR^+$ plasmacytoid dendritic cells also increased upon fasting and was still enriched after refeeding (Fig. 1h, Supplementary Data 1). When looking closer into monocyte subsets, fasting increased (and refeeding reduced) the frequency of classical $CD14^{high}CD16^-$, non-classical $CD14^{low}CD16^{++}$, and intermediate $CD14^{high}CD16^+$ monocytes (Fig. 1i, Supplementary Fig. 1, Data 1), which was confirmed by unbiased FlowSOM analyses (Supplementary Fig. 4A–D). Fasting also affected the relative abundance of differentially activated T cells. Upon fasting, $CD8^+$ T cells showed a higher percentage of terminally differentiated cells (T_{eff}, $CD45RO^-CD62L^-$) and a lower percentage of the naïve phenotype (T_n, $CD45RO^-CD62L^+$), while memory T cells were not affected (Fig. 1i, Supplementary Fig. 3, Data 1). A similar

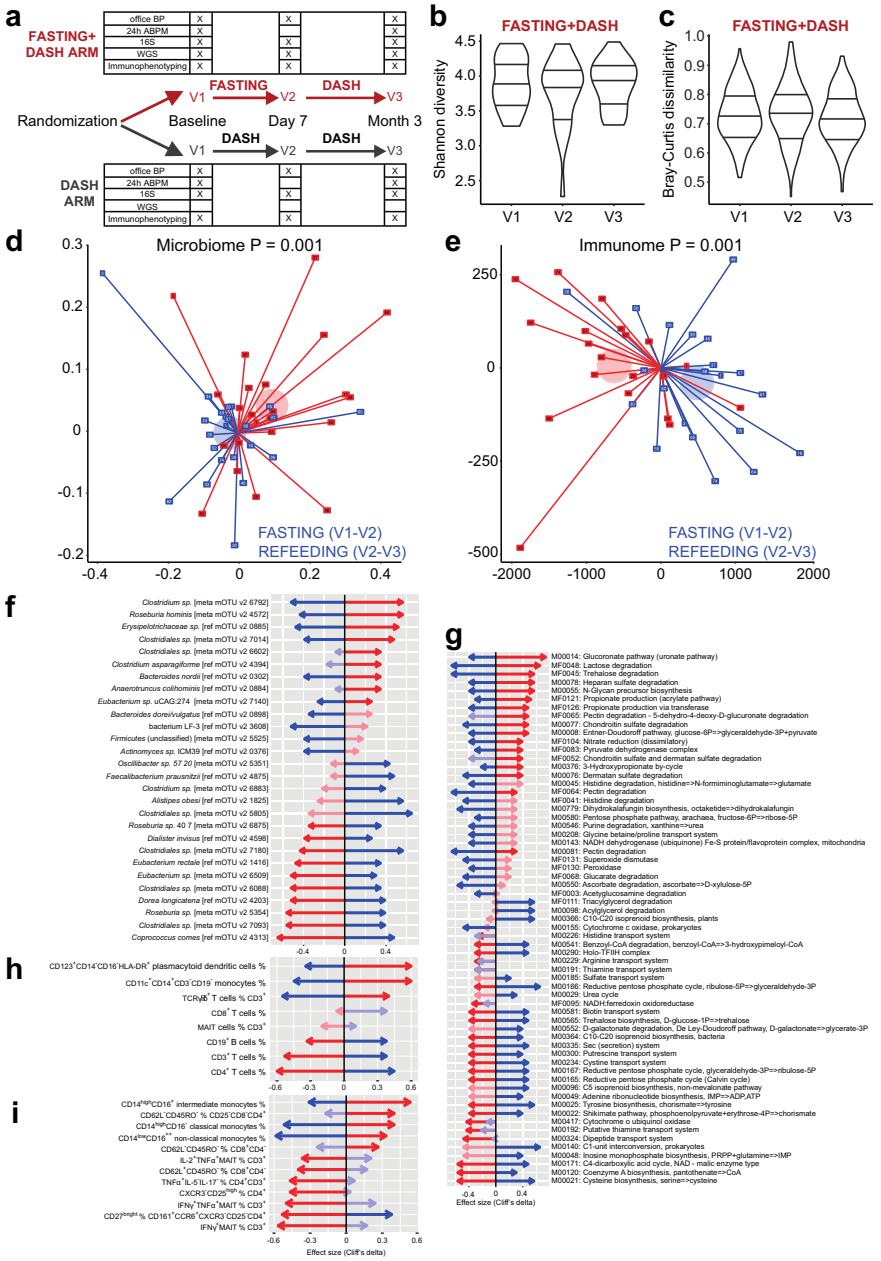

pattern was observed in $CD4^+$ T_{eff} (Fig. 1i, Supplementary Data 1). Further, fasting decreased the frequency of pro-inflammatory Th17 ($CD27^{bright}$ $CD161^+CCR6^+CXCR3^-$ $CD25^-CD4^+$), as well as TNFα- and IFNγ-producing Th1 cells (Fig. 1i, Supplementary Data 1). These changes were partially reverted upon refeeding (Fig. 1i). Neither fasting nor refeeding changed the overall frequency of $CD161^+Vα7.2^+$ $CD3^+$ mucosa-associated invariant cells (MAIT, Fig. 1h, Supplementary Fig. 3). However, frequency of pro-inflammatory MAITs producing TNFα and IFNγ significantly decreased upon fasting and were minimally affected by refeeding (Fig. 1i, Supplementary Data 1).

Next, we tested all gut microbial taxa and gene functional (KEGG[12], GMM[13]) modules for abundance shifts during fasting or refeeding, as well as persistent shifts across the 3-month study

Fig. 1 Fasting has a pervasive host and microbiome impact. a Study design is shown. Subjects are followed from baseline (V1), randomly assigned to begin a modified DASH diet only or to undergo a 5-day fast followed by a modified DASH diet. Follow-up is done at one week (V2) and 3 months (V3). **b** Fasting has no significant (two-sided MWU $P > 0.05$) impact on gut microbiome alpha diversity (Shannon diversity from mOTUv2 OTUs) across observation times V1–V3. **c** Fasting has no significant (two-sided MWU $P > 0.05$) impact on gut microbiome beta diversity (Bray–Curtis dissimilarity from mOTUv2 OTUs, shown are all between donor comparisons per time point) across observation times V1–V3. **d** Fasting significantly shifts the gut microbiome towards a characteristic compositional state, while refeeding reverses this change. Unconstrained Principal Coordinates graph with first two dimensions shown. Axes show Bray–Curtis dissimilarities of rarefied mOTUv2 OTUs between samples; each participant in the fasting arm is shown as two lines, one red (fasting change), one blue (refeeding change) connected (centered) at the origin for ease of visualization. Axes show fasting and refeeding deltas after one-week intervention and 3-month refeeding. Pseudonym participant ID numbers are shown on the point markers. Transparent circle markers show arithmetic mean position of fasting and recovery deltas, respectively. PERMANOVA test *P*-values reveal significant dissimilarity ($P < 0.05$) between samples from each visit V1–V3 in the original distance space, stratifying by donor. **e** Fasting significantly shifts the host immune cell population towards a characteristic state, while refeeding reverses it. Same as in (**d**), using Euclidean distances. **f** Gut microbial taxa significantly enriched/depleted upon fasting/refeeding. Taxa (mOTUv2 OTUs) are shown on the vertical axis, and effect sizes (Cliff's delta) shown on the horizontal axis. Red arrows represent fasting effects (V2–V1 comparison), blue arrows refeeding effects (V3–V2 comparison). Bold arrows are significant (nested model comparison of a linear model for rarefied abundance of each taxon, comparing a model incorporating patient ID, age, sex and all dosages of relevant medications) to a model additionally incorporating time point, requiring likelihood test Benjamini-Hochberg corrected FDR < 0.1 and additionally pairwise post-hoc two-sided MWU test $P < 0.05$. **g** Gut microbial gene functional modules (KEGG and GMM models analyzed together) significantly enriched/depleted upon fasting/refeeding. **h** General immune cell populations significantly enriched/depleted upon fasting/refeeding. **i** Specific immune cell subpopulations. **g–i** Same test as in (**f**), subset of altered features shown for clarity. Effect sizes and FDR-corrected *P* values can be found in Supplementary Data 1,2.

period, controlling for age, sex and any changes in medication (Fig. 1f–h, Supplementary Data 1). Fasting stimulated shifts in the abundance of several core commensals, which were reversed upon refeeding (Fig. 1f, Supplementary Data 1). Many Clostridial Firmicutes shifted significantly in abundance, with an initial decrease in butyrate producers such as *Faecalibacterium prausnitzii*, *Eubacterium rectale* and *Coprococcus comes*, which had also reverted after 3 months. Interestingly, modeling the shift in *C. comes* abundance as a function of body-mass index (BMI) changes during the study yielded a better fit of the data than when it was modeled as a function of the fasting intervention. Bacteroidaceae showed the opposite pattern. At the end of the refeeding period, a persistent depletion could be seen in Enterobacteriaceae, especially *Escherichia coli*. These shifts were accompanied by vast changes in microbial metabolic capacity (Fig. 1g, Supplementary Data 1). Fasting enriched for propionate production capacity, mucin degradation gene modules, and diverse nutrient utilization pathways.

Reanalyzing previously published data, we compared the microbiome signatures of metformin use and MetS to those seen in our dataset[11,14]. For ease of comparability, we proceeded with only human gut-specific functional modules (GMM) assessed from shotgun sequencing data available for the fasting arm. Certain fasting- or refeeding-associated functional gene modules from our data were found to overlap with signatures of metformin usage or MetS, though there was little concordance on a taxonomic composition level, in line with previously described higher functional than taxonomic concordance between microbiomes. Of note, when comparing the metformin signal to the MetS signal, it is clear that these two effects are functionally distinct and often oppose one another. In contrast, the inferred gut functional signature of metformin treatment shared some features with that of our fasting intervention (Supplementary Fig. 5).

Fasting reduces long-term systolic blood pressure and body weight in MetS patients. Assessing the clinical relevance of our intervention, we inspected clinical outcomes in the two study arms. While DASH reduced office SBP after 3 months (Fig. 2h), it did not significantly (MWU $P = 0.27$) affect 24 h ambulatory SBP, the gold standard of clinical BP measurements (Fig. 2a)[3]. In contrast, fasting followed by a modified DASH diet led to a sustained reduction both in 24 h ambulatory SBP and mean arterial pressure (MAP) (MWU $P < 0.05$, Fig. 2a). Further, subjects undergoing fasting could significantly (χ^2 $P = 0.035$) reduce their intake of antihypertensive medication in 43% of cases, compared to only 17% of the cases on DASH alone, while their BP remained under control (Fig. 2b, Supplementary Data 3). Because the BP response to fasting was heterogeneous in our cohort (Fig. 2a, b), we applied a decision tree model to stratify patients based on their ambulatory BP response, adjusted for antihypertensive medication (Supplementary Fig. 6, Data 4). The responder group ($n = 22$) had a median SBP decrease of 8.0 mmHg, irrespective of the high reduction in medications amongst these patients, while the decrease in the non-responder group ($n = 10$) was significantly lower (0.3 mmHg; Fig. 2c). In the DASH-only arm, 17 patients were classified as responders with a median SBP decrease of 8.0 mmHg, while the non-responders ($n = 14$) showed no decrease in median SBP (0.5 mmHg, Fig. 2c). Fasting followed by a modified DASH diet, unlike a modified DASH diet alone, significantly (drug-adjusted post-hoc $P < 0.05$) reduced BMI and body weight even 3 months post-fasting (Fig. 2d, e). Although all fasting+DASH participants showed a reduction in body weight, this reduction alone could not explain the long-term ambulatory SBP and MAP changes exclusive to the fasting arm (Fig. 2f, g), nor the microbiome or immunome changes accompanying it. 95% of significant findings retain significance when BMI is added as a predictor to the nested models for longitudinal data (see Supplementary Data 5). Very few of the significant effects observed in the fasting+DASH arm could be replicated in the equally powered DASH-only arm (Fig. 3a–c).

BP responder-specific changes in the gut microbiome and immunome. Because the BP responsiveness was heterogeneous in the fasting+DASH arm (Fig. 2a–c), despite the similar disease severity indicated by the baseline clinical characteristics of these patients (Supplementary Data 6), we hypothesized that unique characteristics involving the immunome or microbiome of these patients may contribute to their BP response. We compared the impact of fasting and refeeding in the complete fasting arm, in the BP responders of the fasting arm, and in the DASH-only arm (Fig. 4a, b, Supplementary Data 2, 7, 8). Even at reduced statistical power, we were able to capture changes in the abundance of many gut microbial taxa that were uniquely characteristic of successful fasting treatment even 3 months post-fasting (Fig. 4a, Supplementary Data 7, 8). Fasting combined with DASH resulted in the sustained depletion of Actinobacteria family members Corynebacteriaceae and Actinomycetaceae (Fig. 4a). BP responders

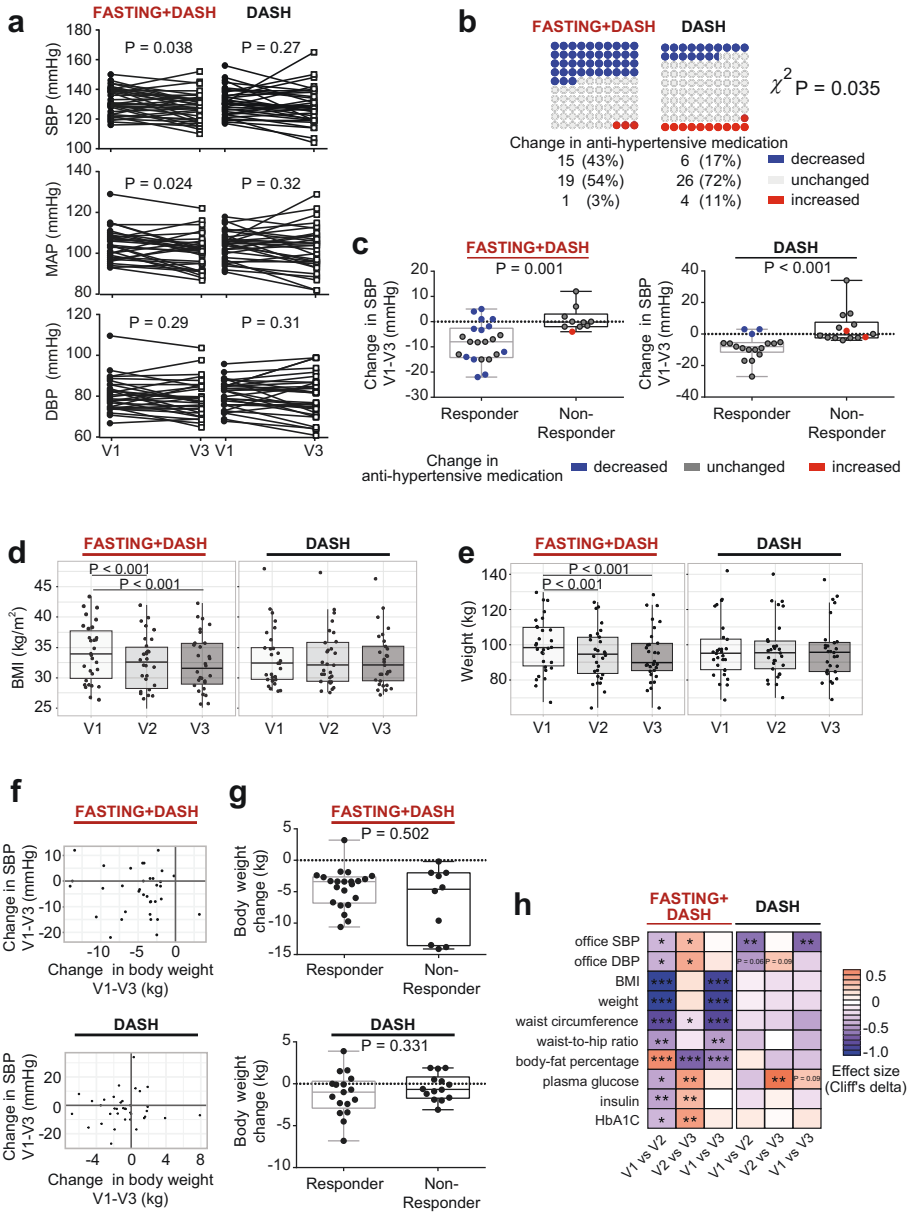

were uniquely characterized by immediate and sustained enrichment of an unclassified *Clostridium* species, with concomitant depletion of *Sphingomonas* (genus-16S) and Prevotellaceae *NK3B31* group (Fig. 4a). In addition, responders experienced a significant and sustained enrichment of the butyrate-producer *F. prausnitzii* upon refeeding (Fig. 4a). We further classified microbiomes in the fasting+DASH arm into enterotypes as previously described[15], finding a trend towards more samples shifting enterotype during intervention in subjects, who achieved BP decrease (Supplementary Fig. 7). Virtually no overlap with effects seen in the equally powered DASH arm were found, indicating that fasting may be needed on top of a BP-reducing diet for these changes to occur (Fig. 4a, b).

In profiling the microbial metabolic potential in BP responders, we focused on gene modules curated for relevance to metabolism in the human gut (GMM)[13]. On a functional level, responder-characteristic changes resemble those in the fasting arm at large, but with even more pronounced relative enrichment for

Fig. 2 Fasting effects are distinct from those of a modified DASH diet only, and connected to vascular health benefits. a Fasting followed by a modified DASH diet, but not a DASH diet alone, significantly improves 24 h ambulatory SBP and MAP 3 months post-intervention (two-sided MWU, FDR-corrected *P*-values are shown). Lines show individual participant trajectories. **b** MetS subjects beginning a modified DASH diet post-fasting significantly reduce their intake of antihypertensive medication by 3 months post-intervention, compared to subjects beginning a DASH diet only. Two-sided χ^2 test, $P = 0.035$. **c** Changes in 24 h ambulatory SBP in responders and non-responders including change in antihypertensive medication (two-sided MWU). **d**, **e** One week of fasting followed by modified DASH diet, but not DASH diet alone, caused significant (two-sided MWU, FDR-corrected *P* values are shown) BMI and body weight reduction in MetS patients, persisting 3 months later. **f** Comparison of changes in 24 h ambulatory SBP and body weight, respectively between baseline and follow-up in both study arms. Each dot represents an individual. **g** Body weight change is not significantly different between responders and non-responders in the fasting arm between baseline and follow-up (two-sided MWU). **h** Selected cardiometabolic risk parameters (vertical axis) altered in the fasting arm compared to the DASH arm. Heatmap hues show Cliff's delta signed effect sizes, with asterisk indicating post-hoc univariate significance after compensating for drug dosage changes (see Methods). Horizontal axis shows each time point comparison: change during fasting/week three of DASH, change during refeeding/3 months of DASH, and change during the study period as a whole. Boxplot hinges denote 25th–75th percentile. Line within the boxplot indicates median. Whiskers on (**c**, **g**) are drawn from minimum to maximum values. Whiskers on (**d**, **e**) are drawn to minimum and maximum values, but not further than 1.5 × IQR.

propionate production (MF0126, MF0121) modules (Fig. 4c). Some modules were significantly altered in abundance only in this stratified subgroup, indicating these changes strongly characterize BP responders compared to non-responders (Supplementary Data 7). For example, pyruvate:formate lyase (MF0085) is depleted during recovery only in responders.

Changes to the immunome of responders are similar to those seen in the unstratified fasting group and differ from those in the DASH arm (Fig. 4d, Supplementary Data 2, 7, 8). In the fasting arm, several immune features related to pathogen-sensing and mucosal immunity (e.g. MAIT cells, IL-17$^+$-producing Th and γδT cells) changed in abundance significantly only when tested in the responder group, indicating relevant differences between responders and non-responders. Upon fasting, the frequency of both pro- and anti-inflammatory adaptive immune cells showed a stronger decrease in responders, indicating a stronger anti-inflammatory effect of fasting in responders.

Network analysis of microbial, immune, and clinical features. We next aimed to explain the beneficial role of fasting on BP by studying interacting microbiome-immune features through network analysis. We assessed all triplets of pairwise interactions between host clinical phenotypes, immune cell populations, and microbiome taxa or functional profiles, respectively, using modified Spearman correlations (requiring FDR < 0.1 in each comparison of two data spaces, and $P < 0.05$ in a post-hoc test accounting for the presence of the same subjects at all three time points (see Methods, Supplementary Data 9). Figure 5a shows a chord diagram constructed from these data, where the colored outer rings are lined with components from one of our three tested system spaces during fasting, refeeding, and over the full duration of the study, and the color of the connectors between factors indicate a positive or negative association (Spearman's rho). We identified a cluster of circulating cytokine-producing MAIT cells (absolute number and fraction of CD3$^+$ T cells), which positively correlated with 24 h ambulatory SBP (Figs. 5a, 6c, Supplementary Fig. 8) and MAP, but not with 24 h diastolic BP (Fig. 5a, Supplementary Data 9).

In addition, abundance of IL-2$^+$ and granulocyte-macrophage colony-stimulating factor (GM-CSF)-producing CD4$^+$ cells significantly correlated with SBP. These immune clusters showed significant interconnection to a remarkable number of microbial SCFA producers (Fig. 5a, b Supplementary Data 10), though some are rather poorly characterized. Notably, abundance of the butyrate producers *E. rectale* (ref mOTU v2 1416) and *Dorea longicatena* (ref mOTU v2 4203), and the acetate producer *Hungatella hathewayi* (ref mOTU v2 0882) negatively correlated with the abundance of the GM-CSF and IL-2-producing CD4$^+$ T cells, and with the absolute number of IFNγ$^+$ and TNFα-producing MAITs, respectively.

16S analyses of the gut microbiome identified a positive correlation between the pro-inflammatory cytokine-producing MAITs and the microbial taxa Acidaminococcaceae (family), and of two *Alistipes spp*. (*shahii* and *inops*) (Fig. 5a, b). While further characterization of these taxa in the context of the gut microbiome is needed, previously published data indicated that these taxa can produce acetate, and likely butyrate and propionate as well (Supplementary Data 10).

Abundance of KEGG module M00209 (osmoprotectant transport system), reported to facilitate the uptake of nutrients mostly found in red meat[16–18], was negatively associated with IFNγ$^+$ and TNFα$^+$ MAIT cells (Fig. 5a, b, Supplementary Data 9). Interestingly, fasting depleted various cytokine-producing MAIT cells with the most pronounced long-lasting decrease seen in IL-2$^+$TNFα$^+$ producing MAIT in BP responders (Figs. 5a, b, 6a, Supplementary Data 9).

The association between MAIT cells and BMI is still a matter of debate[19]. We found in our study that the abundance of MAIT cells did not correlate with BMI, weight, waist circumference, waist-hip ratio, or body fat percentage (Supplementary Fig. 8, Data 9). Though we did find that BMI correlated with the abundance of a subset of circulating Treg-like cells (CD62L$^+$ CD45RO$^-$CD25$^+$CD4$^+$), a cell type previously linked to morbid obesity in human subjects[20].

A recent publication showed non-classical monocyte enrichment in hypertensive patients[21]. Interestingly in our study, circulating non-classical monocytes were enriched upon fasting and then depleted again upon refeeding to remain below baseline levels 3 months after fasting (Figs. 1h, 5a, Supplementary Data 2). Network analysis revealed an association between non-classical monocytes, MAP and gut abundance of *Sutterella* showed an inverse correlation with non-classical monocytes (Figs. 5a, b, 6d, Supplementary Data 9).

Baseline indicators predicting efficacy of fasting on blood pressure. As previously stated, a large proportion of fasting patients responded with a substantial drop in BP, allowing them to reduce their use of antihypertensive medication while BP remained controlled. As not all patients experienced this beneficial effect, we sought to understand whether the factors underlying successful fasting intervention in the BP responders could be predicted at baseline. Responder and non-responder subgroups differ considerably in immunome and microbiome features, not only post-fasting and at three-month follow-up, but also at baseline, suggesting a favorable clinical response may be predictable in single patients (Supplementary Fig. 9A–C).

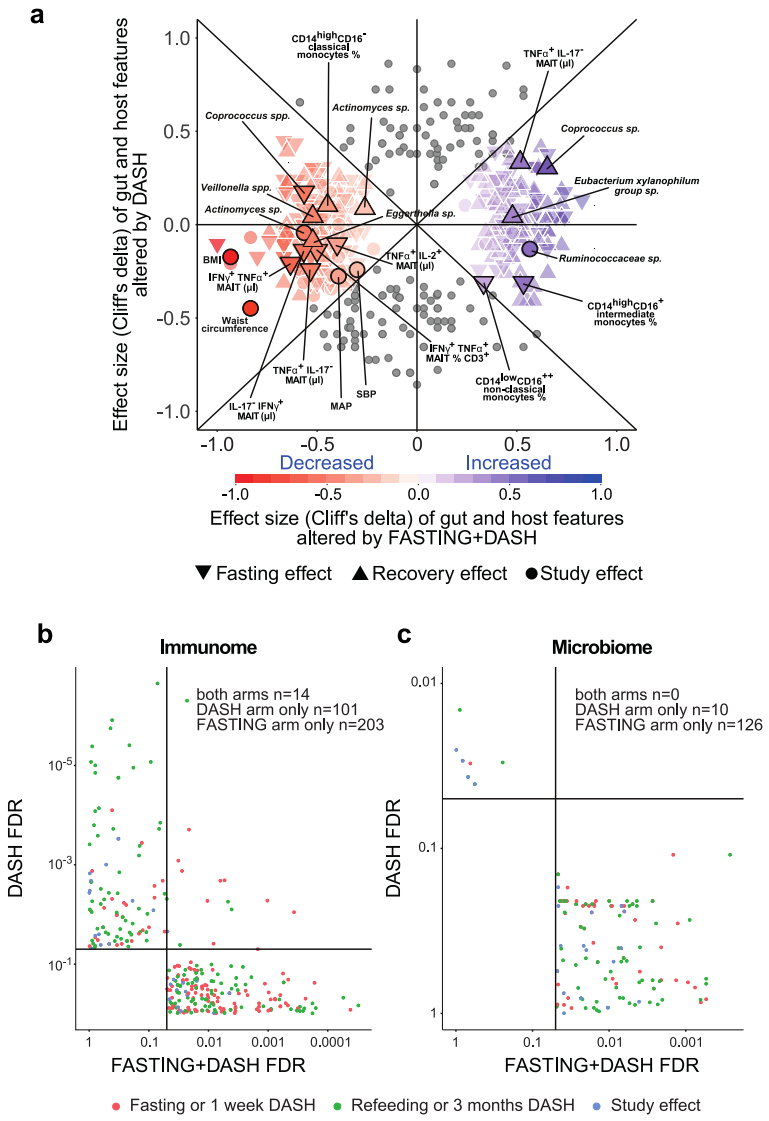

Fig. 3 Fasting and recovery effects are not replicated in an equally powered control cohort, indicating they are intervention-specific. a A majority of host and microbiome effects reported from the fasting+DASH arm are not replicated in DASH-only patients. Comparative effect size plot contrasting features altered significantly only under fasting+DASH (colored markers, $n = 315$) with features altered significantly also under DASH alone, or with absolute effect size greater in DASH alone (gray markers, $n = 146$). For the former category, color hue shows direction of effect, color intensity scope of effect, and marker shape which time point comparison is shown. Vertical axis shows effect size in DASH only, horizontal effect size in fasting+DASH. Selected features are named for reference. **b**, **c** Volcano plots show post-hoc FDR for all features significantly altered in either arm between any two time points in the fasting arm (horizontal axis), compared to the same sample number DASH arm (vertical axis). Point color shows which time point comparison is plotted. Quadrants (formed by the FDR < 0.05 thresholds) and summary counts highlight features significantly altered in each dataset for immune cell (**b**) and functional or taxonomic microbiome features (**c**). Only the fasting arm had a significant effect on the microbiome, and while a smaller fraction of immune features were altered in the DASH-only arm, these were largely not significant in the fasting arm.

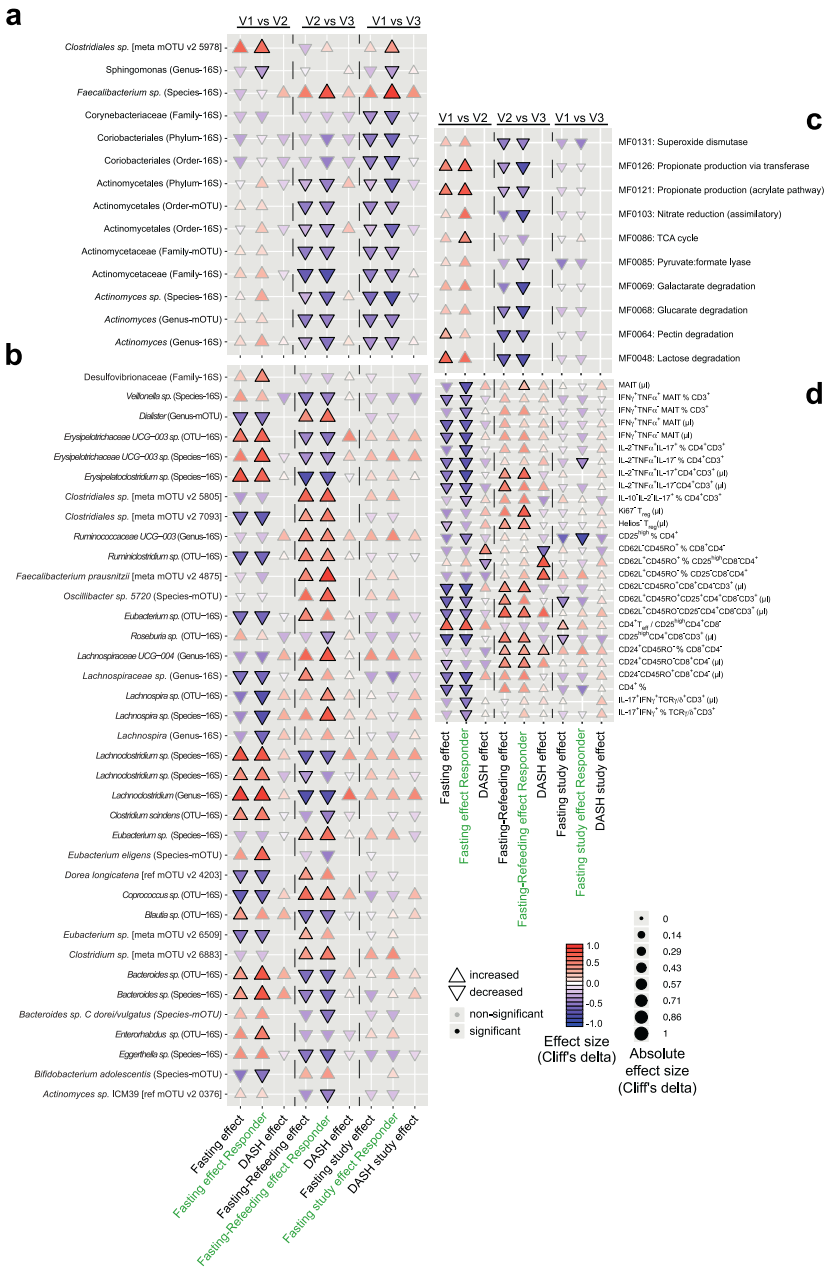

To further elucidate this phenomenon, we applied machine-learning algorithms and empirically show that we can make effective predictions from the immunome data. From 494 total immune variables, stepwise forward regression identified the top ten discriminators of responders from non-responders at baseline. Evaluating the machine-learning model, we constructed for predicting whether fasting+DASH will reduce BP by testing it on unseen data, a prediction accuracy of 71% (sensitivity 75%, specificity 70%, and F1 score 77%) was achieved using a leave-subject-out cross-validation for whether or not a future patient would respond favorably to fasting with regards to BP (Fig. 7a). Within this multivariate analysis, the driving immune features

Fig. 4 Subjects responding favorably to fasting exhibit stronger changes in commensal abundance under intervention. a Cuneiform plot shows subset of bacterial taxa, at different taxonomic levels, and measured either using 16S sequencing or shotgun sequencing, altered significantly (drug-adjusted post-hoc FDR < 0.05) in abundance tested in intervention responders only (vertical axis) and showing a study effect, comparing to baseline and follow-up (V3). Signed effect size are shown through marker direction and color, hue and size represent absolute effect size. Solid borders indicate significance. Markers not shown could not be tested in the DASH arm as shotgun data was unavailable, or showed no difference in rank-transformed values (Cliff's delta=0). Horizontal axis separates tests for fasting (comparison of baseline to after one week), recovery (comparison of after one week to 3 months), and study effect (comparison of baseline to 3-month follow-up). DASH results are from the DASH arm only, responders are tests using only the responders (as per decision tree) in the fasting arm. **b** Same view as (**a**), showing 16S or shotgun sequencing microbial taxa significantly altered either at fasting (V1 vs. V2) or refeeding (V2 vs. V3) in responders excluding features already in (**a**) to avoid redundancy. **c** same view as (**a**), with regards to gut functional modules (selected subset shown for clarity). **d** Same view as (**a**) but with regards to immune cell subpopulations (selected subset shown for clarity). T_{reg}: $FoxP3^+$ cells, MAIT: $V\alpha7.2^+CD161^+CD4^-CD3^+$.

of this classifier highlighted a lower $CXCR3^+CD25^-CD4^+/CD25^{high}CD4^+$ (most likely Th1/Treg ratio), alongside lower abundances of $CD24^+$ memory $CD8^+$ T cells and $IL\text{-}17^+TNF\alpha^+$MAIT cells in responders relative to non-responders (Fig. 7b, Supplementary Fig. 9E). Regarding the top ten features derived as indicative for successful patient classification, responders seem to have less of a pro-inflammatory immune signature at baseline (Fig. 7b). Notably, we could increase the prediction performance of the classifier up to 78% by using changes of immune cell abundances between baseline and 3-month follow-up visit as a basis for prediction of BP response at the single-patient level (Supplementary Fig. 9D, F). In contrast, for subjects on a DASH diet only, corresponding classifiers were unable to predict BP response above chance level.

Regarding responder-specific features, we identified microbial features as both characteristic of responders at baseline and during the intervention (Fig. 8a). Microbiomes of BP responders were depleted pre-intervention for Desulfovibrionaceae, previously shown to be enriched in type 2 diabetic patients in a Chinese cohort[17], and were moreover depleted of propionate biosynthesis genes (Fig. 8a). Fasting strongly elevated the abundance of this taxa and enriched these propionate production modules, indicating that responders suffer a treatable deficit. By 3 months post-intervention, propionate modules are almost back at baseline while BP (relative to medication dosage) remains improved, suggesting that their transient elevation during refeeding may have stabilized a less hypertensive state through mechanisms active beyond the gut (Fig. 8a). An opposing pattern was shown by a poorly characterized *Lachnospira sp*., which had a higher abundance in responders at baseline (Fig. 8a). These findings indicate that baseline state of the gut microbiome in these MetS patients predicts individual degree of success of the fasting+DASH intervention.

The question was raised whether independent data could confirm these findings. We therefore reanalyzed the data from the only other existing cohort investigating the effect of fasting, where both BP data and stool sequencing[22] (herein referred to as "Mesnage data") was available, using the same software pipeline as for our own samples. We compared the results to ours, collapsing species/OTU fasting/refeeding/long-term follow-up signals in either dataset at the genus level for clarity (Fig. 8b, Supplementary Data 11). Despite substantial differences between the two study settings (e.g. MetS vs. healthy, mixed vs. single-sex cohort) even at reduced statistical power (Mesnage $n = 15$), we observe substantial agreement between the two datasets; dynamics of *Bifidobacterium*, *Roseburia*, *Bacteroides*, *Coprococcus* and *Intestinimonas* are comparable (Fig. 8b). Though differences can also be observed in the patterns of *Oscillibacter* and *Alistipes* in these two studies. The SCFA producer *Faecalibacterium* showed discordant fasting responses in the healthy vs. MetS cohort but exhibited consistent growth upon refeeding in both datasets (Fig. 8b).

Due to the similarity of the study designs, we next assessed whether a decrease in BP in the Mesnage cohort could be predicted by a model trained on our 16S dataset. We classified the Mesnage patients according to their BP decrease 3 months post-fasting (Supplementary Data 12). A stepwise selection model was built on our 16S baseline data, filtered for significant responder-specific taxa. The model was then evaluated, using the corresponding features from the Mesnage dataset as input. The model classified correctly 10 out of 15 subjects in the Mesnage cohort as either BP responders or non-responders. Top five contributors to the predictor highlighted gut microbiomes of non-responders to be enriched and responders to be depleted of the taxa Desulfovibrionaceae, Hydrogenoanaerobacterium, *Akkermansia*, Ruminococcaceae GCA-900066225 and *Hydrogenoanaerobacterium sp*. (Fig. 8c).

Discussion

Here we demonstrate that fasting induces changes to the gut microbiome and immune homeostasis with a sustained beneficial effect on body weight and BP in hypertensive MetS patients. There is a growing interest in understanding how dietary interventions shape the gut microbiome and interact with metabolic diseases, including obesity, MetS, type 2 diabetes, and (cardiovascular) health[8–10,23–27]. Several lifestyle interventions aimed at weight loss have shown that the gut microbiome changes in obese, type 2 diabetic or MetS patients[10,23,24,26,27]. Although these interventions led to beneficial clinical outcomes, their effect on the gut microbiome was highly variable[10,23,24,26,27] (more information in Supplementary Data 13). In mice, intermittent fasting decreased obesity-induced cognitive impairment and insulin resistance associated with increased abundance of the *Lactobacillus* and the butyrate-producer *Odoribacter*[25]. In a small human pilot study, Ramadan fasting[9] affected the microbiome of healthy subjects enriching several SCFA producers. Each of the aforementioned studies are described in greater detail in Supplementary Data 13.

We have carried out the first high-resolution multi-omics characterization of (periodic) fasting in patients with MetS, including detailed clinical and immunophenotyping along with gut microbiome sequencing. Our major finding is that periodic fasting followed by 3 months of a modified DASH diet induces concerted and distinct microbiome and immunome changes that are specific to fasting itself, leading to a sustained BP benefit (Fig. 3a), which was not seen in the patients following a DASH diet alone.

Fasting followed by modified DASH also led to a significant long-term reduction in body weight. However, neither the change in BP nor global changes to the microbial composition or immunome appeared to be mediated by this BMI decrease (95% of findings retained significance when deconfounded for BMI change, see Supplementary Data 5, and body weight reduction was not more pervasive in treatment responders than non-

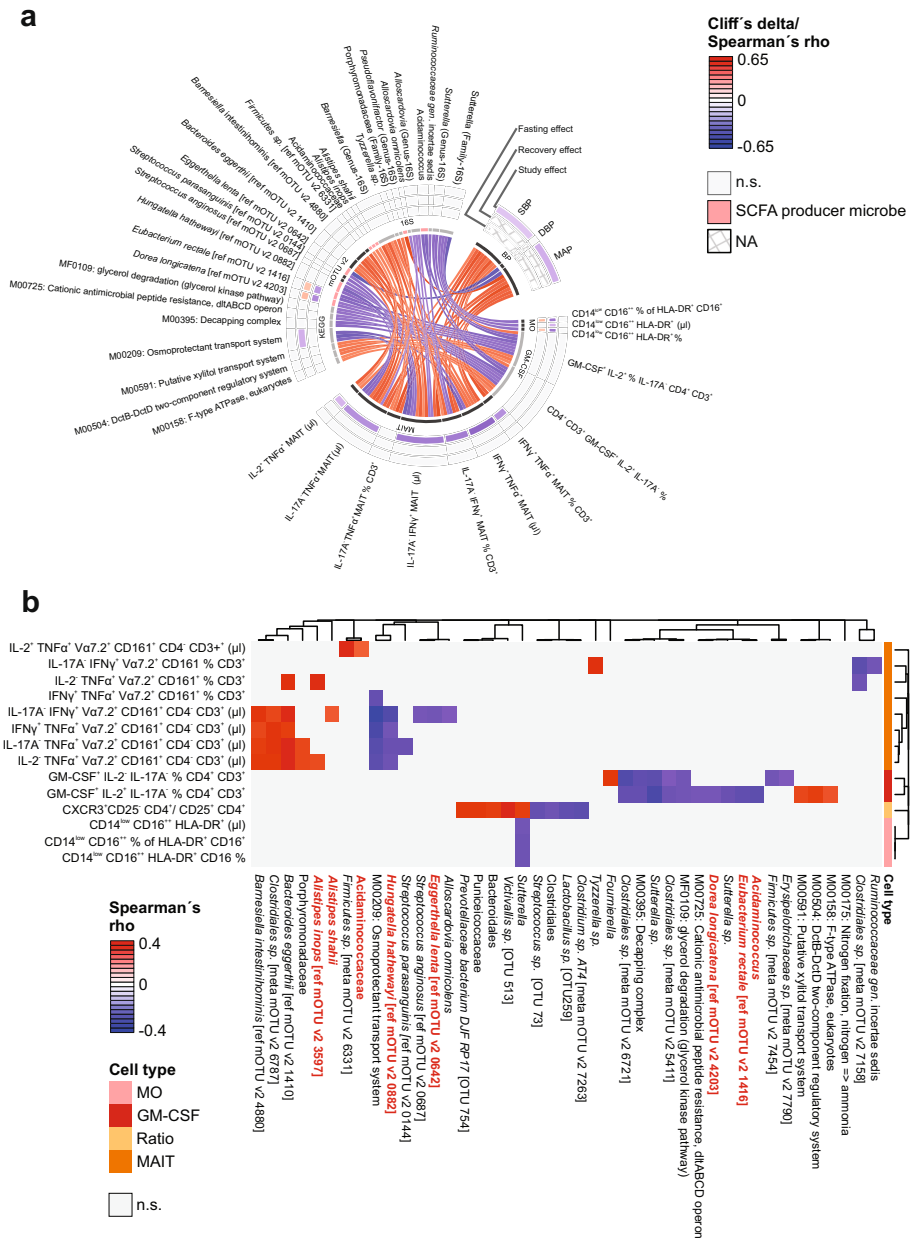

Fig. 5 Blood pressure-microbe-immune association. a Chord diagram visualizes the interrelation between BP (24 h ambulatory systolic, mean or diastolic BP) and fasting-impacted microbiome functional or taxonomic features, and immune cell subsets. Features are shown that form triplets of immune, microbial and phenotype variables where at least two of three correlations are significant (Spearman FDR < 0.05, post-hoc nested model test accounting for same-donor samples < 0.05) in the fasting arm of our cohort, and where in addition one or more features is significantly (drug-adjusted post-hoc FDR < 0.05) affected by the intervention. Color of the connectors indicates positive or negative association (Spearman's rho), color of the cells within the tracks indicates changes upon fasting, refeeding and study effect (Cliff's delta, white if not significant), respectively. **b** Hierarchical clustering of microbiome features-associated immune features. Color indicates Spearman's rho.

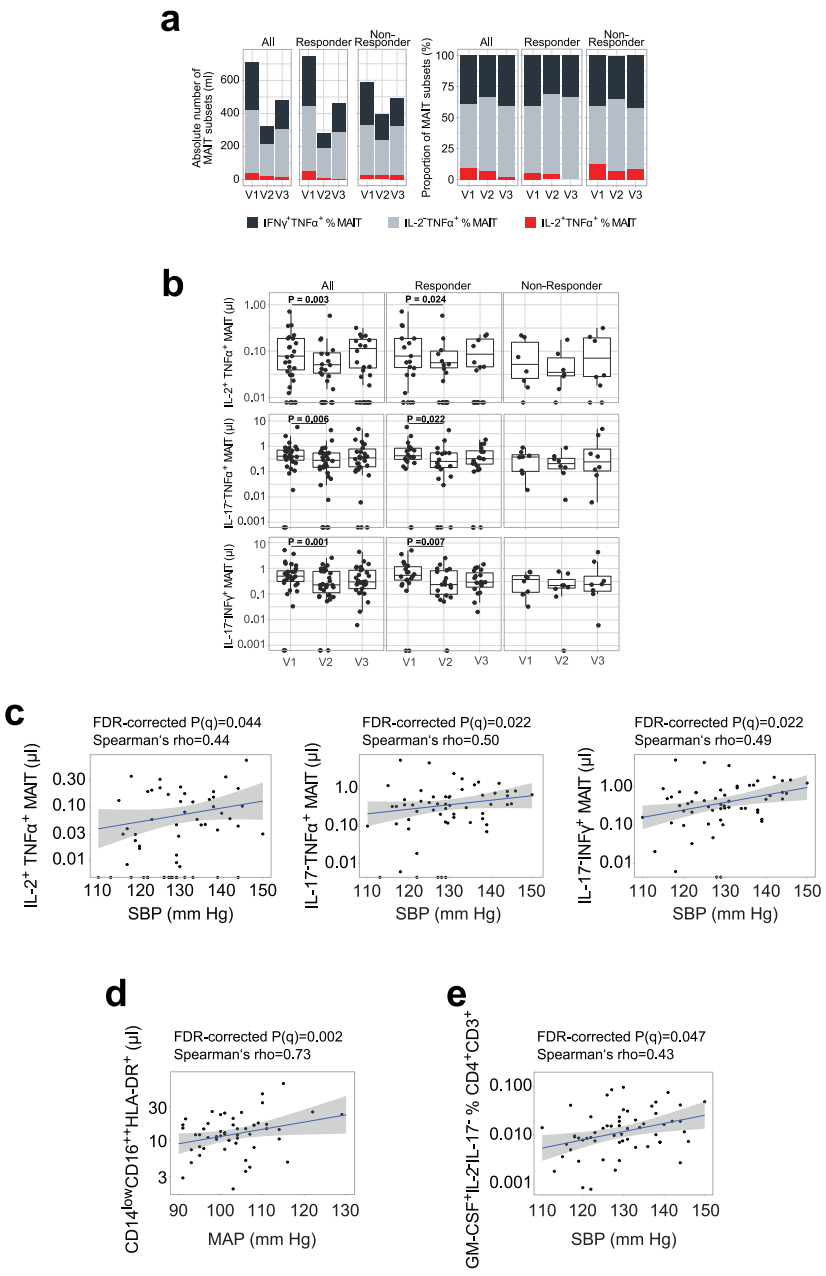

responders, Fig. 2g). Furthermore, BP and BMI were both associated with various immune cell subsets and microbial taxa on a multivariate level, and the effects of fasting on these two features are divergent (shown as chord plots on Fig. 5, Supplementary Fig. 8, respectively). Nevertheless, the data indicate that a 5-day fast exerted an effect on microbiome composition and immune cell subsets. Even though many of these shifts post-fasting are transient, a sustained improvement of BP was seen in our patients. Comparison of V1 to V2 suggests that microbiome and immune cells may reset to some extent during and after the intense caloric restriction, similar to a preconditioning mechanism. The subsequent DASH diet consistent across all patients thus seem to act differently depending on whether this preconditioning took place or not. This interpretation is supported by the fact

Fig. 6 The association between blood pressure and specific circulating immune cell populations. a Cumulative absolute number and relative abundance of circulating IFNγ$^+$TNFα$^+$, IL-2$^-$TNFα$^+$ and IL-2$^+$TNFα$^+$ mucosa-associated invariant T cells (MAIT) cells within the fasting arm subdivided by BP responsiveness (median, $n = 30$ for all, $n = 20$ for responders, $n = 8$ for non-responders, respectively). Absolute number of circulating IL-2$^+$TNFα$^+$ (All: $P = 0.019$, Responder: $P = 0.024$), TNFα$^+$ (All: $P = 0.006$; Responder: $P = 0.022$) and IFNγ$^+$ (All: $P = 0.001$; Responder: $P = 0.007$); (**a**) two-sided MWU test after Benjamini–Hochberg correction. **b** MAIT cells within the fasting arm subdivided by BP responsiveness (n-number as in (**a**); two-sided MWU test after Benjamini–Hochberg correction). **c** Correlations of circulating IL-2$^+$TNFα$^+$, TNFα$^+$, and IFNγ$^+$ MAIT cells and 24 h ambulatory SBP (*FDR-corrected $P = 0.044$, 0.022, and 0.022, respectively). **d** Correlations of circulating non-classical CD14^{low}CD16^{++}HLA-DR$^+$ monocytes and 24 h ambulatory MAP in responder (FDR-corrected $P = 0.002$). **e** Correlations of circulating GM-CSF$^+$IL-2$^-$IL-17$^-$ of % CD3$^+$ and 24 h ambulatory SBP (FDR-corrected $P = 0.047$). n-number for (**c**–**g**) as in (**b**). MAIT: Vα7.2$^+$CD161$^+$CD4$^-$CD3$^+$. Boxplot hinges denote 25th–75th percentile. Line within the boxplot indicates median. Whiskers are drawn to minimum and maximum values, but not further than 1.5 × IQR. **c**–**e** Gray shading represents 95% CI.

that the DASH diet alone neither reduced SBP nor BMI, while affecting different (and substantially fewer) immune cell subsets. In line with the preconditioning hypothesis, we consider that (1) those subjects who benefit most with regards to BP from a fasting+DASH intervention are those depleted at baseline for both SCFA producing taxa (including core butyrate producers) and SCFA production gene modules; (2) that such taxa and gene modules enrich either during the fasting phase or the refeeding phase thus ameliorating the aforementioned baseline depletion; and (3) that at least some enrichment remains at 3-month follow-up in BP responders (less so in non-responders). Our interpretation is that one crucial mechanism for the improvement stems from the effects of increased SCFA availability, either locally in the intestine (impacting immune signaling and intestinal permeability), systemically, or both. While we cannot directly test it in the present cohort, it is a scenario consistent both with expectations from the literature and with our observations of a consistent depletion-then-regrowth pattern. Thus, future work will include studying a larger fasting/refeeding cohort at various intermediate time intervals.

Fasting induced a profound change in circulating immune populations; e.g. depleted Th1 cells and permanently enriched dendritic cells, which both have been shown previously to play a role in the pathogenesis of experimental hypertension[28,29]. Further, we discovered significant correlations between circulating MAIT cells and 24 h ambulatory BP and MAP.

A growing body of evidence suggests that the abundance of certain microbes is associated with cardiovascular health. Previous reports on hypertensive patients have shown taxonomic and functional gut microbiome shifts[6,7]. For example, Firmicutes have been shown to be more abundant in healthy controls compared to pre-hypertensive and hypertensive patients[7]. Upon fasting, several Clostridial Firmicutes shifted significantly in abundance, with an initial decrease in butyrate producers such as *F. prausnitzii*, *E. rectale* and *C. comes*, which were reverted after 3 months upon refeeding; with the latter taxon likely being an indirect effect of the observed weight reduction (Supplementary Data 5). Further, functional microbial metabolism in fasting patients at baseline share some similarities to the previously profiled hypertensive microbiome[7]. In the fasting arm, the functional shift during refeeding enriches for functional modules also enriched in non-hypertensive controls, i.e. for potentially BP-protective factors.

Clinical studies represent a highly heterogeneous situation with multifactorial disease features and strongly variable microbial and lived environments. To account for this heterogeneity, we compared the data from our longitudinal study (post-fasting and 3-month) to the respective baseline values of the study subjects. This intraindividual analysis allowed us to identify BP responder-specific changes in spite of the reduced power in such a sub-stratified analysis. The responder-specific microbiome changes in our fasting arm post-intervention (enrichment of *F. prausnitzii*, *Bacteroides* and Firmicutes, depletion of *Actinomyces*) are likely beneficial to the host. A recent study profiling the hypertensive microbiome showed that during disease, patients experienced an enrichment of Actinomyces, and a depletion of *F. prausnitzii*, *Bacteroides* and Firmicutes[7]. Moreover, Guevara-Cruz et al. recently showed in a Mexican cohort involving 146 MetS patients, that a 75 day long, 500 kcal/day, low-saturated fat dietary intervention improved the clinical phenotype, significantly decreased gut dysbiosis and increased the abundance of *Akkermansia muciniphila* and SCFA producer *F. parausnitzii*[27] (Supplementary Data 13). Furthermore, abundance of some functional gut-specific gene modules was significantly altered in our dataset only in BP responders, for example, the pyruvate:formate lyase module, MF0085, which was decreased after refeeding. This decrease (from a trending elevation at baseline) may contribute to vascular health, as a recent study demonstrated enrichment of the same enzyme in atherosclerosis patients relative to healthy controls[30], and formate production has been previously linked to BP regulation[31,32].

Stratification of the cohort to BP responsiveness showed that also immune changes present in the fasting arm are more pronounced in responders than in non-responders, and are fundamentally different from the changes observed in the DASH-only arm. The DASH-only arm was associated with the decrease of CD8$^+$ Tem cells, previously reported to play a role in hypertension[29,33]. Responders and non-responders not only reacted differentially to fasting, but also differed at baseline with regards to their propionate synthesis capacity pre-intervention and the relative depletion by depletion of Desulfovibrionaceae, which has been linked to a lean phenotype[34,35]. These features were then normalized during fasting. Notably, recent experimental work suggested an antihypertensive effect of propionate treatment in mice[36]. Furthermore, responders were enriched in *Lachnospira sp*. at baseline, which was shown to contribute to diabetes in obese mice and is enriched in obese children[37,38]. Our findings indicate responders and non-responders to our intervention differ with regards to several gut microbiome features relevant to hypertension, with fasting-induced normalization of these differences seen during a successful fasting intervention.

Through network analysis of the immunome, microbiome, and clinical data, we identified significant correlations between circulating MAIT cells and 24 h ambulatory SBP and MAP. MAIT cells represent up to 10% of peripheral blood T cells, but in contrast to other classical T cells[29], have not yet been linked to the regulation of BP. They differ in many aspects from conventional T cells by expressing a semi-invariant TCR α-chain Vα7.2-Jα33. MAITs can produce various cytokines mimicking an effector/memory-like phenotype and yet they behave rather like innate cells. During aging[18] and CMD[19,39], absolute circulating MAIT number and frequencies decrease, while certain subsets of cytokine-producing and adipose tissue MAITs were found to be enriched in obese type 2 diabetic patients[19]. In addition, this network analysis revealed that abundance of SCFA producing microbes correlates significantly with circulating

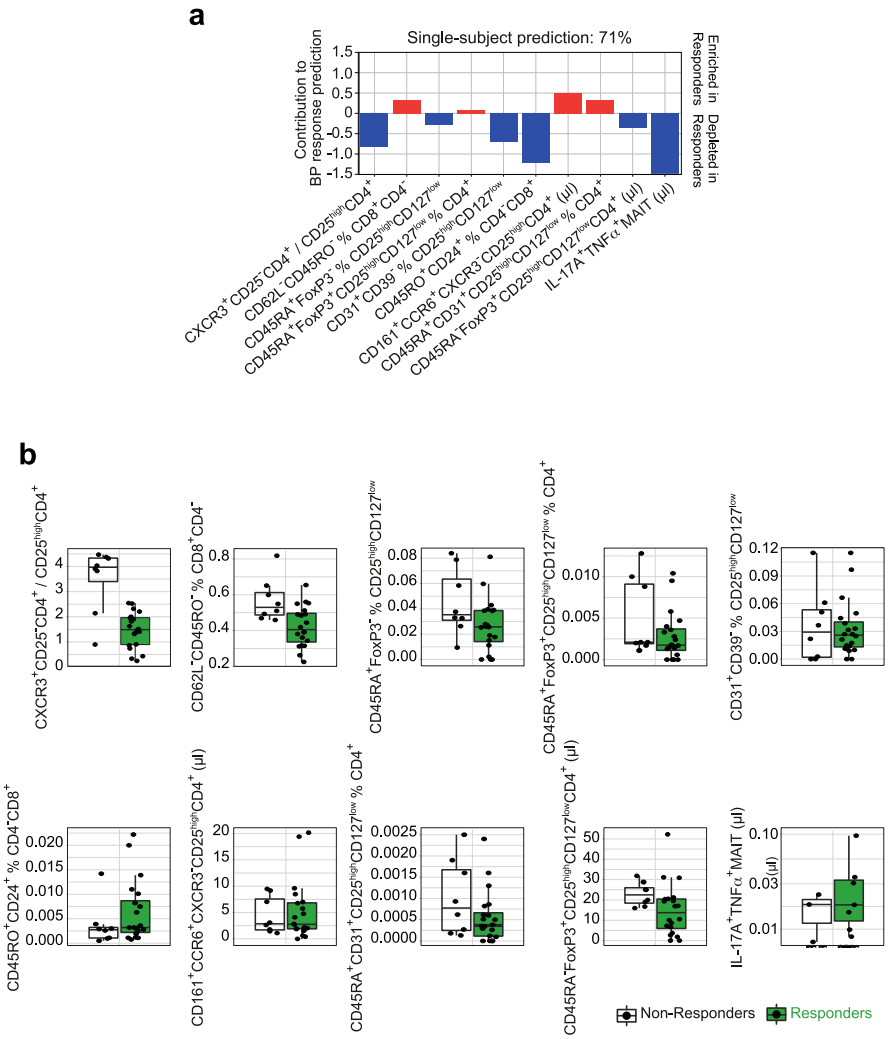

Fig. 7 Long-lasting BP responders and non-responders differ in immunome composition. a Prediction model weights for BP response using the immunome dataset at baseline. The top ten immunome features were used to build a multivariate logistic-regression algorithm. Single-subject prediction was quantified using a leave-one-out cross-validation procedure. The bar plots represent the regression in a model with binary output (responder yes = 1 vs. no = 0) for every feature. **b** Quantification of the immunome features at baseline used in the prediction model to predict BP response in the future, split into responders and non-responders. MAIT: Vα7.2$^+$CD161$^+$CD4$^-$CD3$^+$. Boxplot hinges denote 25th–75th percentile. Line within the boxplot indicates median. Whiskers are drawn to minimum and maximum values, but not further than 1.5 × IQR.

pro-inflammatory cytokine-producing MAIT cells and GM-CSF$^+$ IL-2$^+$ T helper cells. Of note, most of these microbes are relatively poorly characterized taxa and further description is needed to elucidate their role in the gut and as contributors of dys- or eubiosis.

Using machine learning, we were able to utilize deep immunophenotyping data to predict at baseline, which subjects were likely to decrease their BP during fasting despite the small number of subjects. In addition, the accuracy of the prediction was enhanced further taking the dynamics of immune populations along the course of the study into account. No corresponding prediction of a favorable response to a DASH-only intervention was possible. The features informing the predictor indicate BP responders and non-responders present with differing severities of a pro-inflammatory immune signature at baseline, raising the question whether responders and non-responders suffer from varying degrees of MetS severity at baseline. Remarkably, no significant difference in baseline BP, BMI, lipid levels, or glucose homeostasis parameters between BP responders and non-responders was observed before the intervention (Supplementary Data 6). However, BP responders exhibited higher median SBP than non-responders (135 mmHg and 128 mmHg,

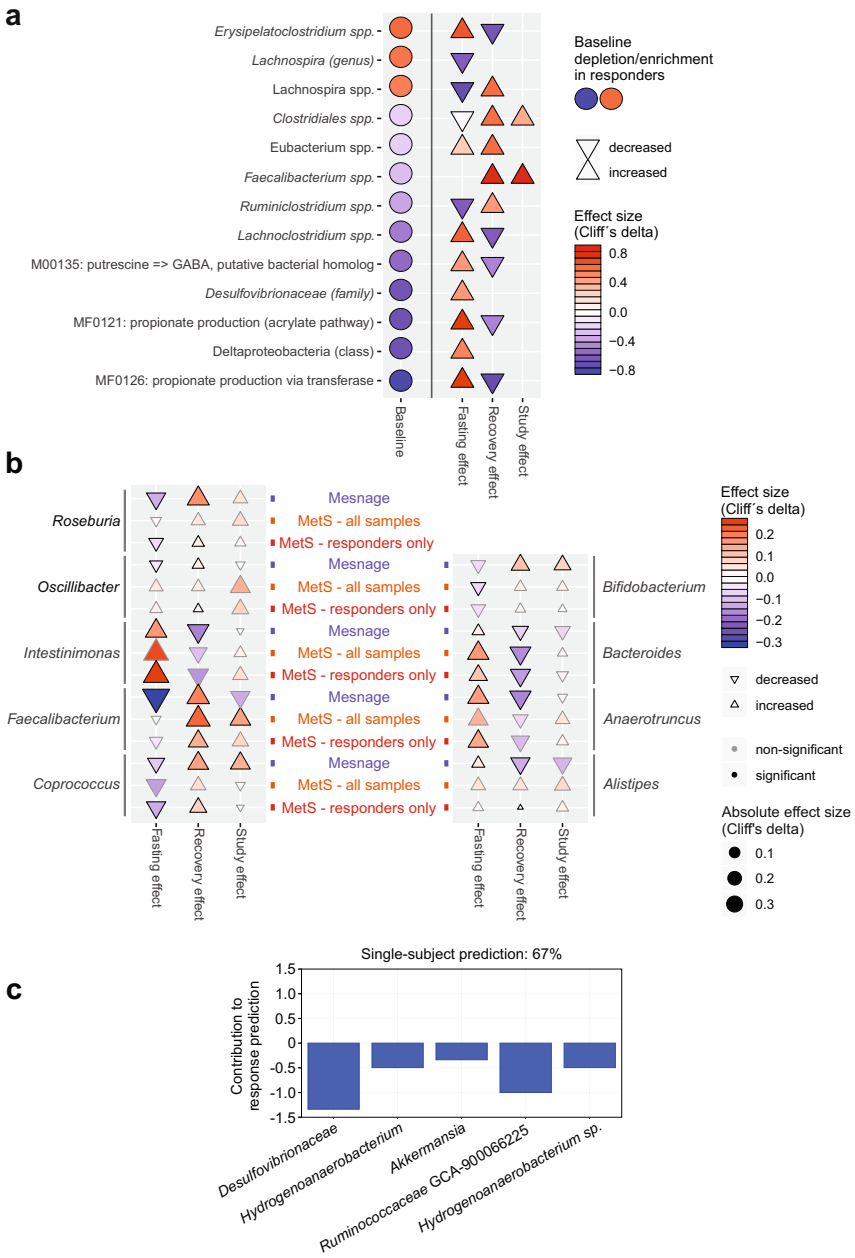

respectively). Baseline antihypertensive medication did not differ significantly between the groups (responders' normalized mean dose: 1.4, non-responders' normalized mean dose: 2.1). Additionally, responders had lower median BMI than non-responders; 32.0 and 36.5, respectively. In addition, body fat percentage was slightly higher in the fasting+DASH group compared to the DASH group (median 42%, 39%, respectively). Furthermore, BP responders had a baseline median LDL of 149 mg/dl compared to 122 mg/dl for non-responders, while HDL did not differ (in both groups 48 mg/dl). These data indicate that although BP

Fig. 8 Baseline microbiome predicts long-lasting BP responsiveness. a Circles denote features differing at baseline in responders vs. non-responders and altered during intervention in responders. Effect size (Cliff's delta) is shown comparing responders and non-responders. **b** Comparison of results from the present study (MetS; all samples and BP responders only shown as orange and red tags, respectively, separately) with those of a recent similar fasting intervention in healthy men (Mesnage; blue tags). Effect sizes at the species or OTU level were averaged at the genus level for clarity, and are shown in the plot (direction rendered as marker shape and hue; scope rendered as marker size and intensity) for all genera where at least one constituent taxon achieved significance either in the Mesnage or MetS study (these are shown in boldface). Columns denote phases of each intervention - fasting phase, refeeding, and follow-up vs. baseline. Substantial agreement between the two studies is seen, which is typically stronger for the subset of BP responders. **c** Prediction model weights for BP response using the MetS 16S dataset at baseline. The top five immunome features were used to build a multivariate logistic-regression algorithm. Single-subject prediction on the Mesnage dataset[22] was quantified using a leave-one-out cross-validation procedure. The bar plots represent the regression in a model with binary output (responder yes = 1 vs. no = 0) for every feature.

responders and non-responders do demonstrate slightly different trends in some clinical parameters, BP responders do not show any less severe disease phenotype.

Through the reanalysis of the Mesnage dataset, the only fasting cohort in the literature with a similar study design and which includes both BP and microbiome data, we were able to demonstrate concordant treatment-related microbiome shifts in both studies. This finding suggests the effects of fasting and refeeding on gut microbiota generalizable. A machine-learning model built from microbiome features differentially abundant at baseline in BP responders in our cohort was able to predict significant long-term BP decrease in the Mesnage et al. subjects with about 70% accuracy, further supporting the idea that these findings are likely generalizable.

Previous works have also shown that some outcomes of dietary interventions in cardiovascular patients might be related to baseline microbiome features. Notably, a recent study demonstrated that higher baseline *Akkermansia* abundance was associated with persistent weight loss in a study investigating MetS/obese patients undergoing a 52-week long weight reduction program[10] (Supplementary Data 13). In addition, Velikonja et al. showed in a study investigating the effect of beta-glucan supplementation in MetS patients that a higher baseline abundance of *Akkermansia muciniphila* and *Bifidobacter* spp. was characteristic of patients whose cholesterol decreased due to the intervention[23] (Supplementary Data 13).

Thus, we demonstrate the practical utility of a machine-learning analysis pipeline for predicting BP benefit of fasting in MetS patients with hypertension using both baseline immunome and microbiome data.

It is important to recognize that our study represents patients with hypertension and MetS solely from a Caucasian-European background. This selection criterion introduces a selection bias in our study design. Additional research is necessary to elucidate whether the results presented here could be applicable in a more heterogeneous patient population. Further, our recruitment procedure could already have introduced a selection bias toward patients who were interested in fasting/dietary studies and therefore are sensitive about their cardiometabolic health. Since the participants were especially interested in the fasting procedure, the allocated DASH participants were offered a cost-free fasting cycle after successful completion of the study. However, we cannot exclude that this led to an increased long-term motivation compared to the participants who started with the fasting protocol. Furthermore, the study design did not allow us to investigate the long-term effects of a fasting intervention without a subsequent DASH diet on the BP, microbiome, or immunome. In our cohort, fasting was required on top of DASH to achieve the observed outcomes, but we cannot conclude (and do not expect) fasting without a subsequent dietary change to do so either. We can only claim fasting was required prior to the DASH diet to achieve the effects observed in our cohort. DASH, which is rich in fibers, might furthermore "fuel" the beneficial microbiome, thus further contributing to cardiovascular health, and may play a part in maintaining this microbiotal state longer. However, some effects are replicated in the similar dataset from healthy males (without MetS and without DASH intervention) in the Mesnage dataset[22], thus indicating the precise DASH setup may not be strictly needed. Most likely, the two components of the intervention synergize—fasting may potentiate the microbiome in these patients to be shifted to a more DASH-compatible microbiota upon diet change. While we identify changes in microbial taxonomic and functional features, bacterial metabolites and immune processes, which could explain the efficacy of the intervention, robust conclusions of causality will require follow-up experimental work, particularly in animal models (e.g. gnotobiotic mice colonized with bacteria strongly associated with BP). In addition, the relatively low patient number could be regarded as a limitation. Although our present study is large enough to allow inference of significance for the strongest contributors to the observed effect, our results are likely not complete, and follow-up in additional and larger studies will be needed for a comprehensive view of subtle fasting-associated host and microbiome features. Our study design did not allow for the blinding of participants regarding their intervention. To maximally reduce the bias, the scientific staff were blinded during the course of processing, measurement, and analysis of collected samples. Further, the present study cannot infer how frequently fasting cycles should be repeated to control BP in at-risk patients, nor whether it is as effective without a concomitant DASH intervention. Despite the low number of participants of the study, machine-learning algorithms were able to predict BP responsiveness based on the immunome and 16S data. Only the latter could be confirmed in an independent dataset, as no equivalent immunome profiling in a fasting dataset has been published to date. Confirmation of the predictive capability of the immunome data and testing further hypothesis raised above (e.g. the interaction between SCFA availability and BP responsiveness) require future prospective clinical studies. The favorable impact of fasting followed by a DASH diet during refeeding phase shown here highlights this intervention as a promising non-pharmacological intervention for the treatment of high BP in MetS patients.

Methods

Study planning and ethical approval. The study was planned as part of a randomized-controlled bi-centric trial conducted by the outpatient center of the department of Internal and Integrative Medicine at Charité-Universitätsmedizin. The study was approved by the ethics committees of the Charité-Universitätsmedizin Berlin (approval number: EA4/141/13) and registered at ClinicalTrials.gov (registration number: NCT02099968).

Participants. Participants were recruited from the existing patients at study centers and through local newspaper announcements. Patients were first screened over the phone by a research assistant to assess eligibility. Eligible patients were invited for an assessment by a physician, where they were examined and provided detailed written information describing the study. If patients met all inclusion criteria and did not meet any exclusion criteria, informed consent was obtained and they were included in the study.

Male and female patients with MetS according to National Cholesterol Education Program Adult Treatment Panel III (NCEP ATP III) criteria were included. MetS was defined as the presence of at least three out of five risk factors: (i) increased waist circumference (>94 cm in men and >80 cm in women), (ii) hypertriglyceridemia (>150 mg/dl (1.7 mmol/l) or lipid-lowering medication), (iii) low levels of high-density lipoprotein cholesterol (HDL-C; < 40 mg/dl (1 mmol/l) in men and <50 mg/dl (1.3 mmol/l) in women or use of HDL-increasing medication (niacin or fibrate), (iv) elevated blood pressure (≥130/85 mm Hg or use of antihypertensive medication), and (v) elevated fasting plasma glucose (≥110 mg/dl or treatment for diabetes mellitus). Beyond NCEP ATP III criteria, patients were required to have been diagnosed with systolic hypertension (either being on antihypertensive medication or untreated). Further inclusion criteria included basic mobility and the ability to provide informed consent.

Exclusion criteria included (i) diabetes mellitus type 1 or insulin bolus therapy (c-peptide < 1.2 ng/ml), (ii) manifest treated coronary artery disease, myocardial infarction, pulmonary embolism, or stroke within the past 3 months, (iii) heart failure ≥ stage I NYHA, (iv) peripheral artery disease ≥ stage 2, (v) chronic kidney disease > stage 2 (GFR < 60 ml/min), (vi) manifest eating disorder, vii) dementia or manifest psychosis, or viii) other severe internal diseases.

Periodic fasting and plant-based Mediterranean diet intervention

Dietary interventions. The interventions in both groups were delivered as an intensive group-based behavioral intervention. The educational concept incorporated aspects of the mind–body program designed by the Benson–Henry Mind/Body Medical Institute of Harvard Medical School[40]. The dietary education included counseling, comprehensive lectures and cooking classes.

Periodic fasting and modified DASH diet intervention. Intervention within the fasting arm (Fig. 1a) started with two calorie-restricted vegan days (max 1200 kcal/day), followed by 5-days with a daily nutritional energy intake of 300–350 kcal/day, derived from vegetable juices and vegetable broth. After completion of fasting, weekly 6 h multimodal sessions were provided for a total of 10 weeks; both groups received intensified nutritional counseling/nutritional classes and additional general lifestyle recommendations for exercise and stress reduction[41]. The program entailed 10 h of group sessions for the initial periodic fasting and 50 h of nutritional education, which included lectures and cooking lessons. Similar to protocols from previous trials on periodic fasting in rheumatoid arthritis and diabetes mellitus type 2[42,43] patients were instructed to follow a modified DASH diet after the fasting period, with additional emphasis on plant-based and Mediterranean diet to optimize refeeding[44–46].

Modified DASH diet intervention. The DASH group (Fig. 1a) was trained in the Dietary Approaches to Stop Hypertension (DASH) diet, a sodium-, fat- and sugar-reduced mainly plant-based diet, which has been shown to reduce high blood pressure[47,48]. The intervention was similarly delivered as an the fasting group-based behavioral intervention with aspects of the mind–body program of the Benson–Henry Mind/Body Medical Institute, Harvard Medical School[40]. Overall, the program consisted of 50 h of group sessions over a period of 10 weeks and also included comprehensive lectures and cooking lessons.

Randomization. Patients were randomly allocated to Fasting or DASH by block-randomization with randomly varying block lengths, stratified by a) study center, and b) the intake/non-intake of antihypertensive medication. The randomization list was created by a biometrician not involved in patient recruitment or assessment using the Random Allocation Software[49]. The list was password-secured and only the biometrician was able to access it. On this basis, sealed, sequentially numbered opaque envelopes containing the treatment assignments were prepared.

Outcome measures. Outcomes were assessed at baseline and at 1 and 12 weeks after randomization by a blinded outcome assessor who was not involved in patient recruitment, allocation, or treatment. Two primary outcome measures were defined: 24 h ambulatory systolic blood pressure at week 12 and the Homeostasis Model Assessment (HOMA)-index at week 12.

Physician-assessed outcomes. Twenty-four-hour ambulatory blood pressure monitoring (ABPM) and pulse pressure recording were performed using a digital blood pressure monitor (Mobil-O-Graph® PWA, I.E.M., Stolberg, Germany)[50]. Baseline ABPM measurements were performed within one week before the starting of the intervention, those at week 12 within a week after the end of the intervention. ABPM was initiated at the same time of day for each successive visit. The monitoring software automatically removed incorrect measurements using built-in algorithms. Blood pressure and heart rate values were further categorized as day or night values using each patient's reported awake and sleep times. Office blood pressure was measured in the hospital by a sphygmomanometer, using the average of three consecutive measurements after 5 min rest while sitting in a quiet room. Office blood pressure was measured at each time point, ambulatory blood pressure only at baseline and week 12.

Body weight, body fat percentage, and lean mass percentage were measured using the Omron BF 511 bioelectrical impedance device[51]. BMI was calculated as the weight in kilograms divided by the square of height in meters. Waist circumference was measured by two research assistants using a measuring tape in the horizontal plane exactly midway between the iliac crest and the costal arch. Measures were repeated twice and the mean of both measures was used. If the two measures differed by more than 1 cm, both measures were repeated. Hip circumference was measured in the horizontal plain at the maximal circumference of the hips or buttock region above the gluteal fold, whichever is larger, using the same approach as for waist circumference. Waist-hip-ratio was measured as the quotient of waist circumference and hip circumference[52].

Laboratory measures. Blood samples were collected from the antecubital vein into vacutainer tubes and analyzed using the Modular P analyzer (Roche, Mannheim, Germany). Metabolic parameters included plasma and blood glucose levels, blood insulin levels, HbA1C, and HbA1C IFCC and were analyzed using standard procedures. HOMA index was calculated as blood insulin level (µU/ml) × blood glucose level (mmol/l)/22.5[53]. Further laboratory parameters included blood lipid levels (total cholesterol, HDL cholesterol, LDL cholesterol, LDL/HDL ratio, triglyceride), uric acid, blood creatinine level, estimated glomerular filtration rate (eGFR), C-reactive protein (CRP), insulin-like growth factor 1 (IGF-1), and interleukin-6 (IL-6), triglyceride, fasting glucose level[54]. Samples were destroyed after the analysis and were not further stored.

Safety. All adverse events occurring during the study period were recorded. Patients experiencing adverse events were asked to see the study physician to assess their status and initiate any necessary response. The most common symptoms during the fasting period were mild weakness, headaches, and mild perception of hunger. No serious adverse effects were reported. During the normocaloric diet periods no adverse effects were reported.

Multiple imputation. All analyses were conducted on an intention-to-treat basis, including all participants being randomized, regardless of whether or not they gave a full set of data or adhered to the study protocol. Missing data were multiply imputed by Markov chain Monte Carlo methods[55,56].

Peripheral blood mononuclear cell analysis. Whole blood staining was performed using antibodies against major leukocyte lineages. Quantitative measurement was performed using a high throughput sampler (BD) and a BD FACS CantoII (BD). Peripheral venous blood was obtained and mononuclear cells were isolated within 24 h of collection by density gradient centrifugation using Biocoll and cryopreserved until further processing. Thawed cell aliquots were either labeled for extracellular antigens using fluorophore-conjugated monoclonal antibodies or CD4$^+$ cells were selected (Miltenyi CD4$^+$ Selection Kit). Cells (10^6) from CD4$^+$ and CD4$^-$ fractions were placed onto U-bottom plates and re-stimulated for 4 h at 37° C and 5% CO_2 in a humidified incubator in a final volume of 200 µl RPMI 1640 (Sigma) supplemented with 10% FBS (Merck), 100U/ml penicillin (Sigma), 100 mg/ml streptomycin (Sigma), 50 ng/ml phorbol 12-myristate 13-acetate (PMA, Sigma), 250 ng/ml ionomycin (Sigma) and 1.3 µl/ml Golgistop (BD). After re-stimulation, cells were labeled with Life/Dead Fixable Aqua Dead Cell Stain Kit, for 405 nm excitation (Invitrogen), followed by labeling with surface antigen-specific fluorophore-conjugated monoclonal antibodies. Cells were then fixated and permeabilized by FoxP3/Transcription Factor Staining Kit (eBioscience), and subsequently labeled with intracellular-antigen-specific fluorophore-conjugated monoclonal antibodies. Antibodies are listed in Table 2. Samples were analyzed using the FACSCanto II multicolor flow cytometer (BD). The acquisition was performed with Diva 6.1.3 (BD). Data analysis was performed using FlowJo 10.3 (FlowJo LLC) and FCSExpress V6.02 (De Novo Software) software. Absolute cell numbers were calculated using the relative percentage of cell population compared to a marker used in the whole blood staining.

FlowSOM. Data were manually gated on single live cells and exported as FCS files in FCS Express V6.02 (De Novo Software). The automated analysis of FCS files was done by the FlowSOM[57] algorithm, an R[58] bio-conductor package that uses self-organizing maps for dimensional reduction and visualization of flow cytometry data. All data were scaled and log-transformed on import. Cells were assigned to a Self-Organizing Map (SOM) with a 10 × 10 grid, grouping similar cells into 100 nodes. Each node in the FlowSOM tree gets a score indicating its correspondence with this requested cell profile. To visualize similar nodes in branches, a minimal spanning tree (MST) was constructed and cell counts were log scaled. To visualize the differences between the two-time points, the mean percentage per sample group was computed in each cluster and then the statistical difference was performed by applying MWU test on every node within metaclusters. *P* values were two-sided and analysis was performed using RStudio (version 3.4.4). The FlowSOM algorithm was run 3 times to ensure reproducibility of the results and $P < 0.05$ was considered to be statistically significant.

Medication data collection and cleanup. Antihypertensive drugs were normalized in order to track changes during intervention. In a first step, antihypertensives (according to the WHO ATC classification system), diuretics, beta-blocking agents, calcium channel blockers, and agents acting on the renin-angiotensin system as well as the given dosage were identified at V1 and at follow-up visit after 3 months (V3).

Table 2 Antibodies used for the flow cytometry analysis.

Antibody	SOURCE	RRID	Dilution
a-CD11c APC	Miltenyi	AB_871587	2:25
a-CD123 PE	Miltenyi	AB 244211	1:10
a-CD127 PE-Vio770	Miltenyi	AB_2659856	1:10
a-CD14 APC	Miltenyi	AB_244301	1:25
a-CD14 PE-Vio770	Miltenyi	AB_2660180	1:25
a-CD16 FITC	Miltenyi	AB_2655402	1:10
a-CD16 PE	Miltenyi	AB_2655404	1:10
a-CD161 FITC	Miltenyi	AB_871631	1:10
a-CD19 PE	Miltenyi	AB_244223	2:25
a-CD196 (CCR6) APC	Miltenyi	AB_2655933	1:10
a-CD24 PerCP-Vio700	Miltenyi	AB_2660665	1:10
a-CD25 APC	Miltenyi	AB_871644	1:10
a-CD25 PE	Miltenyi	AB_244320	1:10
a-CD27 PerCP-Vio700	Miltenyi	AB_2660841	1:10
a-CD27 PE-Vio770	Miltenyi	AB_2660837	1:10
a-CD3 PerCP-Vio700	Miltenyi	AB_2659948	1:10
a-CD31 FITC	Miltenyi	AB_871662	1:10
a-CD39 APC-Vio770	Miltenyi	AB_2660873	1:10
a-CD4 FITC	Miltenyi	AB_871682	1:10
a-CD4 VB	Miltenyi	AB_10829954	1:10
a-CD45 FITC	Miltenyi	AB_244234	1:10
a-CD45RA PerCP-Vio700	Miltenyi	AB_2660987	1:10
a-CD45RO FITC	Miltenyi	AB_10827692	1:10
a-CD56 APC	Miltenyi	AB_244331	1:10
a-CD62L APC	Miltenyi	AB_244246	1:10
a-CD69 APC	Miltenyi	AB_615096	1:10
a-CD8 FITC	Miltenyi	AB_244336	1:10
a-CD8 PE-Vio770	Miltenyi	AB_10829189	1:10
a-CXCR3 PE-Vio770	Miltenyi	AB_2655740u	1:10
a-FoxP3 PE	Biolegend	AB_10579944	1:5
a-GM-CSF PE	Miltenyi	AB_2572656	1:20
a-Helios FITC	eBioscience	AB_2572656	1:120
a-HLA-DR PerCP-Vio700	Miltenyi	AB_10839556	1:10
a-IFNγ PE-Vio770	Miltenyi	AB_2661063	1:30
a-IL10 PE-Cy7	eBioscience	AB_2573523	1:20
a-IL17A APC-Vio770	Miltenyi	AB_2659812	1:10
a-IL2 FITC	eBioscience	AB_2572512	1:20
a-IL2 PE	Miltenyi	AB_244197	1:10
a-IL22 eFluor450	eBioscience	AB_11150956	1:20
a-IL5 APC	Biolegend	AB_315330	1:20
a-Ki67 APC	Miltenyi	AB_2573218	1:120
a-TCRγδ APC-Vio770	Miltenyi	AB_2654040	1:10
a-TCRγδ PE	Miltenyi	AB_2654034	1:10
a-TCRVα 7.2 APC-Vio770	Miltenyi	AB_2653673	1:10
a-TCRVα 7.2 VB	Miltenyi	AB_2653669	1:10
a-TNFα APC	Miltenyi	AB_244201	1:10
a-TNFα eFluor450	eBioscience	AB_2043889	1:20

Secondly, drug dosage was normalized to the lowest drug dosage per patient and drug. The lowest drug dosage at baseline was set to one, while corresponding drug dosages at other time points where either zero if the medication was discontinued, one if there was no change in drug dosage between time points, smaller than one if the drug dosage was decreased or greater than one if the drug dosage was increased at a certain time point. The sum of the agents taken was calculated at each time point.

DNA isolation. For DNA-based 16S rRNA gene and metagenomics sequencing, fecal samples were collected into RNALater containing tubes, shipped at room temperature and stored at −80 °C until processing. The DNA isolation protocol has been previously described[59]. Briefly, samples were treated with 500 µl of extraction buffer (200 mM Tris, 20 mM EDTA, 200 mM NaCl, pH 8.0), 200 µl of 20% SDS, 500 µl of phenol: chloroform:isoamyl alcohol (24:24:1) and 100 µl of zirconia/silica beads (0.1 mm diameter). Samples were homogenized twice with a bead beater (BioSpec) for 2 min. After precipitation of DNA, crude DNA extracts were resuspended in TE Buffer with 100 µg/ml RNase I and column purified to remove PCR inhibitors.

16S rRNA gene amplification and sequencing. Amplification of the V4 region (F515/R806) of the 16S rRNA gene was performed according to previously described protocols[60,61]. Briefly, for DNA-based amplicon sequencing 25 ng of DNA was used per PCR reaction in a final volume 30 µl. The PCR conditions consisted of initial denaturation for 30 s at 98 °C, followed by 25 cycles (10 s at 98 °C, 20 s at 55 °C, and 20 s at 72 °C). Each sample was amplified in triplicates and subsequently pooled. After normalization, PCR amplicons were sequenced on MiSeq PE300 platform (Illumina) at the Helmholtz Centre for Infection Research, Braunschweig, Germany.

Metagenomic DNA library construction and sequencing. Sixty microliters of total DNA was used for shearing by sonication (Covaris). Fragmentation was performed as follows; processing time: 150 s, fragment size: 200 bp, intensity: 5, duty cycle: 10. Library preparation for Illumina sequencing was performed using the NEBNext Ultra DNA library prep Kit (New England Biolabs). The library preparation was performed according to the manufacturer's instructions. An input of 500 ng of sheared DNA was used and the size selection was performed using AMPure XP beads with the following parameters. First bead selection: 55 µl, and second: 25 µl. Adaptor enrichment was performed using seven cycles of PCR using NEBNext Multiplex oligonucleotides for Illumina (Set1 and Set2, New England Biolabs). Sequencing was performed on NovaSeq PE1000 platform (Illumina) at the Helmholtz Centre for Infection Research, Braunschweig, Germany.

16S sequence processing. Reads retrieved from 16S amplicon sequencing were analyzed using the LotuS (1.62) pipeline[62]. The pipeline includes sequence quality filtering[63], read merging[64], adapter and primer removal, chimera removal[65], clustering[66], and taxonomic classification[67] based on the SILVA (v138)[68] database. The validation dataset[22] was reprocessed using the exact same settings.

Shotgun metagenomic processing. Metagenomic shotgun sequences were processed within the NGLess framework (0.10)[69]. Reads were quality filtered by a minimum read length of 45 bp and a minimum Phred quality score of 25. Sequences passing that filter were mapped to the human genome (adapted from hg19; minimum 45 bp match, 90% minimum identity) and filtered. Sequences identified as non-human were mapped with bwa[70] to a) the IGC gene catalog (0.5)[70] with a minimum match size of 45 bp and a minimum identity of 95%, b) 40 reference marker genes described in Ciccarelli et al.[71] and Sorek et al.[72] with a minimum match size of 45 bp and a minimum identity of 97%. Reads mapping to the marker genes were extracted and further mapped to marker gene-based OTUs[73]. Mapping statistics can be found in Supplementary Data 14.

Microbiome statistical analysis

Data pre-processing. Reads mapped to the IGC microbial gene catalog (0.5)[71] were rarefied using the RTK (0.93.1)[74] with default settings (95% of smallest total reads—here 15,247,497 reads/sample). Reads were mapped to the mOTUv2 (2.1) taxonomic marker genes[73] were likewise rarefied (5838 reads/sample). Reads mapped to 16S OTUs (27813 reads), to ensure sample compatibility regardless of sampling depth. For functional microbiome analysis, IGC genes were binned to KEGG KOs[75] based on the annotations in MOCAT2 (2.0.1)[75], then binned by averaging over KOs to KEGG modules and to Gut Microbial Modules (GMMs)[76]. 16S and mOTUv2 (2.1) OTUs were binned at more rootwards taxonomic levels using the taxonomies provided with LotuS (1.62)[62] and the mOTUv2 (2.1) tool[73] respectively.

Alpha and beta diversity analysis. We assessed several metrics for gut alpha diversity using the 16S species data (thus, available in equal form for both arms), namely species richness, Shannon diversity, community evenness, Simpson's and the Inverse Simpson's metric, and the Chao1 index, calculated using the RTK (0.93.1)tool[74]. Unpaired MWU tests failed to reach significance ($P > 0.05$) for all comparisons of subsets of samples: each time point versus each other time point, in each arm separately and pooled, and between the arms within each time separately and pooled. Subsequently, we assessed within-individual changes in alpha diversity for both the DASH and the fasting+DASH arm, analogously to analysis of microbial taxa, functional modules, clinical phenotypes, and immune cell population counts, controlling for medication changes in the same manner. Supplementary Data 1 shows these results. In short, there is a nonsignificant trend for fasting to reduce diversity, which refeeding then restores, in the fasting+DASH arm, whereas no such trend is visible in the DASH-only arm. Beta diversity was assessed as community distances between samples computed using the vegan (2.5-5) R package. For microbiome data, Bray-Curtis distances on rarefied samples were used, and for immunome data, Euclidean distances. Comparisons of distance profiles was performed using Mann–Whitney U tests.

Multivariate analysis. Mutlivariate analysis was carried out using Principal Coordinates Analysis (PcoA) as per the vegan (2.5-5) R package, with the same distance metrics as noted above. Where described, delta metrics for the first two dimensions of unconstrained ordination were computed. PERMANOVA tests for multivariate effect were done using the adonis function in the vegan (2.5-5)[77] R package, stratified for patient ID.

Univariate contrast analysis. For all univariate analysis of clinical, immunome, or microbiome features, medication changes during the course of the study were accounted for as possible confounders using the following two-step procedure. The first step was a nested model comparison of a linear model for each feature, involving as predictors age, patient ID, sex, and normalized dosage of each salient medication tracked at each time point, with the same model but additionally containing time point V1-V3 as a predictor. Models were compared using a likelihood ratio test as implemented in the lmtest (0.9-37)[78] R package, and adjusted for false discovery rate (FDR) using the Benjamini–Hochberg (BH) procedure within each measurement space. In the second step, features with FDR < 0.1 were retained for a second phase of post-hoc tests using Mann–Whitney *U* comparisons between values at each pair of time points, BH FDR-adjusted between time point comparisons ($n = 3$) and requiring FDR < 0.05 to retain the result as significant. Standardized non-parametric effect sizes were taken using the (signed) Cliff's delta metric as implemented in the orddom (3.1)[79] R package. The same methods were used to analyze the validation dataset, with the exception no drugs were adjusted for as subjects were unmedicated[22].

Statistical analysis of 24 h ambulatory blood pressure and body weight changes. Body weight and blood pressure change differences between Responders and Non-Responders were compared with two-sided Mann–Whitney U test using GraphPad Prism (6.01).

Fasting arm enterotyping. Enterotypes of the samples in the fasting arm were performed by implementing the R package DirichletMultinomial (1.32.0.)[15] on the genus-level abundance table.

Correlation analysis. To assess possible interactions between immune cells, taxa, and quantitative phenotypes, another two-step test was used: first a Spearman correlation test using samples pooled across time points, and with Spearman's rho used as standardized signed effect estimate. *P*-values from this were FDR-adjusted with the BH method for each comparison of two data spaces, requiring FDR < 0.05 for significance. Second, a post-hoc test was done to account for dependency between same-donor samples: for each of two correlated features, a mixed-effects model was fitted of the rank-transformed variable using the rank of the other as predictor, with patient ID as a random effect. This model was compared to a simpler model containing only the random effect under a likelihood ratio test as implemented in the lmtest (0.9–37)[78] R package. The highest P-value for the two possible such models was taken, and $P < 0.05$ was additionally required to retain the correlation as robust. Correlation was visualized by the R packages circilize[80] and pheatmap[81].

Re analysis of previous datasets for comparison. Samples from Kushugulova et al.[14] and Forslund et al.[11] were previously mapped to the IGC gene catalog (0.5) and the mOTU marker genes; these abundances (binned at the level of KEGG and GMM modules as per the above in case of functional profiles). The Kushugulova samples were tested for significantly differential abundances between MetS cases and controls using the Mann–Whitney U test, then controlling that a MetS status predictor still significantly improves fit (using the R lmtest ((0.9–37)[78] package) of the rank-transformed abundances when added to a linear model already incorporating metformin status as a predictor, thereby controlling for confounding influence of metformin treatment status. Analogously, the Forslund samples were tested for significantly differential abundances between metformin-treated and untreated patients using the Mann–Whitney U test, then controlling that a metformin status predictor still significantly improves fit (using the R lmtest (0.9–37)[78] package) of the rank-transformed abundances when added to a linear model already incorporating MetS status as a predictor, thereby controlling for confounding influence of MetS status. The validation dataset[22] was analyzed exactly as the main study dataset, as described above.

Machine-learning prediction of treatment response at the single-subject level. To estimate how well the omics data enables forecasting of the blood-pressure response in future patients, we performed a leave-one-patient-out cross-validation procedure. This approach represents the gold standard in the machine-learning community to carry out an acid-test that empirically evaluates the practical value of a predictive model[82]. To this end, the set of n participants was iteratively split into $n - 1$ participants as training set, and the untouched data from the hold-out participant as the test set. All input variables were z-scored by centering to zero mean and unit-scaling to a variance of one[83]. In each of n cross-validation folds, the logistic-regression algorithm was a natural choice of method for binary classification (no intercept term, L2 shrinkage penalty, hyper-parameter C defaulted to 1.0). Given that the number of variables was >10× times larger than the number of participants, dimensionality reduction was necessary for a preliminary selection of a set of ten most promising input variables that could be relevant for outcome prediction. Forward-stepwise selection is an established means[84] to screen the relevance of several hundred quantitative measures. The first step identifies the single input variable among the p candidates, with the best p-value having a statistically significant association with the blood-pressure outcome. After adding this first variable to the empty null model, the second most significant (i.e., smallest p-value) was searched based on the remaining $p - 1$ input variables. Based on a two-variable model, the third most significant variable was searched based on $p - 2$ remaining variables, and so forth. This successive identification of the ten most promising among the p overall input dimensions did not bias the subsequently performed prediction performance estimate, because the entire variable reduction scheme was exclusively carried out on the $n - 1$ participants of the current cross-validation fold. Based on the top 10 variables, the logistic-regression algorithm could be more robustly fit to these subselected ten input dimensions only. The ensuing predictive model was then explicitly validated by computing whether or not the obtained model parameters allowed for accurate derivation of the relevant blood-pressure response for the independent, unseen participant. In this way, the omics data of each patient in our dataset served as test observation once. Averaging these yes-no results over all n predicted, versus observed clinical responses, yielded an estimate of the expected forecasting accuracy of the predictive model in participants that we would observe in other or later acquired datasets.

Reporting summary. Further information on research design is available in the Nature Research Reporting Summary linked to this article.

Data availability

Data supporting the conclusions of this manuscript will be made available by the authors, without undue reservation, to any qualified researcher. The Python code for this analysis can be found online: https://github.com/fastingproject/Fasting_Paper_2020[85]. Databases are to be found under the following links. KEGG: https://www.genome.jp/kegg/, SILVA: https://www.arb-silva.de. mOTU: https://motu-tool.org/, Mesnage dataset: https://www.ncbi.nlm.nih.gov/bioproject/PRJNA531091, IGC: https://db.cngb.org/microbiome/genecatalog/genecatalog_human/. Stool sequencing data: https://www.ncbi.nlm.nih.gov/bioproject/PRJNA698459.

Received: 13 February 2020; Accepted: 26 February 2021;
Published online: 30 March 2021

References

1. Di Francesco, A., Di Germanio, C., Bernier, M. & de Cabo, R. A time to fast. *Science* **362**, 770–775 (2018).
2. Collaborators GBDD. Health effects of dietary risks in 195 countries, 1990-2017: a systematic analysis for the Global Burden of Disease Study 2017. *Lancet* **393**, 1958–1972 (2019).
3. Whelton, P. K. et al. 2017 ACC/AHA/AAPA/ABC/ACPM/AGS/APhA/ASH/ASPC/NMA/PCNA guideline for the prevention, detection, evaluation, and management of high blood pressure in adults: a report of the American College of Cardiology/American Heart Association Task Force on Clinical Practice Guidelines. *Circulation* **138**, e484–e594 (2018).
4. Christ, A. & Latz, E. The Western lifestyle has lasting effects on metaflammation. *Nat. Rev. Immunol.* **19**, 267–268 (2019).
5. Lynch, S. V. & Pedersen, O. The human intestinal microbiome in health and disease. *N. Engl. J. Med.* **375**, 2369–2379 (2016).
6. Yan, Q. et al. Alterations of the gut microbiome in hypertension. *Front Cell Infect. Microbiol.* **7**, 381 (2017).
7. Li, J. et al. Gut microbiota dysbiosis contributes to the development of hypertension. *Microbiome* **5**, 14 (2017).
8. Frost, F. et al. A structured weight loss program increases gut microbiota phylogenetic diversity and reduces levels of Collinsella in obese type 2 diabetics: a pilot study. *PLoS ONE* **14**, e0219489 (2019).
9. Ozkul, C., Yalinay, M. & Karakan, T. Structural changes in gut microbiome after Ramadan fasting: a pilot study. *Beneficial Microbes* **11**, 227–233 (2020).
10. Louis, S., Tappu, R. M., Damms-Machado, A., Huson, D. H. & Bischoff, S. C. Characterization of the gut microbial community of obese patients following a weight-loss intervention using whole metagenome shotgun sequencing. *PLoS ONE* **11**, e0149564 (2016).
11. Forslund, K. et al. Disentangling type 2 diabetes and metformin treatment signatures in the human gut microbiota. *Nature* **528**, 262–266 (2015).
12. Kanehisa, M., Sato, Y., Kawashima, M., Furumichi, M. & Tanabe, M. KEGG as a reference resource for gene and protein annotation. *Nucleic Acids Res.* **44**, D457–D462 (2016).
13. Vieira-Silva, S. et al. Species-function relationships shape ecological properties of the human gut microbiome. *Nat. Microbiol.* **1**, 16088 (2016).
14. Kushugulova, A. et al. Metagenomic analysis of gut microbial communities from a Central Asian population. *BMJ Open* **8**, e021682 (2018).
15. Holmes, I., Harris, K. & Quince, C. Dirichlet multinomial mixtures: generative models for microbial metagenomics. *PLoS ONE* **7**, e30126 (2012).
16. Mende, D. R., Sunagawa, S., Zeller, G. & Bork, P. Accurate and universal delineation of prokaryotic species. *Nat. Methods* **10**, 881–884 (2013).

17. Qin, J. et al. A metagenome-wide association study of gut microbiota in type 2 diabetes. *Nature* **490**, 55–60 (2012).
18. Zhang, C. et al. Impact of a 3-months vegetarian diet on the gut microbiota and immune repertoire. *Front. Immunol.* **9**, 908 (2018).
19. Magalhaes, I. et al. Mucosal-associated invariant T cell alterations in obese and type 2 diabetic patients. *J. Clin. Invest.* **125**, 1752–1762 (2015).
20. van der Weerd, K. et al. Morbidly obese human subjects have increased peripheral blood CD4+ T cells with skewing toward a Treg- and Th2-dominated phenotype. *Diabetes* **61**, 401–408 (2012).
21. Loperena, R. et al. Hypertension and increased endothelial mechanical stretch promote monocyte differentiation and activation: roles of STAT3, interleukin 6 and hydrogen peroxide. *Cardiovasc Res.* **114**, 1547–1563 (2018).
22. Mesnage, R., Grundler, F., Schwiertz, A., Le Maho, Y. & Wilhelmi de Toledo, F. Changes in human gut microbiota composition are linked to the energy metabolic switch during 10 d of Buchinger fasting. *J. Nutritional Sci.* **8**, e36 (2019).
23. Velikonja, A., Lipoglavsek, L., Zorec, M., Orel, R. & Avgustin, G. Alterations in gut microbiota composition and metabolic parameters after dietary intervention with barley beta glucans in patients with high risk for metabolic syndrome development. *Anaerobe* **55**, 67–77 (2019).
24. Roager, H. M. et al. Whole grain-rich diet reduces body weight and systemic low-grade inflammation without inducing major changes of the gut microbiome: a randomised cross-over trial. *Gut* **68**, 83–93 (2019).
25. Liu, Z. et al. Gut microbiota mediates intermittent-fasting alleviation of diabetes-induced cognitive impairment. *Nat. Commun.* **11**, 855 (2020).
26. Kopf, J. C. et al. Role of whole grains versus fruits and vegetables in reducing subclinical inflammation and promoting gastrointestinal health in individuals affected by overweight and obesity: a randomized controlled trial. *Nutr. J.* **17**, 72 (2018).
27. Guevara-Cruz, M. et al. Improvement of lipoprotein profile and metabolic endotoxemia by a lifestyle intervention that modifies the gut microbiota in subjects with metabolic syndrome. *J. Am. Heart Assoc.* **8**, e012401 (2019).
28. Kirabo, A. et al. DC isoketal-modified proteins activate T cells and promote hypertension. *J. Clin. Invest.* **124**, 4642–4656 (2014).
29. Drummond, G. R., Vinh, A., Guzik, T. J. & Sobey, C. G. Immune mechanisms of hypertension. *Nat. Rev. Immunol.* **19**, 517–532 (2019).
30. Jie, Z. et al. The gut microbiome in atherosclerotic cardiovascular disease. *Nat. Commun.* **8**, 845 (2017).
31. Holmes, E. et al. Human metabolic phenotype diversity and its association with diet and blood pressure. *Nature* **453**, 396–400 (2008).
32. Goodrich J. K. et al. Genetic Determinants of the Gut Microbiome in UK Twins. *Cell Host Microbe* **19**, 731–743 (2016).
33. Itani, H. A. et al. CD70 exacerbates blood pressure elevation and renal damage in response to repeated hypertensive stimuli. *Circulation Res.* **118**, 1233–1243 (2016).
34. Andoh, A. et al. Comparison of the gut microbial community between obese and lean peoples using 16S gene sequencing in a Japanese population. *J. Clin. Biochem. Nutr.* **59**, 65–70 (2016).
35. Goodrich, J. K. et al. Human genetics shape the gut microbiome. *Cell* **159**, 789–799 (2014).
36. Bartolomaeus, H. et al. Short-chain fatty acid propionate protects from hypertensive cardiovascular damage. *Circulation* **139**, 1407–1421 (2019).
37. Kameyama, K. & Itoh, K. Intestinal colonization by a Lachnospiraceae bacterium contributes to the development of diabetes in obese mice. *Microbes Environ.* **29**, 427–430 (2014).
38. Chen, X. et al. Alteration of the gut microbiota associated with childhood obesity by 16S rRNA gene sequencing. *PeerJ* **8**, e8317 (2020).
39. Touch, S. et al. Mucosal-associated invariant T (MAIT) cells are depleted and prone to apoptosis in cardiometabolic disorders. *FASEB J.* https://doi.org/10.1096/fj.201800052RR (2018).
40. Benson, H. & Stuart, M. *The Wellness Book. Mind–body Medicine* (Fireside, 1999).
41. Cramer, H., Lauche, R., Paul, A. & Dobos, G. Mindfulness-based stress reduction for breast cancer-a systematic review and meta-analysis. *Curr. Oncol.* **19**, e343–e352 (2012).
42. Li, C. et al. Effects of a one-week fasting therapy in patients with type-2 diabetes mellitus and metabolic syndrome—a randomized controlled explorative study. *Exp. Clin. Endocrinol. Diabetes* **125**, 618–624 (2017).
43. Kjeldsen-Kragh, J. et al. Controlled trial of fasting and one-year vegetarian diet in rheumatoid arthritis. *Lancet* **338**, 899–902 (1991).
44. de Lorgeril, M. et al. Mediterranean alpha-linolenic acid-rich diet in secondary prevention of coronary heart disease. *Lancet* **343**, 1454–1459 (1994).
45. De Lorgeril, M. et al. Effect of a mediterranean type of diet on the rate of cardiovascular complications in patients with coronary artery disease. Insights into the cardioprotective effect of certain nutriments. *J. Am. Coll. Cardiol.* **28**, 1103–1108 (1996).
46. Esposito, K. et al. Effect of a mediterranean-style diet on endothelial dysfunction and markers of vascular inflammation in the metabolic syndrome: a randomized trial. *JAMA* **292**, 1440–1446 (2004).
47. Appel, L. J. et al. Effects of comprehensive lifestyle modification on blood pressure control: main results of the PREMIER clinical trial. *JAMA* **289**, 2083–2093 (2003).
48. Appel, L. J. et al. A clinical trial of the effects of dietary patterns on blood pressure. DASH Collaborative Research Group. *N. Engl. J. Med.* **336**, 1117–1124 (1997).
49. Saghaei, M. Random allocation software for parallel group randomized trials. *BMC Med. Res. Methodol.* **4**, 26 (2004).
50. Westhoff, T. H. et al. Convenience of ambulatory blood pressure monitoring: comparison of different devices. *Blood Press. Monit.* **10**, 239–242 (2005).
51. Bosy-Westphal, A. et al. Accuracy of bioelectrical impedance consumer devices for measurement of body composition in comparison to whole body magnetic resonance imaging and dual X-ray absorptiometry. *Obes. facts* **1**, 319–324 (2008).
52. World Health Organization. *Waist Circumference and Waist–hip ratio: Report of a WHO Expert Consultation* (World Health Organization, 2011).
53. Rudenski, A. S., Matthews, D. R., Levy, J. C. & Turner, R. C. Understanding "insulin resistance": both glucose resistance and insulin resistance are required to model human diabetes. *Metab.: Clin. Exp.* **40**, 908–917 (1991).
54. Assmann, G., Cullen, P. & Schulte, H. Simple scoring scheme for calculating the risk of acute coronary events based on the 10-year follow-up of the prospective cardiovascular Munster (PROCAM) study. *Circulation* **105**, 310–315 (2002).
55. Rubin, D. B. *Multiple Imputation for Nonresponse in Surveys* (Wiley, 1987).
56. Schafer, J. L. *Analysis of Incomplete Multivariate Data* (Chapman & Hall, 1997).
57. Van Gassen, S. et al. FlowSOM: Using self-organizing maps for visualization and interpretation of cytometry data. *Cytom. Part A: J. Int. Soc. Anal. Cytol.* **87**, 636–645 (2015).
58. Team RC. *R: A Language and Environment for Statistical Computing* (R Foundation for Statistical Computing, 2014).
59. Turnbaugh, P. J. et al. A core gut microbiome in obese and lean twins. *Nature* **457**, 480–484 (2009).
60. Thiemann, S. et al. Enhancement of IFNgamma production by distinct commensals ameliorates Salmonella-induced disease. *Cell host microbe* **21**, 682–694 (2017). e685.
61. Caporaso, J. G. et al. Global patterns of 16S rRNA diversity at a depth of millions of sequences per sample. *Proc. Natl Acad. Sci. USA* **108**, 4516–4522 (2011).
62. Hildebrand, F., Tadeo, R., Voigt, A. Y., Bork, P. & Raes, J. LotuS: an efficient and user-friendly OTU processing pipeline. *Microbiome* **2**, 30 (2014).
63. Lange, A. et al. AmpliconDuo: A Split-Sample Filtering Protocol for High-Throughput Amplicon Sequencing of Microbial Communities. *PloS ONE* **10**, e0141590 (2015).
64. Magoc, T. & Salzberg, S. L. FLASH: fast length adjustment of short reads to improve genome assemblies. *Bioinformatics* **27**, 2957–2963 (2011).
65. Edgar, R. C. UCHIME2: improved chimera prediction for amplicon sequencing. *bioRxiv* https://doi.org/10.1101/074252 (2016).
66. Edgar, R. C. UPARSE: highly accurate OTU sequences from microbial amplicon reads. *Nat. Methods* **10**, 996–998 (2013).
67. Altschul, S. F., Gish, W., Miller, W., Myers, E. W. & Lipman, D. J. Basic local alignment search tool. *J. Mol. Biol.* **215**, 403–410 (1990).
68. Yilmaz, P. et al. The SILVA and "All-species Living Tree Project (LTP)" taxonomic frameworks. *Nucleic Acids Res.* **42**, D643–D648 (2014).
69. Coelho, L. P. et al. Similarity of the dog and human gut microbiomes in gene content and response to diet. *Microbiome* **6**, 72 (2018).
70. Li, J. et al. An integrated catalog of reference genes in the human gut microbiome. *Nat. Biotechnol.* **32**, 834–841 (2014).
71. Ciccarelli, F. D. et al. Toward automatic reconstruction of a highly resolved tree of life. *Science* **311**, 1283–1287 (2006).
72. Sorek, R. et al. Genome-wide experimental determination of barriers to horizontal gene transfer. *Science* **318**, 1449–1452 (2007).
73. Milanese, A. et al. Microbial abundance, activity and population genomic profiling with mOTUs2. *Nat. Commun.* **10**, 1014 (2019).
74. Saary, P., Forslund, K., Bork, P. & Hildebrand, F. RTK: efficient rarefaction analysis of large datasets. *Bioinformatics* **33**, 2594–2595 (2017).
75. Kanehisa, M., Furumichi, M., Tanabe, M., Sato, Y. & Morishima, K. KEGG: new perspectives on genomes, pathways, diseases and drugs. *Nucleic Acids Res.* **45**, D353–D361 (2017).
76. Rajilic-Stojanovic, M. et al. Development and application of the human intestinal tract chip, a phylogenetic microarray: analysis of universally conserved phylotypes in the abundant microbiota of young and elderly adults. *Environ. Microbiol.* **11**, 1736–1751 (2009).
77. Oksanen, J. et al. *vegan: Community Ecology Package* (R Core Team, 2018).
78. Zeileis, A. & Hothorn, T. Diagnostic checking in regression relationships. *R. News* **2**, 7–10 (2002).
79. Rogmann, J. J. *Ordinal Dominance Statistics* (CRAN, 2013).

80. Gu, Z., Gu, L., Eils, R., Schlesner, M. & Brors, B. Circlize Implements and enhances circular visualization in R. *Bioinformatics* **30**, 2811–2812 (2014).
81. Kolde, R. *pheatmap: Pretty Heatmaps* 1.0.12 edn (CRAN, 2019).
82. Hastie, T., Tibshirani, R. & Friedman, J. *The Elements of Statistical Learning* (Springer, 2001).
83. Gelman, A. & Hill, J. *Data Analysis Using Regression and Multi-level Hierarchical Models*. (Cambridge University Press 2007).
84. Harrell, F. E. *Regression Modeling Strategies, with Applications to Linear Models, Survival Analysis and Logistic Regression* (Springer, 2001).
85. Bzdok, D. fastingproject/Fasting_Paper_2020: 1st Release of the prediction code.). v1.0.0 edn. Zenodo (2021).

Acknowledgements
The authors thank Juliane Anders, Jana Czychi and Gabriele N'Diaye for the outstanding technical assistance, Falk Hildebrand, Luis Pedro Coelho, and Renato Alves for assistance with metagenomic software adaptation.

Author contributions
A.M. led and designed and performed most experiments, analyzed and interpreted the data. N.S., H.C., G.D., A.Mi. recruited the patient and conducted the clinical study. T.S., T.R.L. performed 16S and metagenomic sequencing. A.M., H.B., E.G.A., I.H., U.S., M.K. performed immunophenotyping experiments and analyzed data. S.K.F., U.L., C.C. performed computational analyses. S.K.F., D.B., A.M. performed statistical analyses. A.M., M.K., R.D., A.M., D.N.M., S.K.F supervised the experiments and analyses. A.M., H.B., L.M., N.W., A.Ma., U.S., M.K., A.Mi., D.N.M., S.K.F. conceived parts of the project, supervised the experiments, and interpreted the data. A.M., H.B., E.G.A., D.B., A.Mi., D.N.M., and S.K.F. wrote the manuscript with key editing by L.M., R.D., M.K. and further input from all authors.

Funding
Open Access funding enabled and organized by Projekt DEAL.

Competing interests
The authors declare no competing interests.

Additional information
Supplementary information The online version contains supplementary material available at https://doi.org/10.1038/s41467-021-22097-0.

Correspondence and requests for materials should be addressed to A.M., D.N.M. or S.K.F.

Peer review information *Nature Communications* thanks the anonymous reviewer(s) for their contribution to the peer review of this work. Peer reviewer reports are available.

Reprints and permission information is available at http://www.nature.com/reprints

Publisher's note Springer Nature remains neutral with regard to jurisdictional claims in published maps and institutional affiliations.

Open Access This article is licensed under a Creative Commons Attribution 4.0 International License, which permits use, sharing, adaptation, distribution and reproduction in any medium or format, as long as you give appropriate credit to the original author(s) and the source, provide a link to the Creative Commons license, and indicate if changes were made. The images or other third party material in this article are included in the article's Creative Commons license, unless indicated otherwise in a credit line to the material. If material is not included in the article's Creative Commons license and your intended use is not permitted by statutory regulation or exceeds the permitted use, you will need to obtain permission directly from the copyright holder. To view a copy of this license, visit http://creativecommons.org/licenses/by/4.0/.

© The Author(s) 2021

[1]Experimental and Clinical Research Center, a joint cooperation of Max Delbruck Center for Molecular Medicine and Charité - Universitätsmedizin Berlin, Berlin, Germany. [2]Charité - Universitätsmedizin Berlin, corporate member of Freie Universität Berlin and Humboldt-Universität zu Berlin, Berlin, Germany. [3]DZHK (German Centre for Cardiovascular Research), partner site Berlin, Berlin, Germany. [4]Max Delbruck Center for Molecular Medicine in the Helmholtz Association (MDC), Berlin, Germany. [5]Department of Biology, Chemistry, and Pharmacy, Freie Universität Berlin, Berlin, Germany. [6]Department of Internal and Integrative Medicine, Immanuel Krankenhaus Berlin, Berlin, Germany. [7]Berlin Institute of Health (BIH), Berlin, Germany. [8]Charité - Universitätsmedizin Berlin, corporate member of Freie Universität Berlin and Humboldt-Universität zu Berlin, Department of Nephrology and Internal Intensive Care Medicine, Berlin, Germany. [9]VIB Laboratory of Translational Immunomodulation, VIB Center for Inflammation Research (IRC), UHasselt, Campus Diepenbeek, Hasselt, Belgium. [10]Department of Immunology, Biomedical Research Institute, UHasselt, Campus Diepenbeek, Hasselt, Belgium. [11]Department of Internal and Integrative Medicine, Kliniken Essen-Mitte, Faculty of Medicine, University of Duisburg-Essen, Essen, Germany. [12]Department of Microbial Immune Regulation, Helmholtz Centre for Infection Research, Braunschweig, Germany. [13]Hannover Medical School, Hannover, Germany. [14]Department of Cardiology and Nephrology, HELIOS-Klinikum, Berlin, Germany. [15]Department of Biomedical Engineering, McConnell Brain Imaging Centre, Montreal Neurological Institute, Faculty of Medicine, McGill University, Montreal, Canada. [16]Mila – Quebec Artificial Intelligence Institute, Montreal, Canada. [17]Parietal Team, Institut National de Recherche en Informatique et en Automatique (INRIA), Neurospin, Commissariat à l'Energie Atomique (CEA) Saclay, Gif-sur-Yvette, France. [18]These authors contributed equally: Andreas Michalsen, Dominik N. Müller, Sofia K. Forslund. ✉email: andreas.michalsen@charite.de; dominik.mueller@mdc-berlin.de; sofia.forslund@mdc-berlin.de

Study 3:

ESC European Society of Cardiology
Cardiovascular Research (2023) **119**, 1441–1452
https://doi.org/10.1093/cvr/cvac121

Quantifying the impact of gut microbiota on inflammation and hypertensive organ damage

Ellen G. Avery [1,2,3,4†], Hendrik Bartolomaeus [1,2,3,5†], Ariana Rauch [1,2,3,5], Chia-Yu Chen [1,2,3,6], Gabriele N'Diaye[1,2,6], Ulrike Löber [1,2,3], Theda U. P. Bartolomaeus [1,2,3,6], Raphaela Fritsche-Guenther [2,7], André F. Rodrigues [2,3,4], Alex Yarritu[1,2,3,5], Cheng Zhong[8], Lingyan Fei[8], Dmitry Tsvetkov [1,3,6,9], Mihail Todiras [2,10], Joon-Keun Park[11], Lajos Markó [1,2,3,6], András Maifeld[1,2,3,6], Andreas Patzak[8], Michael Bader [2,3,6], Stefan Kempa [2,12], Jennifer A. Kirwan [2,7], Sofia K. Forslund [1,2,3,6], Dominik N. Müller [1,2,3,6]*, and Nicola Wilck [1,2,3,5]*

[1]Experimental and Clinical Research Center, A Cooperation of Charité-Universitätsmedizin Berlin and Max-Delbrück-Center for Molecular Medicine, Berlin, Germany; [2]Max-Delbrück-Center for Molecular Medicine in the Helmholtz Association, Berlin, Germany; [3]DZHK (German Centre for Cardiovascular Research), partner site Berlin, Germany; [4]Department of Biology, Chemistry, and Pharmacy, Freie Universität Berlin, Berlin, Germany; [5]Department of Nephrology and Internal Intensive Care Medicine, Charité-Universitätsmedizin Berlin, Corporate member of Freie Universität Berlin and Humboldt-Universität zu Berlin, Berlin, Germany; [6]Charité-Universitätsmedizin Berlin, Corporate member of Freie Universität Berlin and Humboldt-Universität zu Berlin, Berlin, Germany; [7]Metabolomics Platform, Berlin Institute of Health at Charité-Universitätsmedizin Berlin, Berlin, Germany; [8]Institute of Translational Physiology, Charité-Universitätsmedizin Berlin, Corporate Member of Freie Universität Berlin and Humboldt-Universität zu Berlin, Charitéplatz 1, 10117 Berlin, Germany; [9]Department of Geriatrics, University of Greifswald, University District Hospital Wolgast, Greifswald, Germany; [10]Nicolae Testemianu State University of Medicine and Pharmacy, Chisinau, Moldova; [11]Hannover Medical School, Hannover, Germany; and [12]Integrative Proteomics and Metabolomics Platform, Berlin Institute for Medical Systems Biology BIMSB, Berlin, Germany

Received 23 September 2021; revised 4 July 2022; editorial decision 8 July 2022; online publish-ahead-of-print 29 July 2022

Time of primary review: 44 days
This article was guest edited by Thomas F. Lüscher.

Aims Hypertension (HTN) can lead to heart and kidney damage. The gut microbiota has been linked to HTN, although it is difficult to estimate its significance due to the variety of other features known to influence HTN. In the present study, we used germ-free (GF) and colonized (COL) littermate mice to quantify the impact of microbial colonization on organ damage in HTN.

Methods and results 4-week-old male GF C57BL/6J littermates were randomized to remain GF or receive microbial colonization. HTN was induced by subcutaneous infusion with angiotensin (Ang) II (1.44 mg/kg/day) and 1% NaCl in the drinking water; sham-treated mice served as control. Renal damage was exacerbated in GF mice, whereas cardiac damage was more comparable between COL and GF, suggesting that the kidney is more sensitive to microbial influence. Multivariate analysis revealed a larger effect of HTN in GF mice. Serum metabolomics demonstrated that the colonization status influences circulating metabolites relevant to HTN. Importantly, GF mice were deficient in anti-inflammatory faecal short-chain fatty acids (SCFA). Flow cytometry showed that the microbiome has an impact on the induction of anti-hypertensive myeloid-derived suppressor cells and pro-inflammatory Th17 cells in HTN. *In vitro* inducibility of Th17 cells was significantly higher for cells isolated from GF than conventionally raised mice.

Conclusion The microbial colonization status of mice had potent effects on their phenotypic response to a hypertensive stimulus, and the kidney is a highly microbiota-susceptible target organ in HTN. The magnitude of the pathogenic response in GF mice underscores the role of the microbiome in mediating inflammation in HTN.

Keywords Hypertension • Microbiome • Inflammation • Kidney • Heart

Downloaded from https://academic.oup.com/cardiovascres/article/119/6/1441/6651675 by Duke University - Perkins Library user on 21 August 2023

* Corresponding authors. Tel: +49 30 450540459, E-mail: nicola.wilck@charite.de (N.W.); Tel: +49 30 450540286, E-mail: dominik.mueller@mdc-berlin.de (D.N.M.)
† These authors contributed equally.
© The Author(s) 2022. Published by Oxford University Press on behalf of the European Society of Cardiology.
This is an Open Access article distributed under the terms of the Creative Commons Attribution-NonCommercial License (https://creativecommons.org/licenses/by-nc/4.0/), which permits non-commercial re-use, distribution, and reproduction in any medium, provided the original work is properly cited. For commercial re-use, please contact journals.permissions@oup.com

1. Introduction

Hypertension (HTN) is the leading risk factor for non-communicable diseases worldwide,[1] and is known as a multifactorial disease, where complex mechanisms often co-occur to lead to a persistent increase in blood pressure (BP). Several studies have indicated that alterations in the composition and function of the intestinal microbiota may contribute to the burden of hypertensive disease.[2–6] However, it is difficult to estimate the contribution of the microbiota, especially in human studies, where the added complexities of other contributing factors easily obstruct our understanding. The aim of our study is to understand the relative contribution that the microbiota has to the burden of hypertensive disease.

Mounting evidence suggests that inflammation is not only characteristic of hypertensive cardiovascular disease (CVD) but is causally linked to disease progression and severity.[3] Components of both the innate and adaptive immune system have been implicated.[3] T-helper 17 (Th17) cells and Type 1 helper T-cells (Th1) have been shown to be integrally interlinked with hypertensive disease, and have been demonstrated to exacerbate cardiac and renal damage.[5,7,8] Moreover, myeloid-derived suppressor cells (MDSCs) derived from hypertensive mice were shown to have immunosuppressive properties, and upon adoptive transfer were able to mitigate BP increase in response to angiotensin II (Ang II) infusion.[9] MDSC, Th17, and Th1 cells have each been shown in different settings to be influenced by the microbiota.[5,9–11]

We and others could recently demonstrate the role of several anti-inflammatory microbial metabolites in HTN. Short-chain fatty acids (SCFA) such as acetate, propionate, and butyrate, are produced by gut microbiota through the fermentation of indigestible dietary fibre.[12] Acetate has been shown to ameliorate hypertensive damage to the kidney and heart in mice.[13] Our recent work elucidated the protective role of propionate in Ang II-induced inflammation and cardiovascular damage.[14] Furthermore, low butyrate levels have been associated with worsened CVD in several models.[15] In addition to SCFA, we have recently shown that a bacterially produced indole metabolite derived from tryptophan suppresses Th17-driven inflammation in salt-sensitive HTN.[5] In contrast, metabolites of microbial origin can also exacerbate disease in some contexts. For example, pro-inflammatory metabolites like trimethylamine N-oxide (TMAO) and indoxyl sulfate (IS) have been shown to aggravate CVD.[16,17]

To address our central aim, we utilized germ-free (GF) mice. C57BL/6J GF littermates were randomized at 4 weeks of age to either receive a microbiota transfer from our in-house C57BL/6J colony, or to remain GF for the duration of the experiment. Here, we have uncovered several differences between GF and colonized (COL) mice in response to Ang II and 1% NaCl in the drinking water, which underscores the importance of the microbiota in the pathogenesis of HTN-induced organ damage. Of note, we show an exacerbation of damage in GF mice compared with COL mice, which is more distinct in the kidney than in the heart.

2. Materials and Methods

Detailed description of all analytical methods and data analysis used are available in the Supplementary material online.

2.1 Animal ethics

All experiments performed complied with the German/European law for animal protection and were approved by the local ethics committee (G0280/13, G0028/21).

2.2 Animal protocol

Wild-type C57BL/6J mice were bred under axenic conditions in an isolator (Metall + Plastic, Radolfzell-Stahringen, Germany). Mice were maintained on a 12:12 h day: night cycle with constant access to food and water. Until Week 4, mice in both experimental groups grew under GF conditions. At 4 weeks of age, male mice were randomized to either remain GF in the isolator or receive passive bacterial colonization (COL). For colonization, mice were introduced in the regular SPF animal facility and placed in cages from healthy wild-type male C57BL/6J mice. Until 12 weeks of age mice received sterilized tap water as drinking water. At 12 weeks of age, COL and GF mice received Angiotensin II (Ang II, 1.44 mg/kg/day) by subcutaneous infusion via an osmotic minipump (Alzet) and 1% NaCl (Carl Roth) in the drinking water or sham treatment. Sham-treated animals received the same operation procedure without minipump implantation. Minipumps were implanted under sterile conditions, GF mice were kept sterile throughout the experiment. Sterile drinking water was delivered via the Hydropac system (Plexx B.V., Elst, the Netherlands). Throughout the experiment mice were fed autoclaved standard breeding chow (V1124, Ssniff, Soest, Germany). After 2 weeks of Ang II + 1% NaCl or sham treatment mice were euthanized by isoflurane anaesthesia and blood, spot urine (where possible), faeces, and organs were collected. The Ang II infusion model was performed in 40 mice (GF $n = 5$, COL $n = 5$, GF + HTN $n = 16$, COL + HTN $n = 14$). Over the course of the experiments, five animals were taken out of the experiment (GF + HTN $n = 3$, COL + HTN $n = 2$), due to pre-specified ethical termination criteria in order to counteract severe distress in this experiment. These five mice were not included in the analysis. Additionally, invasive BP measurements were performed in 10 animals (GF $n = 5$, COL $n = 5$), these animals were not included in any other analysis. As a control group for *in vitro* experiments, cells, and tissues from age-matched conventionally raised SPF C57BL/6J mice (referred to as CONV) were used.

Mice were euthanized by isoflurane anaesthesia (5% isoflurane–air mixture). Furthermore, echocardiography, BP, and Ang II pressor response measurements were performed in isoflurane inhalation anaesthesia (2–2.5% isoflurane–air mixture). Details are given in Supplementary material online.

3. Results

3.1 Absence of microbiota exacerbates cardiorenal damage

To exclude confounding effects relating to the genetic background of mice used in our study, GF littermates were randomized at 4 weeks of age for colonization with SPF microbiota (COL) or further kept under GF conditions. At 12 weeks of age, we induced HTN by subcutaneous Ang II infusion and 1% NaCl-supplemented drinking water. After 14 days, we analysed hypertensive target organ damage (*Figure 1A*). Of note, we did not include surgical uninephrectomy to avoid bacterial contamination. The standard model in our lab includes uninephrectomy to induce a more severe form of renal damage,[8,18] thus we expected a lower degree of renal damage when compared with the published literature.[19] To validate the integrity of our experiment, we first checked the colonization status of the mice. Gross morphological changes were assessed, and the characteristics typical of the gastrointestinal (GI) tract in GF mice (e.g. megacecum) did not persist in the mice which had been colonized (COL) (see Supplementary material online, *Figure S1A*). To confirm the microbial status of the respective group, we examined faecal pellets

Downloaded from https://academic.oup.com/cardiovascres/article/119/6/1441/6651675 by Duke University - Perkins Library user on 21 August 2023

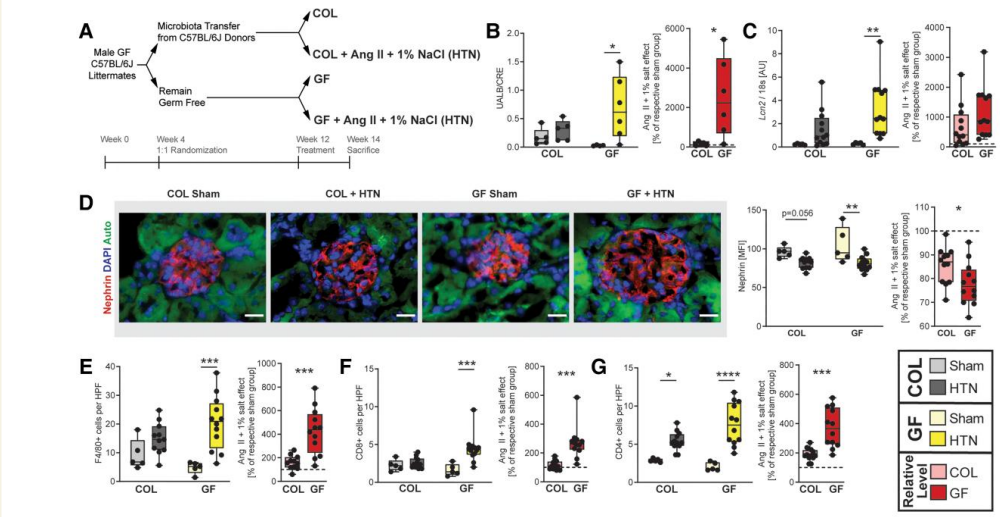

Figure 1 Renal damage is exacerbated under GF conditions. (*A*) Description of experimental protocol (unless otherwise stated, GF Sham $n = 5$, GF + HTN $n = 12$, COL Sham $n = 5$, COL + HTN $n = 12$ for further analyses). (*B*) Urinary albumin-to-creatinine ratio from spot urine collected upon sacrifice from a subset of mice (COL $n = 5$, COL + HTN $n = 5$, GF $n = 4$, GF + HTN $n = 6$). (*C*) *Lcn2* gene expression was measured from kidney tissue by qPCR. (*D*) Histological kidney sections were stained for nephrin. Representative glomeruli are shown (left). Nephrin immunofluorescence was quantified as mean fluorescence intensity (MFI) in the glomerular space averaged per mouse. The scale bar represents 20 µm. (*E*) Macrophages (F4/80+), (*F*) CD8+, and (*G*) CD4+ T-cells from kidney sections were counted from five representative high-power fields within the cortex. For (*B*–*G*), the left graph was tested using a two-way ANOVA and *post hoc* Sidak multiple comparison's test and depicts the raw values for each variable. For (*B*–*F*), HTN was identified as the source of variation using two-way ANOVA, and *post hoc* multiple comparison between sham and HTN within each group revealed that the GF comparison was the source of variation. In (*G*), HTN was identified as the source of variation using two-way ANOVA, and *post hoc* multiple comparison between sham and HTN within each group revealed that both the GF and COL comparison were significant. For *B* through *G*, the right plot depicts the relative change induced by Ang II + 1% NaCl in comparison with the respective sham group, tested using an unpaired two-tailed *t*-test. No change (100%) depicted as dotted line. For all plots, *P*-values are as follows; $*P \leq 0.05$, $**P \leq 0.01$, $***P \leq 0.001$, $****P \leq 0.0001$.

produced on the final day of experimentation. First, pellets were incubated in a thioglycolate medium for 96 h, and GF mice were found to show no bacterial growth (see Supplementary material online, *Figure S1B*). Second, 16S rDNA copies per gram stool measured by qPCR were found to be similar in COL (Sham and HTN) and conventional SPF mice (CONV), whereas GF mice did not have more 16S rDNA copies than blank samples (see Supplementary material online, *Figure S1C*). Finally, unimputed serum metabolomics confirmed the presence of bacterially-derived metabolites in COL mice only (see Supplementary material online, *Figure S1D*). Shotgun metagenomics revealed that the grafted bacteria in COL mice showed the largest overlap with mouse gut metagenomes published in the global microbial gene catalogue (GMGC) (see Supplementary material online, *Figure S2*). We therefore concluded that the GF and COL groups were maintained as intended to confidently proceed with further analyses. Of note, it has been previously reported for the Ang II infusion model that HTN induction leads to changes in the microbiome composition.[20] Likewise, we found Ang II infusion influenced the abundance of various taxa in COL mice (see Supplementary material online, *Figure S1E*) as shown by shotgun sequencing. Indeed, both the caecal and faecal compartments displayed differences between the COL sham and HTN groups on phylum and genus levels (see Supplementary material online, *Figure S1F* and *G*, and *File S1–4*).

One of the hallmarks of hypertensive target organ damage is renal damage, which is characterized by abnormally high excretion of albumin with the urine (albuminuria), fibrosis, and inflammation. In line with the literature,[19] our HTN induction without uninephrectomy lead to a moderate increase in albuminuria in COL mice (*Figure 1B*). GF mice developed a greater degree of albuminuria upon HTN induction, which is abundantly clear when comparing the relative increase of GF and COL mice compared with their respective sham groups (*Figure 1B*). HTN also lead to a significant increase in renal damage marker lipocalin-2 in GF mice (Lcn2), which was not evident in COL mice (*Figure 1C*). Next, we analysed nephrin, a protein in the podocytes' slit membrane, by immunofluorescence. We observed a significant decrease of nephrin immunofluorescence in GF mice, where COL mice exhibited a similar but insignificant trend (*Figure 1D*). HTN led to a significant increase of macrophages (F4/80+ cells, *Figure 1E*) and cytotoxic T-cells (CD8+ cells, *Figure 1F*) in the kidney of GF mice, not reaching significance in COL mice. Likewise, we found that mRNA expression of CC-chemokine ligand 2 (Ccl2, see Supplementary material online, *Figure S3A*) and infiltrating T-cells (CD3+, see Supplementary material online, *Figure S3B*) were selectively increased in the GF group upon HTN. While T-helper cells (CD4+ cells) were shown to increase in both GF and COL mice, GF mice displayed a stronger increase

Downloaded from https://academic.oup.com/cardiovascres/article/119/6/1441/6651675 by Duke University - Perkins Library user on 21 August 2023

(*Figure 1G*). The number of leukocytes (CD45+ cells) within the kidney confirms the stronger effect of HTN on renal inflammation in GF (see Supplementary material online, *Figure S3C*). For all immune populations in the kidney, the change in HTN relative to sham was consistently exacerbated in GF compared with COL (*Figure 1E–G*, and see Supplementary material online, *Figure S3B and C*). Finally, we investigated kidney fibrosis. Expression of *Col3a1* was significantly increased only in GF + HTN mice (see Supplementary material online, *Figure S3D*). Perivascular fibrosis analysed by Masson's trichrome staining was accentuated in GF mice but not statistically different between the groups using two-way analysis of variance (ANOVA); although when comparing the relative increase from sham to HTN, there was a significant difference between GF and COL (see Supplementary material online, *Figure S3E*). Similar to what was previously shown,[21] GF mice tended to have lower baseline values for several damage markers when comparing sham-treated GF and COL mice. Overall, renal pathology upon HTN induction was greater in GF mice when compared with their COL littermates.

Next, we examined the cardiac phenotype. HTN induction led to greater hypertrophy in GF compared with COL mice, as measured by heart weight-to-tibia length ratio (*Figure 2A*). Left ventricular weight taken from echocardiography relative to the tibia length (*Figure 2B*) as well as cardiac *Nppb* expression (*Figure 2C*) confirmed this finding. Neither the GF + HTN nor COL + HTN mice had a reduced ejection fraction (*Figure 2D*), indicating none of these mice were experiencing systolic heart failure. Using two-way ANOVA, both perivascular (*Figure 2E*) and interstitial (*Figure 2F*) fibrosis were significantly increased in GF + HTN and not in COL + HTN mice compared with their respective sham group. Interestingly, when assessing the relative increase in HTN compared with sham for markers of cardiac fibrosis, there was no difference in GF compared with COL mice (*Figure 2E and F*). Next, we examined cardiac inflammation. Despite an increase in *Ccl2* expression in GF and not COL (see Supplementary material online, *Figure S4A*), macrophages (F4/80+) were increased in both GF and COL hearts upon HTN; and GF + HTN showed significantly less macrophages than COL + HTN mice (*Figure 2G*). The change in overall leukocytes (CD45+) within the heart mimics the changes seen for macrophages (see Supplementary material online, *Figure S4B*). Furthermore, no significance was reached when comparing CD4+ T-helper cell infiltration (*Figure 2H*), whereas CD8+ cytotoxic T-cells in the hearts increased in both GF + HTN and COL + HTN mice compared with sham (*Figure 2I*). We also observed an increase in the cardiac expression of pro-inflammatory cytokine *Tnfa* selectively in the GF + HTN group compared with sham (see Supplementary material online, *Figure S4C*). Altogether, cardiac hypertrophy and inflammation following HTN were affected to a greater extent in GF, but when assessing the relative change for GF and COL mice in HTN compared with sham we saw many similarities in the development of the cardiac fibrosis. Whereas in the kidney, there was a clear difference in the development of HTN damage between GF and COL mice, these distinctions were less evident in the heart.

3.2 Hypertensive kidney damage is more sensitive to microbial status than cardiac damage

The aforementioned findings indicate that GF mice respond more sensitively to HTN. Within the context of our initial statistical approach (two-way ANOVA) we often saw a loss of significance for the HTN effect in COL mice under equal statistical power; and the differences between GF and COL response where much clearer when assessing the relative increase for a given marker in HTN (unpaired *t*-test). To expand on this idea to increase our understanding of the differences between GF and COL, we assessed the size of the HTN-induced effect by calculating an effect size (Cliff's delta) and fold change for each marker. Using a comprehensive univariate testing strategy, we assessed the significance in the different tissue spaces using a robust false discovery rate (FDR) correction within GF and COL groups to root out any spurious findings. From the majority of kidney parameters assessed, across the subcategorizations of damage, fibrosis, and inflammatory markers, a very consistent pattern emerged in that the GF mice experienced worsened kidney outcomes compared with COL mice (*Figure 3A*, see Supplementary material online, *Table S1*). In contrast to the renal damage, both GF and COL mice experienced a more similar cardiac damage pattern, particularly regarding markers of cardiac fibrosis (*Figure 3B*, and see Supplementary material online, *Table S2*). Albeit several cardiac parameters reached significance in GF and COL mice, the fold changes observed in GF mice were often larger (e.g. *Nppb*, perivascular fibrosis, *Ccn2*, *Lcn2*, F4/80, CD8; see Supplementary material online, *Table S2*). GF + HTN mice develop a significant increase in lung weight-to-tibia length ratio (*Figure 3B*), indicating the development of lung congestion[22] due to aggravated cardiac dysfunction. Taken together, there was more overlap in the cardiac response to HTN in GF and COL groups than was seen for the kidney parameters.

To further quantify the HTN effect across the renal (*Figure 3C*) and cardiac (*Figure 3D*) tissue space, we performed a multivariate principal coordinate analysis (PCoA) summarizing the overall (dis)similarities amongst the groups. To assess pairwise comparisons of interest, the overall dataset was divided and tested using PERMANOVA (*Figure 3C*). The pairwise comparisons of the kidney phenotypic data show a significant distance in the COL group from sham to HTN (P-value = 0.012, F-value = 4.8). However, the effect of HTN, as measured by the F-value, was greater in the GF mice (P-value = 0.001, F-value = 8.2). In line with our initial univariate targeted analysis (*Figure 1*), this indicates that the overall phenotypic change in the kidney in response to HTN was larger in GF mice than in COL mice. Furthermore, the pairwise PERMANOVA between GF + HTN and COL + HTN groups (P-value = 0.044, F-value = 3.2) indicates that HTN induction resulted in a different outcome on a multivariate level. Despite some slight differences within some univariate kidney data in the sham groups (e.g. albuminuria, F4/80 + cells), pairwise comparison of GF and COL sham samples was insignificant (P-value = 0.262, F-value = 1.4).

For the multivariate analysis of our cardiac data, pairwise comparisons were also used to assess the trajectory of each group (*Figure 3D*). Consistent with our conclusions from the univariate assessment of the overall cardiac phenotype (*Figure 3B*), we saw that the comparison between GF + HTN and COL + HTN group showed significant overlap in the PCoA plot, and the pairwise comparison between these samples was not significant (P-value = 0.391, F-value = 1.1). Conversely, the difference between sham GF and COL samples was significant, suggesting that perhaps the basal cardiac phenotype is sensitive to the host's microbiome status (P-value = 0.01, F-value = 5.6). As expected, the comparison of HTN with sham samples within the GF (P-value = 0.01, F-value = 4.8) and COL (P-value = 0.046, F-value = 3.2) samples were both significant. The cardiac data again indicate larger phenotypic shifts in GF mice most likely driven by significantly different sham groups.

Taken together, our univariate and multivariate approaches indicate a larger effect of HTN in GF mice. In the case of the kidney, this increased effect is indeed driven by a stronger adverse response of GF mice to

Downloaded from https://academic.oup.com/cardiovascres/article/119/6/1441/6651675 by Duke University - Perkins Library user on 21 August 2023

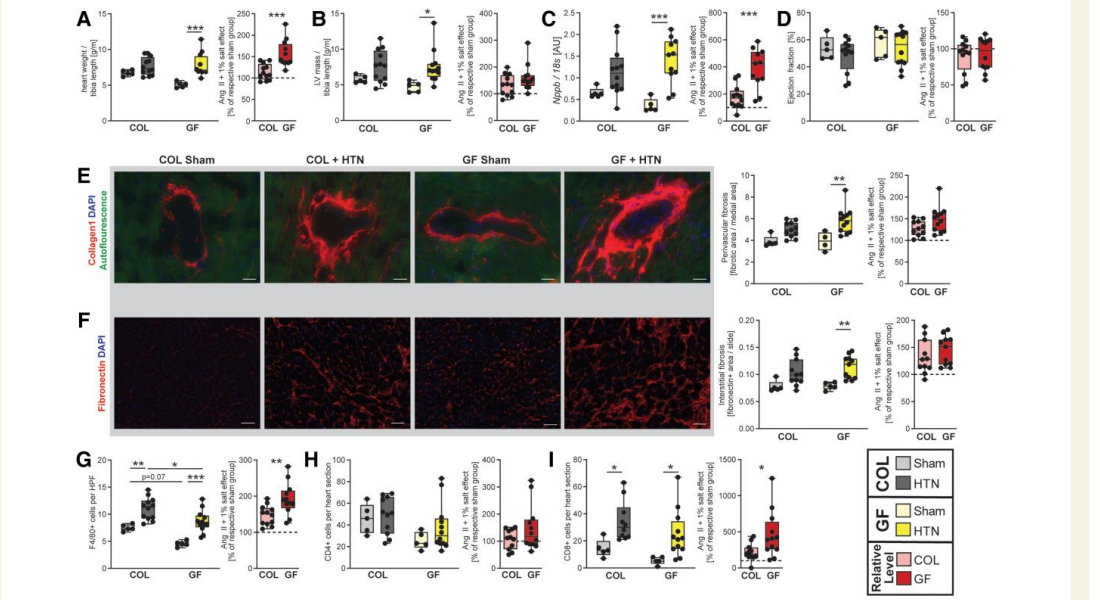

Figure 2 Cardiac inflammation and hypertrophy are aggravated in GF mice. Unless otherwise stated, GF Sham $n = 5$, GF + HTN $n = 12$, COL Sham $n = 5$, COL + HTN $n = 12$. (*A*) Heart weight-to-tibia length (g/m) from mice taken at sacrifice. (*B*) Left ventricular (LV) mass was estimated using echocardiography and normalized to tibia length (g/m). (*C*) Cardiac ventricular natriuretic peptide gene expression (*Nppb*) measured by qPCR. COL + HTN $n = 11$, otherwise as stated above. (*D*) Echocardiography prior to sacrifice revealed no change in the ejection fraction upon HTN induction in GF or COL mice. (*E*) Perivascular fibrosis from cardiac vessels, evaluated by measuring the fibrotic area relative to the medial area of vessels from Collagen 1-stained histology slides. GF Sham $n = 4$, otherwise as stated above. (*F*) Cardiac interstitial fibrosis was evaluated as fibronectin positive area proportionate to total area from five representative 40× magnification pictures from histological slides. In scale bar represents 40 µm. (*G*) Macrophages (F4/80+) were counted from five representative high-power fields, and (H) CD4+, and (*I*) CD8+ T-cells were counted from whole heart sections. Two-way ANOVA and *post hoc* Sidak multiple comparison's test for (*A–I*) was used to test significance in the left plot. In (*A–C*) and (*E and F*), HTN was identified as the source of variation using two-way ANOVA, and *post hoc* multiple comparison between sham and HTN within each group revealed that the GF comparison was the source of variation. In (*G*) HTN and the microbiome were both identified as sources of variation using two-way ANOVA, and significant *post hoc* comparisons are shown. In (*I*), HTN was identified as the source of variation using two-way ANOVA, and *post hoc* multiple comparison between sham and HTN within each group revealed that both the GF and COL comparison were significant. To the right in (*A–I*), the relative change induced by Ang II + 1% NaCl in comparison with the respective sham group was tested using an unpaired two-tailed *t*-test. No change (100%) depicted as dotted line. For all plots, *P*-values are as follows; $*P \leq 0.05$, $**P \leq 0.01$, $***P \leq 0.001$.

HTN, whereas in the case of the heart, this effect is driven by phenotypic differences in the healthy groups (sham-treated mice).

3.3 Vascular response to Angiotensin II is similar in GF and COL mice

There is some evidence from the literature that vascular reactivity may be dependent on microbial colonization.[23,24] We opted not to implant telemetry devices for the measurement of BP in our primary experimental animals, as microscopic vascular surgery was not possible under sterile conditions. Although we decided to forgo this gold-standard for BP measurement, we still questioned whether the axenic status of our GF mice would impact the basal mean arterial pressure (MAP), or BP reactivity to Ang II. We therefore colonized additional mice using the same colonization procedure as previously outlined, and we performed *in vivo* BP measurements using an implanted arterial catheter in freely moving mice. Interestingly, we found that GF mice had a significantly higher MAP (*Figure 4A*) than their colonized counterparts, although the mean of each group (GF mean value = 118.4 mmHg, COL mean value = 107.8 mmHg) was still in a range considered normal for untreated C57BL/6J mice.[25] Acute intravenous infusion of Ang II induced an increase in BP (*Figure 4B*) which was nearly identical for GF and COL mice, suggesting that Ang II-dependent reactivity of the vasculature is similar in these mice. Similarly, we investigated *ex vivo* vascular contractility of mesenteric arteries isolated from conventionally colonized mice (CONV) or GF mice (GF). CONV mice were used for this *in vitro* experiment due to ease of availability because colonization of GF mice is a lengthy procedure. GF mice showed similar contractile response compared with CONV mice in response to Ang II (see Supplementary material online, *Figure S5A*). Additionally, mesenteric arterial rings from GF mice showed similar contraction force in response to KCl to CONV mice (see Supplementary material online, *Figure S5B*). Similarly,

Downloaded from https://academic.oup.com/cardiovascres/article/119/6/1441/6651675 by Duke University - Perkins Library user on 21 August 2023

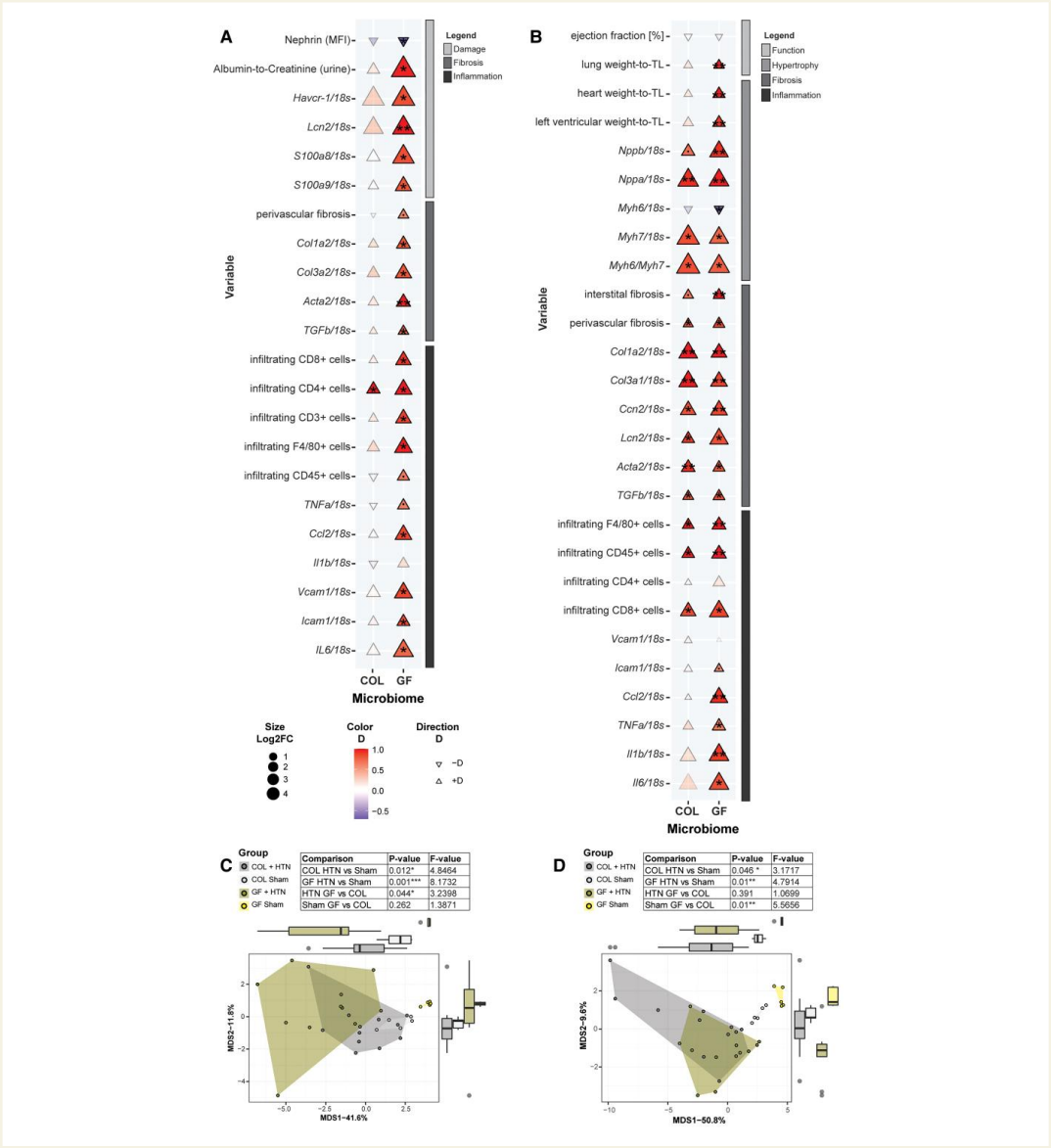

Figure 3 Unbiased assessment of kidney and heart damage in HTN-treated GF vs. COL mice. Unless otherwise stated, GF Sham $n = 5$, GF + HTN $n = 12$, COL Sham $n = 5$, COL + HTN $n = 12$. For cardiac RNA expression COL + HTN $n = 11$, otherwise as stated before. (*A*) Effect sizes [Cliff's delta (*D*)] and fold changes are shown to assess the effect of HTN treatment relative to the respective sham group in GF and COL on the kidney phenotype. Colour and triangle direction indicates effect size. Size indicates log2-transformed fold change (Log2FC) of HTN compared with the respective sham group. Significance was calculated using the Mann–Whitney *U*-test and was FDR-corrected with the Benjamini–Hochberg procedure to account for multiple testing. Markers for significant *Q*-values are superimposed, and transparency indicates non-significant effects. $^{\circ}q < 0.1$, $^{*}q < 0.05$, $^{**}q < 0.01$. Variables are organized by subcategory (damage, fibrosis, inflammation). (*B*) Same univariate analysis as in (*A*) was performed on cardiac phenotypic data. Variables are organized by subcategory (function, hypertrophy, fibrosis, inflammation). (*C*) PCoA was performed based on Euclidean distance scaling of kidney phenotypic data to demonstrate the dissimilarities between study groups in a quantitative phenotypic state space (GF + HTN = 11, otherwise as stated). Pairwise comparisons between groups were preformed using PERMANOVA and reported in the inset table. (*D*) PCoA as in (*C*) was performed on the cardiac phenotypic data.

Downloaded from https://academic.oup.com/cardiovascres/article/119/6/1441/6651675 by Duke University - Perkins Library user on 21 August 2023

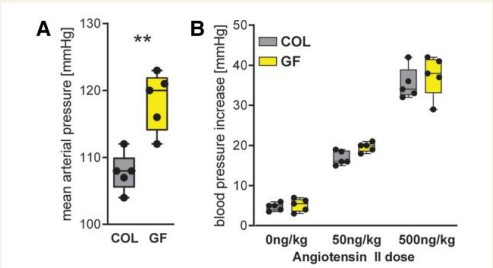

Figure 4 BP and Angiotensin II reactivity in GF and COL mice. $N = 5$ animals per group. (*A*) GF and COL mice were implanted an arterial catheter for BP measurement. MAP was measured in resting and awake animals, and the difference was tested using an unpaired two-tailed *t*-test (**$P \leq 0.01$). (*B*) The increase in BP after acute intravenous infusion of Angiotensin II as a bolus was measured. No statistical difference between GF and COL mice was found using a two-way repeated measurement ANOVA ($P = 0.14$), whereas Ang II dose had a significant influence ($P \leq 0.0001$, not shown).

endothelial-dependent (see Supplementary material online, *Figure S5C*) and –independent (see Supplementary material online, *Figure S5D*) relaxation was not influenced by colonization status.

3.4 Microbiota and microbial metabolites shape serum metabolome changes in HTN

Although the vascular reactivity of GF mice was similar to those housing microbes, we were interested to understand the different phenotypic and inflammatory response to HTN. We therefore decided to investigate the microbiome itself and associated metabolite production, as our group and others have previously shown that some metabolites of microbial origin can be anti-inflammatory in HTN.[5,13,14]

Consistent with the literature,[20] the metabolome of GF and COL animals was affected by HTN induction. We found a multitude of differences when analyzing the serum metabolome (MxP Quant 500, Biocrates) from GF and COL mice in HTN compared with the respective sham, which we grouped together by class to show the composite shift of over 300 individually measured metabolites (*Figure 5A*, and see Supplementary material online, *Table S3*). Of the 15 classes of metabolites where HTN induction had an effect, four of those classes (phosphatidylcholines, hexosylceramides, alkaloids, fatty acids) showed similar trajectories, suggesting these classes changed in a microbiome-independent manner upon HTN (*Figure 5A*, individual metabolites shown in see Supplementary material online, *Figure S6A–D*). For individual metabolites, we compared the impact of HTN induction on metabolite trajectories. When comparing sham with HTN, there was little overlap between the metabolites that decreased (*Figure 5B*) or increased (*Figure 5C*) within GF or COL. Overall, in GF mice more metabolites were regulated by HTN than in COL mice (see Supplementary material online, *Table S11*) (*Figure 5D*). Of note, a subset of metabolites which were upregulated in GF mice were downregulated in COL mice in response to HTN and vice versa (*Figure 5D*, shown in black). Taken together, the alterations of the metabolome in response to HTN show little overlap in GF and COL mice (*Figure 5D*, referred to as 'both'). Unsurprisingly, the serum metabolome was significantly impacted by the microbiome, and we saw a wide range of correlations between individual metabolites and microbial species, as well as functional modules derived from shotgun sequencing data (see Supplementary material online, *Figure S7*). Although the serum metabolite measurements used here were very comprehensive, they did not cover SCFA metabolites, which we and others have shown to have high importance in the progression of HTN. It has been demonstrated elsewhere that GF mice are devoid of some important SCFA.[26] We confirmed this for our mouse colonies (GF and CONV, which were the source populations for our experiments) by performing mass spectrometry measurements of faecal acetate, propionate, and butyrate (*Figure 5E*). We expect that the lack of the potent anti-hypertensive metabolites propionate and butyrate influences the phenotype seen in GF mice.

3.5 Inflammation contributes to the differing phenotypic response to HTN in GF and COL mice

It has been shown that the immune system and the gut microbiome are strongly interconnected, and several studies have shown the importance of immune cells in HTN.[2,3] We and others have also shown that metabolites of microbial origin can influence inflammation in HTN.[5,13,14] We examined the splenic immune cell composition a surrogate for systemic inflammation in GF and COL mice by flow cytometry (gating strategies are shown in see Supplementary material online, *Figure S8*). Of the 23 immune cell subsets we investigated, 12 were differentially influenced by HTN when compared with the respective sham group (*Figure 6A*, and see Supplementary material online, *Table S4*). We then examined all immune parameters multivariately to assess how changes in immune cells would be reflected in the distance between each group using PCoA (*Figure 6B*). It is known that the immune system of GF mice differs from their colonized counterparts.[27] Our data confirms this observation as the pairwise comparison of sham-treated GF and COL mice (*P*-value = 0.011, *F*-value = 6.6) was significant. Interestingly, this difference between COL and GF was still evident after HTN induction (*P*-value = 0.026, *F*-value = 2.8). Pairwise comparisons of individual groups using PERMANOVA indicated that the HTN to sham comparison was significant in the GF group (*P*-value = 0.006, *F*-value = 4.8), but not within the COL group (*P*-value = 0.177, *F*-value = 1.6) (*Figure 6B*). It can be concluded that overall, the inflammatory status of GF mice was disturbed to a greater degree by HTN induction.

Previous studies have shown that splenic MDSC increase in HTN and have anti-hypertensive properties.[9] In line with the literature, there was an increase in monocytic MDSC (mMDSC) upon HTN induction, and this increase was only significant in COL + HTN mice (*Figure 6C*). Furthermore, for both mMDSC and granulocytic MDSC (gMDSC) (*Figure 6D*) subtypes, COL + HTN mice showed a significantly higher frequency of these anti-hypertensive immune cells than GF + HTN mice. The relative increase in HTN compared with sham for mMDSC was lesser in GF mice but greater for gMDSC than in COL (*Figure 6C and D*). The dynamics of whether the relative increase, or absolute number of MDSCs is relevant in HTN is currently unknown. Additionally, we saw an increase in Th17 cells in both GF and COL mice, though this effect only reached significance in GF mice (*Figure 6E*). This increase was driven by pathological Th1-like Th17 cells, defined by their co-expression of RORgt and Tbet (*Figure 6F*).[28] Recent evidence suggest that pre-existing conditions can influence naive T-cell responses towards effector differentiation.[29–31] We hypothesized that the absence of microbes and their metabolites in GF mice would render naive T-cells more vulnerable to

Downloaded from https://academic.oup.com/cardiovascres/article/119/6/1441/6651675 by Duke University - Perkins Library user on 21 August 2023

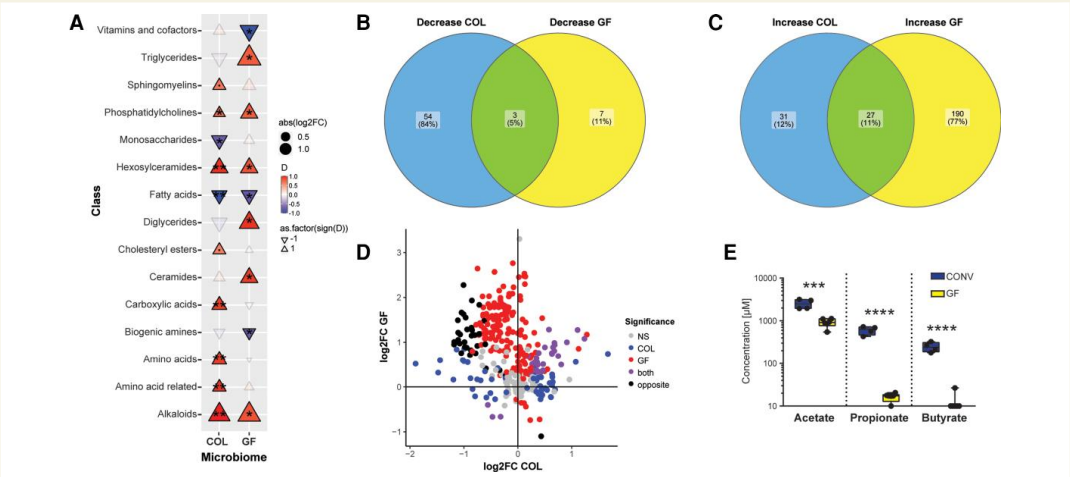

Figure 5 Microbiome heavily influences the metabolome in response to HTN. (*A*) Using the Biocrates MxP500 Quant kit, serum metabolites were analysed from GF and COL mice. Metabolites were grouped by class to demonstrate the overall effect on the serum metabolome (Sham GF $n = 5$, Sham COL $n = 5$, GF + HTN $n = 10$, COL + HTN $n = 11$). Effect size [Cliff's delta (*D*)] is shown to demonstrate the effect of HTN relative to the respective sham group in GF and COL. Colour and triangle direction indicates effect size. Size indicates log2-transformed fold change (Log2FC) of HTN mice compared with the respective sham group. Significance was calculated using the Mann–Whitney *U*-test and was FDR-corrected using the Benjamini–Hochberg procedure to account for multiple testing. Markers for significant Q-values are superimposed, and transparency indicates non-significant effects. °$q < 0.1$, *$q < 0.05$, **$q < 0.01$. For (*B*) and (*C*), individual metabolites rather than metabolite classes within the GF and COL group were compared using the effect size calculation listed in (*A*, see Supplementary material online, *Table S11*). Those metabolites which were significantly altered in the sham to HTN comparison, as tested using the Mann–Whitney *U*-test with Benjamini–Hochberg FDR correction were selected and separated based on the directionality of their shift. Metabolites which decreased (*B*) or increased (*C*) in HTN relative to sham are compared between the COL and GF conditions using a Venn diagram. The number of metabolites and the percentage within each subcategory are overlayed. In (*D*) significant changes to individual metabolites (points) are shown in GF (*y*-axis) and COL (*x*-axis) as log2-fold changes in response to HTN. Metabolites exclusively significantly regulated in GF or in COL are shown in red and blue, respectively. Purple points indicate metabolites significantly regulated similarly in GF and COL (significant in both and same trajectory), while black points indicate metabolites regulated significant in both groups but with opposite trajectories. Grey points are metabolites which were reliably measured but not significantly altered in either group. (*E*) Faecal SCFA from GF or CONV mice demonstrates the absence of potent anti-hypertensive metabolites butyrate and propionate in the GF setting (GF $n = 6$, CONV $n = 4$). Significance was tested using unpaired two-tailed Student's *t*-test (***$P \leq 0.001$, ****$P \leq 0.0001$). LC-MS, liquid chromatography-mass spectrometry; FIA-MS, flow injection analysis-mass spectrometry.

cytokines. Therefore, we performed an *in vitro* Th17 polarization of naive T-cells from GF and CONV mice (which were used in place of COL due to ease of accessibility) in the presence or absence of Ang II. Naive T-cells from GF mice more readily polarized towards Th17 cells than cells from CONV mice, particularly in the presence of Ang II (*Figure 6G*). To demonstrate that the conditions for the polarization of Th17 cells indeed exist *in vivo*, we quantified the expression of each of the Th17-polarizing cytokines (Il-6, Il-1b, and TGFb) by qPCR from kidney (see Supplementary material online, *Figure S9A*, and *Figure 3A*) and heart (see Supplementary material online, *Figure S9B*, and *Figure 3C*) tissue. These key cytokines were increased upon HTN. The comparison of effect sizes (*Figure 3A and C*) often indicated larger effects of HTN in GF mice. We suspected that the reason naive CD4+ T-cells isolated from CONV mice were less inducible toward Th17 in the presence of Ang II may be due to the priming of immune cells by SCFA in the *in vivo* microenvironment. To test this hypothesis, prior to Th17 induction in the presence of Ang II, naive CD4+ cells were pre-treated for 24 h with the SCFA butyrate and propionate. While the pre-treatment did not affect the induction of Th17 in CONV, SCFA pre-treatment prevented the enhanced Th17 induction of naive T-cells from GF mice (*Figure 6H*).

In summary, our *in vitro* findings suggest that the different preconditioning of naive T-cells within GF and COL mice may impact polarization into pro-inflammatory effector T-cells and thus severity of target organ damage. We anticipate that this effect contributes to our *in vivo* findings, where the absence of microbes and microbiota-derived metabolites like SCFA had a potent impact on immune cells relevant in HTN and cardiorenal damage.

4. Discussion

Gut microbial dysbiosis associates with HTN in humans[5,32] and in rodent models.[5,32–34] Faecal microbiota transplantation from hypertensive patients into mice has also been shown to induce an increase in BP.[32] However, few studies have focused on the overall contribution of the microbiome to the pathogenesis of HTN, such that it may be contextualized relative to other known contributors to hypertensive disease

Downloaded from https://academic.oup.com/cardiovascres/article/119/6/1441/6651675 by Duke University - Perkins Library user on 21 August 2023

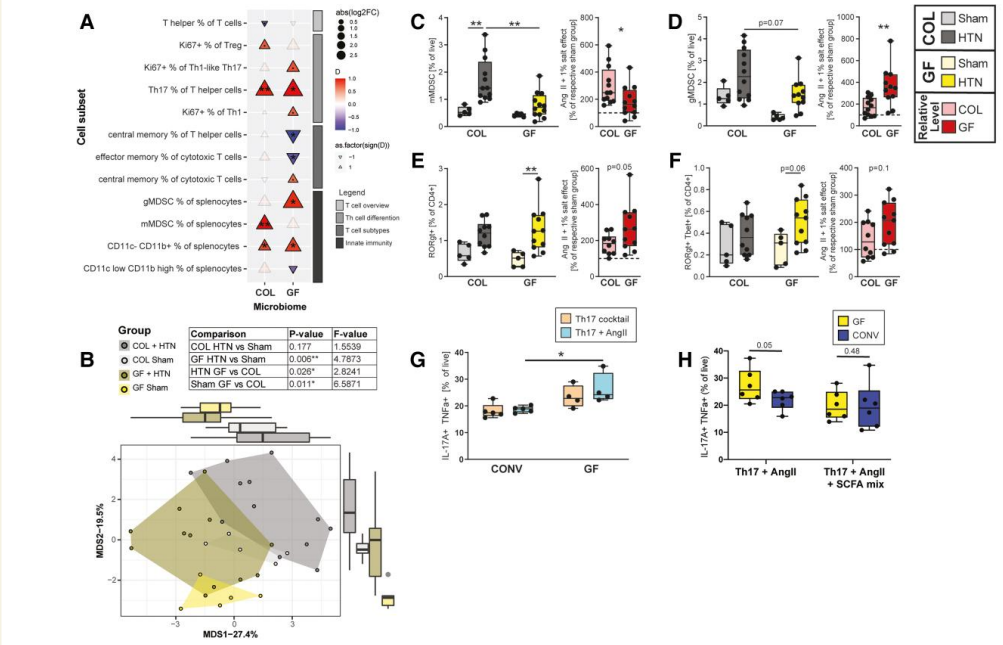

Figure 6 Colonization status influences the inflammatory reaction to HTN. Unless otherwise stated, GF Sham $n = 5$, GF + HTN $n = 12$, COL Sham $n = 5$, COL + HTN $n = 12$. (*A*) Several unique immune cell subsets were measured from the spleen, as a proxy measure of systemic inflammation. Effect size (Cliff's delta [D]) is shown to demonstrate the effect of HTN relative to the respective sham group in GF and COL. Colour and triangle direction indicates effect size. Size indicates log2-transformed fold change (Log2FC) of HTN induction compared with the respective sham group. Significance was calculated using the Mann–Whitney *U*-test and was FDR-corrected using the Benjamini–Hochberg procedure to account for multiple testing. Markers for significant Q-values are superimposed, and transparency indicates non-significant effects. $^{\circ}q < 0.1$, $^{*}q < 0.05$, $^{**}q < 0.01$. Immune cell subsets are organized by sub-category (Innate immunity and T-cell overview, differentiation, and subtypes) and subsets, and cell types where no significant effect in either GF or COL was found are not shown. (*B*) PCoA was performed based on Euclidean distance scaling of immune cell abundances to demonstrate the dissimilarities between study groups. Pairwise comparisons between groups were performed using PERMANOVA and reported in the inset table. Monocytic MDSCs (mMDSC, *C*) and granulocytic MDSCs (gMDSC, *D*), as well as Th17 (*E*) and Th1-like Th17 cells (*F*) from the spleen are shown as boxplots on the left. (*G*) naive CD4+ T-cells from mesenteric lymph nodes of either GF of CONV mice, polarized *in vitro* towards a Th17 using a cocktail of IL-1β, TGFβ, and IL-6 with or without Ang II (GF $n = 4$, CONV $n = 5$). In (H) naive CD4+ T-cells were pre-treated with 1 mM SCFA mix (0.5 mM of each butyrate and propionate) or 1 mM NaCl. Subsequently, the pre-treatment was removed, and cells were polarized toward Th17 in the presence of Ang II as described in G (GF $n = 6$, CONV $n = 6$). To the left in (*C*–*G*), two-way ANOVA and *post hoc* Sidak multiple comparison's test was used to test significance. To the right in (*C*–*F*), the relative change induced by Ang II + 1% NaCl in comparison with the respective sham group was tested using an unpaired two-tailed *t*-test. No change (100%) depicted as dotted line. In (*H*) for the Th17 + Ang II and Th17 + Ang II + SCFA mix a one-tailed *t*-test was performed per group, as a pre-specified hypothesis from *Figure 6G* was tested. For all plots in (*C*–*G*), *P*-values are as follows; $^{*}P \leq 0.05$, $^{**}P \leq 0.01$.

burden. Here we show in a presence/absence scenario, that the microbiota has a potent effect on HTN-induced cardiac and renal damage in mice. GF mice showed a stronger adverse response to HTN than their COL littermates. Interestingly, the kidney seems to be more sensitive to changes in microbial status than the heart. Finally, we propose that the altered inflammatory response in GF mice contributes to their aggravated phenotype in HTN.

We have shown robustly that the kidney damage within GF mice upon HTN is comparatively more severe than the damage experienced by their COL littermates. Some of the larger effects in our univariate analysis may be related to the slightly lower baseline level of putative markers for kidney damage within sham GF mice compared with sham COL, though these groups do not significantly differ. We surmise that the baseline differences between GF and COL mice are likely due to the immunological uniqueness of GF mice, which has been documented in the literature.[27] Indeed, across renal damage, fibrosis and inflammation markers, we consistently saw a significant effect of HTN selectively in the GF group (*Figure 3A*). Furthermore, we show on a multivariate level that the difference between sham GF and GF + HTN mice for the composite of kidney parameters is significant, while the equivalent comparison within the COL mice is insignificant (*Figure 3C*). Consistent with other inflammatory markers, we show an increase of infiltrating macrophages (F4/80+ cells, *Figure 1E*) in GF + HTN kidneys, as well as the increased expression of *Ccl2* (see Supplementary material online,

Downloaded from https://academic.oup.com/cardiovascres/article/119/6/1441/6651675 by Duke University - Perkins Library user on 21 August 2023

Figure S3A), which has been implicated as a major player in worsening kidney damage in mice[35] and humans.[36] Infiltrating macrophages during renal injury are known to contribute to the secretion of cytokines like IL-1β, which enhances the activation and differentiation of Th17 cells.[37] A previous study additionally showed that SCFA-treatment in ischaemia-reperfusion injury (IRI) radically reduced kidney *Ccl2*, *Il-1b*, and associated kidney damage.[38] SCFA have been shown to have anti-inflammatory properties in several cell types,[39–42] which could contribute to the lessened damage in COL mice, since only mice harbouring microbiota have significant SCFA production within the GI tract (*Figure 5C*). Our results are highly compatible with previous studies showing that GF status exacerbates kidney damage in the context of IRI[43] and adenine-induced chronic kidney disease.[21,44]

Intriguingly, we found that the cardiac phenotype was less influenced by the microbial status of the host. Here we have shown that particularly for markers of fibrosis (*Figure 3B*), regardless of the microbiome status, the mice developed significant injury. For CD8+ T-cells, F4/80+ macrophages and overall CD45+ leukocytes, we observed significant changes in GF and COL mice, although GF mice tended to show a higher fold change in response to HTN (see Supplementary material online, *Table S2*). Despite these similarities, both cardiac hypertrophy (*Figure 2A*) and left ventricular mass-to-tibia length (*Figure 2B*) were significantly altered upon HTN induction in the GF but not COL mice. Nonetheless, our data suggest that the kidney, more so than the heart, represents a subspace of hypertensive target organ damage, which is more susceptible to microbial colonization. It is conceivable that cardiac damage could be further exacerbated as renal function declines. Thus, the gut microbiota could be added as an important modulator of the well-known cardiorenal axis. Further research to follow up this idea is required, perhaps using several iterations of variations to a defined community of microbes, to test the universality of this hypothesis.

Metabolites of microbial origin, some of which are known to be associated with CVD and accumulate in chronic kidney disease,[16,17] were measurable within the serum metabolome of our COL but not our GF mice, such as IS and TMAO (see Supplementary material online, *Figure S1D*). Our results very clearly indicate that GF mice experience robust kidney damage to a greater extent than COL mice, despite GF mice being devoid of these harmful metabolites. However, we suggest that the reason COL mice experience less overall damage is likely due to the presence of SCFA. We and others have shown the potent effect of SCFA in mouse models.[13,14] Here we have shown again, for a representative set of animals, that SCFA are depleted in GF mice (*Figure 5C*). We hypothesize that the potency of SCFA in COL mice counterbalances the presence of IS and TMAO. Further research on this topic is required to definitively conclude the effects of the co-occurrence of these various metabolites of microbial origin.

Furthermore, we show that systemic inflammatory response to HTN is altered by colonization status. MSDC, which represent an important subset of innate anti-inflammatory cells in HTN,[9] reacted differently GF mice compared with COL (*Figure 6C and D*). Additionally, we found that Th17 cells were increased during HTN in GF mice (*Figure 6E*). Th1-like Th17 cells, which are known to be pathogenic, trended towards enrichment in GF + HTN mice (*Figure 6F*). We wanted to explore *in vitro* that naive T-cells from GF mice were more sensitive to polarizing cytokines and Ang II. We found that upon polarization, naive T-cells from GF mice skewed more towards Th17, particularly when Ang II was added (*Figure 6G*). As it has been recently demonstrated that the SCFA propionate can decrease the rate of Th17 cell differentiation,[41,42] we suspected that this could be part of the reason naive cells from COL mice were less inducible toward Th17. Indeed, when we pre-treated naive CD4+ T-cells with butyrate and propionate, we observed a decline in Th17 inducibility in the presence of Ang II in GF; an effect that was not seen in cells isolated from CONV mice (*Figure 6H*). Recently, Krebs and colleagues showed that the development of Th17 cells in the kidney is dependent on the cytokine micromilieu and can be blocked with specific antibodies against IL-1b and IL-6.[45] We also could show that the polarization conditions used in our Th17 *in vitro* assay were practically available *in vivo*, and the expression of each polarizing cytokine was increased within heart and kidney tissue of hypertensive mice.

To our knowledge, one study similar to ours exists within the literature, published by Karbach *et al.*[46] It is clear from the extensive phenotyping performed in our study that our findings were not congruent with their data, where they showed that GF mice were protected from developing HTN and related vascular damage. Though this was initially a surprise, upon further examination, there are two likely scenarios that may explain this. First, the protocol of our experiments did differ from one another. The study from Karbach and colleagues compared GF mice with conventionally raised mice, whereas we compared GF mice with littermates that had been colonized early in life. Therefore, our study was able to account for known genetic drifts in gnotobiotic colonies. Additionally, Ang II infusion was only performed for seven days, while we studied a more chronic phenotype. Furthermore, our mice ate different diets, and as Kaye and colleagues recently demonstrated, the composition of the diet can have a profound impact on the resultant hypertensive phenotype.[47] Second, it is highly likely that the microbiome used in our study and in the study by Karbach and colleagues may be distinct from one another. Incongruencies like ours have also been found in other contexts. The comparison of microbiome-rich and GF mice in one study showed the amelioration of an IRI of the kidney by the microbiome,[43] where another study demonstrated the opposite effect.[48]

To investigate the second scenario further, we hypothesized that the microbiome background used in any given study might have drastic implications for the study outcome. Our group and others have shown that microbially-produced metabolites have a potent effect on the pathogenesis of HTN.[5,13,14,49] In reference to that, if the microbiota itself were to change, we expect the circulating metabolites to be likewise altered within the host. Unfortunately, the study from Karbach *et al.*[46] did not include any information regarding the microbiome and metabolome of their microbiota-rich mice. Although, we did find a recent study from Cheema and Pluznick[20] where these data were made available, but their phenotypic data is not reported.[20] Nevertheless, to test our hypothesis regarding the putative comparability of the colonizing microbiome between studies, and the impact this may have on resultant study outcome, we decided to compare our microbiome and metabolome with the published data from Cheema and Pluznick. To compare the microbiomes from these two studies, we re-annotated our shotgun microbiome sequencing data such that it would be comparable to the 16s rDNA sequencing data from Cheema and Pluznick. The microbiome of CONV between the two studies were starkly contrasting in sham and HTN mice (shown as a multivariate PCoA plot derived from genus level information from each of the studies, see Supplementary material online, *Figure S10A*). We surmised that because of the lack of overlapping microbiome signatures within our study and the Pluznick dataset, that the metabolome signal would likewise be dichotomous. We compared the serum metabolome dataset from the two studies by using metabolites which could be measured in both studies from all COL and GF mice. We found that interestingly, there was significantly less distance

Downloaded from https://academic.oup.com/cardiovascres/article/119/6/1441/6651675 by Duke University - Perkins Library user on 21 August 2023

between the effect of HTN on individual metabolites within the serum metabolome of GF mice from these two studies than in the equivalent COL mice comparison (see Supplementary material online, *Figure S10B and C*). This result suggests that the congruence of the serum metabolome in GF groups within these two datasets is higher than the COL groups. These exploratory data support the idea that the structure of the implanted microbiome has a measurable impact on serum metabolome alterations in response to HTN. Because of our and others' findings regarding the importance of microbial metabolites in HTN, we believe that this could be a driving factor behind the contradictory phenotypic results of our study compared with the data from Karbach *et al.*[46] It is nonetheless critical in future studies for the microbiome to be well documented and openly accessible to avoid questions regarding the reproducibility of existing studies.

5. Conclusion

We have shown that the microbiota has a profound effect on hypertensive disease pathogenesis. Furthermore, we have shown that GF mice, when compared with their colonized littermates, experienced an aggravation of target organ damage, which was more distinct in the kidney than in the heart. Additionally, we demonstrated that the metabolome is influenced significantly by the microbiome used for experimentation, which underscores the need for standardization of experimentation and reporting within the field. The immunophenotype of HTN mice, and in particular, the alteration of MDSC and Th17 cells, which have been previously implicated in HTN, give us some indication of how GF mice may have developed an exacerbated hypertensive phenotype in our study. *In vitro*, SCFA rescued the pro-inflammatory phenotype of T-cells isolated from GF mice. We propose that the COL mice were protected from damage in comparison with their GF counterparts due to the absence of the potent anti-inflammatory SCFA metabolites under GF conditions.

Supplementary material

Supplementary material is available at *Cardiovascular Research* online.

Authors' Contributions

N.W., D.N.M., and H.B. designed the study. E.G.A., H.B., A.R., G.N., D.T., A.Y., C.Z., L. Y., L.M., A.M., A.P., and N.W. performed animal experiments and analysed the data. A.F.R, M.T., and M.B. performed *in vivo* BP measurement. C.-Y.C., U.L., and T.U.P.B. performed the microbiome analysis. E.G.A., R.F.G., S.K., and J.A.K. performed and analysed the metabolomics experiments. S.K.F. helped with data analysis and interpretation. E.G.A., N.W., H.B., and D.N.M. wrote the manuscript with input from all authors.

Acknowledgments

We thank Petra Voss, Ilona Kramer, May-Britt Köhler, Jana Czychi, Ute Gerhardt, Alina Eisenberger, Martin Taube, and Stefanie Schelenz for their technical assistance.

Conflict of interest: none declared.

Funding

N.W. is supported by the European Research Council (ERC) under the European Union's Horizon 2020 research and innovation programme (852796) and by a grant from the Corona-Stiftung, Deutsches Stiftungszentrum, Essen, Germany. A.P., N.W., D.N.M., and S.K.F. are supported by the Deutsche Forschungsgemeinschaft (DFG, German Research Foundation) Projektnummer 394046635—SFB 1365. The DZHK (German Centre for Cardiovascular Research, 81Z1100101) supported D.N.M. N.W. was participant in the Clinician Scientist Programme funded by the Berlin Institute of Health (BIH).

Data availability

The data underlying this article are available in the article and in its online supplementary material. The microbiome data underlying this article are available in NCBI database and can be accessed as BioProject PRJNA812410. The metabolomics data underlying this article are available via FigShare, please see Supplementary material online, *Table S10* for access links.

References

1. Ezzati M, Riboli E. Behavioral and dietary risk factors for noncommunicable diseases. *N Engl J Med* 2013;**369**:954–964.
2. Avery EG, Bartolomaeus H, Maifeld A, Marko L, Wiig H, Wilck N, Rosshart SP, Forslund SK, Muller DN. The gut microbiome in hypertension: recent advances and future perspectives. *Circ Res* 2021;**128**:934–950.
3. Madhur MS, Elijovich F, Alexander MR, Pitzer A, Ishimwe J, Van Beusecum JP, Patrick DM, Smart CD, Kleyman TR, Kingery J, Peck RN, Laffer CL, Kirabo A. Hypertension: do inflammation and immunity hold the key to solving this epidemic? *Circ Res* 2021;**128**:908–933.
4. Verhaar BJH, Collard D, Prodan A, Levels JHM, Zwinderman AH, Backhed F, Vogt L, Peters MJL, Muller M, Nieuwdorp M, van den Born BH. Associations between gut microbiota, faecal short-chain fatty acids, and blood pressure across ethnic groups: the HELIUS study. *Eur Heart J* 2020;**41**:4259–4267.
5. Wilck N, Matus MG, Kearney SM, Olesen SW, Forslund K, Bartolomaeus H, Haase S, Mahler A, Balogh A, Marko L, Vvedenskaya O, Kleiner FH, Tsvetkov D, Klug L, Costea PI, Sunagawa S, Maier L, Rakova N, Schatz V, Neubert P, Fratzer C, Krannich A, Gollasch M, Grohme DA, Corte-Real BF, Gerlach RG, Basic M, Typas A, Wu C, Titze JM, Jantsch J, Boschmann M, Dechend R, Kleinewietfeld M, Kempa S, Bork P, Linker RA, Alm EJ, Muller DN. Salt-responsive gut commensal modulates TH17 axis and disease. *Nature* 2017;**551**:585–589.
6. Yang T, Santisteban MM, Rodriguez V, Li E, Ahmari N, Carvajal JM, Zadeh M, Gong M, Qi Y, Zubcevic J, Sahay B, Pepine CJ, Raizada MK, Mohamadzadeh M. Gut dysbiosis is linked to hypertension. *Hypertension* 2015;**65**:1331–1340.
7. Madhur MS, Lob HE, McCann LA, Iwakura Y, Blinder Y, Guzik TJ, Harrison DG. Interleukin 17 promotes angiotensin II-induced hypertension and vascular dysfunction. *Hypertension* 2010;**55**:500–507.
8. Marko L, Kvakan H, Park JK, Qadri F, Spallek B, Binger KJ, Bowman EP, Kleinewietfeld M, Fokuhl V, Dechend R, Muller DN. Interferon-γ signaling inhibition ameliorates angiotensin II-induced cardiac damage. *Hypertension* 2012;**60**:1430–1436.
9. Shah KH, Shi P, Giani JF, Janjulia T, Bernstein EA, Li Y, Zhao T, Harrison DG, Bernstein KE, Shen XZ. Myeloid suppressor cells accumulate and regulate blood pressure in hypertension. *Circ Res* 2015;**117**:858–869.
10. Ivanov II, Atarashi K, Manel N, Brodie EL, Shima T, Karaoz U, Wei D, Goldfarb KC, Santee CA, Lynch SV, Tanoue T, Imaoka A, Itoh K, Takeda K, Umesaki Y, Honda K, Littman DR. Induction of intestinal Th17 cells by segmented filamentous bacteria. *Cell* 2009;**139**:485–498.
11. Zaccone P, Raine T, Sidobre S, Kronenberg M, Mastroeni P, Cooke A. Salmonella typhimurium infection halts development of type 1 diabetes in NOD mice. *Eur J Immunol* 2004;**34**:3246–3256.
12. Tan J, McKenzie C, Potamitis M, Thorburn AN, Mackay CR, Macia L. The role of short-chain fatty acids in health and disease. *Adv Immunol* 2014;**121**:91–119.
13. Marques FZ, Nelson E, Chu PY, Horlock D, Fiedler A, Ziemann M, Tan JK, Kuruppu S, Rajapakse NW, El-Osta A, Mackay CR, Kaye DM. High-fiber diet and acetate supplementation change the gut microbiota and prevent the development of hypertension and heart failure in hypertensive mice. *Circulation* 2017;**135**:964–977.
14. Bartolomaeus H, Balogh A, Yakoub M, Homann S, Marko L, Hoges S, Tsvetkov D, Krannich A, Wundersitz S, Avery EG, Haase N, Kraker K, Hering L, Maase M, Kusche-Vihrog K, Grandoch M, Fielitz J, Kempa S, Gollasch M, Zhumadilov Z, Kozhakhmetov S, Kushugulova A, Eckardt KU, Dechend R, Rump LC, Forslund SK, Muller DN, Stegbauer J, Wilck N. Short-chain fatty acid propionate protects from hypertensive cardiovascular damage. *Circulation* 2019;**139**:1407–1421.
15. Poll BG, Cheema MU, Pluznick JL. Gut microbial metabolites and blood pressure regulation: focus on SCFAs and TMAO. *Physiology (Bethesda)* 2020; **35**:275–284.
16. Zhu W, Gregory JC, Org E, Buffa JA, Gupta N, Wang Z, Li L, Fu X, Wu Y, Mehrabian M, Sartor RB, McIntyre TM, Silverstein RL, Tang WHW, DiDonato JA, Brown JM, Lusis AJ,

Downloaded from https://academic.oup.com/cardiovascres/article/119/6/1441/6651675 by Duke University - Perkins Library user on 21 August 2023

Hazen SL. Gut microbial metabolite TMAO enhances platelet hyperreactivity and thrombosis risk. *Cell* 2016;**165**:111–124.
17. Nakano T, Katsuki S, Chen M, Decano JL, Halu A, Lee LH, Pestana DVS, Kum AST, Kuromoto RK, Golden WS, Boff MS, Guimaraes GC, Higashi H, Kauffman KJ, Maejima T, Suzuki T, Iwata H, Barabasi AL, Aster JC, Anderson DG, Sharma A, Singh SA, Aikawa E, Aikawa M. Uremic toxin indoxyl sulfate promotes proinflammatory macrophage activation via the interplay of OATP2B1 and Dll4-notch signaling. *Circulation* 2019;**139**:78–96.
18. Marko L, Park JK, Henke N, Rong S, Balogh A, Klamer S, Bartolomaeus H, Wilck N, Ruland J, Forslund SK, Luft FC, Dechend R, Muller DN. B-cell lymphoma/leukaemia 10 and angiotensin II-induced kidney injury. *Cardiovasc Res* 2020;**116**:1059–1070.
19. Leelahavanichkul A, Yan Q, Hu X, Eisner C, Huang Y, Chen R, Mizel D, Zhou H, Wright EC, Kopp JB, Schnermann J, Yuen PS, Star RA. Angiotensin II overcomes strain-dependent resistance of rapid CKD progression in a new remnant kidney mouse model. *Kidney Int* 2010;**78**:1136–1153.
20. Cheema MU, Pluznick JL. Gut microbiota plays a central role to modulate the plasma and fecal metabolomes in response to angiotensin II. *Hypertension* 2019;**74**:184–193.
21. Mishima E, Ichijo M, Kawabe T, Kikuchi K, Akiyama Y, Toyohara T, Suzuki T, Suzuki C, Asao A, Ishii N, Fukuda S, Abe T. Germ-free conditions modulate host purine metabolism, exacerbating adenine-induced kidney damage. *Toxins (Basel)* 2020;**12**:547.
22. Richards DA, Aronovitz MJ, Calamaras TD, Tam K, Martin GL, Liu P, Bowditch HK, Zhang P, Huggins GS, Blanton RM. Distinct phenotypes induced by three degrees of transverse aortic constriction in mice. *Sci Rep* 2019;**9**:5844.
23. Joe B, McCarthy CG, Edwards JM, Cheng X, Chakraborty S, Yang T, Golonka RM, Mell B, Yeo JY, Bearss NR, Furtado J, Saha P, Yeoh BS, Vijay-Kumar M, Wenceslau CF. Microbiota introduced to germ-free rats restores vascular contractility and blood pressure. *Hypertension* 2020;**76**:1847–1855.
24. Edwards JM, Roy S, Tomcho JC, Schreckenberger ZJ, Chakraborty S, Bearss NR, Saha P, McCarthy CG, Vijay-Kumar M, Joe B, Wenceslau CF. Microbiota are critical for vascular physiology: germ-free status weakens contractility and induces sex-specific vascular remodeling in mice. *Vascul Pharmacol* 2020;**125-126**:106633.
25. Mattson DL. Comparison of arterial blood pressure in different strains of mice. *Am J Hypertens* 2001;**14**:405–408.
26. Hoverstad T, Midtvedt T. Short-chain fatty acids in germfree mice and rats. *J Nutr* 1986;**116**:1772–1776.
27. Smith K, McCoy KD, Macpherson AJ. Use of axenic animals in studying the adaptation of mammals to their commensal intestinal microbiota. *Semin Immunol* 2007;**19**:59–69.
28. Kamali AN, Noorbakhsh SM, Hamedifar H, Jadidi-Niaragh F, Yazdani R, Bautista JM, Azizi G. A role for Th1-like Th17 cells in the pathogenesis of inflammatory and autoimmune disorders. *Mol Immunol* 2019;**105**:107–115.
29. Coit P, Dozmorov MG, Merrill JT, McCune WJ, Maksimowicz-McKinnon K, Wren JD, Sawalha AH. Epigenetic reprogramming in naive CD4+ T cells favoring T Cell activation and non-Th1 effector T cell immune response as an early event in lupus flares. *Arthritis Rheumatol* 2016;**68**:2200–2209.
30. Altorok N, Coit P, Hughes T, Koelsch KA, Stone DU, Rasmussen A, Radfar L, Scofield RH, Sivils KL, Farris AD, Sawalha AH. Genome-wide DNA methylation patterns in naive CD4+ T cells from patients with primary Sjogren's syndrome. *Arthritis Rheumatol* 2014;**66**:731–739.
31. Heninger AK, Eugster A, Kuehn D, Buettner F, Kuhn M, Lindner A, Dietz S, Jergens S, Wilhelm C, Beyerlein A, Ziegler AG, Bonifacio E. A divergent population of autoantigen-responsive CD4(+) T cells in infants prior to beta cell autoimmunity. *Sci Transl Med* 2017;**9**:eaaf8848.
32. Li J, Zhao F, Wang Y, Chen J, Tao J, Tian G, Wu S, Liu W, Cui Q, Geng B, Zhang W, Weldon R, Auguste K, Yang L, Liu X, Chen L, Yang X, Zhu B, Cai J. Gut microbiota dysbiosis contributes to the development of hypertension. *Microbiome* 2017;**5**:14.
33. Adnan S, Nelson JW, Ajami NJ, Venna VR, Petrosino JF, Bryan RM Jr, Durgan DJ. Alterations in the gut microbiota can elicit hypertension in rats. *Physiol Genomics* 2017;**49**:96–104.
34. Santisteban MM, Qi Y, Zubcevic J, Kim S, Yang T, Shenoy V, Cole-Jeffrey CT, Lobaton GO, Stewart DC, Rubiano A, Simmons CS, Garcia-Pereira F, Johnson RD, Pepine CJ, Raizada MK. Hypertension-linked pathophysiological alterations in the gut. *Circ Res* 2017;**120**:312–323.
35. Kashyap S, Osman M, Ferguson CM, Nath MC, Roy B, Lien KR, Nath KA, Garovic VD, Lerman LO, Grande JP. Ccl2 deficiency protects against chronic renal injury in murine renovascular hypertension. *Sci Rep* 2018;**8**:8598.
36. Eardley KS, Zehnder D, Quinkler M, Lepenies J, Bates RL, Savage CO, Howie AJ, Adu D, Cockwell P. The relationship between albuminuria, MCP-1/CCL2, and interstitial macrophages in chronic kidney disease. *Kidney Int* 2006;**69**:1189–1197.
37. Pindjakova J, Hanley SA, Duffy MM, Sutton CE, Weidhofer GA, Miller MN, Nath KA, Mills KH, Ceredig R, Griffin MD. Interleukin-1 accounts for intrarenal Th17 cell activation during ureteral obstruction. *Kidney Int* 2012;**81**:379–390.
38. Andrade-Oliveira V, Amano MT, Correa-Costa M, Castoldi A, Felizardo RJ, de Almeida DC, Bassi EJ, Moraes-Vieira PM, Hiyane MI, Rodas AC, Peron JP, Aguiar CF, Reis MA, Ribeiro WR, Valduga CJ, Curi R, Vinolo MA, Ferreira CM, Camara NO. Gut bacteria products prevent AKI induced by ischemia-reperfusion. *J Am Soc Nephrol* 2015;**26**:1877–1888.
39. Singh N, Thangaraju M, Prasad PD, Martin PM, Lambert NA, Boettger T, Offermanns S, Ganapathy V. Blockade of dendritic cell development by bacterial fermentation products butyrate and propionate through a transporter (Slc5a8)-dependent inhibition of histone deacetylases. *J Biol Chem* 2010;**285**:27601–27608.
40. Wang F, Liu J, Weng T, Shen K, Chen Z, Yu Y, Huang Q, Wang G, Liu Z, Jin S. The inflammation induced by lipopolysaccharide can be mitigated by short-chain fatty acid. Butyrate, through upregulation of IL;10, in septic shock. *Scand J Immunol* 2017;**85**:258–263.
41. Duscha A, Gisevius B, Hirschberg S, Yissachar N, Stangl GI, Eilers E, Bader V, Haase S, Kaisler J, David C, Schneider R, Troisi R, Zent D, Hegelmaier T, Dokalis N, Gerstein S, Del Mare-Roumani S, Amidror S, Staszewski O, Poschmann G, Stuhler K, Hirche F, Balogh A, Kempa S, Trager P, Zaiss MM, Holm JB, Massa MG, Nielsen HB, Faissner A, Lukas C, Gatermann SG, Scholz M, Przuntek H, Prinz M, Forslund SK, Winklhofer KF, Muller DN, Linker RA, Gold R, Haghikia A. Propionic acid shapes the multiple sclerosis disease course by an immunomodulatory mechanism. *Cell* 2020;**180**:1067–1080.e16.
42. Haghikia A, Jorg S, Duscha A, Berg J, Manzel A, Waschbisch A, Hammer A, Lee DH, May C, Wilck N, Balogh A, Ostermann AI, Schebb NH, Akkad DA, Grohme DA, Kleinewietfeld M, Kempa S, Thone J, Demir S, Muller DN, Gold R, Linker RA. Dietary fatty acids directly impact central nervous system autoimmunity via the small intestine. *Immunity* 2015;**43**:817–829.
43. Jang HR, Gandolfo MT, Ko GJ, Satpute S, Racusen L, Rabb H. Early exposure to germs modifies kidney damage and inflammation after experimental ischemia-reperfusion injury. *Am J Physiol Renal Physiol* 2009;**297**:F1457–F1465.
44. Mishima E, Fukuda S, Mukawa C, Yuri A, Kanemitsu Y, Matsumoto Y, Akiyama Y, Fukuda NN, Tsukamoto H, Asaji K, Shima H, Kikuchi K, Suzuki C, Suzuki T, Tomioka Y, Soga T, Ito S, Abe T. Evaluation of the impact of gut microbiota on uremic solute accumulation by a CE-TOFMS-based metabolomics approach. *Kidney Int* 2017;**92**:634–645.
45. Krebs CF, Reimers D, Zhao Y, Paust HJ, Bartsch P, Nunez S, Rosemblatt MV, Hellmig M, Kilian C, Borchers A, Enk LUB, Zinke M, Becker M, Schmid J, Klinge S, Wong MN, Puelles VG, Schmidt C, Bertram T, Stumpf N, Hoxha E, Meyer-Schwesinger C, Lindenmeyer MT, Cohen CD, Rink M, Kurts C, Franzenburg S, Koch-Nolte F, Turner JE, Riedel JH, Huber S, Gagliani N, Huber TB, Wiech T, Rohde H, Bono MR, Bonn S, Panzer U, Mittrucker HW. Pathogen-induced tissue-resident memory TH17 (TRM17) cells amplify autoimmune kidney disease. *Sci Immunol* 2020;**5**:eaba4163.
46. Karbach SH, Schonfelder T, Brandao I, Wilms E, Hormann N, Jackel S, Schuler R, Finger S, Knorr M, Lagrange J, Brandt M, Waisman A, Kossmann S, Schafer K, Munzel T, Reinhardt C, Wenzel P. Gut microbiota promote angiotensin II-induced arterial hypertension and vascular dysfunction. *J Am Heart Assoc* 2016;**5**:e003698.
47. Kaye DM, Shihata WA, Jama HA, Tsyganov K, Ziemann M, Kiriazis H, Horlock D, Vijay A, Giam B, Vinh A, Johnson C, Fiedler A, Donner D, Snelson M, Coughlan MT, Phillips S, Du XJ, El-Osta A, Drummond G, Lambert GW, Spector TD, Valdes AM, Mackay CR, Marques FZ. Deficiency of prebiotic fiber and insufficient signaling through gut metabolite-sensing receptors leads to cardiovascular disease. *Circulation* 2020;**141**:1393–1403.
48. Emal D, Rampanelli E, Stroo I, Butter LM, Teske GJ, Claessen N, Stokman G, Florquin S, Leemans JC, Dessing MC. Depletion of gut microbiota protects against renal ischemia-reperfusion injury. *J Am Soc Nephrol* 2017;**28**:1450–1461.
49. Heianza Y, Ma W, Manson JE, Rexrode KM, Qi L. Gut microbiota metabolites and risk of major adverse cardiovascular disease events and death: a systematic review and meta-analysis of prospective studies. *J Am Heart Assoc* 2017;**6**:e004947.

Translational perspective

To assess the potential of microbiota-targeted interventions to prevent organ damage in hypertension, an accurate quantification of microbial influence is necessary. We provide evidence that the development of hypertensive organ damage is dependent on colonization status and suggest that a healthy microbiota provides anti-hypertensive immune and metabolic signals to the host. In the absence of normal symbiotic host-microbiome interactions, hypertensive damage to the kidney in particular is exacerbated. We suggest that hypertensive patients experiencing perturbations to the microbiota, which are common in CVD, may be at a greater risk for target-organ damage than those with a healthy microbiome.

Downloaded from https://academic.oup.com/cardiovascres/article/119/6/1441/6651675 by Duke University - Perkins Library user on 21 August 2023

Curriculum Vitae

My curriculum vitae does not appear in the electronic version of my paper for reasons of data protection.

My curriculum vitae does not appear in the electronic version of my paper for reasons of data protection.

My curriculum vitae does not appear in the electronic version of my paper for reasons of data protection.

Publication list

1. Hsiao, G., Wang, S. W., Chiang, Y. R., Chi, W. C., Kuo, Y. H., Phong, D. A., **Chen, C.-Y.** & Lee, T. H. Anti-inflammatory effects of peptides from a marine algicolous fungus Acremonium sp. NTU492 in BV-2 microglial cells. *J Food Drug Anal* 28, 283-291 (2020). https://doi.org/10.38212/2224-6614.1062
   Impact factor: 6.2

2. Carley, L. N., Mojica, J. P., Wang, B., **Chen, C.-Y.**, Lin, Y.-P., Prasad, K. V. S. K., Chan, E., Hsu, C.-W., Keith, R., Nuñez, C. L., Olson-Manning, C. F., Rushworth, C. A., Wagner, M. R., Wang, J., Yeh, P.-M., Reichelt, M., Ghattas, K., Gershenzon, J., Lee, C.-R., Mitchell-Olds, T. Ecological factors influence balancing selection on leaf chemical profiles of a wildflower. *Nature Ecology & Evolution* 5, 1135-1144 (2021). https://doi.org/10.1038/s41559-021-01486-0
   Impact factor: 16.8

3. Maifeld, A., Bartolomaeus, H., Lober, U., Avery, E. G., Steckhan, N., Marko, L., Wilck, N., Hamad, I., Susnjar, U., Mahler, A., Hohmann, C., **Chen, C.-Y.**, Cramer, H., Dobos, G., Lesker, T. R., Strowig, T., Dechend, R., Bzdok, D., Kleinewietfeld, M., Michalsen, A., Muller, D. N., Forslund, S. K. Fasting alters the gut microbiome reducing blood pressure and body weight in metabolic syndrome patients. *Nat Commun* 12, 1970 (2021). https://doi.org/10.1038/s41467-021-22097-0
   Impact factor: 16.6

4. Avery, E. G., Bartolomaeus, H., Rauch, A., **Chen, C.-Y.**, N'Diaye, G., Löber, U., Bartolomaeus, T. U. P., Fritsche-Guenther, R., Rodrigues, A. F., Yarritu, A., Zhong, C., Fei, L., Tsvetkov, D., Todiras, M., Park, J. K., Markó, L., Maifeld, A., Patzak, A., Bader, M., Kempa, S., Kirwan, J. A., Forslund, S. K., Müller, D. N., Wilck, N. Quantifying the impact of gut microbiota on inflammation and hypertensive organ damage. *Cardiovascular Research* (2022). https://doi.org/10.1093/cvr/cvac121
   Impact factor: 10.8

5. Mähler, A., Klamer, S., Maifeld, A., Bartolomaeus, H., Markó, L., **Chen, C.-Y.**, Forslund, S.K., Boschmann, M., Müller, D.N., Wilck, N. Increased Salt Intake Decreases Diet-Induced Thermogenesis in Healthy Volunteers: A Randomized Placebo-Controlled Study. *Nutrients* 14, 253 (2022). https://doi.org/10.3390/nu14020253
   Impact factor: 5.9

6. **Chen, C.-Y.**, Löber, U., Forslund, S. K. LongDat: an R package for covariate-sensitive longitudinal analysis of high-dimensional data. *Bioinformatics Advances* 3 (2023). https://doi.org/10.1093/bioadv/vbad063
   This journal is currently without an impact factor due to its recent establishment.

Acknowledgments

My sincerest gratitude goes to my supervisors, Dr. Sofia Forslund, Dr. Dominik N. Müller and Dr. Nicola Wilck at ECRC, Charité – Universitätsmedizin Berlin. I wish to convey my profound appreciation to Sofia for affording me the invaluable opportunity to become a part of the SFB 1365 Renoprotection program and her outstanding team. Words are inadequate to express my gratitude for your unwavering support and guidance. Your role as a supervisor and a mentor is exceptional in every regard. Our regular discussions and meeting have been pivotal in improving my skills and enriching my knowledge base. I attribute my growth to the trust, flexibility, and insights that you graciously extend to me. Without your constant support, I could not have navigated the myriad challenges of this Ph.D. journey which was full of ups and downs. To Dominik and Nicola, thank you for your guidance that has shaped my research direction, and for our collaborative efforts on multiple projects. Your expertise has greatly enriched my academic journey.

I am also thankful to all the PIs, post-docs, and fellow Ph.D. students who have enhanced my Ph.D. journey with their insights and perspectives, expanding my horizons in both science and life. A special note of gratitude goes to Dr. Young-Ae Lee, a member of my thesis committee, for your insight and guidance. I would like to recognize the invaluable support provided by post-docs Dr. Ulrike Löber, Dr. Lajos Marko, and Dr. Victor Hugo Jarquin Diaz, who have been essential in both scientific and administrative aspects. Your assistance and collaboration have played a crucial role in enabling me to successfully complete my studies. Furthermore, I want to express my appreciation to my fellow Ph.D. students, Morgan Essex, Till Birkner, Friederike Gutmann, and Theda Bartolomaeus. Your contributions have been instrumental in my development, as you've generously shared your expertise and experiences in statistics, programming, paper writing, and administrative affairs, sparking fresh and creative ideas for my projects. Collaborating with excellent post-docs and Ph.D. students within the lab has been both fortunate and enriching.

Finally, I want to extend my heartfelt thanks to my husband and family, which includes our cute dog Happy and the charming cat Charcoal. Your fond support has been important in enabling me to successfully complete my Ph.D. study in Germany. Particularly,

my husband, Che-Wei Hsu, deserves special recognition for the profound love and care you have given me. Throughout this journey, you have been my steadfast pillar and closest confidant. Your inspiration initially led me onto the path of pursuing a Ph.D., and your encouragement became the driving force that carried me to its completion. Your support has been indispensable, contributing significantly to not only achieving the fulfillment of my studies but also to creating countless precious memories during our time in Berlin.